POLY (AMIDO AMINE) DENDRIMERS: ROLE OF ARCHITECTURAL FEATURES ON BIODISTRIBUTION AND ORAL ABSORPTION ENHANCEMENT

by

Shraddha Shirish Sadekar

A dissertation submitted to the faculty of
The University of Utah
in partial fulfillment of the requirements for the degree of

Doctor of Philosophy

Department of Pharmaceutics and Pharmaceutical Chemistry

The University of Utah

August 2013

The University of Utah Graduate School

STATEMENT OF DISSERTATION APPROVAL

The dissertation of **Shraddha Shirish Sadekar**

has been approved by the following supervisory committee members:

Hamidreza Ghandehari	, Chair	**02/28/2013** Date Approved
Margit Janàt-Amsbury	, Member	**02/28/2013** Date Approved
James Herron	, Member	**03/01/2013** Date Approved
Steven Kern	, Member	**03/01/2013** Date Approved
Jindřich Kopeček	, Member	**03/01/2013** Date Approved

and by **David Grainger** , Chair of

the Department of **Pharmaceutics and Pharmaceutical Chemistry**

and by Donna M. White, Interim Dean of The Graduate School.

ABSTRACT

Most of the chemotherapeutics used in the clinic indiscriminately act on healthy proliferating cells along with malignant cells resulting in nonspecific toxicities, a narrow therapeutic index and reduced patient quality of life. Most of such agents are also limited by very low aqueous solubility. One strategy to overcome these challenges is to use biocompatible, water-soluble polymeric carriers to deliver chemotherapeutics with higher selectivity to sites of action (tumors), resulting in a better safety profile, increased maximum tolerated dose, and potentially better efficacy. Poly(amido amine) or PAMAM dendrimers are a class of branched polymers being extensively investigated for their potential as carriers for the delivery of anticancer agents. Their commercial availability, well-defined physicochemical and architectural features, ease of surface functionalization and encapsulation make PAMAM dendrimers useful for the delivery of chemotherapeutics. This dissertation focusses on two aspects of PAMAM dendrimers as drug carriers. The influence of PAMAM's molecular architecture on biodistribution and pharmacokinetics is compared with traditionally used and clinically investigated linear polymers at various molecular weights. Architecture of the polymer affected its hydrodynamic size at different molecular weights. A difference in accumulation of polymers of varying architecture in nonspecific elimination organs (kidney, liver) as well as site-specific organs (tumor) was observed. Variation in polymer architecture also resulted in a decrease in blood clearance with increase in hydrodynamic size and affinity

to passively target the tumor by the enhanced permeability and retention effect when circulating in the blood. This dissertation also explored the use of PAMAM dendrimers for oral delivery of chemotherapeutics. By virtue of their unique three-dimensional architecture, PAMAM dendrimers are known to encapsulate, complex and solubilize hydrophobic drugs, modify epithelial tight junctions and act as drug carriers for oral delivery. It was observed that co-administration with dendrimers increased oral bioavailability of camptothecin, a schedule-dependent drug limited in oral use by low and variable absorption. Results suggest that this increase in absorption was not due to epithelial tight junction modulation and that drug inclusion in PAMAM interior controlled solubilization in gastric conditions and increased oral bioavailability.

CONTENTS

ABBREVIATIONS

2D-NOESY	Two-dimensional-nuclear overhauser effect spectroscopy
AB	Apical to basolateral
AIBN	Azobisisobutyronitrile
AIC	Akaike information criterion
AUC_{plasma}	Area under the curve of the plasma concentration profile
AUC_{tumor}	Area under the curve of the tumor concentration profile
BA	Basolateral to apical
BCS	Biopharmaceutical classification system
CF	5(6)-carboxyfluorescein
CL_R	Renal clearance
C_p	Concentration in the plasma
CPT	Camptothecin
CPT-11	Irinotecan hydrochloride
CsA	Cyclosporin A
C_{t1}	Concentration in tumor compartment 1
C_{t2}	Concentration in tumor compartment 2
DAPI	4V,6-diamidino-2-phenylindole
DI water	Deionized water
DIC	Disseminated intravascular coagulation

DLS	Dynamic light scattering
DMSO	Dimethyl sulfoxide
DTPA	1,2-diamine-N,N-N′,N′,N″,N″-pentaacetic acid
E.CL	Elimination clearance
EDTA	Ethylenediaminetetraacetic acid
EEA-1	Early endosome antigen-1
EPR	Enhanced permeability and retention
FD	Fluorescein isothiocyanate-labeled dextrans
FDP	Fibrin degradation product
FITC	Fluorescein isothiocyanate
FPLC	Fast protein liquid chromatography
G0-deg-NAP	Naproxen conjugated to G0.0 via a diethyleneglycol spacer
G0-lact-NAP	Naproxen conjugated to G0.0 via a lactic acid spacer
G3.5-gly-SN38	SN38 conjugated with G3.5-COOH via a glycine spacer
G3.5-βala-SN38	SN38 conjugated with G3.5-COOH via a β-alanine spacer
GIT	Gastrointestinal tract
GX.0-NH_2	Amine-terminated PAMAM dendrimer generation X.0
GX.0-NH_2-FITC	Fluorescein isothiocyanate- labeled amine terminated PAMAM dendrimer of generation X.0
GX.0-OH	Hydroxyl terminated PAMAM, generation X.0
GX.0-OH	Hydroxyl-terminated PAMAM dendrimer generation X.0
GX.5-COOH	Carboxyl-terminated PAMAM dendrimer generation X.5

GXLY	Amine-terminated PAMAM dendrimer of generation X.0 modified with Y moles of lauric acid per mole of PAMAM
H and E stain	Hematoxylin and eosin stain
HPLC	High performance liquid chromatography
HPMA	*N*-(2-hydroxypropyl)methacrylamide
LAMP-1	Lysosome-associated membrane protein 1
LDH	Lactate dehydrogenase
MA-GG-EtOH	*N*-methacryloyl-glycylglycyl-ethanolamine
MA-GG-ONP	*N*-methacryloyl-glycylglycyl-para-nitrophenyl ester
MA-GG-TT	*N*-methacryloyl-glycylglycyl-thiazolidine-2-thione
MALLS	Multi-angle laser light scattering
MA-Tyr-$COCH_3$	*N*-methacryloyl tyrosine-methyl ester
MA-Tyr-$CONH_2$	*N*-methacryloyl tyrosinamide
MDCK	Madin-Darby canine kidney
MRI	Magnetic resonance imaging
MTD	Maximum tolerated dose
MTT	(3-(4,5-Dimethylthiazol-2-yl)-2,5-diphenyltetrazolium bromide)
MW	Molecular weight
NMR	Nuclear magnetic resonance
NSAIDS	Nonsteroidal anti-inflammatory drugs
PAMAM	Poly(amido amine)
PAMAM-COOH	Carboxylic-terminated PAMAM dendrimer
PAMAM-NH_2	Amine-terminated PAMAM dendrimer

PAMAM-OH	Hydroxyl terminated poly(amido amine)
P_{app}	Apparent permeability coefficient
PBS	Phosphate Buffer Saline
PEG	Poly(ethylene glycol)
PEI	Poly(ethyleneimine)
PEO	Poly(ethylene oxide)
PGA	Poly(glutamic acid)
P-gp	P-glycoprotein
PLL	Polylysine
PPI	Poly(propyleneimine)
RES	Reticuloendothelial system
R_h	Hydrodynamic radius
SEC	Size exclusion chromatography
SGF	Simulated gastric fluid
SIF	Simulated intestinal fluid
SN-38	7-ethyl-10-hydroxy-camptothecin
TEER	Transepithelial electrical resistance
TEM	Transmission electron microscopy
TES	N-tris(hydroxymethyl)methyl-2-aminoethanesulfonic acid
WST-1	(4-[3-(4-iodophenyl)-2-(4-nitrophenyl)-2H-5-tetrazolio]-1,3-benzene disulfonate)

ACKNOWLEDGEMENTS

My journey in graduate school was an excellent opportunity to discover my personal strengths and limitations. This journey would not have been possible without the support of all the people I connected with, near and away.

Dr. Hamid Ghandehari has been the primary facilitator and mentor to build this dissertation. He has been very prompt in giving feedback on research as well as writing and has always remained accessible despite his many commitments. Dr. Ghandehari has contributed immensely towards improving my writing skills. His focus, hard work and drive are qualities I wish to inculcate in my scientific career.

All of my committee members have been instrumental in improving my proposal for advancing to candidacy in the program. As a first year student, I enjoyed rotating in Dr. Jindřich Kopeček laboratory. I admire the detailed-oriented culture in his laboratory and often seek help from his lab members. Dr. James Herron's understanding of the physical sciences is inspiring and discussions with him on my research have been very insightful. Dr. Steven Kern inspired me in his class on compartmental pharmacokinetics. He initiated me into research on pharmacokinetics and pharmacodynamics. I admire his teaching and also wish to emulate his career path. Dr. Margit Amsbury has always had an encouraging word to say. She has also facilitated the collaboration for the tumor model employed in this dissertation.

The Ghandehari Lab members have helped with trouble-shooting on a daily basis. Dr. Abhijit Ray and Dr. Khaled Greish have trained me in experimenting with chemistry and animal studies respectively. My fellow project mates and graduate students in Bioengineering- Giridhar Thiagarajan and Dallin Hubbard- have helped extensively with intellectual inputs and manual labor for animal experiments. In the past few months, I have had the opportunity to mentor Kristopher Bartlett, a sophomore in the Bioengineering program and a budding scientist. Kristopher went above and beyond the call of duty every week in order to help with my experiments. I want to thank him for his eagerness to learn and for the satisfaction I got from teaching him. Nate Larson and Brandon Buckway, graduate students in pharmaceutics, have always been very resourceful and instrumental in problem-solving.

I was fortunate to find fruitful collaborations during my research. Yong-En Sun, a research associate who works with Dr. Margit Amsbury, hugely assisted with tumor inoculation and animal harvesting. Without his surgical skillset, it would not have been possible to use the orthotopic ovarian tumor model employed in the experiments of Chapter 3. Olinto Linares-Perdomo from the Department of Biomedical Informatics initiated the pharmacokinetic analysis of some of my experimental data.

I also want to take this opportunity to thank Dr. David Grainger in his role as Chair of the Department of Pharmaceutics and Pharmaceutical Chemistry. He has been a student advocate and his endeavors have ensured that students of our department get the highest level of education.

My husband, Shantanu Rajwade, endured distance and provided me with constant emotional support in order for me to pursue my education and build this dissertation. He

also tutored me in MATLAB®, a tool I used to model some of my experimental data and helped format this dissertation. Lastly, I would like to thank my parents Deeksha and Shirish Sadekar. Their wisdom and perspective towards life has helped me in tough times.

CHAPTER 1

INTRODUCTION

1.1. Introduction

Most anticancer drugs used in the clinic have disadvantages of a narrow therapeutic index, indiscriminately acting on healthy proliferating cells along with malignant cells and resulting in nonspecific toxicities. Conjugating and complexing small molecular weight anticancer drugs to biocompatible, water-soluble polymeric carriers increases therapeutic index, facilitates passive targeting to solid tumors, decreases toxicities and has the potential to increase efficacy [1, 2].

One such class of polymers being explored as drug carriers is poly(amido amine) or PAMAM dendrimers. PAMAM dendrimers are hyperbranched polymers with a very well-defined architecture due to their controlled synthesis [3]. With increase in the extent of branching, the generation of the dendrimer increases and the number of surface terminal groups double [4]. As a result of the divergent branching, PAMAM dendrimers have a relatively hollow core and a dense surface exterior that can be tailor-made to have different terminal groups [4]. The large number of functional groups on the exterior as well as the relatively hollow interior provides the opportunity of loading various cargo like drugs, imaging agents and targeting moieties by surface conjugation, complexation

or encapsulation within the dendrimer core (Figure 1-1) [5-15]. Their commercial availability, monodisperse physicochemical characteristics, ease of functionalization and potential for encapsulation make PAMAM dendrimers excellent carriers for polymer therapeutics. They are extensively being investigated as carriers for delivery of anticancer drugs to solid tumors [16].

Traditionally, polymer therapeutics have been linear or random coil conformations in solutions. Many polymer therapeutics in clinical investigation have had poly(*N*-(2-hydroxypropyl)methacrylamide) (HPMA) as carriers that are known to assume a random coil conformation in solution [17, 18]. The passive targeting of polymer-conjugated drugs based on the enhanced permeability and retention (EPR) effect has also been primarily investigated with such linear polymers [19-21]. PAMAM dendrimers, on the other hand, are hyperbranched in architecture. They are known to undergo a conformational change with increase in generation, with the lower generation dendrimers (G0.0-G3.0) being more flexible in conformation [4]. The intermediate generation dendrimers (G4.0-G6.0) have a relatively hollow core and dense surface possessing nano-container-like properties allowing host-guest interactions, and the higher generation ones (G7.0-G9.0) becoming increasingly rigid and globular in conformation [4]. This difference in molecular conformation and polymer architecture of PAMAM dendrimers from clinically used random-coiled polymers like HPMA is likely to affect its biodistribution and pharmacokinetics *in vivo*.

The unique three-dimensional architecture of PAMAM dendrimers has also been exploited for delivery of drugs across epithelial barriers by virtue of 1) encapsulation within the relatively hydrophobic, hollow interior of PAMAM dendrimers resulting in

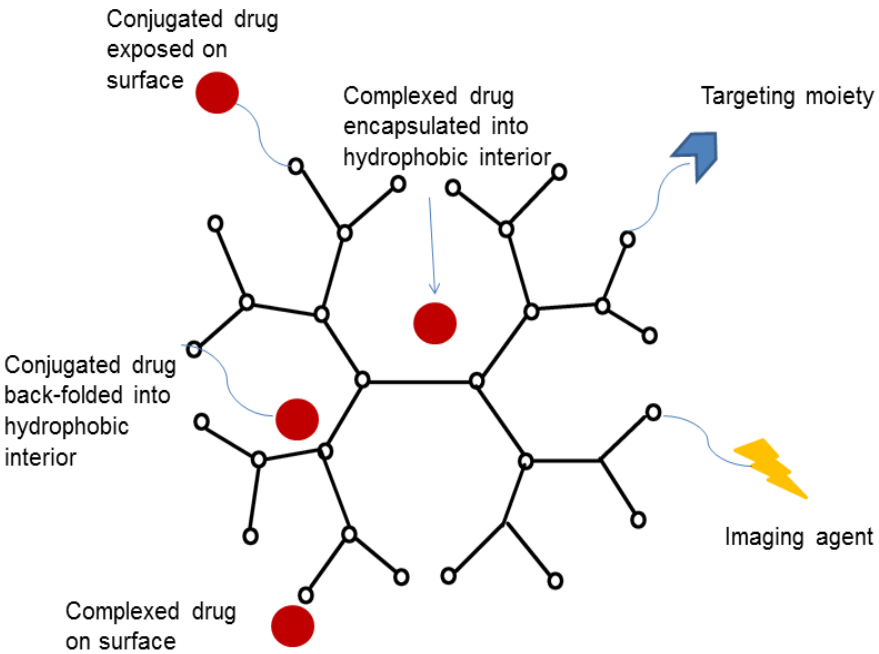

Figure 1-1. Schematic of a dendrimer-based delivery system functionalized with conjugated or complexed drug, targeting moiety and imaging agent.

solubilization of hydrophobic drugs [13, 14], 2) tight junction modulation of epithelial barriers by densely charged positive or negative surface groups [22, 23], and 3) endocytotic uptake of PAMAM dendrimers [24-26]. PAMAM dendrimers have been extensively studied *in vitro* across Caco-2 monolayers for their transepithelial transport and as oral delivery systems for hydrophobic drugs [27, 28]. *In vitro* studies lacked the variables of mucous layer, gastrointestinal transit time and harsh enzymatic and pH conditions of the gastrointestinal tract (GIT). There have been very limited studies *in vivo* to assess PAMAM dendrimers as oral drug carriers [29, 30].

1.2. Aims and scope of this dissertation

This dissertation focusses on two aspects of PAMAM dendrimers as drug carriers for delivery of anticancer drugs. In the first part of the dissertation (Chapters 3 and 4), the effect of architectural difference between hyperbranched PAMAM dendrimers and clinically used linear polymers on *in vivo* biodistribution and pharmacokinetics is described. In the second part of this dissertation (Chapter 5), the unique three-dimensional architecture of the PAMAM dendrimer consisting of a densely-charged surface exterior and relatively hollow and hydrophobic core is exploited for oral delivery of a chemotherapeutic. Three specific aims were pursued:

Specific aim 1: To compare the biodistribution of hyperbrancehd PAMAM-OH dendrimers and linear HPMA copolymers of comparable MW over a physiologically relevant MW range.

In Chapter 3, the biodistribution of a series of hydroxyl-terminated PAMAM dendrimers were compared with HPMA copolymers of comparable molecular weights in

physiologically relevant molecular weight range of kidney filtration, extended plasma circulation and tumor accumulation. The biodistribution studies of both the polymer series were done under consistent experimental conditions of physicochemical characterization, animal model, and *in vivo* detection system in order to facilitate a head to head comparison and to evaluate the effect of hydrodynamic size and polymer architecture on accumulation in target organ, tumor, and nonspecific organs like kidney and liver. The studies were carried out in animals bearing orthotopic ovarian carcinoma tumors, which is a non-metastatic, solid tumor model known to better simulate ovarian malignancy. Biodistribution studies were performed by dosing tumor-bearing mice with ^{125}Iodine-labeled polymers. Radiolabeled polymers were detected in organ systems by measuring gamma emission of the ^{125}Iodine radiolabel which facilitated a direct and accurate measurement. Polymer architecture affected hydrodynamic size at different molecular weights [31]. In addition to molecular weight, hydrodynamic size and polymer architecture affected the accumulation of these constructs in nonspecific elimination organs, kidney and liver, and site-specific organs, tumor and blood [31].

Specific aim 2: To compare the blood and tumor pharmacokinetics of hyperbranched PAMAM-OH dendrimers and linear HPMA copolymers of comparable MW over a physiologically relevant MW range.

In Chapter 4, the biodistribution data collected in Chapter 3 were analyzed by compartmental pharmacokinetic analysis. Specifically, blood and tumor pharmacokinetic parameters were computed that gave additional insight onto the effect of polymer architecture on *in vivo* fate of the carriers. Blood concentration data were modeled by two-compartment analysis comprising of a central blood compartment and a peripheral

fast-distribution compartment. Polymer architecture influenced elimination and renal clearance [32]. These results suggest a difference in extravasation of polymers of varying architecture through the glomerular basement membrane. A blood-tumor link model was fitted to experimental blood and tumor data by varying the tumor extravasation (K_4, K_6) and elimination (K_5) rate constants using multivariable constrained optimization. Polymer architecture affected tumor extravasation rates and tumor to blood exposure ratios [32]. Along with MW and Rh, the difference in polymer architecture of PAMAM-OH dendrimers and HPMA copolymers was critical in affecting the blood and tumor pharmacokinetics of these polymeric carriers.

Specific aim 3: To evaluate PAMAM dendrimers as absorption enhancers for the oral delivery of chemotherapeutic.

By virtue of their unique three-dimensional architecture, PAMAM dendrimers of certain generations are known to solubilize and/or encapsulate hydrophobic drugs, modify epithelial tight junctions and act as drug carriers for oral delivery of conjugated or complexed drugs. Their potential in oral delivery has been extensively evaluated *in vitro* and *in situ*, however there have been very limited studies *in vivo*. In Chapter 5, cationic, amine-terminated PAMAM dendrimer generation 4.0 and anionic, carboxylate-terminated PAMAM generation 3.5, known to solubilize drugs and modulate tight junctions, were evaluated as absorption enhancers for the oral delivery of anticancer drug camptothecin [33]. Camptothecin is a BCS class IV drug with poor solubility and permeability. It is a schedule-dependent drug that benefits from low and frequent oral dosing. Its oral use for hepatic metastasis of colorectal cancer is limited by low and variable oral bioavailability. Camptothecin was formulated and co-delivered orally with

G4.0-NH_2 and G3.5-COOH in CD-1 mice at different ratios of drug to dendrimer. PAMAM surface charge influenced camptothecin association with the dendrimer [33]. The hypothesis was that PAMAM dendrimers at nontoxic concentrations can increase oral absorption of drug either by 1) drug solubilization in gastric conditions or 2) by tight junction modulation. Both PAMAM G4.0 and G3.5 controlled drug solubilization in gastric conditions and increased oral absorption of camptothecin [33]. PAMAM G4.0 and G3.5 did not increase oral absorption of mannitol, a paracellular marker, suggesting that increase in oral absorption of camptothecin was not due to tight junction modulation [33]. This study demonstrated that both cationic and anionic PAMAM dendrimers were equally effective in enhancing the oral absorption of camptothecin [33]. Results suggest that drug inclusion in PAMAM interior controlled drug solubilization in gastric conditions and increased oral bioavailability [33].

The following chapters of this dissertation include a review of the relevant literature (Chapter 2), parts of which were published elsewhere [27], the scientific work used to address specific aims 1-3 (Chapters 3-5) [31-33] and the project's conclusions and future directions (partly adapted from [27]) (Chapter 6).

1.3. References

1. Duncan R. Polymer conjugates as anticancer nanomedicines. Nat Rev Cancer. 2006;6(9):688-701.

2. Li C, Wallace S. Polymer-drug conjugates: Recent development in clinical oncology. Adv Drug Del Rev. 2008;60(8):886-98.

3. Tomalia DA, Baker H, Dewald J, Hall M, Kallos G, Martin S et al. A new class of polymers: starburst-dendritic macromolecules. Polym J. 1985;17(1):117-32.

4. Tomalia DA, Naylor AM, Goddard III WA. Starburst dendrimers: molecular-level control of size, shape, surface chemistry, topology, and flexibility from atoms to macroscopic matter. Angew Chem Int Ed. 1990;29(2):138-75.

5. Gu S, Zhao X, Zhang L, Li L, Wang Z, Meng M et al. Anti-angiogenesis effect of generation 4 polyamidoamine/vascular endothelial growth factor antisense oligodeoxynucleotide on breast cancer *in vitro*. J Zhejiang Univ Sci B. 2009;10(3):159-67.

6. Bhadra D, Bhadra S, Jain S, Jain N. A PEGylated dendritic nanoparticulate carrier of fluorouracil. Int J Pharm. 2003;257(1-2):111-24.

7. Kukowska-Latallo JF, Bielinska AU, Johnson J, Spindler R, Tomalia DA, Baker JR. Efficient transfer of genetic material into mammalian cells using Starburst polyamidoamine dendrimers. Proc Natl Acad Sci USA. 1996;93(10):4897-902.

8. Thiagarajan G, Ray A, Malugin A, Ghandehari H. PAMAM-camptothecin conjugate inhibits proliferation and induces nuclear fragmentation in colorectal carcinoma cells. Pharm Res. 2010;27:2307-16.

9. Asthana A, Chauhan AS, Diwan PV, Jain NK. Poly (amidoamine)(PAMAM) dendritic nanostructures for controlled sitespecific delivery of acidic anti-inflammatory active ingredient. AAPS PharmSciTech. 2005;6(3):536-42.

10. Yiyun C, Na M, Tongwen X, Rongqiang F, Xueyuan W, Xiaomin W et al. Transdermal delivery of nonsteroidal anti inflammatory drugs mediated by polyamidoamine (PAMAM) dendrimers. J Pharm Sci. 2007;96(3):595-602.

11. Cheng Y, Qu H, Ma M, Xu Z, Xu P, Fang Y et al. Polyamidoamine (PAMAM) dendrimers as biocompatible carriers of quinolone antimicrobials: an *in vitro* study. Eur J Med Chem. 2007;42(7):1032-8.

12. Ma M, Cheng Y, Xu Z, Xu P, Qu H, Fang Y et al. Evaluation of polyamidoamine (PAMAM) dendrimers as drug carriers of anti-bacterial drugs using sulfamethoxazole (SMZ) as a model drug. Eur J Med Chem. 2007;42(1):93-8.

13. Gupta U, Agashe HB, Asthana A, Jain N. Dendrimers: novel polymeric nanoarchitectures for solubility enhancement. Biomacromolecules. 2006;7(3):649-58.

14. D'Emanuele A, Attwood D. Dendrimer–drug interactions. Adv Drug Del Rev. 2005;57(15):2147-62.

15. Svenson S, Tomalia DA. Dendrimers in biomedical applications—reflections on the field. Adv Drug Del Rev. 2005;57(15):2106-29.

16. Tomalia D, Reyna L, Svenson S. Dendrimers as multi-purpose nanodevices for oncology drug delivery and diagnostic imaging. Biochem Soc Trans. 2007;35:61-7.

17. Duncan R. Development of HPMA copolymer–anticancer conjugates: clinical experience and lessons learnt. Adv Drug Del Rev. 2009;61(13):1131-48.

18. Kopeček J, Kopečková P. HPMA copolymers: origins, early developments, present, and future. Adv Drug Del Rev. 2010;62(2):122-49.

19. Yamaoka T, Tabata Y, Ikada Y. Distribution and tissue uptake of poly (ethylene glycol) with different molecular weights after intravenous administration to mice. J Pharm Sci. 1994;83(4):601-6.

20. Seymour L, Miyamoto Y, Maeda H, Brereton M, Strohalm J, Ulbrich K et al. Influence of molecular weight on passive tumour accumulation of a soluble macromolecular drug carrier. Eur J Cancer. 1995;31(5):766-70.

21. Noguchi Y, Wu J, Duncan R, Strohalm J, Ulbrich K, Akaike T et al. Early phase tumor accumulation of macromolecules: a great difference in clearance rate between tumor and normal tissues. Cancer Science. 1998;89(3):307-14.

22. El-Sayed M, Ginski M, Rhodes CA, Ghandehari H. Influence of surface chemistry of poly (amidoamine) dendrimers on Caco-2 cell monolayers. J Bioact Compatible Polym. 2003;18(1):7-22.

23. Kitchens KM, Kolhatkar RB, Swaan PW, Eddington ND, Ghandehari H. Transport of poly (amidoamine) dendrimers across Caco-2 cell monolayers: influence of size, charge and fluorescent labeling. Pharm Res. 2006;23(12):2818-26.

24. Kitchens KM, Kolhatkar RB, Swaan PW, Ghandehari H. Endocytosis inhibitors prevent poly (amidoamine) dendrimer internalization and permeability across Caco-2 cells. Mol Pharm. 2008;5(2):364-9.

25. Kitchens KM, Foraker AB, Kolhatkar RB, Swaan PW, Ghandehari H. Endocytosis and interaction of poly (amidoamine) dendrimers with Caco-2 cells. Pharm Res. 2007;24(11):2138-45.

26. El-Sayed M, Rhodes CA, Ginski M, Ghandehari H. Transport mechanism (s) of poly (amidoamine) dendrimers across Caco-2 cell monolayers. Int J Pharm. 2003;265(1-2):151-7.

27. Sadekar S, Ghandehari H. Transepithelial transport and toxicity of PAMAM dendrimers: implications for oral drug delivery. Adv Drug Del Rev. 2012;64(6):571-88.

28. Kitchens KM, El-Sayed MEH, Ghandehari H. Transepithelial and endothelial transport of poly (amidoamine) dendrimers. Adv Drug Del Rev. 2005;57(15):2163-76.

29. Ke W, Zhao Y, Huang R, Jiang C, Pei Y. Enhanced oral bioavailability of doxorubicin in a dendrimer drug delivery system. J Pharm Sci. 2008;97(6):2208-16.

30. Huang X, Wu Z, Gao W, Chen Q, Yu B. Polyamidoamine dendrimers as potential drug carriers for enhanced aqueous solubility and oral bioavailability of silybin. Drug Dev Ind Pharm. 2011;37(00):419-27.

31. Sadekar S, Ray A, Jana t-Amsbury M, Peterson C, Ghandehari H. Comparative biodistribution of PAMAM dendrimers and HPMA copolymers in ovarian-tumor-bearing mice. Biomacromolecules. 2011;12:88-96.

32. Sadekar S, Linares O, Noh GJ, Hubbard D, Ray A, Janát-Amsbury M et al. Comparative pharmacokinetics of PAMAM-OH dendrimers and HPMA copolymers in ovarian tumor-bearing mice. Drug Deliv Transl Res. 2012. doi:10.1007/s13346-012-0119-6.

33. Sadekar S, Thiagarajan G, Bartlett K, Hubbard D, Ray A, L.D.McGill et al. Poly(amido amine) dendrimers as absorption enhancers for oral delivery of camptothecin. Int J Pharm. *submitted*.

CHAPTER 2[1]

LITERATURE BACKGROUND

2.1. Polymer therapeutics

The term 'polymer therapeutics' encompasses polymer-drug conjugates, polymer-protein conjugates and supramolecular polymer-drug systems such as drug-containing polymeric micelles, polymer-drug complexes, polyplexes as non-viral vectors for nucleic acid delivery [1, 2]. Conjugation or complexation of small molecular weight drugs to polymeric carriers can result in increased drug solubility, prolonged circulation half-life , increased concentration at the site of action (such as tumors) and decreased non-specific toxicity. [1, 3-6]. The rationale of polymer therapeutics is similar to other macromolecular therapeutics such as proteins, antibodies as well as their prodrugs [7, 8]. However, it is possible to synthetically tailor the polymeric carrier with greater versatility in the right size range, required molecular conformation and with specific functionalities [1, 9-14].

---

[1]Note-Parts of literature background reprinted with permission from S. Sadekar, H. Ghandehari, Transepithelial Transport and Toxicity of PAMAM Dendrimers: Implications for Oral Drug Delivery, *Advanced Drug Delivery Reviews*, 2012, 64, 6, 571-588.

2.1.1. Polymer-drug conjugates

A model polymer-drug conjugate was first described by Ringsdorf, consisting of a linear polymeric backbone and pendant side chains containing drugs, targeting moieties and imaging agents [15]. Polymer-drug conjugates are known to passively target the tumor by the enhanced permeability and retention (EPR) effect (discussed in Section 2.1.2) and can also be actively targeted to the tumor [16-19]. These conjugates are known to be taken up in tumor cells via receptor-mediated endocytosis [20, 21]. Drug release is by hydrolytic or enzymatic cleavage of the spacer group in the extracellular tumor environment or intracellular lysosomal compartment [3, 22-26]. An ideal polymeric carrier should be water-soluble, biocompatible, have attachment sites for linkers carrying cargo and should have reproducible synthetic methodology with the ability to tailor molecular weight, size and cargo load [1].

All polymer-drug conjugates evaluated in the clinic except one (HPMA-doxorubicin-galactosamine) rely on passive targeting to the tumor via the EPR effect (discussed in Section 2.1.2) [27, 28]. The synthetic polymeric carriers used to synthesize polymer-drug conjugates in the clinic are *N*-(2-hydroxypropyl)methacrylamide (HPMA) copolymers, poly(ethylene glycol) (PEG) and poly(glutamic acid) (PGA) [2, 27, 28]. Majority of the polymeric carriers employed under clinical investigation have a linear backbone (e.g., HPMA, PEG) (Table 2-1). Polymeric carriers of increasing complexity (described in Section 2.2.) have evolved and are being assessed as drug carriers. The dendritic systems offer advantages of being more defined in their chemical composition and architecture resulting in monodisperse systems that can be tailor-made to have multivalent surface functionalities or to host guest molecules within their interior [29].

Table 2-1. Polymer-anticancer drug conjugates investigated clinically. (Compiled from Ref [2, 27, 28])

Polymer-drug conjugate	**Polymeric carrier architecture/conformation**
HPMA copolymer-doxorubicin [30]	Linear-random coil- side chains
HPMA copolymer-doxorubicin-galactosamine [17]	Linear-random coil- side chains
HPMA copolymer-paclitaxel [31]	Linear-random coil- side chains
AP5280, HPMA copolymer-carboplatinate analogue [32]	Linear-random coil- side chains
AP5346, HPMA copolymer-diaminocyclohexane palatinate analogue [33, 34]	Linear-random coil- side chains
HPMA copolymer-camptothecin [35]	Linear-random coil- side chains
PEG-camptothecin [36]	Linear-random coil- side chains
PEG-Irinotecan [37]	4-arm branched
PEG-SN38 [38]	4-arm branched
PEG-docetaxel [39]	4-arm branched
PGA-taxol [40]	Linear-extended- side chains
PGA-camptothecin [6, 41]	Linear-extended- side chains

Note: Drug conjugation can alter architectures and conformations of polymeric carriers

2.1.2. The enhanced permeability and retention (EPR) effect-Passive tumor targeting of polymer therapeutics

The enhanced permeability and retention (EPR) effect was first reported by Maeda and coworkers postulating that particles of a certain size accumulate and retain in solid tumors [42]. Elevated levels of vascular permeability factors cause high vascular density in a short period of time [43]. The abnormally fast growth of vasculature results in a defective architecture of endothelial cells with wide fenestrations that lack a smooth muscle layer and an interstitium that has a compromised lymphatic drainage [43].

A time dependent accumulation of macromolecules has been noted for proteins, polymers, liposomes and other nanocarriers as a result of increased blood circulation time and the enhanced permeability and retention in the tumor [16, 19, 44, 45]. Amongst polymeric carriers, the EPR effect has been extensively studied in random coil polymers like poly(ethylene glycol) and *N*-(2-hydroxy)propyl methacrylamide copolymers to study the effect of polymer molecular weight (MW) on the extent of tumor accumulation (Figure 2-1) [46-48]. It has, however, not been well established in polymers of varying architecture.

For the random coil HPMA copolymers evaluated *in vivo* in subcutaneous sarcoma models, the EPR effect was observed for polymers in the MW range of 40 to 800 kDa [48]. At about 6 hours after intravenous administration, the EPR effect was observed to kick in and a tumor to blood accumulation ratio of 10 to 30 was achieved. Retention of about 10-20 % injected dose/g was observed for up to months [48].

While molecular weight (MW) is an important indicator of hydrodynamic size of a polymer, the correlation of MW to hydrodynamic radius (R_h) can be different for

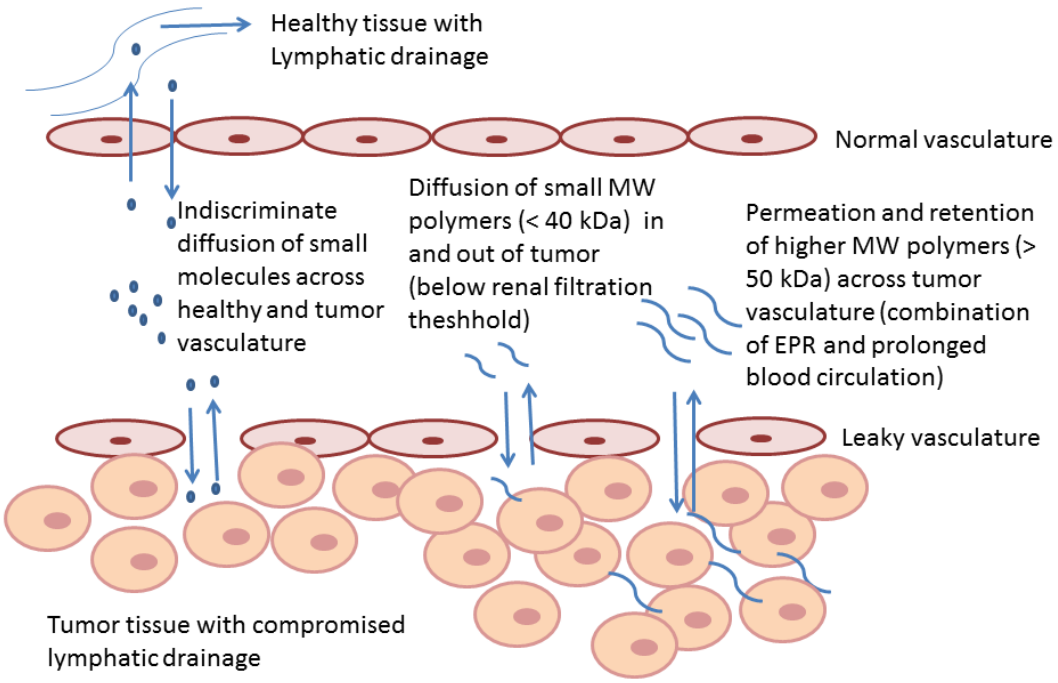

Figure 2-1. Schematic representing the effect of particle size on the enhanced permebability and retention (EPR) effect. (After 6 hours in blood circulation)

polymers of different architectures. Hydrodynamic size and conformational flexibility are more physiologically relevant parameters over MW, that are likely to control passive targeting via the EPR effect [49, 50].

Jain and coworkers have characterized the EPR effect on a micro-scale where they took a closer look at transport barriers within the tumor for the delivery of macromolecules [51, 52]. Transport barrier to drug transport within the tumor include 1) transvascular transport across capillaries into tumor interstitial space, 2) movement in the tumor interstitial space to reach tumor cells and 3) cellular uptake [53]. The unique pathophysiology of the tumor, while making it more permeable to macromolecules, can also augment their transport barriers by: 1) growth-induced solid stress, 2) tortuous vasculature, 3) elevated interstitial fluid pressure and 4) dense interstitial structure [53-56].

There has been extensive research on increasing the transport of macromolecules to the tumor and augmenting the EPR effect [57]. One of the strategies includes tuning the properties of the therapeutic moiety [58-60]. While size and surface charge of a macromolecule have been exploited to increase plasma circulation and target the tumor, conformation and flexibility of the molecule have been the least studied properties [47, 48, 61-67].

The diffusion coefficients of structures comparable in size but having different flexibilities (proteins, dextrans, polymer beads and DNA) were measured in agarose gels, that simulated the porous structure of the extracellular matrix in biological systems [63]. Flexible macromolecules like DNA chains had a higher diffusion coefficient in the gel

than rigid spherical particles of comparable hydrodynamic size in solution [63]. Chain like macromolecules also showed reptation-like behavior in the gel [63].

The tumor uptake of polymeric contrast agents of different conformations was compared [64-66]. Polylysine chains were substituted with 1,2-diamine-N,N-N′,N′,N″,N″-pentaacetic acid (DTPA). The extent of substitution controlled conformation of the polymer in solution. A higher degree of substitution (5-10%) caused the polymers to assume an extended conformation in solution distinct from the coiled conformation of the lower substituted polymers [64, 65]. Polymers with an extended rod-like conformation showed higher tumor uptake than ones with coiled conformations inspite of a similar opportunity to partition into the tumor (with comparable plasma circulation) [64, 65]. It was hypothesized that the rod-like polymer had more efficient cell-surface assisted reptation in the porous tissue matrix, explaining its higher tumor uptake [66]. These studies suggested that flexible chain-like macromolecules would be more effective in permeating the tumor and delivering drug.

2.2. Architecture and its effect on *in vivo* fate of polymeric carriers

Polymer architecture is determined by molecular conformation, chain flexibility, deforming capacity and extent of branching in solution [68]. Polymeric carriers in drug delivery may be linear or graft, dendritic, cyclic and hybrid architectures (structure-physicochemical property relationships of linear and dendritic polymers summarized in Table 2-2).

Physicochemical properties of a polymeric carrier such as composition, molecular weight, hydrodynamic size and architecture are known to affect *in vivo* fate. Polymer

Table 2-2. Structure-physicochemical property relationships of linear and dendritic carriers explored in drug delivery applications. (Compiled from Ref [49])

Structure-physicochemical property	Linear	Dendrimers/Dendritic polymers
Conformation in solution (good solvent)	Uncharged backbone-Random coil Charged backbone-Extended	Higher generations (> G3) are globular, shape-persistant molecular spheres [69] Backfolding of end groups to some extent [70]
Solubility and reactivity	Uncharged backbone-solubility decreases with increase in MW [49].	Spherical shape results in maximum surface area to volume ratio. Increased solubility and reactivity over linear polymers is observed [71].
Rheology	Chain entanglement causes increase in viscosity with increased chain length [72].	Intermolecular chain entanglement suppressed at higher generations [69] Intrinsic viscosity initially increases with MW, goes through a maximum and then decreases with further increase in MW [73]
Examples	HPMA, PEG, PGA	PAMAM, polyester, PLL, PEI, PPI dendrimers

Note- Conjugation of drugs or other moieties is known to alter physicochemical properties and drastically modify conformation.

Note- Hybrid of linear and dendritic architectures such as dendronized polymers or bow-tie architecture show a range of physicochemical properties between those of linear and dendritic systems.

architecture is one of the least studied physicochemical properties that can affect biodistribution and pharmacokinetics.

Architecture of a polymer can influence its renal clearance, blood circulation time, tumor penetration and uptake. One of the first reports in literature to assess the effect of polymer architecture on biodistribution and pharmacokinetics was the evaluation of polyester dendrimers-poly(ethylene oxide) (PEO) hybrids with tunable molecular weight and architecture [74]. The architecture was controlled by dendrimer generation and number of PEO arms (2-8) [74]. The molecular weights ranged from 20 to 160 kDa. Polymers above 40 kDa had a longer plasma elimination half-life and showed reduced renal clearance. For polymers of comparable MW, renal clearance decreased with extent of branching, attributed to decreased flexibility [74].

Polyester backbones with PEG grafts in linear and cyclized forms were evaluated for their circulation half-life [75]. For polymers just above renal filtration threshold, at 50 kDa, the cyclized polymer that lacked a chain end showed a longer plasma elimination half-life [75]. The authors attributed this to the ability of the linear polymer to reptate through pores of vasculature in elimination systems of the body (specifically the kidney filtration system). However, the cyclized polymers lacked a chain end and had to deform in order to extravasate [75].

A series of PEGylated poly acrylic comb-shaped polymers were also synthesized at different molecular weights as linear and cyclized versions [76]. The same phenomenon was observed again with the cyclized polymer showing a greater plasma half-life than the linear counterpart above renal filtration threshold [76]. This study was carried out in tumor-bearing mice (subcutaneous colorectal carcinoma tumors). As a

consequence of increased plasma circulation, the tumor accumulation of the cyclic polymers was also greater than the linear polymer of comparable molecular weight [76].

In all of these studies molecular weight was used as an indicator for polymer size. Hydrodynamic radius is a more physiologically relevant indicator of polymer size *in vivo*. These studies also used plasma elimination half-life as the primary pharmacokinetic parameter to define effect of polymer architecture on plasma circulation. The terminal half-life expresses the overall rate of polymer elimination process during the terminal phase. This rate of elimination depends upon extent of polymer clearance and polymer distribution. A long terminal half-life can be attributed to either a large volume of distribution or a small plasma clearance or both [77]. Therefore, terminal half-life is not the most robust parameter to assess the ability of the body to eliminate the polymer [77]. On the other hand, plasma clearance expresses the ability of the body to eliminate the polymer and is a more robust pharmacokinetic parameter to evaluate the effect of polymer architecture on elimination through vasculature systems of the body. It has been postulated that at comparable hydrodynamic sizes, polymer architecture affects the rate at which it transports across pores in vasculature of elimination systems of the body, which are of the same order of magnitude as the polymer size (2-10 nm) (Figure 2-2) [50].

The hypothesis was that the shape and deforming capability of a polymer impacts its passage through a pore, which in turn influences the glomerular filtration rate and hence plasma exposure [50]. In Figure 2-2 (a) a random coil polymer orients one chain end into the pore and reptates through, (b) a globular polymer has to deform in order to pass through, (c) a cyclic polymer also has to deform in order to pass through, (d) a linear polymer or a rod shaped nanoparticle has to orient along its vertical axis in order to

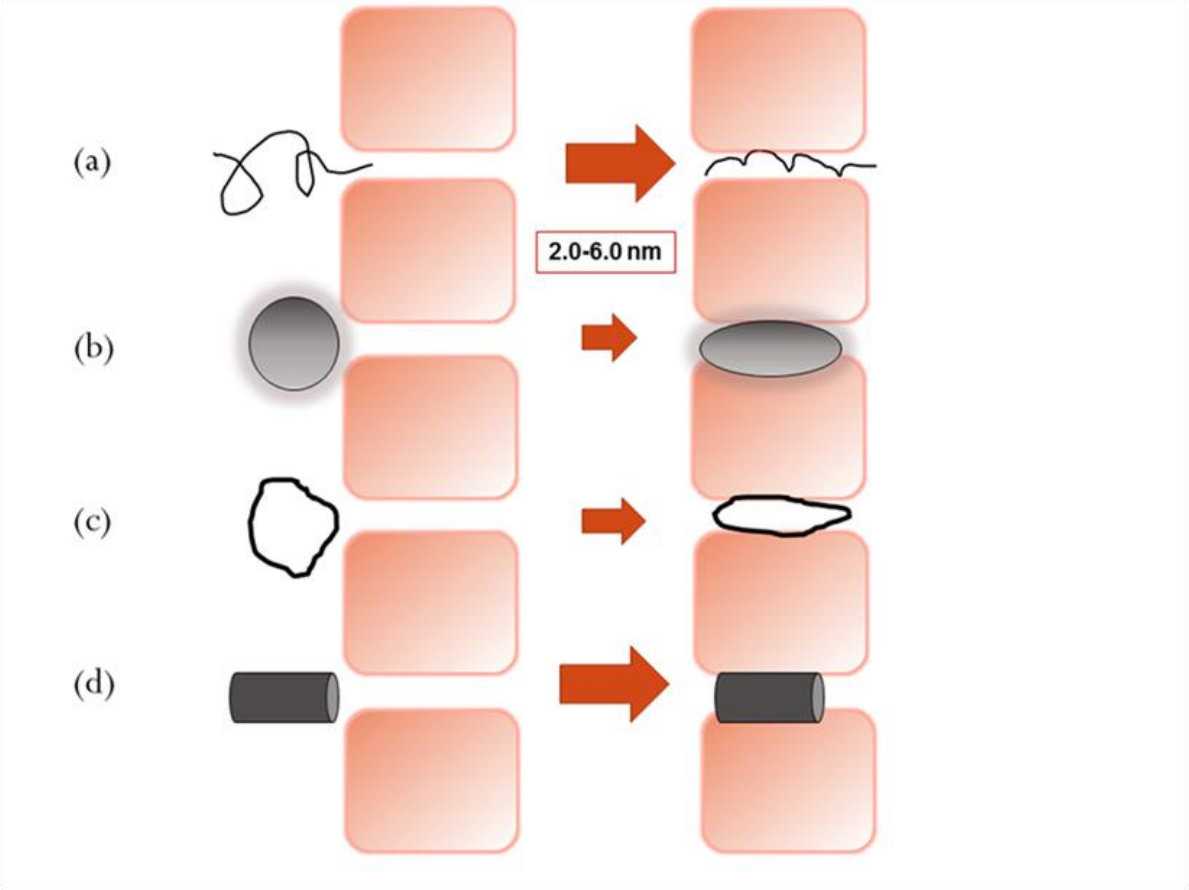

Figure 2-2. Polymers of varying architecture and equivalent hydrodynamic size passing through pores. Size of pores is comparable to size of polymers (2.0-6.0 nm). Size of arrow is indicative of ease of transport.

permeate [50]. It was also suggested that this difference in extravasation of polymers of varying architecture would not be observed if the pore size was an order of magnitude greater than that of the polymer size, which is the case for transendothelial openings of fenestrated capillaries in the tumor and liver fenestrations (40-80 nm) [50].

The review also data mined for plasma elimination half-lives of macromolecules of different molecular conformations as a function of molecular weight [50]. It was noted that the plasma elimination half-lives increased more drastically with increase in MW for the branched or globular polymers than polymers with a random coil conformation in solution [50]. Half-life increase was the slowest for linear polymers with an extended conformation [50]. It should be noted that these trends were generated out of experiments performed under inconsistent conditions of polymer characterization, animal models and detection systems.

Some studies have focused on the effect of polymer architecture on the extravasation of macromolecules across capillary endothelium [78-80]. Capillary endothelium may be continuous such as those found in skeletal and smooth muscle as well as subcutaneous and mucous membrane with fenestrations that do not allow passage of macromolecules > 2.0 nm in size [81]. It may be discontinuous such as those found in organs of the reticuloendothelial system such as liver, spleen, and bone marrow with fenestrations of up to 150 nm [81]. It may also be fenestrated such as in the kidney but with a continuous basement membrane [81].

Elsayed et al compared the extravasation of fluorescently-labeled linear PEG and branched PAMAM-NH_2 across a hamster cremaster muscle preparation (continuous endothelium) using intravital microscopy [79]. The PAMAM dendrimer extravasated

faster than the linear polymer of comparable MW [79]. This difference in extravasation rates were attributed to the difference in molecular conformation as well as surface charge of the two polymer types.

Research to evaluate the effect of molecular shape on the glomerular filtration rates of macromolecules suggests that at comparable sizes, the deforming capability of macromolecules determines the rate of glomerular filtration [78, 80]. The fractional clearances or sieving coefficients of linear polysaccharide dextran, spherical, highly compressible polysacharide ficoll and globular proteins were measured across the glomerular capillary wall [80]. The glomerular capillary wall consists of a fenestrated endothelial cell layer, a continuous basement membrane and an epithelial cell layer [80]. Linear extended conformation of dextran and the highly compressible conformation of ficoll aided their fast filtration across the glomerular capillaries [80]. The globular proteins filtered at a slower rate that was associated with their slower deforming rate through pores of vasculature [80]. A similar observation was made in a study where polysaccharides filtered at a faster rate through glomerular capillary walls than globular proteins [78]. Amongst the polysaccharides, the more extended linear structure of poly(ethylene oxide) showed a faster filtration rate than dextran [78].

2.3. Poly(amido amine) dendrimers

Poly(amido amine) or PAMAM dendrimers are a class of hyper-branched polymers originally developed by Tomalia in 1979 [11]. The ethylene diamine core and amido amine branching structure of the PAMAM lead alternatively to amine-terminated full generation or carboxyl-terminated half-generation dendrimers after each addition step

in the synthesis (Figure 2-3) [11]. For every increase in generation, the number of functional groups double, while the dendrimer diameter increases by about 1 nm [82]. Due to their controlled synthesis, these polymers have the unique advantage of having very low polydispersities. A full generation PAMAM dendrimer has primary amine groups on the surface (pKa =6.85) and tertiary amine groups within the core (pKa = 3.86) [82].

Due to their high degree of branching, PAMAM dendrimers have unique physical and structural properties distinct from linear polymers. PAMAM dendrimers undergo a conformational change with increasing generation [82]. They are more flexible at lower generations (0.0-3.0) [82]. With increase in surface branching, their surface density increases, leading to a dense exterior and a relatively hollow interior (G4.0-G6.0) [82]. This nano-container like conformation allows for entrapment of guest molecules, exploited for drug delivery applications (discussed in Section 2.5.1). As the surface branching increases, it leads to more crowding resulting in a more compact, globular shape for higher generation dendrimers (G7.0- G9.0) [82]. This change in conformation results in an intrinsic viscosity trend different from that of linear polymers. The intrinsic viscosity of PAMAM dendrimers goes through a maximum for certain dendrimer generations (around G6.0) and then decreases as the generation increases [83]. Higher generation dendrimers behave as rigid molecular spheres [83]. Conformational studies have suggested some backfolding of surface groups into the interior void [84]. The extent of backfolding depends on the solvent. In a good solvent, minimum backfolding of peripheral groups is observed [84]. The solubility of PAMAM dendrimers is higher than most linear polymers, attributed to spherical molecular conformation, resulting in the

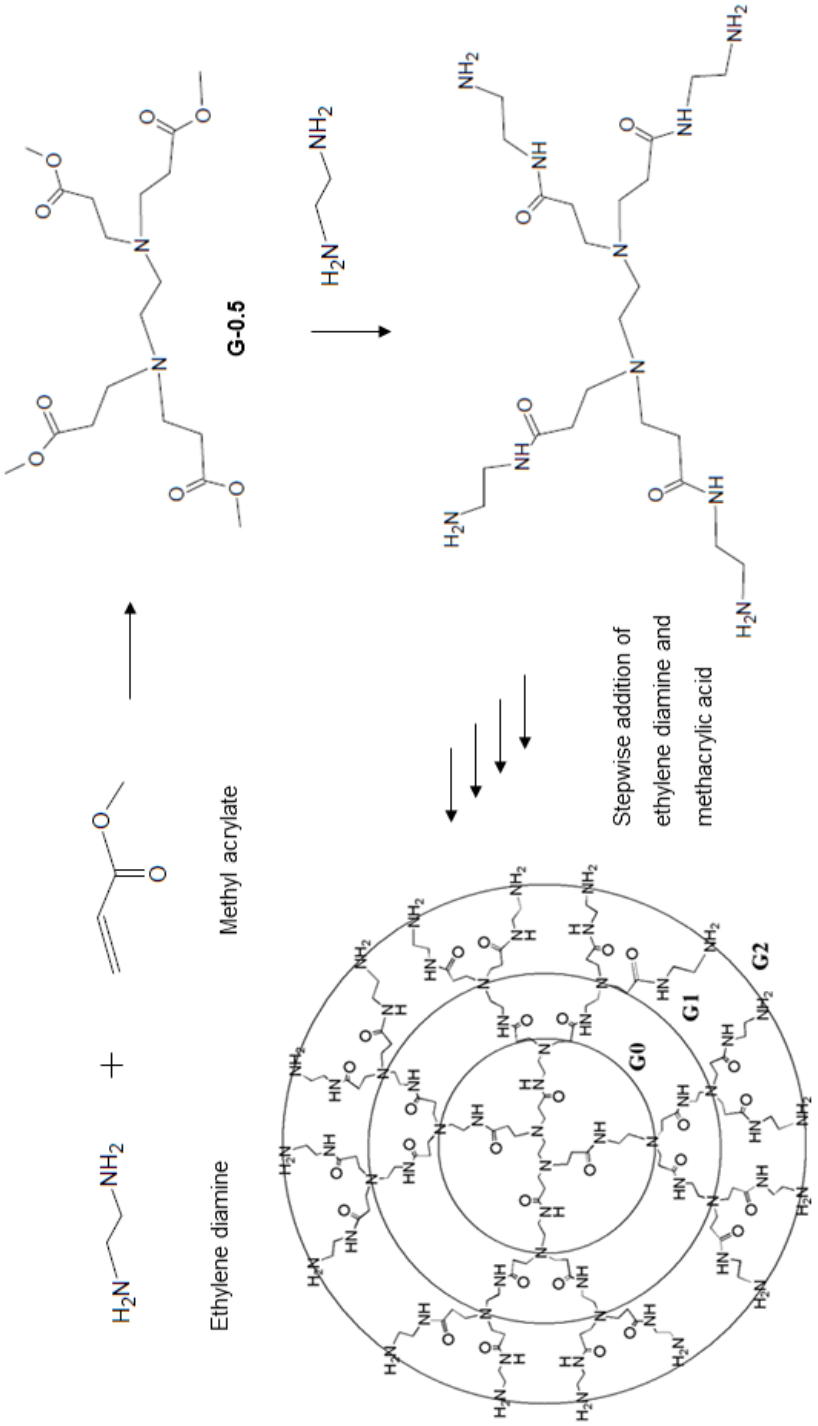

Figure 2-3. Synthesis of PAMAM dendrimers. Stepwise addition of ethylene diamine and methyl acrylate to alternatively form a half generation, carboxylic acid PAMAM and a full generation, amine-terminated PAMAM.

highest surface area to volume ratio [71]. PAMAM dendrimers also have better end-group reactivity due to their increased solubility and better accessibility [71]. The high density of surface functional groups on PAMAM dendrimers presents the opportunity of functionalizing these polymers with various drugs, nucleic acids and imaging system components [85-92]. It also presents a suitable scaffold to facilitate efficient multivalent interactions, critical for biological processes such as cellular recognition [93]. Their surface charge density has also been exploited for interactions with epithelial cell monolayers and tight junction modulation with implications for oral drug delivery (discussed in Section 2.5.2).

2.4. PAMAM dendrimer-drug complexes

The relatively hollow and hydrophobic interiors and dense surface exteriors of dendritic structures allow for host-guest encapsulation of drugs resulting in polymer-drug complexes with a pH sensitive drug release profile [95, 96]. Dendrimers like poly(glycerol), poly(ethyleneimine) (PEI), poly(propyleneimine) (PPI) and poly(amido amine) (PAMAM) have been explored to encapsulate anticancer drugs [95, 96]. Due to their commercial availability and ease of tailoring terminal groups, PAMAM dendrimers have been the most widely studied dendritic architectures in polymer-drug complexes.

Dendrimer-drug interactions can occur electrostatically on the surface and within the core, hydrophobically or hydrogen bonding within the core (Figure 2-4) [95, 96]. Primary factors that influence this interaction are: 1) dendrimer characteristics such as generation, hydrophobicity of core, pH, terminal groups, 2) ratio of dendrimer to drug

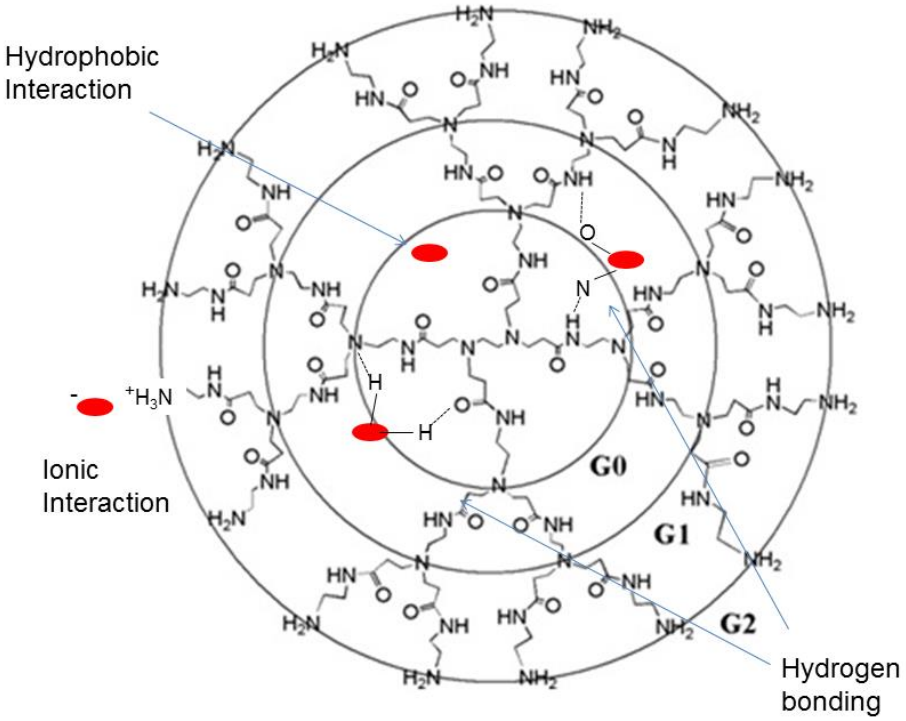

Figure 2-4. Possible mechanisms of dendrimer-drug interactions.

and 3) physicochemical properties of drugs like size, hydrophobicity, nature of functional groups, and pKa.

Reports indicate that PAMAM encapsulation and solubilization potential increases with increase in generation as seen for hydrophobes like nifedipine, indomethacin and NSAIDS like ibuprofen [97, 98]. Majority of the reports evaluate generation 4.0, due to its ideal molecular conformation of a hollow core and dense surface exterior, which allows for encapsulation as well as multiple surface interaction sites. Dendrimers smaller than G3.0 have an open conformation, that will allow guest molecules to easily escape while higher generation dendrimers, G7.0 onwards, become increasingly rigid and have biocompatibility issues with high surface charge density [82].

Along with PAMAM size, surface terminal groups largely influence the complexation of drugs. For drugs containing acidic groups like indomethacin, and ibuprofen, the solubilization potential of amine-terminated dendrimers at pH above the pKa of the drug is much higher than that of neutral or anionic dendrimers [98, 99]. This is due to the electrostatic interaction of the oppositely charged drug and dendrimer. The opposite is true for drugs containing basic functional groups like nifedipine at pH below pKa, where they electrostatically interact with ionic dendrimers on the surface [97, 99].

The pH of the formulating solution influences protonation of tertiary nitrogens in the interior of the PAMAM dendrimer. At pH below pKa of tertiary nitrogens (pKa 3.0-6.0), when nitrogens are protonated, the PAMAM core becomes less hydrophobic, decreasing its drug encapsulation and consequently solubilization. Protonation of amine terminal groups and deprotonation of carboxylic acid surface groups at certain pH values increases surface electrostatic interaction, which aids in drug solubilization and

complexation. One such example is ibuprofen complexed with PAMAM G4.0-NH_2 [100]. It showed a pH-dependent enhancement in solubility with the solubilization potential of the dendrimer being highest at pH 10.5, when both primary surface amines of dendrimer and carboxylic acid group of ibuprofen were ionized [100].

The contributions of dendrimer surface ionic complexation with drugs versus encapsulation within their interior have been assessed. Evaluation was done using nuclear magnetic resonance and two-dimensional Overhausner effect spectroscopy (2D-NOESY) [101]. It was observed that electrostatic interaction on the surface of PAMAM with oppositely charged drug contributed more to solubility than internal encapsulation at the pH value where surface groups and cargo were ionized with opposite charge [102]. It was also observed that positively charged drugs locate only on the surface of negatively charged dendrimers, while negatively-charged drugs were seen to localize both on the surface and interior cavities [99].

Complexation of drugs with dendrimers has the potential to control drug release and improve bioavailability (discussed in Section 2.5.4 and 2.5.5).

2.5. PAMAM dendrimers in oral delivery

PAMAM dendrimers of certain generations and surface charge can permeate the epithelial barrier of the gut, suggesting their potential as oral drug carriers [103-124]. It is important to evaluate the toxicity of PAMAM dendrimers on epithelial barriers to ensure that the permeation across these barriers does not irreversibly damage the epithelial barrier.

2.5.1. Toxicity on Caco-2 cells

Caco-2 cells are human colorectal carcinoma cells that develop a cell polarity when grown in monolayers and allow the study of transepithelial transport [125]. It is known that PAMAM dendrimers demonstrate a generation-, surface charge-, concentration- and incubation time - dependent cytotoxicity profile [126]. Initial studies suggested that the rank order of cytotoxicity of PAMAM dendrimers is hydroxyl-terminated < carboxyl-terminated < amine-terminated systems [69]. As per the lactate dehydrogenase (LDH) assay which assessed membrane damage on Caco-2 cells, carboxyl-terminated dendrimers of generations 3.5 and 4.5 (G3.5-COOH and G4.5-COOH) are toxic only at a higher donor concentration of 10.0 mM compared to amine-terminated dendrimers of generations 3.0 and 4.0 which are toxic at 1.0 mM (G3.0-NH_2 and G4.0-NH_2) [105, 107]. The LDH assay revealed plasma membrane damage of Caco-2 cells by PAMAM dendrimers as a function of generation number, surface charge, incubation time and concentration.

Transmission electron microscopy (TEM) analysis further showed a concentration-, generation- and surface charge-dependent effect of PAMAM dendrimers on Caco-2 microvilli morphology [115]. Cells treated with a concentration of 0.1 mM or higher G4.0-NH_2 showed membrane disruption and loss of Caco-2 microvilli while those treated with G3.5-COOH at the same concentration were unaffected [115]. The extent of disruption and loss of microvilli increased with G4.0-NH_2 concentration. At lower concentration of 0.01 mM, dendrimers did not influence microvilli morphology as per TEM images. Higher generation cationic dendrimers showed increased intestinal membrane damage compared to lower generation ones [115].

In summary, *in vitro* toxicity studies on PAMAM dendrimers revealed that cationic systems are nontoxic on Caco-2 cells at lower concentrations of 0.01 mM as per LDH assay and microscopic evaluation. Anionic PAMAM dendrimers are tolerated to a higher extent than cationic dendrimers making it possible to give higher doses of the carboxylic acid-terminated systems. In the range of dendrimers evaluated from generations 0.0 to 4.0 with varying surface functional groups, it was observed that there is a workable nontoxic window for PAMAM dendrimers to be used as carriers for oral drug delivery. These studies set the stage for the *in vitro* evaluation of transepithelial transport and cellular uptake of PAMAM dendrimers across epithelial barriers.

2.5.2. Biocompatibility and biodistribution

One of the first reports of dendrimer biocompatibility *in vivo* was a preliminary toxicity and immunological evaluation of amine-terminated PAMAM dendrimers G3.0, G5.0 and G7.0 in male swiss-webster mice by intravenous administration [127]. Acute (7 days), sub-chronic (30 days) and chronic toxicity (6 months) was evaluated at intravenous dendrimer doses of 5×10^{-6} mmol/kg, 5×10^{-5} mmol/kg, and 5×10^{-4} mmol/kg. For chronic toxicity, a dose of 5×10^{-4} mmol/kg was administered intravenously for PAMAM G3.0-NH_2 and G5.0-NH_2, and 5×10^{-5} mmol/kg for PAMAM G7.0-NH_2 [127]. PAMAM G7.0-NH_2 was administered at a lower dose for the chronic toxicity study because acute toxicity was observed for PAMAM G7.0-NH_2 at the higher dose of 5×10^{-4} mmol/kg [127]. Animals were monitored for routine behavioral abnormalities and changes in body weight. Upon sacrifice, certain tissues (liver and spleen) were observed for macroscopic and microscopic abnormalities by hematoxylin

and eosin staining. Signs of toxicity were observed only for PAMAM G7.0-NH_2 at the highest dose tested, with 1 out of 5 animal deaths 24 hours after injection [127]. For immunogenicity testing, New Zealand rabbits were subcutaneously injected with PAMAM G3.0-NH_2, G5-NH_2, or G7-NH_2 at two doses of 5 X 10^{-5} mmol with 3 week intervals. The immunogenicity of the PAMAM dendrimers was studied using two different methods: immunoprecipitation and an Ouchterlony double diffusion assay. Ouchterlony double diffusion assay is an agar immunodiffusion assay for detecting extractable nuclear antigens. With blood samples collected at 10 days after injection, no immunological reactions were seen at doses tested. This study was one of the first reports of the *in vivo* evaluation of PAMAM dendrimers. It was a preliminary evaluation of toxicity of cationic PAMAM dendrimers at a fixed dose and showed that PAMAM toxicity increased with increase in generation and surface charge density of amine groups [127]. PAMAMs of G5.0 or below were well tolerated up to doses $5x10^{-4}$ mmol/Kg but higher generation PAMAMs showed biological complications at the same dose. This toxicity study of intravenously administered PAMAM throws light on possible biological complications that may occur upon systemic absorption of orally dosed constructs.

In another study the biocompatibility of cationic PAMAM dendrimers G1.0-G4.0 and anionic PAMAM dendrimers G1.5-G5.5 was systematically investigated to evaluate the effect of dendrimer generation and surface functionality on biological properties *in vitro* [128]. PAMAM dendrimers were incubated with fresh rat blood cells in phosphate buffer saline (PBS) with shaking at 37^0C for 1 hour. The hemoglobin released was spectrophotometrically determined to measure extent of hemolysis. Amine terminated PAMAM dendrimers displayed concentration and generation-dependent hemolysis.

Rounding and clumping of red blood cells was observed in the first hour even at non-hemolytic concentrations (10 µg/ml) [128]. All cationic PAMAM dendrimers except G1.0 were hemolytic above 1.0 mg/mL. Anionic dendrimers caused no morphological changes to RBCs upto 2.0 mg/mL as per scanning electron microscopy [128]. These results correlated well with *in vitro* cytotoxicity studies in Caco-2 cells, in that anionic PAMAM dendrimers were more biocompatible than their cationic counterparts and that the cationic dendrimers showed reduced biocompatibility at higher generations.

Recent *in vivo* studies have focused on establishing the maximum tolerated doses for PAMAM dendrimers of different generations and surface charge, administered orally and intravenously to CD-1 mice [129]. PAMAMs of two different generations 4.0 and 7.0 and three different surface functionalities: amine, carboxylic acid and hydroxyl terminated were tested. Acute toxicity (10 days) was inferred by monitoring routine behavioral changes, body weight changes, and upon animal sacrifice, changes in organ weight, macroscopic tissue abnormalities, blood chemistry and blood picture. It was observed that when intravenously administered, amine terminated dendrimers (both G4.0-NH_2 and G7.0-NH_2) were safe only at doses less than 10 mg/kg [129]. This finding is in agreement with a previous study by Roberts et al. summarized above, where biological complications were observed for G7.0-NH2 dendrimers, dosed at 5.0 x 10^{-4} mmol/Kg which translates to about 58.3 mg/kg of the dendrimer [129]. In the same study, lower generation dendrimers G3.0-NH_2 and G5.0-NH_2, dosed at 5x10^4 mmol/Kg (about 3.4 and 14.4 mg/Kg respectively) were nontoxic [129]. In contrast carboxyl- (G3.5-COOH and G6.5-COOH) and hydroxyl- (G4.0-OH and G7.0-OH) terminated dendrimers were tolerated intravenously at 50-fold or higher doses. Blood analysis of mice treated

with amine terminated dendrimers at 2 weeks showed decreased levels of fibrinogen, platelets and high levels of fibrin degradation products (FDP) which is known to result in intravascular coagulation and hemorrhage [129].

Orally administered dendrimers demonstrated the same trend where the higher generation positively charged systems caused more toxicity than negatively charged ones [130]. Orally administered G7.0-NH2 and G7.0-OH showed signs of hemobilia and splenomegaly at doses above MTD. The oral MTD for these dendrimers ranged from 30mg/kg to 200mg/kg. Anionic G6.5 or smaller generation carboxyl-, amine- or hydroxyl-terminated dendrimers (G3.5-COOH, G4-NH2, G4-OH) on the other hand were tolerated at doses of up to 500mg/kg [130].

Overall these studies revealed that PAMAM dendrimers showed similar toxicity trends when administered orally and intravenously, with the higher generation cationic dendrimers being more toxic than their lower generation counterparts and the anionic dendrimers being less toxic than the cationic ones. PAMAM dendrimers were tolerated at 10-fold higher doses when administered orally as compared to intravenously. This could be due to a rate limiting absorption process that reduces exposure of the dendrimers to blood. However, detailed oral histological evaluation of the gastrointestinal epithelium needs to be carried out to understand possible tissue toxicity due to PAMAM exposure *in vivo*.

An attempt to understand histological damage to intestinal epithelial barrier by PAMAM was carried out *in situ.* Lin et al., evaluated the intestinal membrane damage in SD rats of amine-terminated PAMAMs generations 0.0-3.0 (0.05 to 0.5% w/v), when evaluating *in situ* absorption of hydrophilic molecules in the presence of PAMAM

dendrimers [131]. PAMAM dendrimers were incubated for 4 hours in the canulated intestinal loop and the amounts of LDH and protein released from the small intestinal membranes were measured, which was an indication of plasma membrane damage. At the highest concentration tested (0.5% w/v), PAMAM G2.0-NH_2 showed signs of plasma membrane damage [131]. However, the extent of toxicity was less than that of 3% (v/v) Triton X-100, a commonly used intestinal absorption enhancer, used as a positive control. While co-delivery of PAMAM G2.0-NH_2 enhanced the intestinal absorption of 5(6)-Carboxyfluorescein (CF), a water-soluble dye, pretreatment with G2.0-NH_2 (0.5%,w/v), did not alter absorption of the dye. This suggested that the absorption-enhancing effect of G2.0-NH_2 is reversible and might not cause irreversible membrane damage in the rat small intestine. Data correlate with cytotoxicity and *in vivo* data of PAMAM-NH_2 dendrimers, with the toxicity increasing as a function of generation and concentration. At the highest dose employed of 0.5% w/v of PAMAM G2.0, signs of histological toxicity observed were found to be reversible.

Studies on the *in vivo* biodistribution of ^{125}I-labelled, intravenously administered poly(amido amine) dendrimers in rats have shown that anionic dendrimers circulate longer in the blood than cationic dendrimers [128]. In 1 hour, only 0.1-1.0 % of dose of PAMAM-NH2 dendrimers was recovered in the blood while 15-40 % of the dose of PAMAM-COOH of various generations was recovered. Both types of dendrimers showed high liver accumulation, with the cationic dendrimers showing slightly higher liver concentration (60-90 %) than the anionic dendrimers (25-70 %) [128].

2.5.3. Transepithelial transport and intracellular fate

An important barrier to oral absorption of PAMAM dendrimers is limited transepithelial transport. Several methods are available to study transport of compounds across the epithelial barrier of the gut [125]. These include, but are not limited to, isolated intestinal tissue techniques, cell culture monolayer systems such as Caco-2 cells, and *in situ* perfusion models. The effect of PAMAM generation, surface group, concentration and incubation time with cells on transport across epithelial barriers has been extensively studied on epithelial cell monolayers and isolated intestinal tissue *in vitro* [103-109, 111-117, 119]. In an initial study, the isolated intestinal tissue model using the everted sac technique was employed to assess the transepithelial transport of PAMAM dendrimers [16]. This technique, along with the Ussing chamber technique involving isolated intestinal tissue, provides mechanistic insights and additionally allows the comparison of differences in the segmental transport throughout different regions of the GIT [125]. The everted sac setup involves everting an intestinal segment, 2-4 cm long over a glass rod, 3 mm in diameter. The setup is then put into culture medium containing desired concentration of substance, whose permeability is being evaluated. The flux of the compound is evaluated from the outside mucosal side to the inside serosal sac [132]. The model is a simple, quick, reproducible and inexpensive technique. However, the volume inside the sac is small, because of which physiologically relevant sink conditions cannot be maintained. In an Ussing chamber, a small segment of the intestine is clamped between two chambers: the serosal and the mucosal side [132]. It is also possible to connect electrodes in the two compartments to measure changes in transepthelial electrical resistance (TEER) and therefore tight junction modulation. A small amount of

sample is needed to evaluate absorption. However, the preparation of the intestinal epithelial layer can be complicated. Incomplete removal of the serosal muscle layer can result in false measurements of transport and puncture of the segment can drastically decrease TEER [132]. These *ex vivo* techniques may be useful to determine the segmental transport of compounds at different regions of the intestine. It is also useful to evaluate the site of action of effect of penetration enhancers [125]. Maintaining tissue viability is the most critical step of evaluating transport using isolated tissue.

^{125}I-labelled PAMAM dendrimers were first evaluated for their uptake and transport *in vitro* using the everted intestinal sac system in rat [103]. While amine-terminated cationic PAMAM dendrimers showed greater tissue uptake than transport across the isolated everted rat intestinal sac, carboxylic acid-terminated dendrimers showed greater serosal transfer rates than their tissue uptake. Higher generation anionic G5.5 had a 2-fold greater tissue uptake than that of lower generation anionic G2.5 and G3.5 dendrimers. The serosal transport rate of higher generation anionic dendrimers was less than that of lower generation dendrimers. PAMAM G5.5 was recovered on the serosal side (60-70%), while 80-85 % of G2.5 and G3.5 was recovered [103]. This study demonstrated that PAMAM generation and surface charge influence their transepithelial transport as well as tissue uptake and that there is an optimum range of generation and surface charge to use PAMAM dendrimers as drug carriers for oral delivery.

A variety of factors before and after the epithelial barrier influence the transport of compounds across the isolated intestinal tissues including everted sacs. To avoid the influence of pre- and post-epithelial factors, and gain a detailed understanding of the influence of physicochemical properties of dendrimers on the extent and mechanism of

transepithelial transport, a series of studies were conducted to examine the effect of the physicochemical and structural properties of PAMAMs of various generations and surface charges on their transport across epithelial cell culture monolayers [103-109, 111-117, 119]. Amongst cultured cells, Madin-Darby canine kidney (MDCK) cells, Caco-2 monolayers, and IPEC-J2 monolayers have been used to assess the transepithelial transport of PAMAM dendrimers. When cultured as monolayers, these cells undergo differentiation, maintain a cell polarity and develop a transepithelial resistance [125]. The cell line polarity facilitates the study of directional transport from apical to basolateral side. Measuring transepithelial resistance allows the monitoring of tight junction integrity in cultured monolayer cells. Both cellular uptake and transepithelial transport can be studied. Cell monolayers can be used to evaluate transport mechanism by inhibiting certain cellular uptake pathways and by monitoring tight junction modulation. Cultured intestinal cell monolayers are useful in rank ordering permeabilities of compounds of the same class. A study attempting to correlate *in vitro* results in Caco-2 cell monolayers to *in vivo* data has demonstrated that compounds with apparent permeability coefficients (P_{app}) above 1×10^{-6} cm/sec are likely to be well absorbed [133]. However, cultured monolayers such as the Caco-2 cell monolayers widely used to assess PAMAM intestinal transport lack mucous secretion and therefore do not present a mucosal barrier to transport [125]. Caco-2 cells, which are derived from the colon also lack the cellular heterogeneity found in the intestinal mucosa like presence of payer's patches and more closely represent the colonic than the small intestinal epithelium. Similar to isolated intestinal models, the cultured intestinal cells do not account for other gastrointestinal

physiological variables like transit time, motility, hepatic first pass clearance, hydrolytic and enzymatic degradation, which contribute to reduced oral bioavailability [125].

The influence of size, charge, incubation time, and concentration of amine-terminated PAMAM dendrimers G0.0 to G4.0 across Caco-2 cell monolayers was first studied by El-Sayed *et al.* [105]. In this study, it was observed that the basolateral to apical (BA) permeability of each dendrimer was generally higher than the corresponding apical to basolateral (AB) permeability which was attributed to the difference in tight junction characteristics at the apical and basolateral sides. TEER measurements and the permeability of a known paracellular permeability marker, ^{14}C-mannitol showed that PAMAM dendrimers modulated tight junctions. Tight junction modulation was a function of PAMAM generation, nature of surface functional groups, surface charge density and concentration [105]. Detailed studies on the influence of surface charge of PAMAM dendrimers on transepithelial transport of ^{14}C-mannitol across Caco-2 cells and their cytotoxicity showed that neutral PAMAM dendrimers with hydroxyl surface terminal groups (PAMAM–OH) did not significantly influence TEER or ^{14}C-mannitol permeability across Caco-2 monolayers [107]. Anionic, carboxylic acid-terminated PAMAMs (PAMAM–COOH) had a generation-dependent effect on TEER and ^{14}C-mannitol permeability. Owing to a low surface charge density, smaller generation G-0.5, G0.5 and G1.5 did not cause decrease in TEER values or increase in ^{14}C-mannitol permeability. Due to an increase in surface charge density, G2.5 and G3.5 caused a significant decline in TEER compared to control values and a 6-fold increase in ^{14}C-mannitol permeability and were not cytotoxic to cells at concentrations tested as per the lactate dehydrogenase (LDH) assay indicating no damage to plasma membrane [107].

Amine-terminated dendrimers also decreased TEER and increased mannitol paracellular transport by modulating tight junctions of Caco-2 cell monolayers.

In a subsequent study it was demonstrated that in addition to enhancing paracellular transport, PAMAM dendrimers are also translocated across the epithelial barrier of Caco-2 cells by endocytosis mechanisms [106]. The permeability of G2.0–NH_2 was significantly lower at 4^0C than at 37^0C, suggesting active cellular uptake and endocytic mechansims of transport. It was observed that the BA permeability of G2.0–NH_2 as well as ^{14}C-paclitaxel, a known P-gp substrate were higher than that of AB permeability, suggesting a functioning P-gp efflux pump in the Caco-2 cell monolayers being used [106]. It was also noted that there was no significant difference in AB and BA permeability of ^{14}C-paclitaxel in the presence of G2.0-NH_2. The AB and BA permeability of G2.0–NH_2 did not change in the presence of paclitaxel, which suggests G2.0-NH_2 is not competing with paclitaxel for the P-gp efflux [106].

Since these initial studies demonstrated that PAMAM dendrimers are transported by both para- and transcellular routes, more detailed studies on the mechanism of transport of PAMAM dendrimers have been carried out which are summarized below:

^{14}C-Mannitol permeability was found to significantly increase in the presence of both cationic (G2.0-NH_2 and G4.0-NH_2) and anionic (G1.5-COOH and G3.5-COOH) PAMAM dendrimers indicating the opening of tight junctions [112]. It did not increase for the hydroxyl-terminated PAMAM G2.0-OH. TEER values also decreased for cells incubated with charged PAMAM dendrimers. Amine-terminated PAMAM of generation 2.0 showed the greatest decline in TEER suggesting that it caused the highest tight junction modulation amongst dendrimers tested. An interesting finding was that TEER

modulation of surface modified-G4.0-NH_2 was reversible and TEER values came back to 90% of original within 24 hours. A $1/8^{th}$ surface coverage with FITC masked the surface positive charge to some extent and possibly also altered the PAMAM conformation thus altering its tight junction modulation capability. Occludin is one of the major proteins of the tight junction protein complex, responsible for fusion of adjacent plasma membranes. Increased accumulation of occludin at the cellular junctions indicates tight junction opening. Immunofluorescence microscopy revealed increased occluding accumulation in Caco-cells treated with charged PAMAM dendrimers [112]. The same trend was seen for Actin, a cytoskeletal protein responsible for cellular integrity. Actin disruption was seen for cells treated with PAMAM dendrimers [112]. Immunofluorescence studies qualitatively demonstrated that PAMAM dendrimers modulate tight junctions. These studies further confirmed that PAMAM dendrimers modulated tight junction proteins occludin and actin and that increased permeability of dendrimers is partly due to opening of tight junctions, which can be reversible depending on the concentration, generation and surface charge of the dendrimers.

The endocytic pathway is known to be an important route for intracellular uptake of macromolecules [115]. Confocoal microscopy of FITC-labeled PAMAM dendrimers revealed that both cationic and anionic PAMAM dendrimers were internalized within 20 min, and localized within coated invaginated pits of the plasma membrane, early endosomes and lysosomes [115]. Clathrin-mediated endocytosis was found to be the primary mechanism of cellular uptake for the PAMAMs. Over time, the dendrimers were seen to concentrate within lysosomes.

The detailed mechanistic investigation of Caco-2 uptake of G4.0-NH_2 by endocytosis was carried out [119]. The endocytosis inhibitors used were 1) brefeldin A and 2) colchicine to inhibit trafficking via formation of microtubules, 3) filipin to inhibit claveolin-mediated endocytosis and 4) sucrose to inhibit clathrin mediated endocytosis. Brefeldin A and colchicine reduced G4.0-NH_2 uptake 2-fold and 3-fold, respectively [119]. Both filipin and sucrose reduced uptake 3-fold [119]. Along with cellular uptake, apparent permeabilities of G4.0-NH2 were also reduced in presence of these inhibitors, suggesting that cellular uptake contributed to increased transepithelial transport (Figure 2-5). These findings support previous results that in addition to paracellular transport, cationic dendrimers are also endocytosed.

While the above studies were conducted on amine terminated systems, given that surface charge may influence the pathway of cellular uptake, the mechanisms of PAMAM G3.5-COOH dendrimer cellular uptake, intracellular trafficking, transepithelial transport and tight junction modulation in Caco-2 cell monolayers was evaluated [123]. G3.5 PAMAM dendrimer showed reduction in cellular uptake in the presence of inhibitors for clathrin, caveolin and a combination of the two that is dynamin-mediated endocytosis, suggesting the involvement of both clathrin- and caveolin-mediated endocytosis pathways in cellular uptake [123]. The greatest reduction in uptake of PAMAM G3.5 was shown in the presence of dynasore, an inhibitor for dynamin-mediated endocytosis. Upon cellular uptake, PAMAM dendrimers (tracked by labeling them with Oregon green dye) were seen to localize within early endosomes and lysosome [123]. As expected, cells treated with PAMAM G3.5 showed increased occludin, indicating tight junction opening. Interestingly, when dynamin-mediated endocytosis was

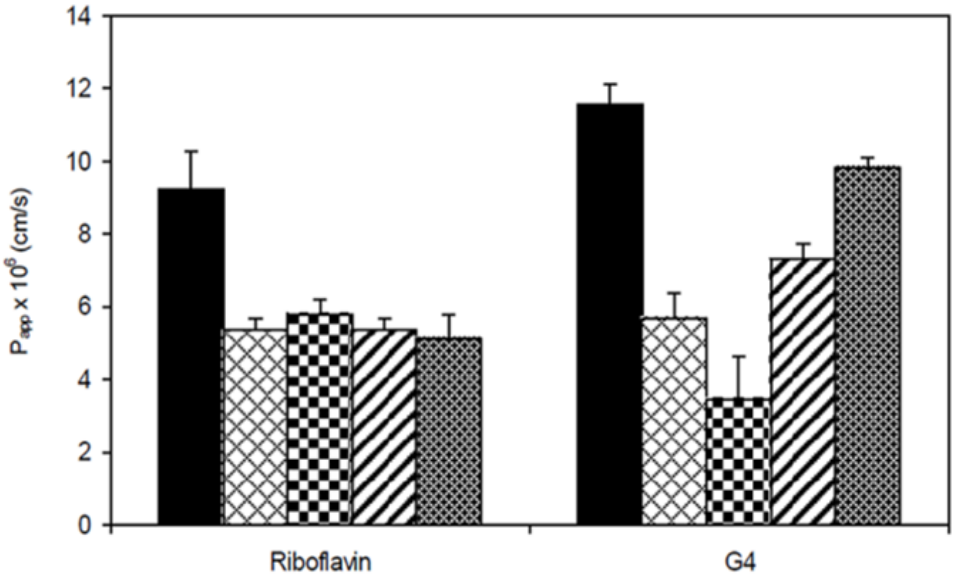

Figure 2-5. Reduced apparent permeability (P_{app} x 10^6 cm/s) of Riboflavin (500 nM) and G4.0-NH_2 (1 μM) across Caco-2 cell monolayers in the presence of endocytosis inhibitors. Bars from left to right indicate: 1-5 μM brefeldin A; 10 μM colchicine; 1 μg/ml filipin; 200 mM sucrose. Results are reported as mean ± SD (n = 3). **, $p < 0.01$: ***, $p < 0.001$. With permission from Ref [119]. Copyright 2008 American Chemical Society.

inhibited, tight junction modulation also decreased, seen by occludin staining (Figure 2-6). This suggests that dendrimers self-catalyze their paracellular transport by being taken up intracellularly and acting on intracellular proteins [123]. Monitoring changes in TEER with and without inhibition of cellular uptake, when cells are incubated with PAMAM dendrimers will confirm the need for dendrimer internalization to modulate tight junctions. More studies are needed to evaluate whether such phenomenon is indeed responsible for tight junction opening of other dendrimers with a different surface charge or generation, and to further delineate the contributions of extracellular vs intracellular factors in opening of the tight junctions in the presence of dendrimers.

More recent reports have focused on modeling the porosity of epithelial layers as a function of dendrimer generation, surface charge, concentration and incubation time [122]. Simulations show that the increase in concentration, incubation time and generation number (surface charge density) of cationic G0.0-NH_2 to G2.0-NH_2 and anionic G2.5-COOH to G3.5-COOH cause an increase in porosity of epithelial cell monolayers. These findings suggest that the transepithelial transport of PAMAM is due to disorganization of cell membranes along with experimentally established tight junction modulation and endocytic uptake [122].

Together, these studies show that PAMAM dendrimers are transported across Caco-2 cell monolayers by a combination of the paracellular pathway and an energy-dependent process, such as endocytosis (Figure 2-7). These studies have set the stage for evaluation of PAMAM dendrimers as drug carriers across epithelial barriers.

Researchers have demonstrated that by engineering the surface groups of PAMAM dendrimers, it is possible to alter cytotoxicity, permeability and cellular uptake

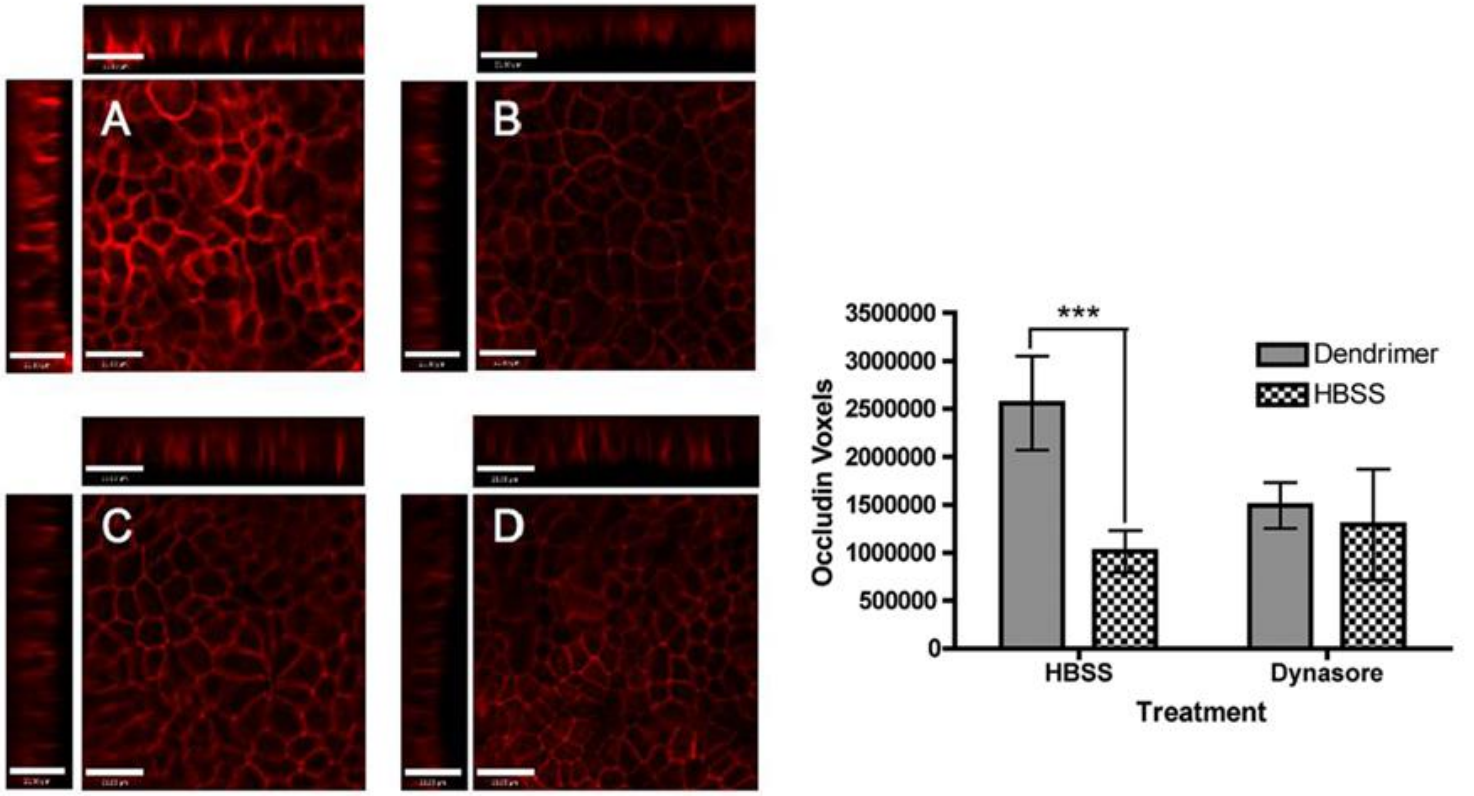

Figure 2-6. Transpeithelial transport and cellular uptake mechanism of PAMAM G3.5-COOH (A-D). Occludin staining in the presence and absence of Oregon green labeled G3.5-COOH dendrimers in Caco-2 cells treated with HBSS or Dynasore. A. G3.5-COOH / HBSS, B. HBSS only C. G3.5-COOH / Dynasore and D. Dynasore only. Main panels illustrate the xy plane; horizontal bars illustrate the xz plane; vertical bars illustrate the yz plane. Scale bars equal 21 μm. E. Quantification of Occludin staining. Results are reported as mean +/- standard deviation with n=4. (***) indicates $p<0.001$. From Ref [123].

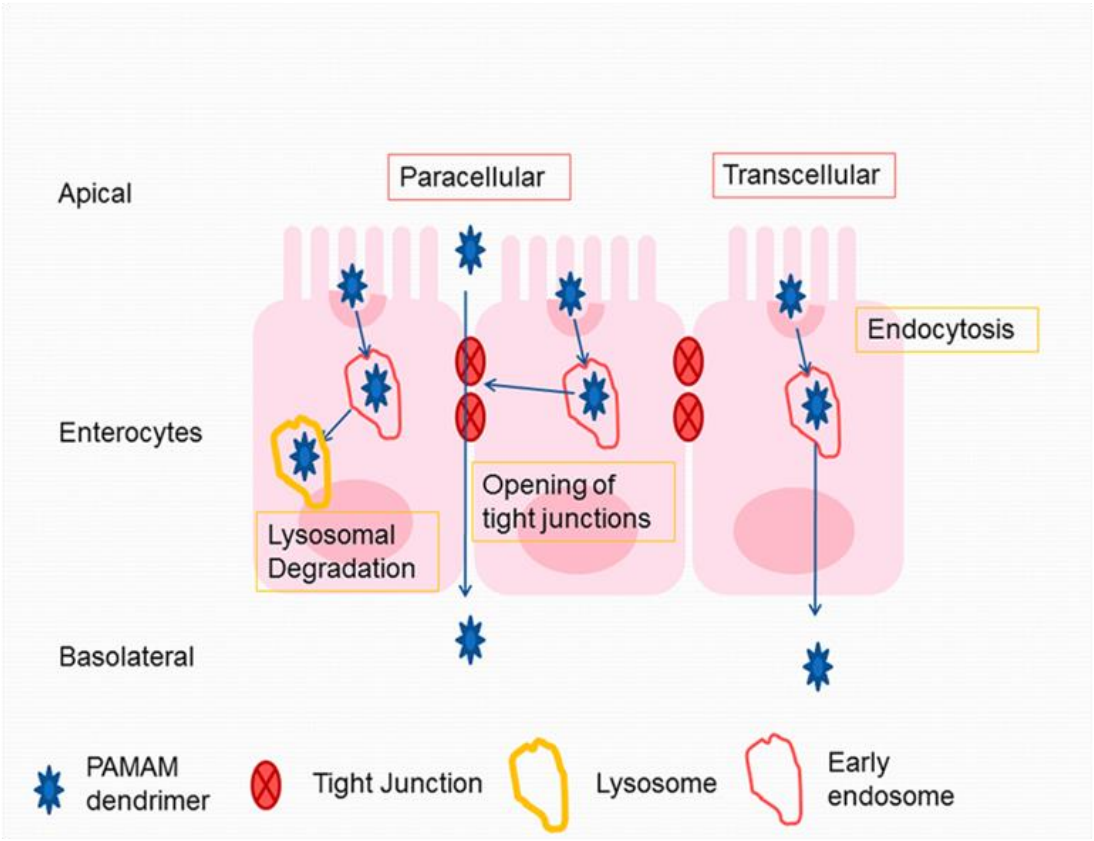

Figure 2-7. Transepithelial transport mechanisms of PAMAM dendrimers. With permission from [94].

[108, 109, 113, 121]. It was shown that surface modification by uncharged groups (PEG, lauroyl, acetyl) reduced toxicity by charge masking of the primary amine groups [108, 109, 113, 121]. Hydrophobic surface modifiers such as the acetyl groups and lauric acid increased permeability while hydrophilic polymers such as PEG reduced permeability [108, 109, 113, 121]. Thus, surface modification provides a tool to reduce toxicity and influence permeability of PAMAM dendrimers across epithelial barriers.

2.5.4. Transepithelial transport of PAMAM – drug complexes and conjugates

Drugs can be attached to PAMAM dendrimers by covalent conjugation, complexed by surface ionic interactions or encapsulated by van der waals and hydrophobic interactions. Although, there has been extensive research on dendrimer-based drug carriers for a variety of routes of delivery, very few studies have demonstrated transepithelial transport of such conjugates or complexes.

Earlier studies by D'Emanuele and coworkers used PAMAM G3.0-NH_2 or lauroyl-modified PAMAM G3.0-NH_2 conjugated to propranolol in varying stoichiometric ratios of the drug [111]. Propranolol was conjugated to PAMAM G3.0 via a chloroacetyl spacer. PAMAM G3.0 was chosen because it has been shown to effectively permeate Caco-2 cell monolayers and was not a P-gp substrate [106]. P-glycoprotein efflux pump reduces the absorption of orally administered drugs such as propranolol and decreases bioavailability. Lauroyl modification of PAMAM G3.0-NH_2 is known to increase its permeability across Caco-2 monolayers [108]. The amine-terminated PAMAM dendrimer was cytotoxic to Caco-2 cells and cytotoxicity decreased

with an increase in the amount of propranolol and lauric acid conjugated, attributed to the shielding of positive surface charge of primary amine groups on PAMAM G3.0-NH_2. Co-administration of P-gp inhibitors such as cyclosporine A can increase bioavailability by blocking the P-gp efflux. As expected, the P_{app} of free propranolol was increased in the presence of the P-gp inhibitor cyclosporin A but not in the presence of PAMAM G3.0-NH_2 conjugated propranolol, suggesting that the conjugate was not a substrate of the P-gp efflux pump. The enhancement of propranolol transepithelial transport was independent of attachment ratio of drug to dendrimer over the range studied (2–6 moles of propranolol per mole of G3.0-NH_2). The maximum enhancement (3.5 fold) was achieved when 6 lauroyl chains were attached to PAMAM G3.0-NH_2 containing 2 propranolol moieties [111]. The conjugate permeability decreased at 4^0C as compared to 37^0C, suggestive of active endocytic uptake of the conjugate in Caco-2 cells followed by transcellular transport [111]. TEER values suggested that paracellular route did not contribute to transport of the lauroyl-modified conjugate. Overall this study showed that conjugation of propranolol with dendrimers increased transepithelial transport of the drug by increasing drug solubility and circumvention of the P-gp efflux pump [111]. However, detailed evaluation of the stability of the conjugated system in presence of Caco-2 cell culture medium and GI conditions warranted further investigation in order to understand stability of the conjugate.

A conjugate of Naproxen, a poorly water-soluble drug, and PAMAM G0.0 was also evaluated as an oral prodrug. The drug was linked to the dendrimers directly by an amide bond or by ester bond or using spacers-l-lactic acid and diethylene glycol [134]. The type of linkage between the dendrimer and drug affected the release characteristics

of the drug from the delivery system. While the direct amide linkage was stable under the conditions of plasma and liver homogenate tested, the ester linkage could be tailored to be stable in plasma and release the drug at the desired site of action in the liver [114, 134]. The conjugates were hydrolytically stable under different pH conditions ranging from gastric to intestinal and colonic pH. However, conjugates were susceptible to enzymatic hydrolysis. Efficient drug release was achieved for both ester conjugates in plasma with the lactic ester conjugate (G0-lact-Nap) hydrolyzing more slowly than the diethylene glycol ester conjugate (G0-deg-Nap) [134]. The same trend was observed in presence of plasma [134]. The length of the spacer affected enzymatic release of the drug. The longer spacer (diethylene glycol) is likely to cause less steric hindrance for enzymatic cleavage and hence may cause faster cleavage of drug in the plasma and liver homogenate. Conjugation of naproxen to dendrimer increased its transepithelial transport across Caco-2 cells [134]. The transport of drug was further improved by lauroyl-modifying PAMAM G0.0. [134]. The study shows that PAMAM based drug conjugates with appropriate linkers have the potential to improve drug solubility, increase transepithelial transport and act as carriers for the oral delivery of drugs such as naproxen.

In another study Kolhatkar *et al.* complexed SN-38, a potent camptothecin analogue to PAMAM G4.0-NH_2 (Figure 2-8) and assessed the transport of the dendrimer-drug complex across Caco-2 monolayers (Figure 2-9) [118]. SN38 has poor aqueous solubility (<10 µg/mL), poor and variable permeability and severe dose-limiting gastric as well as other nonspecific toxicity, thus limiting its oral use. It was hypothesized that complexing SN-38 to G4.0-NH_2 will result in increased solubility and permeability of the

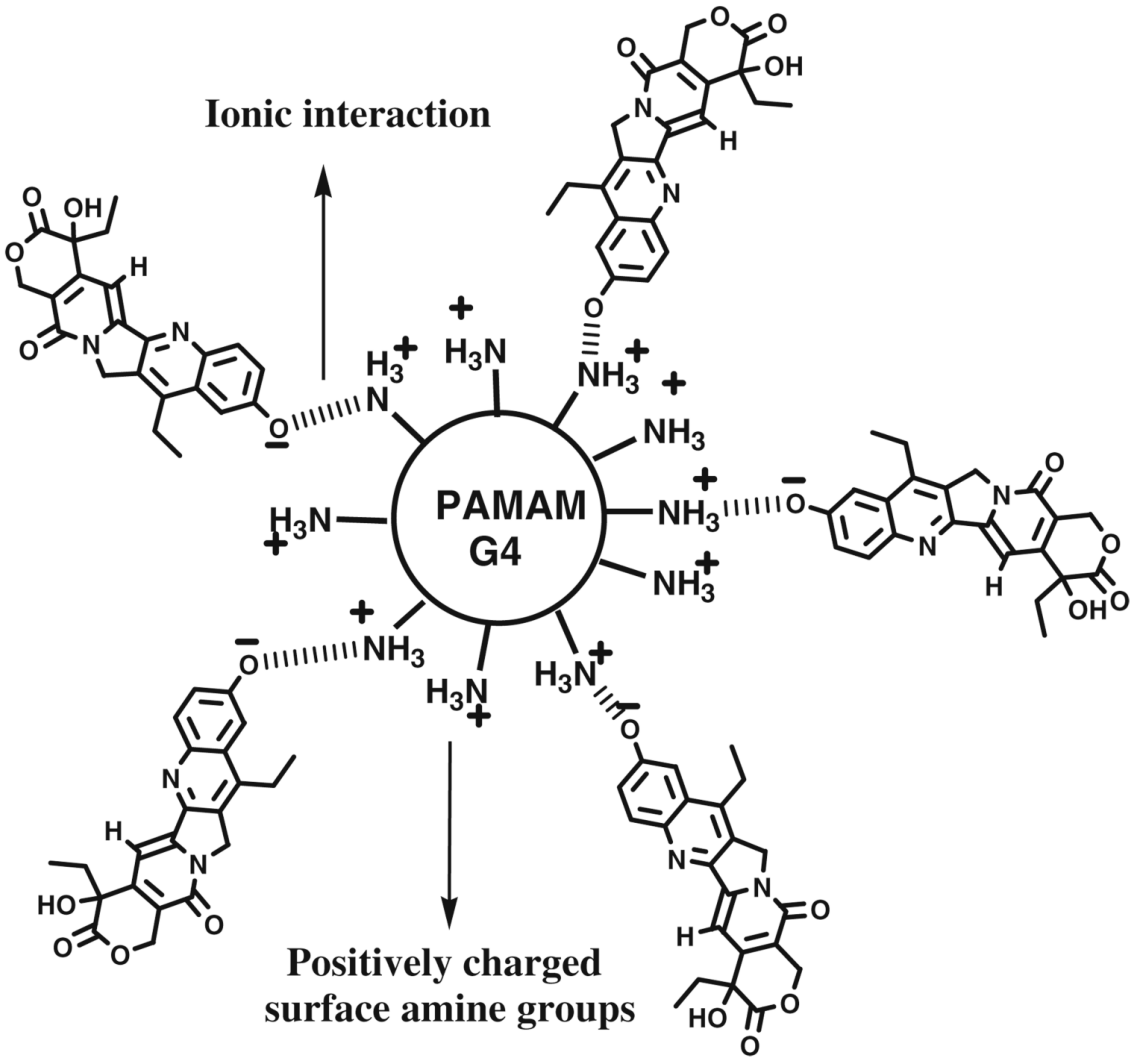

Figure 2-8. Schematic representation of G4S5 complex. With permission from Ref [118].

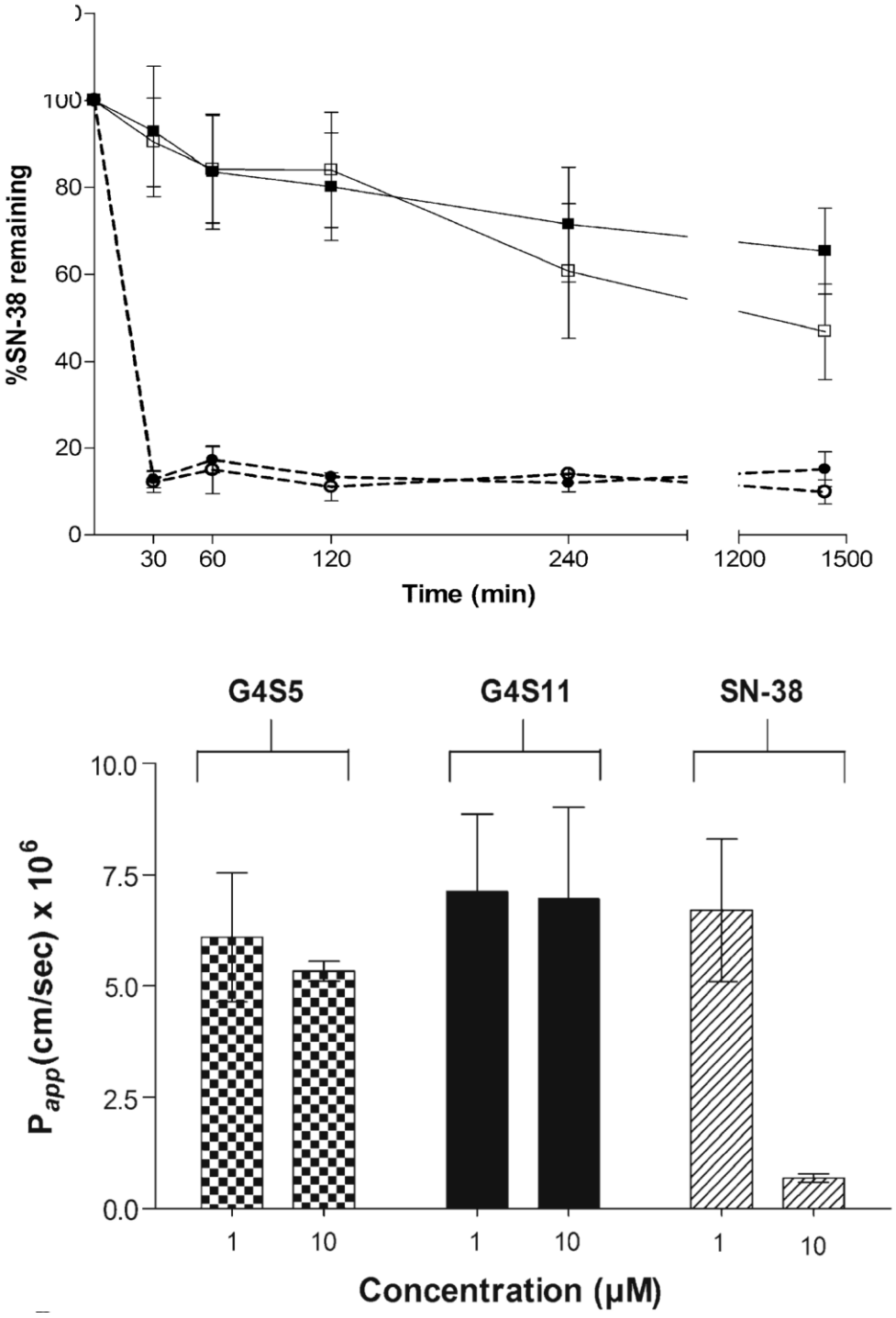

Figure 2-9A. Gastrointestinal stability and transepithelial transport of PAMAM-SN38 complex. Stability of polymer-SN-38 complexes G4S5 (open squares, solid line) and G4S11 (filled squares, solid line) at pH 7.4, and G4S5 (open circles, dotted line) and G4S11 (filled circles, dotted line) at pH 5. G4S5, G4S11: 5 and 11 moles of SN38 complexed to PAMAM G4.0 respectively. B. Permeability of G4S5, G4S11 and SN-38, across Caco-2 cell monolayers after 120 min. With permission from Ref [118].

drug and will help reduce toxicity of SN-38. When complexed with PAMAM G4.0-NH_2, SN-38 showed up to 10 fold higher permeability and 100 fold higher uptake than free SN-38 (Figure 2-9B) [118]. PAMAM-SN38 complexation was attributed to surface electrostatic interaction, which is sensitive to pH. Therefore, the complex was not stable under acidic conditions. Only 10% of the drug remained complexed with the PAMAM after 30 minutes of exposure to pH 5.5 buffer (Figure 2-9A) [118]. These studies indicate that while complexation is a simple and viable approach, it has distinct drawbacks of instability and premature release.

To overcome stability problems of the G4.0-SN38 complex and toxicity of the cationic G4.0-NH_2 carrier, covalent conjugates of the non-toxic PAMAM G3.5-COOH and SN-38 with glycine and β-alanine spacers were synthesized, characterized (Figure 2-10) and evaluated for cytotoxicity, mechanism of action (Figure 2-11), gastrointestinal stability (Figure 2-12A-B) and enzymatic release (Figure 2-12C) in the liver environment, as well as transepithelial transport *in vitro* (Figure 2-13) [124, 135]. PAMAM G3.5-COOH was chosen for its optimum balance of biocompatibility and Caco-2 permeability. The glycine spacer has been used in the clinically evaluated PEG and PGA-camptothecin conjugates [23, 136, 137]. Architecture of the polymeric carrier is likely to influence release and for the same spacer, a sterically hindered carrier like PAMAM will potentially cause drug to be released more slowly than a linear polymer like PEG or PGA, thus making the conjugate more stable to hydrolysis. An ester linkage is likely to be cleaved in the presence of carboxylesterase in the liver. Small spacers differing in one carbon atom were chosen in order to prevent indiscriminate acid and base hydrolysis and to evaluate effect of spacer length on release. SN-38 is a topoisomerase I

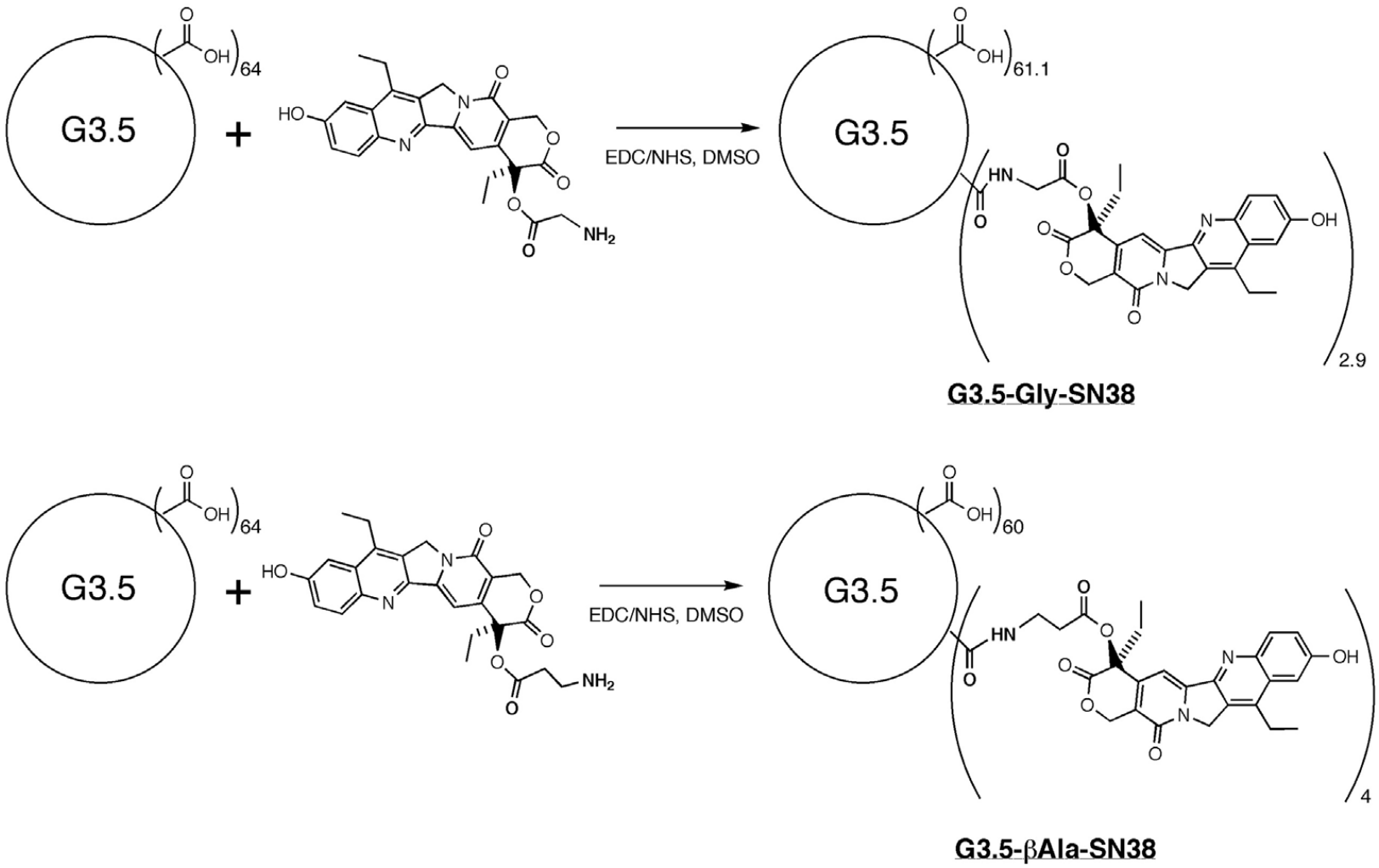

Figure 2-10. Synthetic schemes of G3.5-Gly-SN38 (top) and G3.5-βAla-SN38 (bottom) conjugates. With permission from Ref [135].

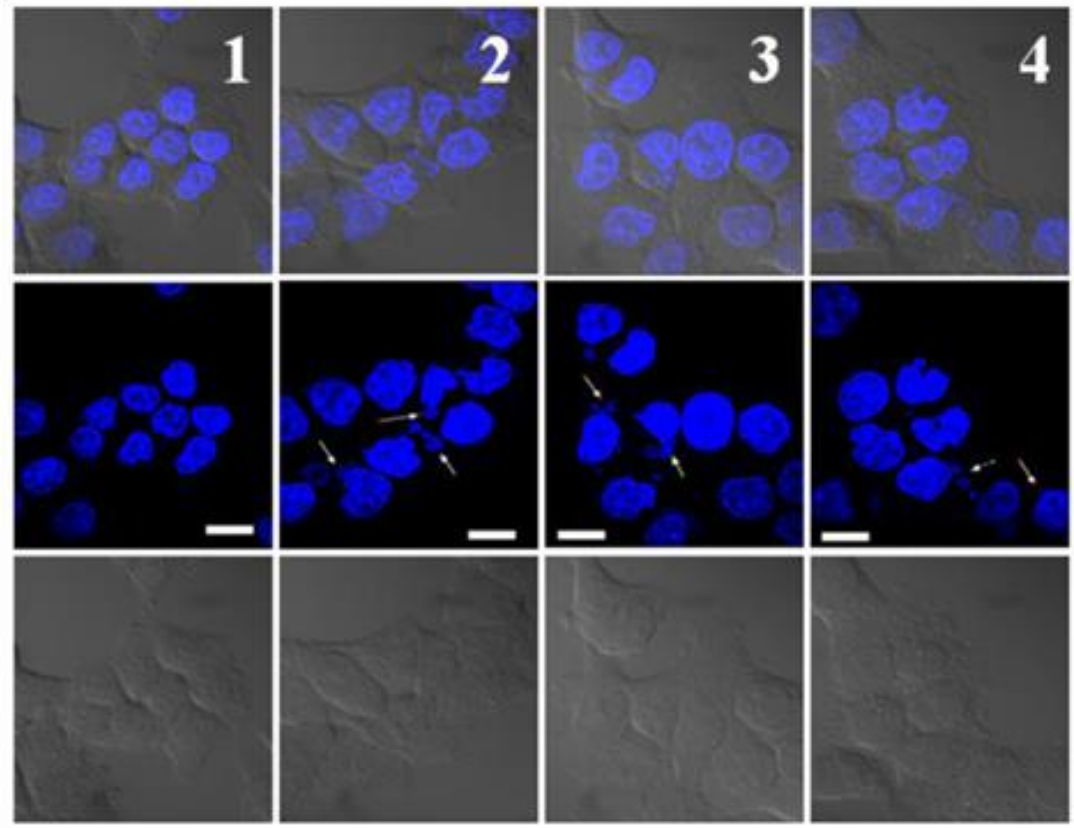

Figure 2-11. Nuclear fragmentation in HCT-116 cells treated with drug/conjugates. Untreated cells (column 1); 5 nM SN38 (column 2); 40 nM G3.5-gly-SN38 (column 3); 120 nM G3.5-βala-SN38 (column 4). Scale bar is 10 μm. Arrows indicate nuclear fragments. From bottom: 1st row, differential interference contrast image; 2nd row, fluorescence image; 3rd row, overlay of differential interference contrast and fluorescence images. Reprinted with permission from Ref [135]. Copyright 2010 American Chemical Society.

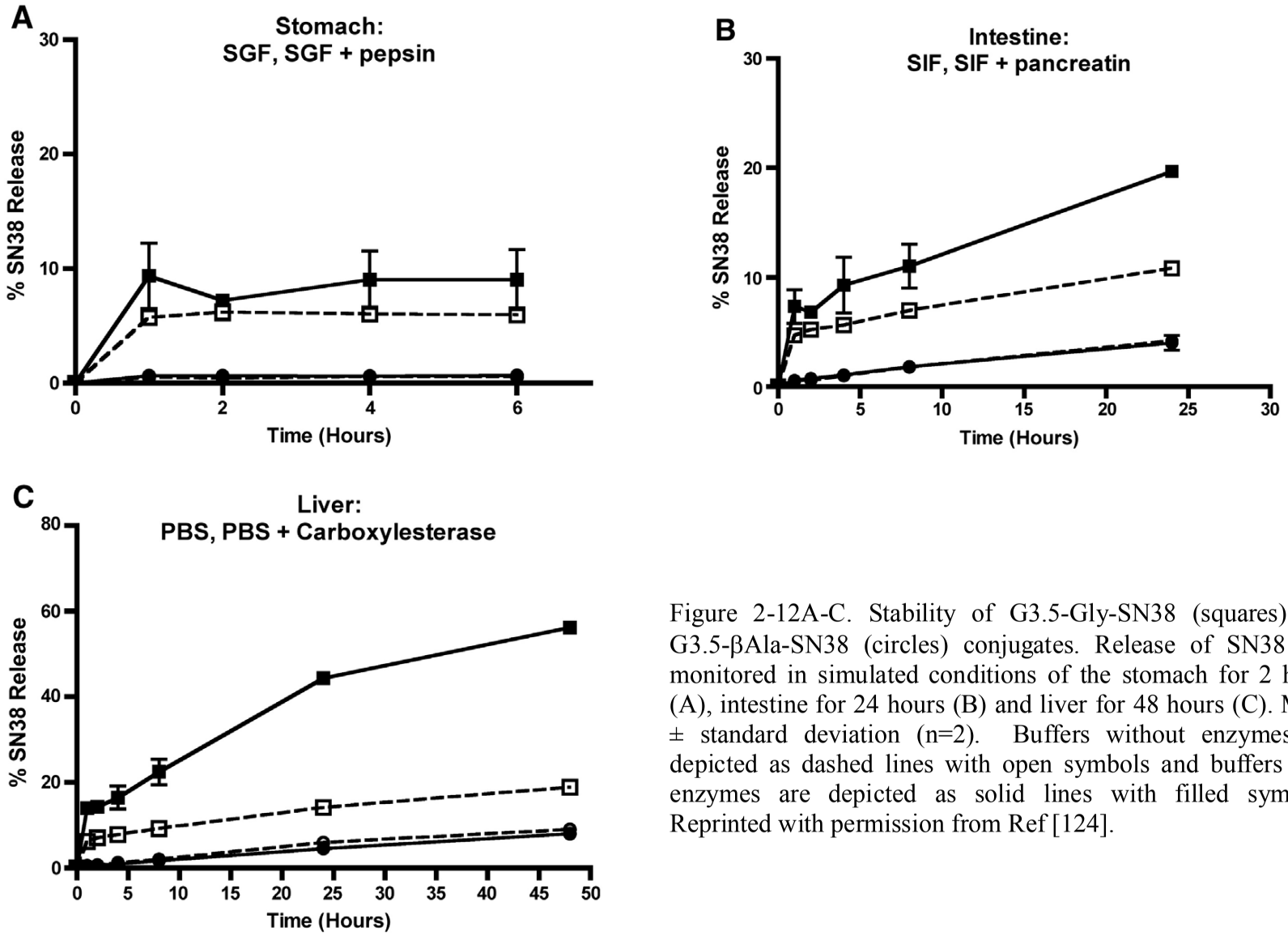

Figure 2-12A-C. Stability of G3.5-Gly-SN38 (squares) and G3.5-βAla-SN38 (circles) conjugates. Release of SN38 was monitored in simulated conditions of the stomach for 2 hours (A), intestine for 24 hours (B) and liver for 48 hours (C). Mean ± standard deviation (n=2). Buffers without enzymes are depicted as dashed lines with open symbols and buffers with enzymes are depicted as solid lines with filled symbols. Reprinted with permission from Ref [124].

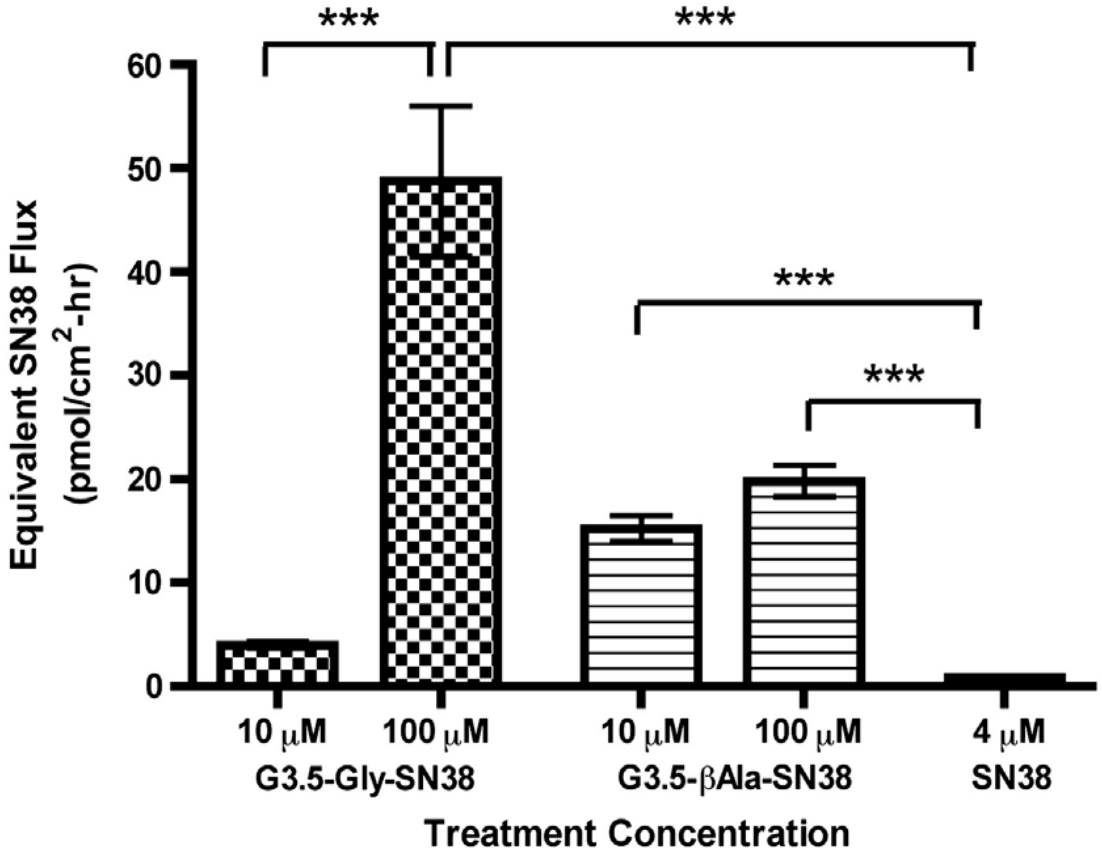

Figure 2-13. Transepithelial transport of G3.5-Gly-SN38 and G3.5-βAla-SN38 conjugates. Equivalent SN38 flux across differentiated Caco-2 monolayers treated with G3.5-SN38 conjugates and SN38. Equivalent SN38 flux was calculated by multiplying the measured molar flux of the conjugates with the number of SN38 molecules per dendrimer. Mean ± standard deviation (n=4). (***) indicates a significant difference with $p<0.001$. Reprinted with permission from Ref [124].

inhibitor and is known to arrest cell cycle in the G2/M phase. Both free drug and conjugates caused majority of the cells to arrest in the G2/M phase and caused condensed nuclear fragments and mitotic cells when nuclear morphology was observed using fluorescence microscopy (Figure 2-11) [135]. This suggests that the PAMAM-SN38 conjugates had a similar mechanism of action as the free SN38 and that release of the free drug from the PAMAM carrier was necessary for it to exert cytotoxic action. These observations are also indicative of apoptosis or necrosis and suggest that free and conjugated SN38 has the same mode of action.

The conjugates were further evaluated for stability in the GIT and enzymatic release. The glycine conjugate (G3.5-gly-SN38) was more susceptible to hydrolytic as well as enzymatic release. Hydrolytic release under different conditions was less than enzymatic release for the glycine conjugate, minimizing nonspecific release and toxicity of the drug in the GIT and maximizing site-specific release in presence of carboxylesterases [124]. The glycine conjugate showed a good balance of gastrointestinal stability, transepithelial transport and cytotoxicity against colorectal carcinoma cells (HT-29 cells) and effective release of free drug in the presence of liver carboxylesterases. The alanine conjugate (G3.5-βala-SN38) was mostly stable under all conditions (Figure 2-12A-C) [124]. The extent of drug release correlated to cytotoxicity of the conjugates with the glycine conjugate being more cytotoxic than the alanine conjugate [124]. The transepithelial transport of SN38 when conjugated via the glycine spacer to G3.5 was concentration dependent and higher than the SN38 flux for the alanine conjugate, which was unchanged over the concentration range tested (10 and 100 μM) (Figure 2-13) [124]. This suggested a different mechanism of transport for the two conjugates-the glycine

conjugate by a more passive diffusion-related process (paracellular) and the alanine conjugate by a more active, cellular uptake related process (transcellular).

The PAMAM dendrimer used for complexation was amine-terminated while that used for conjugation was carboxylic acid-terminated. Hence, it is not possible to do a head to head comparison of the conjugate to the complex. But an interesting observation was that the increase in SN38 flux across Caco-2 cell monolayers was similar for the PAMAM-SN38 conjugates and complexes.

The choice of linker or mechanism of drug association to dendrimer is critical to the stability of the dendrimer-drug conjugate/complex in the harsh conditions of the gastrointestinal tract and to the efficient release of the drug at the site of action. In the context of solid state malignancies, both the GIT and tumor physiology can have a common range of enzymes and pH. It is a chemical paradox to design a system perfectly stable in one condition and completely hydrolyzed in the other. It is therefore important to strike a balance between stability in the GIT and site-specific release. Identifying tumor-specific elevated enzymes and designing linkers to be specifically cleaved by them can potentially overcome this problem.

2.5.5. *In vivo* oral bioavailability of PAMAM – drug complexes

The work summarized in the above sections includes the *in vitro* evaluation of the transepithelial transport of dendrimer-drug conjugates or complexes. It was seen than conjugation and complexation of drugs to dendrimers has the potential to control release and improve bioavailability. *In vitro* models lack the variables of gastric emptying, intestinal tract motility and enzymatic environment of the gastrointestinal tract present in

in vivo models. However, they are useful to provide mechanistic insight into transepithelial transport and absorption and help come up with strategies to enhance the same. The choice of technique will depend on the research question and a combination of different models will ultimately provide an answer to the use of PAMAM dendrimers as oral drug delivery carriers. Two recent studies have evaluated the *in vivo* bioavailability of PAMAM-drug complexes.

The extent of complexation of silybin, a potent hydrophobic alkaloid by cationic and anionic PAMAM dendrimers of varying generations, i.e., G1.5, G2.0, G2.5, and G3.0 was evaluated at different molar ratios of dendrimer and drug [138]. G1.5 and G2.5 incorporated 4 and 6 moles of silybin per mole of PAMAM while G2.0 and G3.0 incorporated 20 and 32 moles of silybin per mole of PAMAM. At basic pH (9-10), around pKa of the primary amine terminal groups of the full generation dendrimers, both the amine groups of the dendrimer and the phenolic groups of silybin are ionized. This facilitates an additional electrostatic interaction between the surface amine groups and the oppositely-charged phenolic hydroxyl groups of silybin, explaining the higher association of silybin to full generation dendrimers. The *in vitro* release experiments suggested a controlled release of the drug from the complexes in simulated gastric (SGF) and intestinal (SIF) fluids. G2.0-silybin and G3.0-silybin complexes released up to 20% silybin in SGF at 2 hours and up to 90% silybin release in SIF at 10 hours [138]. The complexes were not highly stable in gastric conditions indicating that part of the drug is going to be released from the PAMAM in the small intestine, effectively resulting in free as well as complexed drug presented for oral absorption. The relative oral bioavailability of silybin was enhanced 2-fold by complexing with amine terminated PAMAM G2.0-

NH_2 when administered by oral gavage to male rats [138]. Part of the drug might have remained complexed to the dendrimer explaining an extended T_{max} (15 minutes) of absorption as compared to silybin alone (T_{max} = 10 minutes) [138]. The anionic PAMAM-silybin complex was not evaluated *in vivo* in this study. Authors speculated that increased oral absorption of silybin when complexed with PAMAM was due to a combination of increased solubility, controlled release, tight junction modulation and absorptive endocytosis of PAMAM-silybin complex [138].

The cellular uptake in Caco-2 cells, transport across rat intestinal segments and oral absorption pharmacokinetics of doxorubicin complexed with amine terminated PAMAM G3.0-NH_2 in rats by oral gavage has also been investigated [120]. Controlled release of doxorubicin from doxorubicin–PAMAM (1:2 molar ratio) complex (74.5% during 24 hours) was observed in the presence of N-tris(hydroxymethyl)methyl-2-aminoethanesulfonic acid (TES) buffer (pH 6.0-8.0) [120]. However, in the GIT, the PAMAM-doxorubicin complex can be subjected to lower pH in gastric fluid and also to enzymatic degradation. Release in simulated GIT conditions was not evaluated in this study. Doxorubicin is known to be a P-gp substrate. Its uptake in Caco-2 cells was enhanced in the presence of Cyclosporin A (CsA), due to the inhibition of P-gp efflux by CsA [120]. However, the doxorubicin uptake was higher when complexed with PAMAM compared to free doxorubicin alone or free doxorubicin with P-gp inhibitor. Addition of a P-gp inhibitor did not cause significant increase of uptake of the drug suggesting that when complexed with PAMAM, doxorubicin bypassed the P-gp efflux pump. Transport studies in everted intestinal rat segments of duodenum, ileum and jejunum showed that the transport of doxorubicin was higher (4-7 times at 90 min) when complexed with

PAMAM. The transport of doxorubicin was highest in the ileum. [120]. When the PAMAM-doxorubicin complex was incubated with different segments of the small intestine, a slight increase in permeability of mannitol, a paracellular marker, was observed. This is indicative of tight junction modulation by the complex and increased paracellular transport. The complex was evaluated *in vivo* by administration of a single oral dose in rats. A 300 fold increase in bioavailability of the doxorubicin was achieved when complexed with the dendrimer [120]. Increase in plasma exposure of doxorubicin when complexed with PAMAM was attributed to the solubilization effect of the PAMAM on doxorubicin, a highly hydrophobic drug. The GIT stability profile of the two dendrimer-drug complexes of doxorubicin and silybin has not been investigated in detail. Thus, there might be partial or complete release of the free drug complexed to the dendrimer in the GIT before absorption. The increased amount of drug detected in the blood stream could therefore also be due to a combination of the following factors: 1) increased solubilization by the dendrimer, 2) controlled release of the drug from the dendrimer, 3) intestinal penetration enhancement of the free drug by the dendrimer, and 4) increased permeability of the PAMAM-drug complex.

2.5.6. PAMAM dendrimers as intestinal penetration enhancers

With its large surface area, the small intestine offers the opportunity for increased absorption. Cationic PAMAM dendrimers have been recently explored as a class of intestinal penetration enhancers that act on increasing the permeability of hydrophilic small molecules as well as hydrophobic macromolecules throughout the small intestine [131].

In situ intestinal models have been used to evaluate PAMAM dendrimers as penetration enhancers [131]. In an *in situ* method, the segment of the gut lumen to be evaluated is cannulated in the anesthetized animal. All physiological functions of the intestine remains intact and it is possible to access both apical and basolateral sides [125]. This model preserves mucous layer and sink conditions created by vasculature. However, it allows the assessment of absorption without the interference of gastric emptying and motility [125].

The penetration enhancement was achieved using *in situ* closed loop method in SD rats at nontoxic doses and was reversible [131]. Effects of amine-terminated PAMAM generations 0-3 were examined on the absorption of 5(6)-carboxyfluorescein, a hydrophilic small-molecular weight dye. The absorption enhancing effects of PAMAM on the small intestinal segment were concentration and generation dependent. Of the dendrimers tested, PAMAM G2.0-NH_2 showed maximum absorption enhancement, up to 11.1 fold, at 0.5 % w/v. At this concentration, PAMAM G2.0-NH_2 caused membrane damage as evaluated by the LDH assay [131]. However, the damage was found to be reversible. The absorption-enhancing effects of G2.0-NH_2 were tested in the small intestinal segment at 0.5% w/v for hydrophillic macromolecular compounds like fluorescein isothiocyanate-dextrans (FDs) of various molecular weights, calcitonin and insulin. PAMAM G2.0-NH_2 was effective in increasing the absorption of hydrophilic, macromolecular FDs up to 4000 dalton through the small intestine [131]. However, PAMAM G2.0-NH_2 did not significantly increase the permeability of hydrophilic macromolecules of a molecular weight above 4,000 dalton, such as insulin and calcitonin [131]. Absorption enhancement across the small intestinal segment was found to be a

function of molecular weight with the absorption enhancement ratio being highest (about 11.0) for 5(6)-carboxyfluorescein, a small molecular weight hydrophilic compound [131]. It has been speculated that amine-terminated PAMAM dendrimers modulated the tight junctions, suggested by decrease in TEER values, leading to an increase in absorption of the smaller sized hydrophilic molecules tested. Authors also suggest that the enlargement of the tight junction holes may not have been large enough to allow larger sized macromolecules like insulin to pass through [131]. Unlike conventional absorption enhancers, the absorption enhancing effects for PAMAM G2.0-NH_2 observed in the small intestine was much greater than that seen in the large intestine in this study. Authors speculate that these differences could be due to segmental difference in the physiology of the intestine. Variations in the mucosal layer or tight junction arrangement can result in different interaction of the PAMAM dendrimer with the epithelial layer, resulting in different absorption enhancement action. Further research is needed in order to understand the mechanism of penetration enhancement of PAMAM dendrimers in order to exploit their absorption enhancement capacity.

The study summarized above investigated cationic PAMAM dendrimers as penetration enhancers *in situ*. Previous research has shown in Caco-2 cell monolayers and isolated intestinal tissue that along with cationic PAMAM dendrimers, anionic, carboxyl-terminated PAMAM dendrimers can also translocate across the intestinal barrier effectively while being less toxic to the epithelium as compared to the cationic dendrimers [103, 123]. Anionic PAMAM dendrimers also need to be evaluated for absorption enhancing effects. Both cationic and anionic dendrimers have to be evaluated for the penetration enhancement *in vivo*.

Co-delivery of poorly-soluble and poorly-absorbable drugs (BCS class IV) with PAMAM dendrimers that can act as penetration enhancers (Section 2.5.6) and solubilizing agents (Section 2.4) will help solubilize the drug and improve its permeability leading to increased oral bioavailability (Section 2.5.5).

2.6. Oral delivery of chemotherapeutics

Oral administration of chemotherapeutics has treatment advantages of patient preference and convenience and cost-effectiveness [139]. It is also advantageous for improving patient quality of life in palliative care. In terms of treatment outcomes, oral chemotherapeutics are advantageous for protracted dosage regimens as is the case for schedule-dependent cytotoxic drugs [139]. The major limitations for oral chemotherapy are significantly low bioavailability, intra and inter-patient variability attributed to intestinal metabolic and efflux systems like the CYP3A4 and the P-gp efflux, respectively [140]. Most cytotoxic chemotherapeutic drugs have a narrow therapeutic index which makes drug exposure variability a substantial concern. For such drugs, slight variations in bioavailability can lead to suboptimal exposure and inadequate efficacy or greater than optimal exposure and consequently excessive toxicities.

2.6.1. Camptothecins as model chemotherapeutics for oral delivery

Camptothecin and its derivatives are potent topoisomerase-I inhibitors [141]. The pharmacophore of camptothecins is known to be the closed α-hydroxylactone E ring. The lactone ring hydrolyzes under physiological conditions- pH 7.0 or above and in presence of serum albumin, that preferentially binds the ring-opened form [142]. Although the ring

opened form is pharmacologically inactive, this equilibrium is reversible and the lactone form can be obtained under acidic pH (Figure 2-14) [143]. Camptothecins show a schedule-dependent activity which means that they are more efficacious with low and frequent dosage regimens [140].

Topotecan, 9-aminocamptothecin and Irinotecan have been evaluated for oral dosing preclinically and clinically. Topotecan had moderate bioavailability (30.0 +/- 7.7 %) in Phase I with equivalent efficacy to IV administration [140]. It showed similar ratio of lactone to carboxylate exposure when administered orally as compared to IV along with an increased half-life upon oral administration. Irinotecan, evaluated in Phase I studies, showed poor and variable bioavailability (8-12 %) [144].

2.6.2. Hepatic metastasis of colorectal cancer as a model for oral delivery of camptothecins

Colorectal cancer is the third leading cause of cancer in the United States with an estimated 103,170 new cases and 51,690 deaths in 2012 [145]. Approximately 50% of the patients develop metastatic disease, the most common site being the liver, followed by the lung [145]. With improved screening, colorectal cancers are being detected at early surgery remains the primary treatment. However, for metastatic disease, very few patients qualify for surgical resection. Chemotherapeutics indicated for metastatic colorectal cancer include derivatives of floxuridine, 5-fluorouracil, camptothecin and cisplatin. Irinotecan, the prodrug of 7-ethyl-10-hydroxy-camptothecin (SN-38), administered intravenously, is indicated along with 5-fluorouracil and folic acid (FOLFIRI) for the first line treatment and as a single agent therapy for second line treatment of distant metastasis

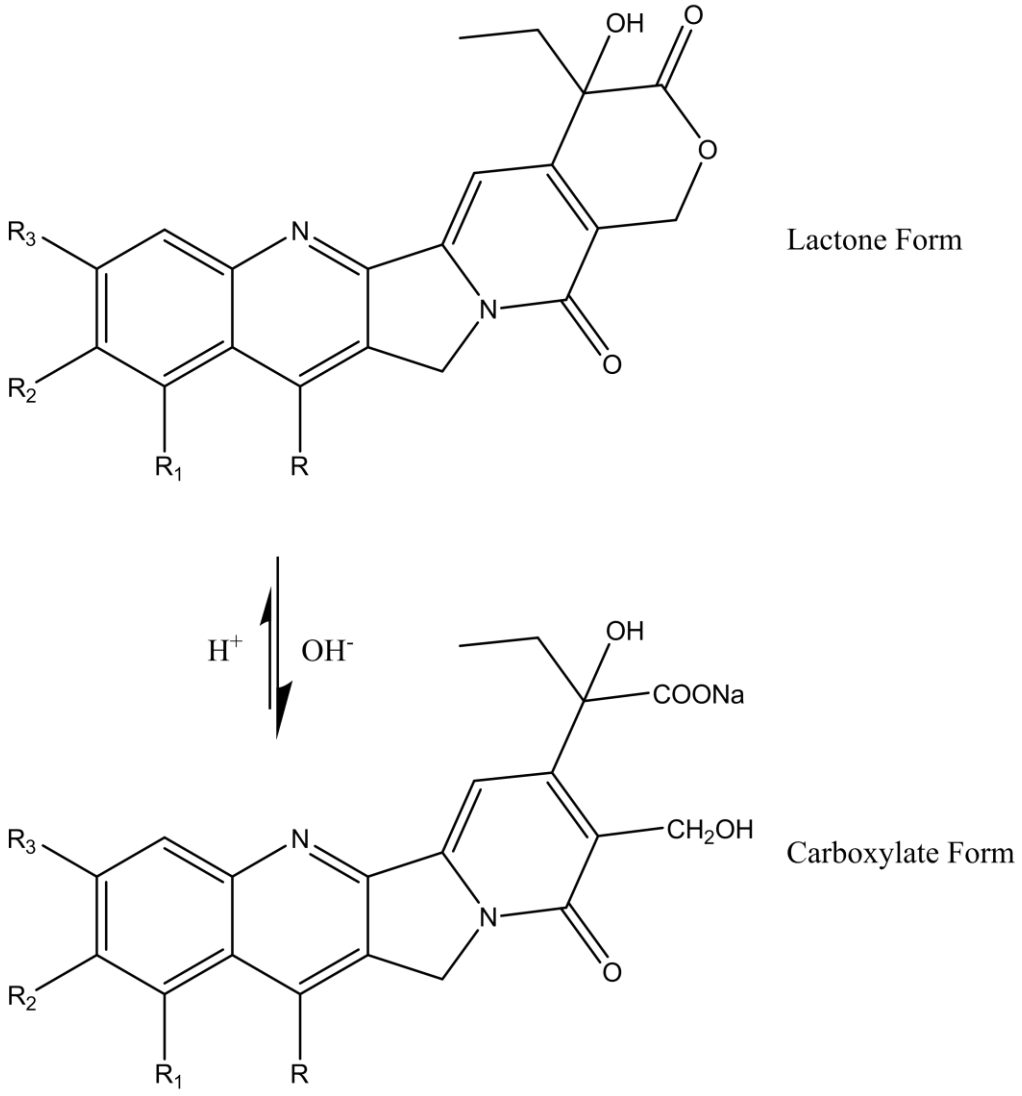

Figure 2-14. Camptothecin (lactone and carboxylate forms) and its analogues.

Note: Camptothecin: R=R1=R2=R3=H; 10-Hydroxycamptothecin: R=R1=R3=H, R2=OH; 10-Methoxycamptothecin: R=R1=R3=H, R2=OCH_3; 9-Nitrocamptothecin: R=R2=R3=H, R1=NO_2; 9-Aminocamptothecin: R=R2=R3=H, R1=NH_2.

of colorectal cancer [145]. IV administration of Irinotecan along with oral prodrug of 5-fluorouracil (cepecitabine) is a treatment regimen that has shown promise of increased efficacy, decreased toxicity and increased patient compliance [145]. Some of the problems with existing systemic chemotherapies are high non-specific toxicities like diarrhea and neutropenia along with long infusion times (48 hours). Oral delivery of these chemotherapeutics can enable low dose regimens with frequent administration (prolonged exposure) required for drugs like camptothecins that show schedule-dependent activity [144, 146]. Camptothecins, when administered orally, take advantage of the first pass effect and accumulate in the liver and liver metastasis. They are primarily detoxified via glucoronidation by P450 CYP3A4 in the liver [147]. The liver metastasis does not have a mechanism of detoxifying camptothecins via glucuronidation thereby generating sufficient drug to be cytotoxic to the tumor [147]. However, irinotecan administered orally shows very low (8-12%) oral bioavailability [144, 146]. Enhancement in oral bioavailability of camptothecins will improve efficacy of treatment and avoid invasive routes of drug administration.

2.7. References

1. Duncan R. The dawning era of polymer therapeutics. Nat Rev Drug Discov. 2003;2(5):347-60.

2. Haag R, Kratz F. Polymer therapeutics: concepts and applications. Angew Chem Int Ed. 2006;45(8):1198-215.

3. Duncan R. Polymer conjugates as anticancer nanomedicines. Nat Rev Cancer. 2006;6(9):688-701.

4. Boddy AV, Plummer ER, Todd R, Sludden J, Griffin M, Robson L et al. A phase I and pharmacokinetic study of paclitaxel poliglumex (XYOTAX), investigating both 3-weekly and 2-weekly schedules. Clin Cancer Res. 2005;11(21):7834-40.

5. Yen Y, Synold T, Schluep T, Hwang J, Oliver J, Davis M. First-in-human phase I trial of a cyclodextrin-containing polymer-camptothecin nanoparticle in patients with solid tumors. J Clin Oncol. 2007;25(18S):14078.

6. Homsi J, Simon GR, Garrett CR, Springett G, De Conti R, Chiappori AA et al. Phase I trial of poly-L-glutamate camptothecin (CT-2106) administered weekly in patients with advanced solid malignancies. Clin Cancer Res. 2007;13(19):5855-61.

7. Sparreboom A, Scripture CD, Trieu V, Williams PJ, De T, Yang A et al. Comparative preclinical and clinical pharmacokinetics of a cremophor-free, nanoparticle albumin-bound paclitaxel (ABI-007) and paclitaxel formulated in Cremophor (Taxol). Clin Cancer Res. 2005;11(11):4136-43.

8. Larson RA, Sievers EL, Stadtmauer EA, Löwenberg B, Estey EH, Dombret H et al. Final report of the efficacy and safety of gemtuzumab ozogamicin (Mylotarg) in patients with CD33-positive acute myeloid leukemia in first recurrence. Cancer. 2005;104(7):1442-52.

9. York AW, Kirkland SE, McCormick CL. Advances in the synthesis of amphiphilic block copolymers via RAFT polymerization: stimuli-responsive drug and gene delivery. Adv Drug Del Rev. 2008;60(9):1018-36.

10. Tomlinson R, Klee M, Garrett S, Heller J, Duncan R, Brocchini S. Pendent chain functionalized polyacetals that display pH-dependent degradation: a platform for the development of novel polymer therapeutics. Macromolecules. 2002;35(2):473-80.

11. Tomalia DA, Baker H, Dewald J, Hall M, Kallos G, Martin S et al. A new class of polymers: starburst-dendritic macromolecules. Polym J. 1985;17(1):117-32.

12. Godwin A, Hartenstein M, Müller AHE, Brocchini S. Narrow molecular weight distribution precursors for polymer–drug conjugates. Angew Chem. 2001;113(3):614-7.

13. Wu K, Yang J, Koňák Č, Kopečková P, Kopeček J. Novel synthesis of HPMA copolymers containing peptide grafts and their self-assembly into hybrid hydrogels. Macromol Chem Phys. 2007;209(5):467-75.

14. Parrish B, Emrick T. Soluble camptothecin derivatives prepared by click cycloaddition chemistry on functional aliphatic polyesters. Bioconjug Chem. 2007;18(1):263-7.

15. Ringsdorf H. Structure and properties of pharmacologically active polymers. J Polym Sci Polym Symp. 1975;51(1):135-53.

16. Maeda H, Wu J, Sawa T, Matsumura Y, Hori K. Tumor vascular permeability and the EPR effect in macromolecular therapeutics: a review. J Control Release. 2000;65(1):271-84.

17. Hopewell J, Duncan R, Wilding D, Chakrabarti K. Preclinical evaluation of the cardiotoxicity of PK2: a novel HPMA copolymer–doxorubicin–galactosamine conjugate antitumour agent. Hum Exp Toxicol. 2001;20(9):461-70.

18. Julyan PJ, Seymour LW, Ferry DR, Daryani S, Boivin CM, Doran J et al. Preliminary clinical study of the distribution of HPMA copolymers bearing doxorubicin and galactosamine. J Control Release. 1999;57(3):281-90.

19. Muggia FM. Doxorubicin-polymer conjugates: further demonstration of the concept of enhanced permeability and retention. Clin Cancer Res. 1999;5(1):7-8.

20. Liu J, Bauer H, Callahan J, Kopečková P, Pan H, Kopeček J. Endocytic uptake of a large array of HPMA copolymers: elucidation into the dependence on the physicochemical characteristics. J Control Release. 2010;143(1):71-9.

21. Perumal OP, Inapagolla R, Kannan S, Kannan RM. The effect of surface functionality on cellular trafficking of dendrimers. Biomaterials. 2008;29(24):3469-76.

22. Duncan R. Designing polymer conjugates as lysosomotropic nanomedicines. Biochem Soc Trans. 2007;35:56-60.

23. Zhao H, Rubio B, Sapra P, Wu D, Reddy P, Sai P et al. Novel prodrugs of SN38 using multiarm poly (ethylene glycol) linkers. Bioconjug Chem. 2008;19(4):849-59.

24. Etrych T, Chytil P, Jelínková M, Říhová B, Ulbrich K. Synthesis of HPMA copolymers containing doxorubicin bound via a hydrazone linkage. Effect of spacer on drug release and *in vitro* cytotoxicity. Macromol Biosci. 2002;2(1):43-52.

25. Kopeček J, Cífková I, Rejmanová P, Strohalm J, Obereigner B, Ulbrich K. Polymers containing enzymatically degradable bonds, 4. Preliminary experiments *in vivo*. Die Makromolekulare Chemie. 1981;182(11):2941-9.

26. Rejmanová P, Kopeček J, Pohl J, Baudyš M, Kostka V. Polymers containing enzymatically degradable bonds, 8. Degradation of oligopeptide sequences in N-(2-hydroxypropyl) methacrylamide copolymers by bovine spleen cathepsin B. Die Makromolekulare Chemie. 2003;184(10):2009-20.

27. Vicent MJ, Ringsdorf H, Duncan R. Polymer therapeutics: clinical applications and challenges for development. Adv Drug Del Rev. 2009;61(13):1117.

28. Li C, Wallace S. Polymer-drug conjugates: Recent development in clinical oncology. Adv Drug Del Rev. 2008;60(8):886-98.

29. Gillies ER, Frechet JMJ. Dendrimers and dendritic polymers in drug delivery. Drug Discovery Today. 2005;10(1):35-43.

30. Vasey PA, Kaye SB, Morrison R, Twelves C, Wilson P, Duncan R et al. Phase I clinical and pharmacokinetic study of PK1 [N-(2-hydroxypropyl) methacrylamide

copolymer doxorubicin]: first member of a new class of chemotherapeutic agents—drug-polymer conjugates. Clin Cancer Res. 1999;5(1):83-94.

31. Meerum Terwogt JM, ten Bokkel Huinink WW, Schellens JHM, Schot M, Mandjes IAM, Zurlo MG et al. Phase I clinical and pharmacokinetic study of PNU166945, a novel water-soluble polymer-conjugated prodrug of paclitaxel. Anti-cancer Drug. 2001;12(4):315.

32. Rademaker-Lakhai JM, Terret C, Howell SB, Baud CM, de Boer RF, Pluim D et al. A Phase I and pharmacological study of the platinum polymer AP5280 given as an intravenous infusion once every 3 weeks in patients with solid tumors. Clin Cancer Res. 2004;10(10):3386-95.

33. Nowotnik DP, Cvitkovic E. ProLindac™(AP5346): a review of the development of an HPMA DACH platinum polymer therapeutic. Adv Drug Del Rev. 2009;61(13):1214-9.

34. Campone M, Rademaker-Lakhai JM, Bennouna J, Howell SB, Nowotnik DP, Beijnen JH et al. Phase I and pharmacokinetic trial of AP5346, a DACH–platinum–polymer conjugate, administered weekly for three out of every 4 weeks to advanced solid tumor patients. Cancer Chemother Pharmacol. 2007;60(4):523-33.

35. Schoemaker N, Van Kesteren C, Rosing H, Jansen S, Swart M, Lieverst J et al. A phase I and pharmacokinetic study of MAG-CPT, a water-soluble polymer conjugate of camptothecin. Br J Cancer. 2002;87(6):608-14.

36. Rowinsky EK, Rizzo J, Ochoa L, Takimoto CH, Forouzesh B, Schwartz G et al. A phase I and pharmacokinetic study of pegylated camptothecin as a 1-hour infusion every 3 weeks in patients with advanced solid malignancies. J Clin Oncol. 2003;21(1):148-57.

37. Von Hoff D, Jameson G, Borad M, Rosen L, Utz J, Basche M et al., editors. First Phase 1 trial of NKTR-102 (Peg-Irinotecan) reveals early evidence of broad anti-tumor activity in three different schedules. 20th EORTC-NCI-AACR Symposium on Molecular Targets and Cancer Therapeutics Meeting, Geneva, Switzerland; 2008.

38. Guo Z, Wheler J, Naing A, Mani S, Goel S, Mulcahy M et al. Clinical pharmacokinetics (PK) of EZN-2208, a novel anticancer agent, in patients (pts) with advanced malignancies: a phase I, first-in-human, dose-escalation study. J Clin Oncol. 2008;26(20 suppl):2556.

39. Wolff R, Routt S, Hartsook R, Riggs J, Zhang W, Persson H et al. NKTR-105, a novel pegylated-docetaxel, demonstrates superior anti-tumor activity versus docetaxel in human non-small cell lung and colon mouse xenograft models. Eur J Cancer Suppl. 2008;6:141.

40. Singer JW, Baker B, Vries P, Kumar A, Shaffer S, Vawter E et al. Poly-(L)-glutamic acid-paclitaxel (CT-2103)[XYOTAX™], a biodegradable polymeric drug conjugate. In: Polymer Drugs in the Clinical Stage, Springer, U.S.A.; 2004; p.81-99.

41. Springett G, Takimoto C, McNamara M, Doroshow J, Syed S, Eastham E et al. Phase I study of CT-2106 (polyglutamate camptothecin) in patients with advanced malignancies. J Clin Oncol. 2004;22(14):3127.

42. Matsumura Y, Maeda H. A new concept for macromolecular therapeutics in cancer chemotherapy: mechanism of tumoritropic accumulation of proteins and the antitumor agent smancs. Cancer Res. 1986;46(12 Part 1):6387-92.

43. Maeda H, Fang J, Inutsuka T, Kitamoto Y. Vascular permeability enhancement in solid tumor: various factors, mechanisms involved and its implications. Int Immunopharmacol. 2003;3(3):319-28.

44. Maeda H. SMANCS and polymer-conjugated macromolecular drugs: advantages in cancer chemotherapy. Adv Drug Del Rev. 2001;46(1):169-85.

45. Maeda H, Seymour LW, Miyamoto Y. Conjugates of anticancer agents and polymers: advantages of macromolecular therapeutics *in vivo*. Bioconjug Chem. 1992;3(5):351-62.

46. Yamaoka T, Tabata Y, Ikada Y. Distribution and tissue uptake of poly (ethylene glycol) with different molecular weights after intravenous administration to mice. J Pharm Sci. 1994;83(4):601-6.

47. Seymour L, Miyamoto Y, Maeda H, Brereton M, Strohalm J, Ulbrich K et al. Influence of molecular weight on passive tumour accumulation of a soluble macromolecular drug carrier. Eur J Cancer. 1995;31(5):766-70.

48. Noguchi Y, Wu J, Duncan R, Strohalm J, Ulbrich K, Akaike T et al. Early phase tumor accumulation of macromolecules: a great difference in clearance rate between tumor and normal tissues. Cancer Sci. 1998;89(3):307-14.

49. Grayson SM, Godbey WT. The role of macromolecular architecture in passively targeted polymeric carriers for drug and gene delivery. J Drug Target. 2008;16(5):329-56.

50. Fox ME, Szoka FC, Fre chet JMJ. Soluble polymer carriers for the treatment of cancer: the importance of molecular architecture. Acc Chem Res. 2009;42(8):1141-51.

51. Jain RK. Transport of molecules in the tumor interstitium: a review. Cancer Res. 1987;47(12):3039-51.

52. Jain RK. Transport of molecules across tumor vasculature. Cancer Metast Rev. 1987;6(4):559-93.

53. Chauhan VP, Stylianopoulos T, Boucher Y, Jain RK. Delivery of molecular and nanoscale medicine to tumors: transport barriers and strategies. Annu Rev Chem Biomol. 2011;2:281-98.

54. Baxter LT, Jain RK. Transport of fluid and macromolecules in tumors. I. Role of interstitial pressure and convection. Microvasc Res. 1989;37(1):77-104.

55. Baxter LT, Jain RK. Transport of fluid and macromolecules in tumors. II. Role of heterogeneous perfusion and lymphatics. Microvasc Res. 1990;40(2):246-63.

56. Baxter LT, Jain RK. Transport of fluid and macromolecules in tumors: III. Role of binding and metabolism. Microvasc Res. 1991;41(1):5-23.

57. Fang J, Nakamura H, Maeda H. The EPR effect: unique features of tumor blood vessels for drug delivery, factors involved, and limitations and augmentation of the effect. Adv Drug Deliv Rev. 2011;63(3):130-51.

58. Choi HS, Liu W, Liu F, Nasr K, Misra P, Bawendi MG et al. Design considerations for tumour-targeted nanoparticles. Nat Nanotechnol. 2009;5(1):42-7.

59. Yuan F, Dellian M, Fukumura D, Leunig M, Berk DA, Torchilin VP et al. Vascular permeability in a human tumor xenograft: molecular size dependence and cutoff size. Cancer Res. 1995;55(17):3752-6.

60. Dellian M, Yuan F, Trubetskoy V, Torchilin V, Jain R. Vascular permeability in a human tumour xenograft: molecular charge dependence. Br J Cancer. 2000;82(9):1513.

61. Campbell RB, Fukumura D, Brown EB, Mazzola LM, Izumi Y, Jain RK et al. Cationic charge determines the distribution of liposomes between the vascular and extravascular compartments of tumors. Cancer Res. 2002;62(23):6831-6.

62. Geng Y, Dalhaimer P, Cai S, Tsai R, Tewari M, Minko T et al. Shape effects of filaments versus spherical particles in flow and drug delivery. Nat Nanotechnol. 2007;2(4):249-55.

63. Pluen A, Netti PA, Jain RK, Berk DA. Diffusion of macromolecules in agarose gels: comparison of linear and globular configurations. Biophys J. 1999;77(1):542-52.

64. Uzgiris E. The role of molecular conformation on tumor uptake of polymeric contrast agents. Invest Radiol. 2004;39(3):131-7.

65. Uzgiris E, Cline H, Moasser B, Grimmond B, Amaratunga M, Smith JF et al. Conformation and structure of polymeric contrast agents for medical imaging. Biomacromolecules. 2004;5(1):54-61.

66. Uzgiris EE. A cell-surface polymer reptation mechanism for tumor transendothelial transport of macromolecules. Technol Cancer Res T. 2008;7(3):257-68.

67. Dreher MR, Liu W, Michelich CR, Dewhirst MW, Yuan F, Chilkoti A. Tumor vascular permeability, accumulation, and penetration of macromolecular drug carriers. J Natl Cancer Inst. 2006;98(5):335-44.

68. Fox ME, Szoka FC, Frechet JMJ. Soluble polymer carriers for the treatment of cancer: the importance of molecular architecture. Acc Chem Res. 2009;42(8):1141-51.

69. Hawker CJ, Frechet JMJ. Comparison of linear, hyperbranched, and dendritic macromolecules. ACS Symposium Series. ACS Publications, Washington DC; 1996.

70. Lescanec RL, Muthukumar M. Configurational characteristics and scaling behavior of starburst molecules: a computational study. Macromolecules. 1990;23(8):2280-8.

71. Wooley KL, Fréchet JMJ, Hawker CJ. Influence of shape on the reactivity and properties of dendritic, hyperbranched and linear aromatic polyesters. Polymer. 1994;35(21):4489-95.

72. Edwards S. The statistical mechanics of polymerized material. Proc Phys Soc. 1967;92(1):1-9.

73. Mourey T, Turner S, Rubinstein M, Fréchet J, Hawker C, Wooley K. Unique behavior of dendritic macromolecules: intrinsic viscosity of polyether dendrimers. Macromolecules. 1992;25(9):2401-6.

74. Gillies ER, Dy E, Fréchet JMJ, Szoka FC. Biological evaluation of polyester dendrimer: poly (ethylene oxide)"bow-tie" hybrids with tunable molecular weight and architecture. Mol Pharm. 2005;2(2):129-38.

75. Nasongkla N, Chen B, Macaraeg N, Fox ME, Fre chet JMJ, Szoka FC. Dependence of pharmacokinetics and biodistribution on polymer architecture: effect of cyclic versus linear polymers. J Am Chem Soc. 2009;131(11):3842-3.

76. Chen B, Jerger K, Fréchet JMJ, Szoka Jr FC. The influence of polymer topology on pharmacokinetics: differences between cyclic and linear PEGylated poly (acrylic acid) comb polymers. J Control Release. 2009;140(3):203-9.

77. Toutain PL, Bousquet-Mélou A. Plasma terminal half-life. J Vet Pharmacol Ther. 2004;27(6):427-39.

78. Asgeirsson D, Venturoli D, Fries E, Rippe B, Rippe C. Glomerular sieving of three neutral polysaccharides, polyethylene oxide and bikunin in rat. Effects of molecular size and conformation. Acta Physiologica. 2007;191(3):237-46.

79. El-Sayed M, Kiani MF, Naimark MD, Hikal AH, Ghandehari H. Extravasation of poly (amidoamine)(PAMAM) dendrimers across microvascular network endothelium. Pharm Res. 2001;18(1):23-8.

80. Venturoli D, Rippe B. Ficoll and dextran vs. globular proteins as probes for testing glomerular permselectivity: effects of molecular size, shape, charge, and deformability. Am J of Physiol Renal Physiol. 2005;288(4):F605-13.

81. Takakura Y, Mahato RI, Hashida M. Extravasation of macromolecules. Adv Drug Deliv Rev. 1998;34(1):93-108.

82. Tomalia DA, Naylor AM, Goddard III WA. Starburst dendrimers: molecular-level control of size, shape, surface chemistry, topology, and flexibility from atoms to macroscopic matter. Angew Chem Int Ed. 1990;29(2):138-75.

83. Mansfield ML, Klushin L. Intrinsic viscosity of model starburst dendrimers. J Phys Chem. 1992;96(10):3994-8.

84. Maiti PK, Cagin T, Wang G, Goddard III WA. Structure of PAMAM dendrimers: generations 1 through 11. Macromolecules. 2004;37(16):6236-54.

85. Gu S, Zhao X, Zhang L, Li L, Wang Z, Meng M et al. Anti-angiogenesis effect of generation 4 polyamidoamine/vascular endothelial growth factor antisense oligodeoxynucleotide on breast cancer *in vitro*. J Zhejiang Univ Sci B. 2009;10(3):159-67.

86. Bhadra D, Bhadra S, Jain S, Jain N. A PEGylated dendritic nanoparticulate carrier of fluorouracil. Int J Pharm. 2003;257(1-2):111-24.

87. Kukowska-Latallo JF, Bielinska AU, Johnson J, Spindler R, Tomalia DA, Baker JR. Efficient transfer of genetic material into mammalian cells using starburst™ polyamidoamine dendrimers. Proc Natl Acad Sci U S A. 1996;93(10):4897-902.

88. Thiagarajan G, Ray A, Malugin A, Ghandehari H. PAMAM-camptothecin conjugate inhibits proliferation and induces nuclear fragmentation in colorectal carcinoma cells. Pharm Res. 2010;27:2307-16.

89. Asthana A, Chauhan AS, Diwan PV, Jain NK. Poly (amidoamine)(PAMAM) dendritic nanostructures for controlled sitespecific delivery of acidic anti-inflammatory active ingredient. AAPS PharmSciTech. 2005;6(3):536-42.

90. Yiyun C, Na M, Tongwen X, Rongqiang F, Xueyuan W, Xiaomin W et al. Transdermal delivery of nonsteroidal anti inflammatory drugs mediated by polyamidoamine (PAMAM) dendrimers. J Pharm Sci. 2007;96(3):595-602.

91. Cheng Y, Qu H, Ma M, Xu Z, Xu P, Fang Y et al. Polyamidoamine (PAMAM) dendrimers as biocompatible carriers of quinolone antimicrobials: an *in vitro* study. Eur J Med Chem. 2007;42(7):1032-8.

92. Ma M, Cheng Y, Xu Z, Xu P, Qu H, Fang Y et al. Evaluation of polyamidoamine (PAMAM) dendrimers as drug carriers of anti-bacterial drugs using sulfamethoxazole (SMZ) as a model drug. Eur J Med Chem. 2007;42(1):93-8.

93. Rupp R, Rosenthal SL, Stanberry LR. VivaGel™(SPL7013 Gel): a candidate dendrimer–microbicide for the prevention of HIV and HSV infection. Int J Nanomedicine. 2007;2(4):561.

94. Sadekar S, Ghandehari H. Transepithelial transport and toxicity of PAMAM dendrimers: implications for oral drug delivery. Adv Drug Del Rev. 2012;64(6):571-88.

95. Gupta U, Agashe HB, Asthana A, Jain N. Dendrimers: novel polymeric nanoarchitectures for solubility enhancement. Biomacromolecules. 2006;7(3):649-58.

96. D'Emanuele A, Attwood D. Dendrimer–drug interactions. Adv Drug Del Rev. 2005;57(15):2147-62.

97. Devarakonda B, Hill RA, de Villiers MM. The effect of PAMAM dendrimer generation size and surface functional group on the aqueous solubility of nifedipine. Int J Pharm. 2004;284(1):133-40.

98. Chauhan AS, Jain NK, Diwan PV, Khopade AJ. Solubility enhancement of indomethacin with poly (amidoamine) dendrimers and targeting to inflammatory regions of arthritic rats. J Drug Target. 2004;12(9-10):575-83.

99. Hu J, Cheng Y, Wu Q, Zhao L, Xu T. Host−guest chemistry of dendrimer-drug complexes. 2. Effects of molecular properties of guests and surface functionalities of dendrimers. J Phys Chem B. 2009;113(31):10650-9.

100. Milhem O, Myles C, McKeown N, Attwood D, D'Emanuele A. Polyamidoamine Starburst® dendrimers as solubility enhancers. Int J Pharm. 2000;197(1):239-41.

101. Markowicz M, Szymański P, Ciszewski M, Kłys A, Mikiciuk-Olasik E. Evaluation of poly (amidoamine) dendrimers as potential carriers of iminodiacetic derivatives using solubility studies and 2D-NOESY NMR spectroscopy. J Biol Phys. 2012:1-20.

102. Cheng Y, Wu Q, Li Y, Xu T. External electrostatic interaction versus internal encapsulation between cationic dendrimers and negatively charged drugs: which contributes more to solubility enhancement of the drugs? J Phys Chem B. 2008;112(30):8884-90.

103. Wiwattanapatapee R, Carreño-Gómez B, Malik N, Duncan R. Anionic PAMAM dendrimers rapidly cross adult rat intestine *in vitro*: a potential oral delivery system? Pharm Res. 2000;17(8):991-8.

104. Tajarobi F, El-Sayed M, Rege B, Polli J, Ghandehari H. Transport of poly amidoamine dendrimers across Madin-Darby canine kidney cells. Int J Pharm. 2001;215(1-2):263-7.

105. El-Sayed M, Ginski M, Rhodes C, Ghandehari H. Transepithelial transport of poly (amidoamine) dendrimers across Caco-2 cell monolayers. J Control Release. 2002;81(3):355-65.

106. El-Sayed M, Rhodes CA, Ginski M, Ghandehari H. Transport mechanism (s) of poly (amidoamine) dendrimers across Caco-2 cell monolayers. Int J Pharm. 2003;265(1-2):151-7.

107. El-Sayed M, Ginski M, Rhodes CA, Ghandehari H. Influence of surface chemistry of poly (amidoamine) dendrimers on Caco-2 cell monolayers. J Bioact Compatible Polym. 2003;18(1):7-22.

108. Jevprasesphant R, Penny J, Jalal R, Attwood D, McKeown NB, D'Emanuele A. The influence of surface modification on the cytotoxicity of PAMAM dendrimers. Int J Pharm. 2003;252(1-2):263-6.

109. Jevprasesphant R, Penny J, Attwood D, McKeown NB, D'Emanuele A. Engineering of dendrimer surfaces to enhance transepithelial transport and reduce cytotoxicity. Pharm Res. 2003;20(10):1543-50.

110. Jevprasesphant R, Penny J, Attwood D, D'Emanuele A. Transport of dendrimer nanocarriers through epithelial cells via the transcellular route. J Control Release. 2004;97(2):259-67.

111. D'Emanuele A, Jevprasesphant R, Penny J, Attwood D. The use of a dendrimer-propranolol prodrug to bypass efflux transporters and enhance oral bioavailability. J Control Release. 2004;95(3):447-53.

112. Kitchens KM, Kolhatkar RB, Swaan PW, Eddington ND, Ghandehari H. Transport of poly (amidoamine) dendrimers across Caco-2 cell monolayers: influence of size, charge and fluorescent labeling. Pharm Res. 2006;23(12):2818-26.

113. Kolhatkar RB, Kitchens KM, Swaan PW, Ghandehari H. Surface acetylation of polyamidoamine (PAMAM) dendrimers decreases cytotoxicity while maintaining membrane permeability. Bioconjug Chem. 2007;18(6):2054-60.

114. Najlah M, Freeman S, Attwood D, D'Emanuele A. *In vitro* evaluation of dendrimer prodrugs for oral drug delivery. Int J Pharm. 2007;336(1):183-90.

115. Kitchens KM, Foraker AB, Kolhatkar RB, Swaan PW, Ghandehari H. Endocytosis and interaction of poly (amidoamine) dendrimers with Caco-2 cells. Pharm Res. 2007;24(11):2138-45.

116. Pisal DS, Yellepeddi VK, Kumar A, Palakurthi S. Transport of surface engineered polyamidoamine (PAMAM) dendrimers across IPEC-J2 cell monolayers. Drug Deliv. 2008;15(8):515-22.

117. Pisal DS, Yellepeddi VK, Kumar A, Kaushik RS, Hildreth MB, Guan X et al. Permeability of surface-modified polyamidoamine (PAMAM) dendrimers across Caco-2 cell monolayers. Int J Pharm. 2008;350(1-2):113-21.

118. Kolhatkar RB, Swaan P, Ghandehari H. Potential oral delivery of 7-Ethyl-10-Hydroxy-camptothecin (SN-38) using poly (amidoamine) dendrimers. Pharm Res. 2008;25(7):1723-9.

119. Kitchens KM, Kolhatkar RB, Swaan PW, Ghandehari H. Endocytosis inhibitors prevent poly (amidoamine) dendrimer internalization and permeability across Caco-2 cells. Mol Pharm. 2008;5(2):364-9.

120. Ke W, Zhao Y, Huang R, Jiang C, Pei Y. Enhanced oral bioavailability of doxorubicin in a dendrimer drug delivery system. J Pharm Sci. 2008;97(6):2208-16.

121. Sweet DM, Kolhatkar RB, Ray A, Swaan P, Ghandehari H. Transepithelial transport of PEGylated anionic poly (amidoamine) dendrimers: implications for oral drug delivery. J Control Release. 2009;138(1):78-85.

122. Lin Y, Khanafer K, El-Sayed MEH. Quantitative evaluation of the effect of poly (amidoamine) dendrimers on the porosity of epithelial monolayers. Nanoscale. 2010;2(5):755-62.

123. Goldberg D, Ghandehari H, Swaan P. Cellular entry of G3.5 poly (amido amine) dendrimers by clathrin-and dynamin-dependent endocytosis promotes tight junctional opening in intestinal epithelia. Pharm Res. 2010;27:1547-57.

124. Goldberg D, Vijayalakshmi N, Swaan P, Ghandehari H. G3.5 PAMAM dendrimers enhance transepithelial transport of SN38 while minimizing gastrointestinal toxicity. J Control Release. 2011;150:318-25.

125. Borchardt R SP, Wilson G, editor. Models for assessing drug absopriton and metabolism: Pharmaceutical biotechnology volume 8, New York, N.Y., Plenum Press, A division of Plenum Publishing Corporation; 1996.

126. Kitchens KM, El-Sayed MEH, Ghandehari H. Transepithelial and endothelial transport of poly (amidoamine) dendrimers. Adv Drug Del Rev. 2005;57(15):2163-76.

127. Roberts JC, Bhalgat MK, Zera RT. Preliminary biological evaluation of polyamidoamine (PAMAM) starburst^{TM} dendrimers. J Biomed Mater Res. 1996;30(1):53-65.

128. Malik N, Wiwattanapatapee R, Klopsch R, Lorenz K, Frey H, Weener JW et al. Dendrimers: relationship between structure and biocompatibility *in vitro*, and preliminary studies on the biodistribution of 125I-labelled polyamidoamine dendrimers *in vivo*. J Control Release. 2000;65(1-2):133-48.

129. Greish K, Thiagarajan G, Herd H, Price R, Bauer H, Hubbard D et al. Size and surface charge significantly influence the toxicity of silica and dendritic nanoparticles. Nanotoxicology. 2012;6(7):713-23.

130. Thiagarajan G, Greish K, Ghandehari H. Charge affects the oral toxicity of poly(amido amide) dendrimers. Submitted 2012.

131. Lin Y, Fujimori T, Kawaguchi N, Tsujimoto Y, Nishimi M, Zhengqi D et al. Polyamidoamine dendrimers as novel potential absorption enhancers for improving the

small intestinal absorption of poorly absorbable drugs in rats. J Control Release. 2011;149:21-8.

132. Qiu Y, Chen Y, Liu L, Zhang GGZ. Developing solid oral dosage forms: pharmaceutical theory and practice. Academic Press, London, United Kingdon; 2008.

133. Artursson P, Karlsson J. Correlation between oral drug absorption in humans and apparent drug permeability coefficients in human intestinal epithelial (Caco-2) cells. Biochem Biophys Res Commun. 1991;175(3):880-5.

134. Najlah M, Freeman S, Attwood D, D'Emanuele A. Synthesis, characterization and stability of dendrimer prodrugs. Int J Pharm. 2006;308(1-2):175-82.

135. Vijayalakshmi N, Ray A, Malugin A, Ghandehari H. Carboxyl-terminated PAMAM-SN38 conjugates: synthesis, characterization, and *in vitro* evaluation. Bioconjug Chem. 2010;21:1804-10.

136. Singer JW, Vries P, Bhatt R, Tulinsky J, Klein P, Li C et al. Conjugation of camptothecins to poly(l-glutamic acid). Ann N Y Acad Sci. 2000;922(1):136-50.

137. Fox ME, Guillaudeu S, Fre chet JMJ, Jerger K, Macaraeg N, Szoka FC. Synthesis and *in vivo* antitumor efficacy of PEGylated poly (l-lysine) dendrimer- camptothecin conjugates. Mol Pharm. 2009;6(5):1562-72.

138. Huang X, Wu Z, Gao W, Chen Q, Yu B. Polyamidoamine dendrimers as potential drug carriers for enhanced aqueous solubility and oral bioavailability of silybin. Drug Dev Ind Pharm. 2011;37(00):419-27.

139. DeMario MD, Ratain MJ. Oral chemotherapy: rationale and future directions. J Clin Oncol. 1998;16(7):2557-67.

140. Terwogt JMM, Schellens JHM, Huinink WW, Beijnen JH. Clinical pharmacology of anticancer agents in relation to formulations and administration routes. Cancer Treat Rev. 1999;25(2):83-101.

141. Liu LF, Desai SD, LI TKUN, Mao Y, Sun M, SIM SAIP. Mechanism of action of camptothecin. Ann N Y Acad Sci. 2000;922(1):1-10.

142. Burke TG, Mi Z. The structural basis of camptothecin interactions with human serum albumin: impact on drug stability. J Med Chem. 1994;37(1):40-6.

143. Hatefi A, Amsden B. Camptothecin delivery methods. Pharm Res. 2002;19(10):1389-99.

144. Drengler RL, Kuhn JG, Schaaf LJ, Rodriguez GI, Villalona-Calero MA, Hammond LA et al. Phase I and pharmacokinetic trial of oral irinotecan administered daily for 5 days every 3 weeks in patients with solid tumors. J Clin Oncol. 1999;17(2):685.

145. Colon Cancer Treatment. National Cancer Institute. Available from: http://www.cancer.gov/cancertopics/pdq/treatment/colon/HealthProfessional#Section_506. Accessed: 12/26/12

146. Soepenberg O, Dumez H, Verweij J, de Jong FA, de Jonge MJA, Thomas J et al. Phase I pharmacokinetic, food effect, and pharmacogenetic study of oral irinotecan given as semisolid matrix capsules in patients with solid tumors. Clin Cancer Res. 2005;11(4):1504.

147. Rothenberg ML. Irinotecan (CPT-11): recent developments and future directions-colorectal cancer and beyond. Oncologist. 2001;6(1):66.

CHAPTER 3[1]

COMPARATIVE BIODISTRIBUTION OF PAMAM-OH DENDRIMERS AND HPMA COPOLYMERS

3.1. Introduction

Biocompatible water-soluble polymers have been widely used for biomedical applications such as drug-delivery and *in vivo* imaging [1]. Conjugation of anticancer drugs to polymers has facilitated increased efficacy due to longer blood circulation and preferential accumulation in solid tumors as per the enhanced permeability and retention (EPR) effect [2]. Polymeric prodrugs have also been actively targeted to receptors of malignant cells or endothelial cells of the tumor to increase site-specific localization [3-5]. Owing to the stealth properties of water-soluble polymers and their ability to passively and/or actively target solid tumors, polymer therapeutics demonstrate reduced toxicity and higher maximum tolerated doses than small MW anticancer drugs [6]. Polymeric carriers may be linear such as poly(*N*-(2-hydroxypropyl)methacrylamide) (HPMA) or branched such as poly (amido amine) or PAMAM dendrimers (Figure 3-1).

---

[1]Note- Reprinted with permission from S. Sadekar, A. Ray, M. Janàt-Amsbury, C. M. Peterson, H. Ghandehari, Comparative Biodistribution of PAMAM Dendrimers and HPMA Copolymers in Ovarian-Tumor-Bearing Mice, *Biomacromolecules,* 2011, *12*, 88–96. Copyright 2011 American Chemical Society.

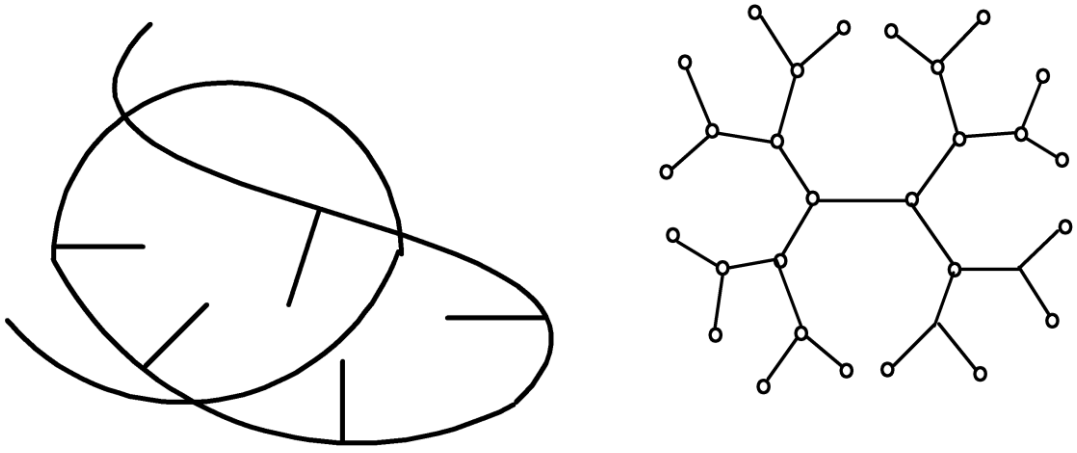

Figure 3-1. Schematics of linear random coil HPMA copolymer with side chains (left) and branched PAMAM dendrimer (right).

Copolymers of *N*-(2-hydroxypropyl)methacrylamide (HPMA) with drugs, targeting moieties and imaging modalities have been well characterized for the influence of comonomer structure and composition on solution properties and *in vivo* biodistribution [3-5] . Attachment of drugs and targeting moieties alters the random coil conformation of the HPMA homopolymer into a more folded structure, thereby reducing hydrodynamic size, circulation half-live and tumor accumulation [7]. The charge on the polymer side chains also affects half-life and biodistribution with charged HPMA copolymers being excreted more rapidly than their neutral counterparts [8].

Hyperbranched polymers such as PAMAM dendrimers have shown promise as drug carriers for targeted delivery to solid tumors, owing to the nature of synthesis, an extraordinary level of structural control that is achieved for these constructs [9-12]. The extent of branching, and nature and number of surface groups have been correlated with toxicity and biodistribution [13-15]. Lower generation PAMAM dendrimers have flexible scaffolding, whereas the higher generation systems have a globular, rigid surface [10]. The lower generation PAMAM dendrimers are excreted through the kidneys whereas the higher generation ones are excreted either by liver alone or by a combination of renal and hepatic routes [10]. The nature of surface groups influences dendrimer charge, which in turn, is correlated to toxicity both *in vitro* and *in vivo* [14, 16, 17]. The cationic, amine terminated PAMAMs are more toxic than their anionic or neutral counterparts [14, 16].

Majority of the anticancer water-soluble polymer-drug conjugates in clinical trials have so far been linear in architecture [18]. The EPR effect, therefore, has been better studied for polymer-drug conjugates with a linear backbone as compared to branched polymeric carriers. Recent work has focused on the influence of polymer architecture on

tumor targeting and drug delivery [19]. A systematic comparison of the effect of polymer architecture on biodistribution, tumor localization, *in vivo* toxicity and elimination will aid in a rational, pharmacokinetically-guided design of an anticancer drug delivery system.

The purpose of this study was to conduct a head to head comparison of the *in vivo* fate of PAMAM dendrimers with linear HPMA copolymers in order to understand the influence of polymer architecture on biodistribution in tumor-bearing mice. This comparison has been done under consistent experimental conditions of polymer characterization and animal model used for biodistribution thus providing valid comparative data of the biodistribution of the two polymer types. The animal model of choice is an orthotopic ovarian tumor model, which is an improvement over widely used xenograft tumor models and better simulates ovarian malignancy. Biodistribution studies were performed by dosing mice with ^{125}Iodine-labeled PAMAM dendrimers and HPMA copolymers of comparable molecular weights. All major organ systems, carcass and excreta were collected at defined time points. Radiolabeled polymers were detected in organ systems by measuring gamma emission of the ^{125}Iodine radiolabel.

Attachment of probes to a polymeric carriers is known to affect size, shape and physicochemical properties of the carrier and this would introduce a separate variable in a head to head comparison study [8]. The influence of architecture on drug loading, drug release, cellular delivery and pharmacological activity *in vitro* has been investigated previously [20]. In this study, we have evaluated the influence of polymer architecture on *in vivo* fate in orthotopic tumor-bearing mouse models. The study has implications in rational choice of polymeric carriers for drug delivery.

3.2. Materials

PAMAM-OH generations 5.0, 6.0 and 7.0 were purchased from Sigma Aldrich (St. Louis, MO, USA). N-Succinimidyl-3-(4-hydroxy-3-[^{125}I] iodophenyl) propionate (^{125}Iodine labeled Bolton Hunter reagent) and radioactive sodium iodide (Na^{125}I) were purchased from American Radiolabeled Chemicals (St. Louis, MO, USA). 6-8 weeks old Nu/Nu mice were purchased from Charles River Laboratories (Wilmington, MA, USA). A2780 was procured from American Type Culture Collection (Manassas, Virginia). HPMA homopolymer standards were a gift from Dr. Jindrich Kopecek's laboratory at the University of Utah.

3.3. Methods

3.3.1. Polymer synthesis and fractionation

HPMA copolymers were synthesized and fractionated to obtain weight average MW of 26 and 52 kDa and 131 kDa in order to have comparable molecular weights with PAMAM-OH: G5.0-OH, G6.0-OH and G7.0-OH (Table 3-1). The HPMA copolymers of 26, 52 and 131 kDa were synthesized with 20, 20 and 5 mole percent glycine-glycine-ethanolamine respectively in order to provide a linear polymer backbone with pendant groups, that facilitate drug loading mimicking previously studied polymers (Figure 3-2 & 3-3) [4, 21]. Since the glycine-glycine-ethanolamine side chains are hydrophilic in nature, we do not expect 5-20 mole percent of these side chains to affect the random coil architecture of the HPMA copolymers. The side chains were terminated in hydroxyl groups, similar to terminal groups of PAMAM-OH dendrimers under study to minimize the influence of the chemical nature of side chains and terminal groups on biodistribution.

Table 3-1. Composition of HPMA-based copolymers

Monomer	**HPMA copolymer (26 kDa)**		**HPMA copolymer (52 kDa)**		**HPMA copolymer (131 kDa)**		**HPMA homopolymer**	
	Feed mole %	mmol/g polymer	Feed mole %	mmol/g polymer	Feed mole %	mmol/g polymer	Feed mole %	mmol/g polymer
MA-Tyr-$COCH_3$	2	0.11 0.04#	2	0.12 0.22#	0	0	0	0
MA-Tyr-$CONH_2$	0	0	0	0	2	0.13	1	0.07
MA-GG-EtOH	0	0	20	1.2	0	0	0	0
MA-GG-TT	0	0	0	0	5	0.33	0	0
MA-GG-ONP	20	1.1	0	0	0	0	0	0
HPMA	78	4.30	78	4.71	93	6.07	99	6.85

Numbers are theoretical values based on feed mole composition; # Measured values based on amino acid analysis

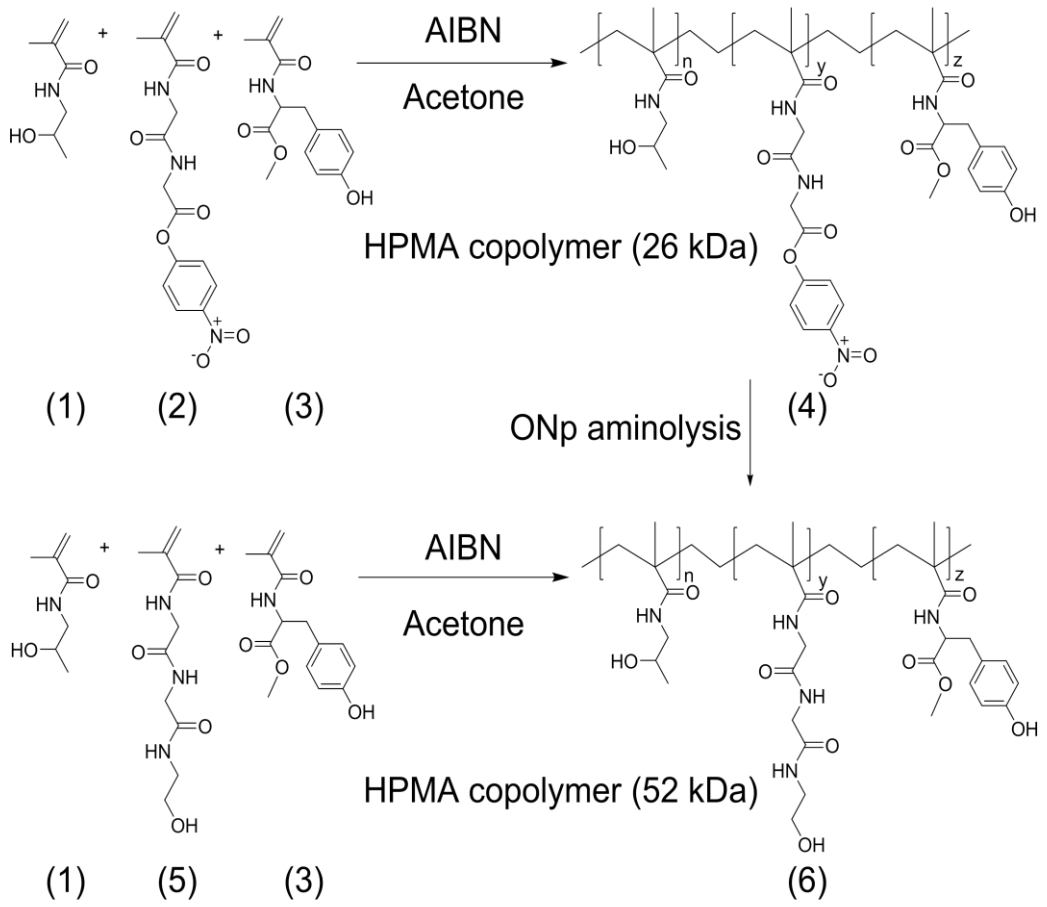

Figure 3-2. Synthetic scheme of HPMA copolymers (26 and 52 kDa).
Copolymerization of the comonomers of HPMA (1), MA-GG-ONp (2) and MA-Tyr-$COCH_3$ (3) by free radical precipitation copolymerization with azobisisobutyronitrile (AIBN) as the initiator to form low MW HPMA copolymer (26 kDa) poly(HPMA-*co*-(MA-GG-ONp)-*co*-(MA-Tyr-$COCH_3$) (4) (Feed composition in Table 3-1). ONP aminolysis of (4) with ethanolamine to form low MW poly(HPMA-*co*-(MA-GG-EtOH)-*co*-(MA-Tyr-$COCH_3$) (6). Copolymerization of the comonomers HPMA (1), MA-GG-EtOH (5) and MA-Tyr-$COCH_3$ (3) by free radical precipitation copolymerization with azobisisobutyronitrile (AIBN) as the initiator to form HPMA copolymer (52 kDa) poly(HPMA-*co*-(MA-GG-EtOH)-*co*-(MA-Tyr-$COCH_3$) (6) (Feed composition in Table 3-1).

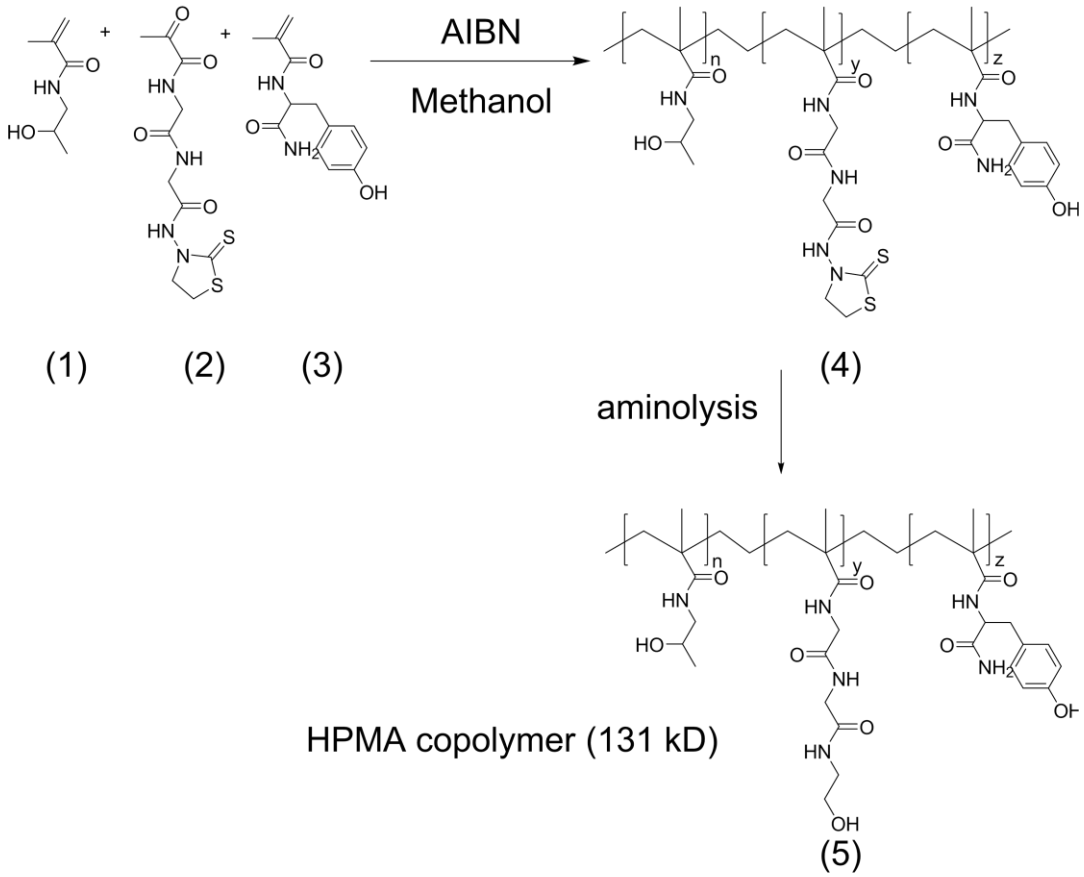

Figure 3-3. Synthetic scheme of HPMA copolymers (131 kDa).
Copolymerization of the comonomers HPMA (1), MA-GG-TT (2) and MA-Tyr-$CONH_2$ (3) by free radical precipitation copolymerization with azobisisobutyronitrile (AIBN) as the initiator to form high MW HPMA copolymer poly(HPMA-*co*-(MA-GG-TT)-*co*-(MA-Tyr-$CONH_2$) (4) (Feed composition in Table 3-1). ONP aminolysis of (4) with ethanolamine to form HPMA copolymer (131 kDa) poly(HPMA-*co*-(MA-GG-EtOH)-*co*-(MA-Tyr-$CONH_2$) (5)

The comonomers *N*-(2-hydroxypropyl)methacrylamide (HPMA), *N*-methacryloyl-glycylglycyl-para-nitrophenyl ester (MA-GG-ONp), and *N*-methacryloyl-glycylglycyl-ethanolamine (MA-GG-EtOH), *N*-methacryloyl-glycylglycyl-thiazolidine-2-thione (MA-GG- TT), *N*-methacryloyl tyrosine-methyl ester (MA-Tyr-$COCH_3$) and *N*-methacryloyl tyrosinamide (MA-Tyr-$CONH_2$) were synthesized by previously reported procedures [22]. To synthesize the lower molecular weight HPMA copolymer of 26 kDa, poly(HPMA-*co*-(MA-GG-ONp)-*co*-(MA-Tyr-$COCH_3$), the comonomers HPMA (78 mole %), MA-GG-ONp (20 mole %) and MA-Tyr-$COCH_3$ (2 mole %) were copolymerized by free radical precipitation copolymerization with azobisisobutyronitrile (AIBN) as the initiator at 50^0C for 24 hours using acetone with 10% dimethyl sulfoxide as the solvent and 12.5 weight % monomer and 0.6 weight % initiator concentration (Table 3-1). The copolymer was reacted with ethanolamine at room temperature for 3-4 hours to yield hydroxyl-terminated side chains (Figure 3-2). To synthesize the higher molecular weight HPMA copolymer of 52 kDa, poly(HPMA-*co*-(MA-GG-EtOH)-*co*-(MA-Tyr-$COCH_3$), the comonomers HPMA (78 mole %), MA-GG-EtOH (20 mole %) and MA-Tyr-$COCH_3$ (2 mole %) were copolymerized by free radical precipitation copolymerization with AIBN as the initiator at 50^0C for 24 hours using acetone with 10% dimethyl sulfoxide as solvent and 12.5 weight % monomer and 0.6 weight % initiator concentration (Table 3-1, Figure 3-2). To synthesize the high molecular weight HPMA copolymer of 131 kDa, poly(HPMA-*co*-(MA-GG-TT)-*co*-(MA-Tyr-$CONH_2$), the comonomers HPMA (93 mole %), MA-GG-TT (5 mole %) and MA-Tyr-$CONH_2$ (2 mole %) were copolymerized by free radical precipitation copolymerization with azobisisobutyronitrile (AIBN) as the initiator at 50^0C for 24 hours using methanol as the

solvent and 18.5 weight % monomer and 0.5 weight % initiator concentration (Table 3-1). The copolymer was reacted with ethanolamine at room temperature for 3-4 hours to yield hydroxyl-terminated side chains (Figure 3-3). The HPMA copolymers and PAMAM G7.0-OH were fractionated by Size Exclusion Chromatography using a Fast Protein Liquid Chromatography system with a Hiload 16/60 Superdex^{TM} preparatory grade column and an ultraviolet detector (GE Healthcare, Piscataway, NJ). PAMAM G5.0-OH and G6.0-OH eluted as monodisperse peaks in a size exclusion chromatograph and did not need to be fractionated. The mobile phase for fractionation was 20% (v/v) acetonitrile and 80% (v/v) phosphate buffer saline (137 mM NaCl, 2.7 mM KCl, 10 mM Na_2HPO_4, 1.76 mM KH_2PO_4, pH 7.4) at a flow rate of 0.5 mL/minute. Eluted peaks were detected at a wavelength of 280 nm.

3.3.2. Polymer characterization

The chromatographic elution profiles of all the HPMA copolymers and PAMAM-OH dendrimers under study were obtained using a Fast Protein Liquid Chromatography (FPLC) system with Superose 6^{TM} 10/300 GL column (GE Healthcare, Piscataway, NJ) and an ultraviolet detector (GE Healthcare, Piscataway, NJ) in order to evaluate relative elution volumes and to check for the absence of small molecular weight impurities (Appendix A). The mobile phase for elution was 20% (v/v) acetonitrile and 80% (v/v) phosphate buffer saline (137 mM NaCl, 2.7 mM KCl, 10 mM Na_2HPO_4, 1.76 mM KH_2PO_4, pH 7.4) at a flow rate of 1.0 mL/minute. Eluted peaks were detected at a wavelength of 280 nm. The molecular weights and molecular weight distributions of the fractionated HPMA copolymers were estimated on the same FPLC setup using HPMA

homopolymer standards of known molecular weights. The molecular weight distribution profile was estimated using multiangle light scattering setup attached to the FPLC system using a Dynamic Light Scattering (DLS) detector (Helleos II) attached to the FPLC system and analyzed using Astra^{TM} 5.3.4.13 software (Wyatt Technologies, Santa Barbara, CA). The HPMA copolymers, HPMA homopolymer standards and PAMAM-OH dendrimers were further characterized for hydrodynamic radius (R_h) using a Dynamic Light Scattering (DLS) detector (Helleos II) attached to the FPLC system and analyzed using Astra^{TM} 5.3.4.13 software (Wyatt Technologies, Santa Barbara, CA). The tyrosine content in the HPMA copolymers of 26 and 52 kDa was analyzed by amino acid analysis (University of Utah Core Facility). The zeta potential of polymers dispersed in distilled (DI) water at a concentration of 5.0 mg/ml was measured using a Malvern Instruments Zetasizer Nano ZS (Westborough, MA).

3.3.3. Radiolabeling of polymers

The fractionated HPMA copolymers, containing tyrosine methyl ester in the side chains, were reacted with Na^{125}I (American Radiolabeled Chemicals, St. Louis, MO) at room temperature in phosphate buffer (pH7.4, 0.02M) for 30 minutes with intermittent shaking. Ten mg of HPMA copolymer was reacted with 2 millicurie (mCi) of Na^{125}I, dissolved in 0.5 mL of buffer each making up a reaction volume of 1.0 mL. PAMAM dendrimers were reacted with 2200 Ci/mmol of ^{125}Iodine-labeled Bolton Hunter reagent (American Radiolabeled Chemicals, St. Louis, MO) over ice in Borate Buffer (pH 8.5, 0.05M) for 30 minutes with intermittent shaking [15]. 10 mg of PAMAM dendrimer was reacted with 1 mCi of ^{125}Iodine labeled Bolton Hunter reagent, dissolved in 0.5 mL of

buffer each reaching a reaction volume of 1.0 mL. The radiolabeled polymers were dialyzed using clear cellulose ester FloatALyzer® tubes with a cutoff of 3.5 to 5.0 kDa (Spectrum® Laboratories Inc., Houston, TX) against five-4 Liter changes of deionised water over a period of 5 days (one water change per day). Upon dialysis, they were checked for absence of free iodine using a PD-10 size exclusion chromatography column (GE Healthcare, Piscataway, NJ) before use (Appendix A). Following dialysis of the reaction volume, the HPMA copolymers showed a specific radioactivity of 1.35 microcurie/mg and the PAMAM dendrimers exhibited radioactivity of 4.5 microcurie/mg of polymer, as measured by a Gamma counter (Cobra Autogamma, Perkin Elmer, Wellesley, MA).

3.3.4. Animal model and tumor inoculation

Six- to eight-week old female Nude/Nude (Nu/Nu) mice were orthotopically inoculated by injecting a cell suspension of $1x10^6$ A2780 cells in 10μL of phosphate buffer saline directly beneath the left ovarian bursa for all the study groups except PAMAM G7.0-OH [23]. Animals used to assess the biodistribution of G7.0-OH were inoculated with $2x10^5$ A2780 cells. The tumor sizes at the time of animal sacrifice and organ harvesting were in the same range as those obtained by inoculation of $1x10^6$ cells for other groups. The non-metastatic tumors were allowed to grow for 4 weeks. Tumor size was monitored by palpating the tumors and by change in animal weight. All animal experiments were performed in accordance with the University of Utah IACUC guidelines with approved protocols.

3.3.5. Biodistribution

Five groups of tumor-bearing mice were dosed intravenously by tail vein injection with 50 mg/Kg of radiolabeled G5.0-OH, HPMA copolymer (26 kDa), 40 mg/Kg of HPMA copolymer (52 kDa) and 20 mg/Kg of HPMA copolymer (131 kDa), PAMAM G6.0-OH, and G7.0-OH in 0.2 mL sterile saline. The solution of radiolabeled polymers was mixed with accurately weighed nonradiolabeled polymers in saline to prepare a radioactive dose of about 50,000 cpm per animal. The amount of polymer contributed by the radiolabeled polymer solution in preparing the dose was considered negligible. The mice were sacrificed at defined time points of 5 minute, 30 minute, 2 hour, 6 hour, 24 hour and 1 week. All major organ systems were collected including blood, heart, lung, liver, spleen, kidney, tumor, contralateral ovary, brain and the rest of the carcass that included skin, muscle and intestines. Urine and stool were collected by housing animals in metabolic cages and were pooled for all the animals for a given study group at a particular time point. Blood and homogenized carcass were sampled whereas the rest of the organs collected were measured as a whole for radioactive count using a Gamma counter (Cobra Autogamma, Perkin Elmer, Wellesley, MA). All animal experiments were performed in accordance with the University of Utah IACUC guidelines under approved protocols.

3.3.6. *In vivo* data analysis

The radioactive readings obtained for the individual organs were expressed as a percentage of injected dose normalized to weight of the organ. Statistical Analysis was done using Analysis of Variance (Graphpad Prism®, version 5.01).

3.4. Results and discussion

3.4.1. Characteristics of the polymers

The PAMAM-OH dendrimers under study were generations 5.0, 6.0 and 7.0 with hydroxyl surface groups. These generations were chosen such that their molecular weights (29, 58 and 117 kDa) lie in the physiologically relevant range for kidney filtration, extended plasma circulation and tumor retention. The HPMA copolymers were synthesized and fractionated in order to have comparable molecular weights with the PAMAM-OH dendrimers. The HPMA copolymers were synthesized with 5-20 mole percent glycine-glycine-ethanolamine side chains in order to provide the linear polymer backbone with pendant groups that typically facilitate the attachment of bioactive and imaging agents [4, 21]. The polymeric side chains terminated in hydroxyl groups, similar to the terminal groups of PAMAM-OH dendrimers under study in order to minimize the influence of surface or pendant functional group characteristics on comparative biodistribution.

Polymer architecture affected molecular conformation and hence hydrodynamic size of the PAMAM dendrimers and HPMA copolymers of comparable molecular weights. The increment in hydrodynamic size (R_h) of HPMA copolymers with increase in molecular weight (MW) was greater than the increment in R_h of PAMAM dendrimers with the same increments in MW (Figure 3-4).

Below a MW of about 40 kDa, PAMAM G5.0-OH (MW = 29 kDa) was larger (R_h = 2.3 nm) than HPMA copolymer of comparable MW (MW= 26 kDa, R_h = 1.4 nm) (Table 3-2). Above this cutoff of 40 kDa, the opposite trend was observed. PAMAM G6.0-OH (MW = 58 kDa, R_h = 3.0 nm) was smaller than HPMA copolymer of

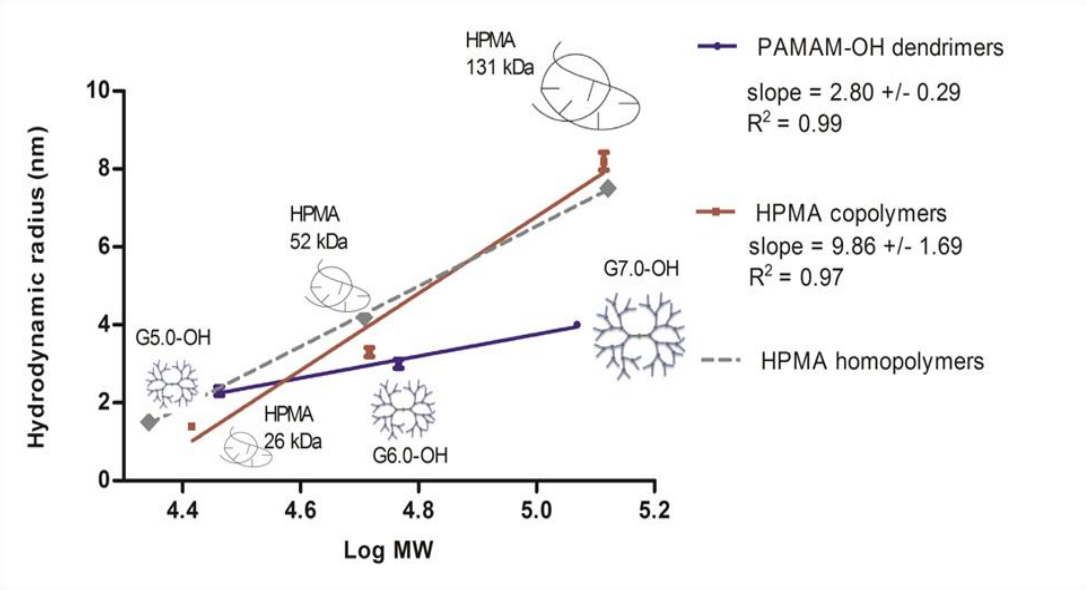

Figure 3-4. Correlation of molecular weight with hydrodynamic radius of PAMAM-OH dendrimers, HPMA copolymers and HPMA homopolymer standards. Values are mean +/- S.D.; n=3.

Table 3-2. Characterization of PAMAM dendrimers and HPMA copolymers

Polymer	**G5.0-OH**	**G6.0-OH**	**G7.0-OH**	**HPMA copolymers**		
Weight average molecular weight (kDa)	28.950*	58.298*	116.993*	26.0 ± 2.0	52.0 ± 5.0	131.0 ± 0.3
Poly dispersity Index (SEC)	ND	ND	ND	1.3 ± 0.2	1.9 ± 0.2	1.7 ± 0.1
Poly dispersity Index (MALLS)	1.12 ± 0.07	1.30 ± 0.02	1.30 ± 0.01	1.20 ± 0.09	1.30 ± 0.05	1.24 ± 0.05
Hydrodynamic radius (R_h) (nm)	2.3 ± 0.2	3.0 ± 0.2	4.0 ± 0.1	1.4 ± 0.0	3.3 ± 0.2	8.2 ± 0.4
Zeta Potential (mV)	1.69 ± 0.21	2.28 ± 0.48	-1.3 ± 0.06	-14.66 ± 0.83	-1.46 ± 0.29	-19.2 ± 1.4
Number of surface hydroxyl groups	128*	256*	512*	ND	ND	ND

*Theoretical values based on perfect dendrimer synthesis [11]; Values are Mean +/- SD (n=3).

comparable MW (MW = 52 kDa, R_h = 3.3 nm) (Table 3-2). The trend was consistent amongst the higher MW polymers with the HPMA copolymer (MW = 131 kDa, Rh = 8.2 nm) being twice the hydrodynamic size of G7.0-OH (MW = 117 kDa, R_h = 4.0 nm) of comparable MW (Table 3-2). This difference in size increment with MW can be attributed to the difference in architecture of linear HPMA copolymers that have a random coil conformation compared to hyperbranched PAMAM dendrimers which are more compact.

The conformation of hyperbranched polymers such as PAMAM depends on generation with the smaller dendrimers having a flexible scaffolding and higher generations assuming a more compact, globular shape with a dense exterior and relatively hollow interior [10]. The hydrodynamic sizes of amine-terminated dendrimers measured by dilute solution viscometry, light scattering, diffusion nuclear magnetic resonance and theoretically calculated by computer simulations that have been widely reported in literature are slightly higher than the hydrodynamic sizes measured for hydroxyl-terminated dendrimers of the same generation (Table 3-1) [24-26]. This can be attributed to a more extended structure of the amine-terminated PAMAMs with charged surface groups as compared to neutral terminal groups in case of the hydroxyl terminated PAMAMs.

Depending on the chemical nature of the pendant side chains, linear polymers may possess a random-coil architecture in case of hydrophilic groups, an extended chain conformation for negatively charged moieties or a unimicellar folded structure in the case of hydrophobic side groups [3]. The HPMA copolymers under study possess hydrophilic, hydroxyl-terminated ethanolamine side chains that are not likely to disrupt the random-

coil conformation of the polymers. Upon comparing the sizes of the HPMA copolymers containing 5-20 mole % glycine-glycine ethanolamine and 2% tyrosine groups with HPMA homopolymer standards containing 1 % pendant tyrosine groups, the HPMA copolymer of 26 kDa had a hydrodynamic radius of 1.4 nm, comparable to that of the HPMA homopolymer standard (22 kDa) with a hydrodynamic radius of 1.5 nm. The HPMA copolymer of 52 kDa, however, had a hydrodynamic radius of 3.3 nm, smaller than that of the HPMA homopolymer standard (51 kDa) with a hydrodynamic radius of 4.2 nm. This can be attributed to a higher tyrosine content in the HPMA copolymer of 52 kDa (0.22 mmol tyrosine/g polymer), as measured by amino acid analysis; than the theoretical tyrosine content in the HPMA homopolymer (0.07 mmol/g polymer) (Table 3-1). An increased number of tyrosine grafts on the HPMA copolymer backbone can lead to intra-molecular, hydrophobic interactions leading to a decrease in the hydrodynamic radius of the HPMA copolymer (52 kDa). Similarly, literature reported values of hydrodynamic radii of HPMA copolymers of similar molecular weights also vary depending on nature and percentage of side chains [7]. HPMA copolymer (131 kDa) had a slightly higher hydrodynamic radius than HPMA homopolymer standard (132 kDa) with a hydrodynamic radius of 7.5 nm. HPMA copolymer of 131 kDa was noted to have a slightly negative charge due to a hydrolysis side reaction, resulting in pendent carboxylic acid groups (Table 3-2). This side reaction can occur in the final aminolysis step in the copolymer synthesis reaction that imparts a majority of hydroxyl-terminated surface groups. The slight negative charge could result in a more extended coiled structure of the HPMA copolymer. This extended structure could potentially result in a greater hydrodynamic size of the copolymer in solution.

3.4.2. *In vivo* biodistribution

The smallest of the PAMAM dendrimers under study, G5.0-OH showed predominant and persistent accumulation in the kidney compared to all other organs (Figure 3-5). G6.0-OH was taken up both by the kidney and the liver (Figure 3-6). However, it did not demonstrate extended circulation in the plasma. G7.0-OH is known to have a rigid sphere-like conformation [10]. It had a hydrodynamic radius of 4.0 nm and showed the highest plasma circulation time (Figure 3-7). This polymer was distributed over all organ systems due to retention in the plasma. Tumor accumulation profile of G7.0-OH was characteristic of macromolecules with slow accumulation that peaked at 6 hours and retained for 1 week.

Small changes in hydrodynamic size of macromolecules in the nanometer range have been known to drastically affect pharmacokinetics [27, 28]. MRI contrast agents based on PAMAM cores have shown a similar trend when increase in generation affected biodistribution, extravasation and mode of excretion [27, 28]. PAMAM based gadolinium contrast agents have shown that constructs below 6.0 nm were predominantly excreted via the kidneys, while larger constructs were taken up by the liver instead [27]. Those constructs in the size range of 5 to 8.0 nm were observed to extravasate into the tumor tissue from tumor vasculature. However, this data had limitations in quantitative interpretation owing to the detection technique (magnetic resonance). The size and conformation of the native PAMAM dendrimers of different generations may have also caused its interaction with plasma proteins, platelets and other components in the blood to differ. Detailed studies on interactions of these native PAMAM dendrimers with blood components could help better explain the effect of size and generation regarding its *in*

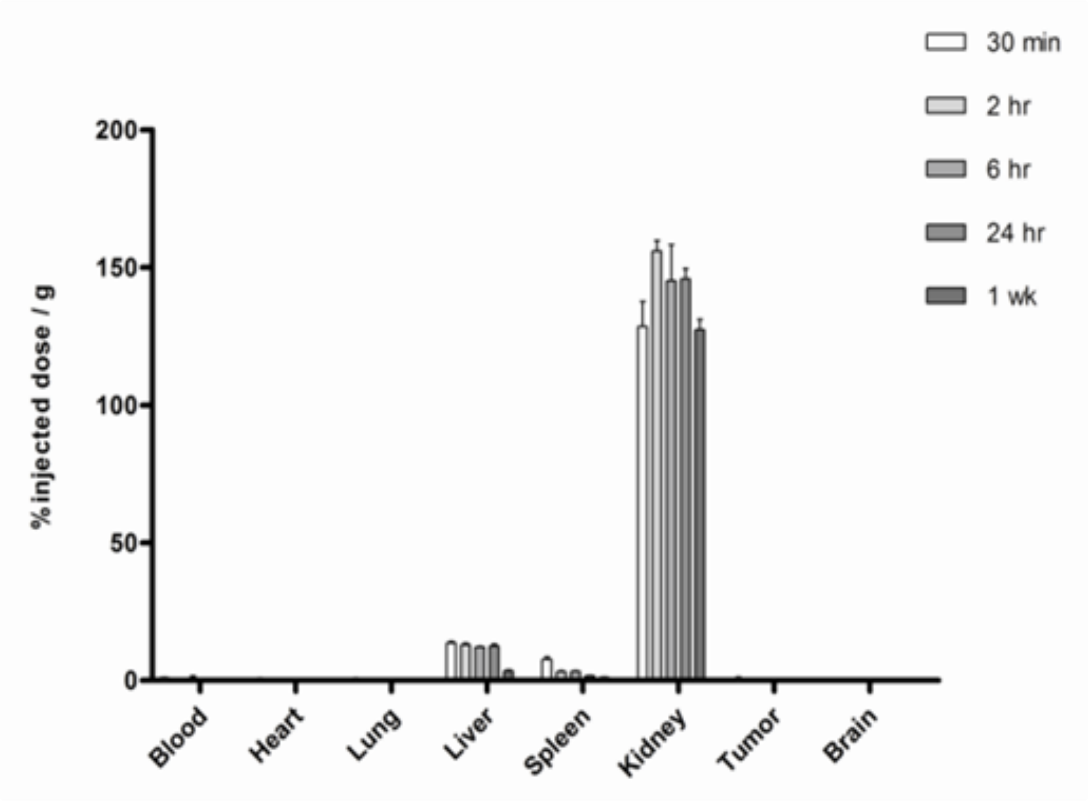

Figure 3-5. Percentage of injected dose / g of tissue for G5.0-OH in principal organs. Values are Mean +/- SEM; n=5.

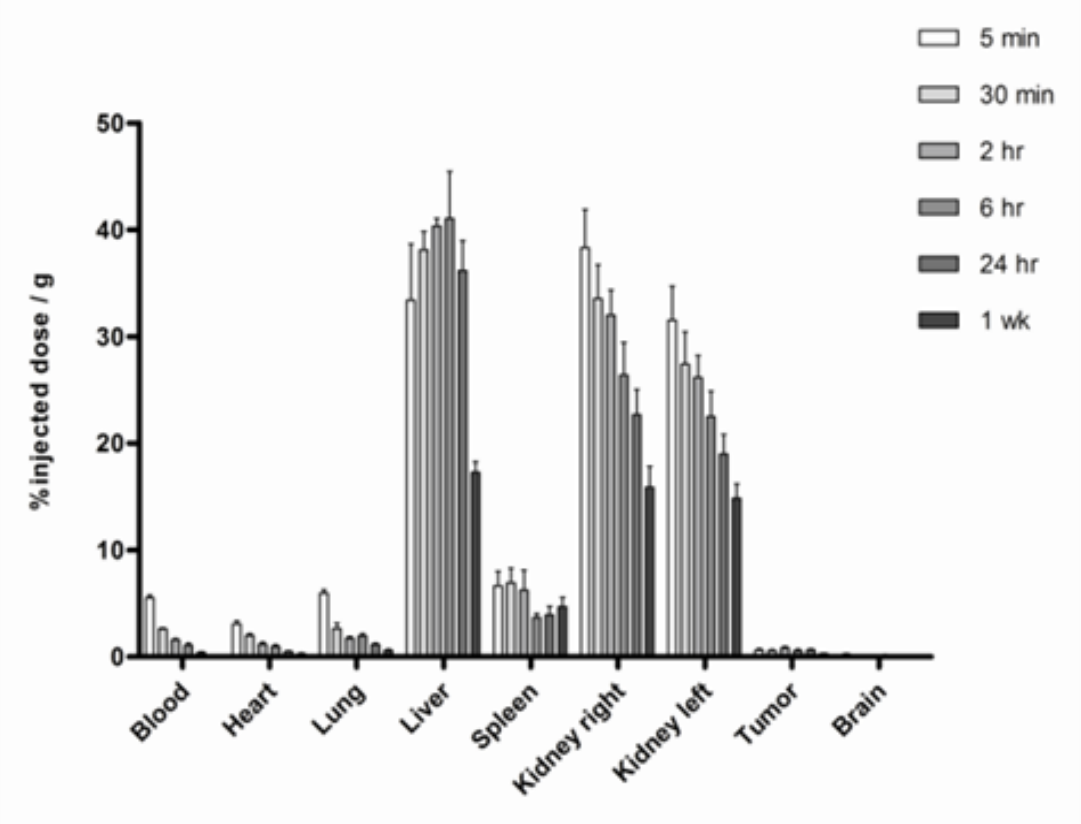

Figure 3-6. Percentage of injected dose / g of tissue for G6.0-OH; in principal organs. Values are Mean +/- SEM; n=5.

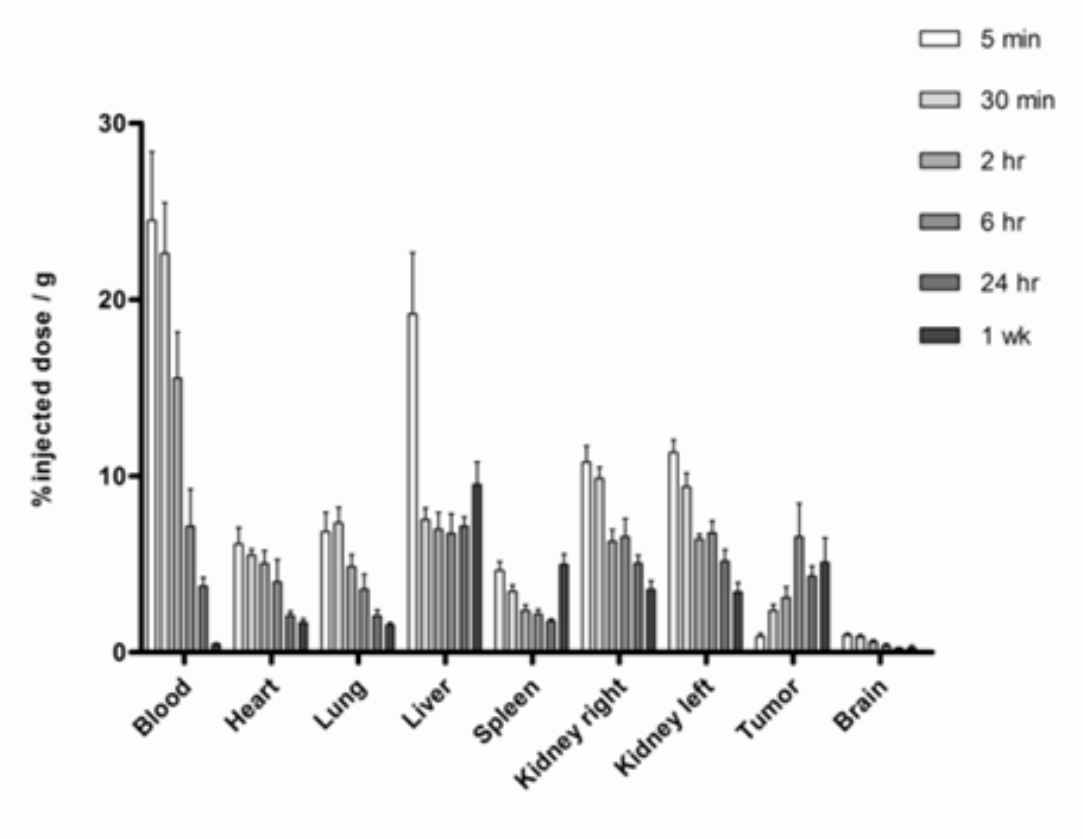

Figure 3-7. Percentage of injected dose / g of tissue for G7.0-OH in principal organs; Values are Mean +/- SEM; n=5; except n=4 for 6 hour and 24 hour.

vivo fate. HPMA copolymer of 26 kDa with the smallest hydrodynamic radius (1.4 nm) amongst the polymers tested, was excreted through the kidney (Figure 3-8) within two hours of administration and recovered in the urine (12% of injected dose, Appendix A). It showed slight kidney accumulation (20 % injected dose/g) with slow renal clearance for up to 1 week (6 % injected dose/g). A neutral HPMA copolymer with 5 mol% GFLG-OH and 0.6 mol% tyrosine in the side chains has been reported to have a similar biodistribution profile in a tumor-bearing rat model [8]. All major organ systems at one week were measured to have less than 1 % of injected dose/g including the kidneys [8]. The difference in kidney accumulation between the reported HPMA-GFLG-OH copolymer and the HPMA copolymer under study can be attributed to the electronegative charge on the HPMA copolymer under study (zeta potential of -15.0mV, Table 3-2). Reports in literature have demonstrated that ionized linear polymers accumulate in kidneys as a function of electronegative charge [29, 30]. The HPMA copolymer of 52 kDa and 131 kDa circulated in the plasma slightly longer than HPMA copolymer of 26 kDa and showed distribution in all organ systems (Figure 3-9 & 3-10). HPMA 52 kDa showed slight tumor accumulation that peaked at 6 hours but did not show prolonged retention at 24 hours. Its tumor accumulation seemed less than that reported for HPMA homopolymer of similar molecular weight studied in a tumor-bearing rat model [8]. This can be explained due to the difference in hydrodynamic radius of the HPMA copolymer (52 kDa) under study and the HPMA homopolymer standard as discussed in the polymer characterization section, thereby highlighting the importance of hydrodynamic size of the polymer in deciding the *in vivo* fate. The HPMA copolymer (52 kDa) under study was seen to be eliminated through urinary excretion with 16 % of the

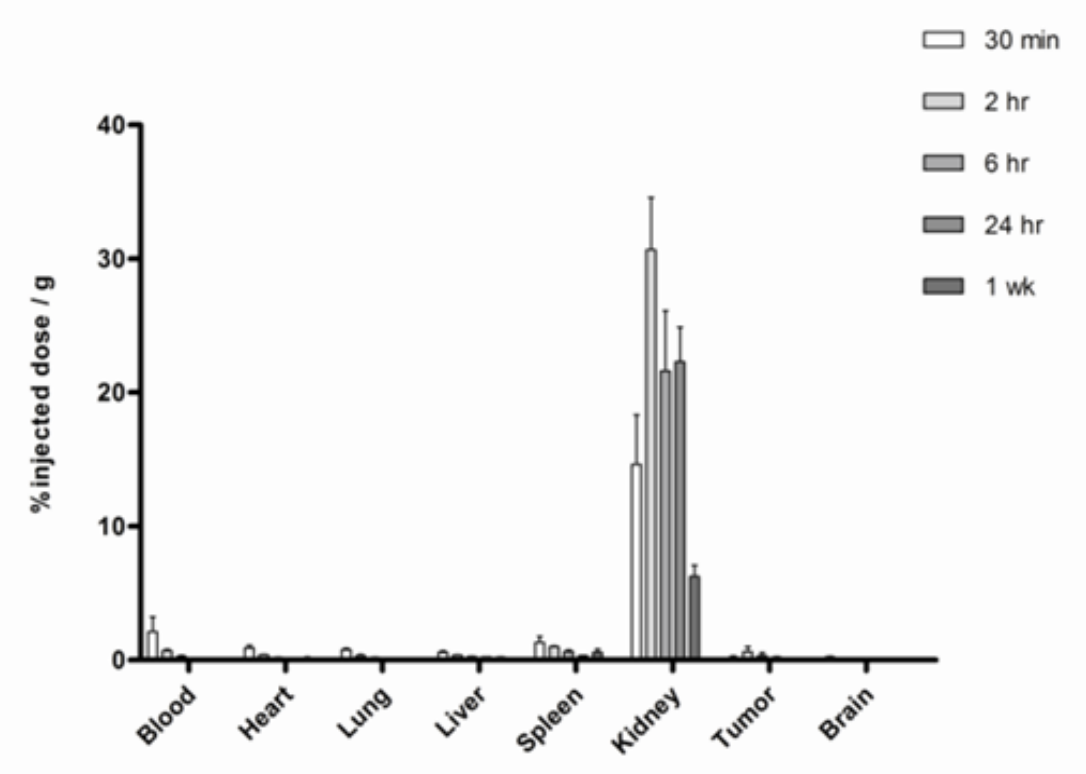

Figure 3-8. Percentage of injected dose / g of tissue for HPMA copolymer 26 kDa in principal organs; Values are Mean +/- SEM; n=5; except n=4 for 2 hour HPMA copolymer (26 kDa).

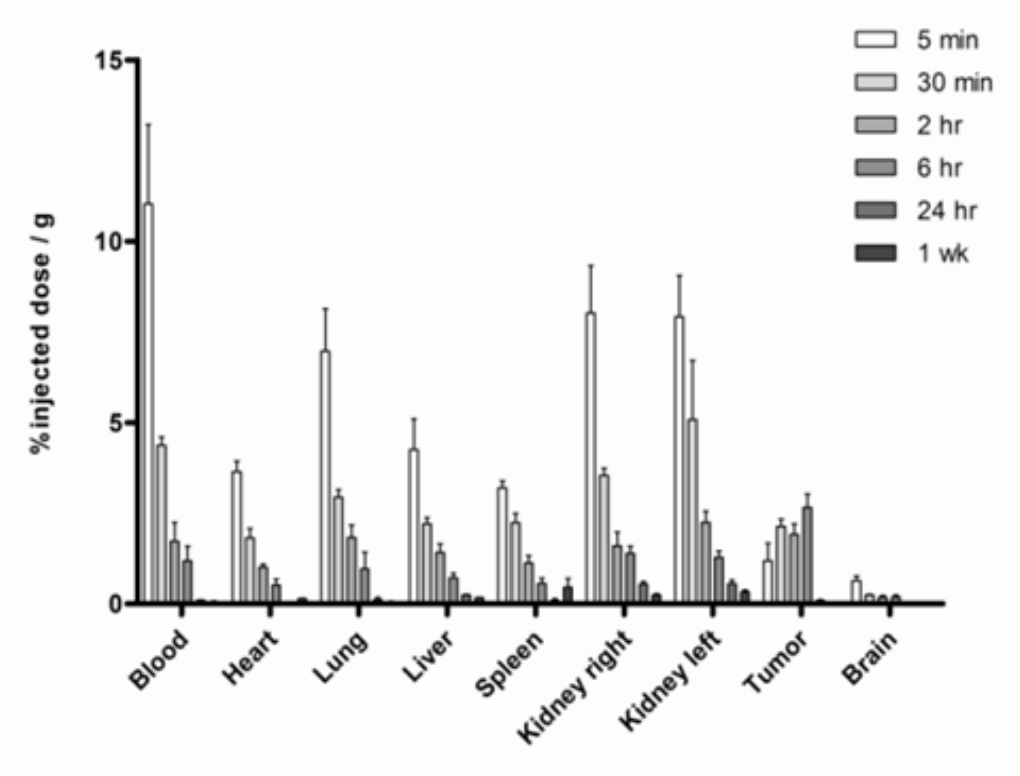

Figure 3-9. Percentage of injected dose / g of tissue for HPMA copolymer 52 kDa in principal organs; Values are Mean +/- SEM; n=5; except n=4 for 5 minute and n=3 for 1 week.

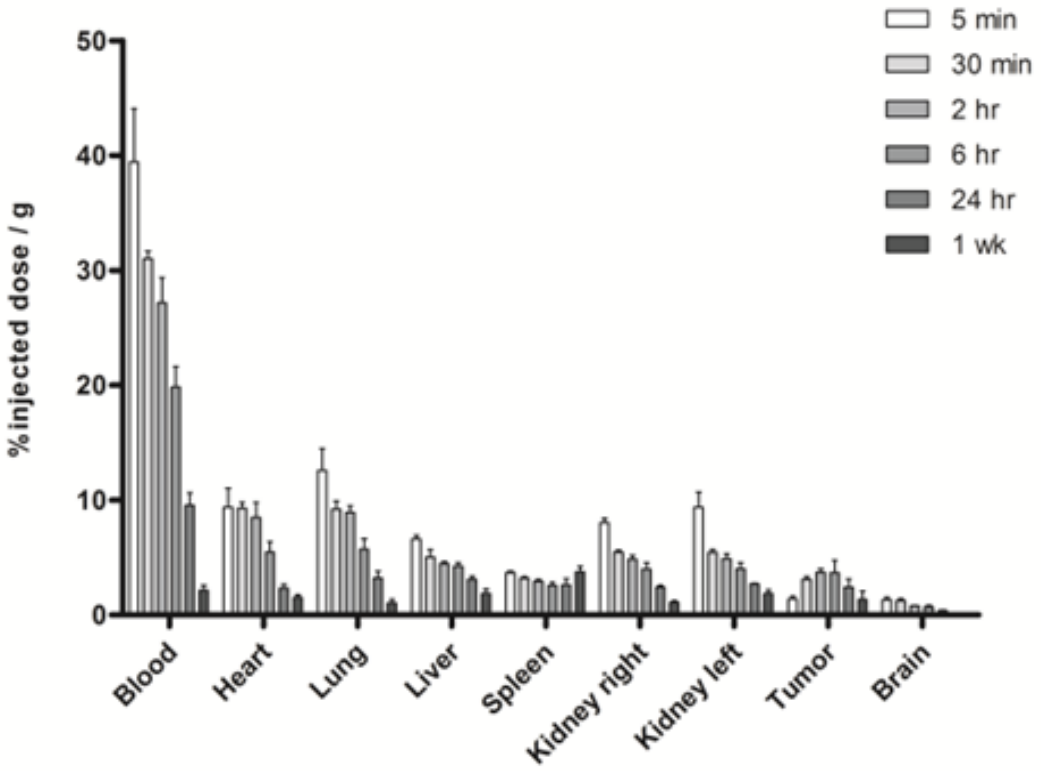

Figure 3-10. Percentage of injected dose / g of tissue for HPMA copolymer 131 kDa in principal organs; Values are Mean +/- SEM; n=3 for 5 minute, 30 minute, 2 hour; n=4 for 6 hour and n=5 for 24 hours and 1 week.

injected dose in the urine 24 hours after injection (Appendix A) and showed negligible liver accumulation. The HPMA copolymer (131 kDa) was long circulating in the plasma owing to its large hydrodynamic size. It did not show persistent kidney or liver accumulation. However, it did show characteristic tumor permeability and enhanced retention greater than the smaller HPMA copolymers (Figure 3-10). The filtration size cut-off for the kidney is known to range from a hydrodynamic diameter of 3.7 to 6.0 nm [31]. PAMAM G5.0-OH and HPMA copolymer of 26 kDa (<5.0 nm in hydrodynamic diameter) can be readily filtered through the glomeruli. We observed kidney retention for G5.0-OH for 1 week up to 150 percent injected dose/gram of tissue (Figure 3-11). HPMA copolymer of comparable molecular weight showed a lesser extent of kidney accumulation and did not persist in the kidney for a week indicating that polymer conformation affected renal reabsorption and retention. Data in literature reports 80 percent of injected dose of PAMAM dendrimer, amine terminated, generation 4.0 (G4.0-NH_2)/gram of kidney tissue, which reduced to 10 percent of injected dose/gram of kidney upon PEGylating the dendrimer [32]. It has been reported that PAMAM G4.0-gadolinium complexes accumulate in the proximal straight tubules in the outer medulla stripe of the kidney [33]. Limited mechanistic studies for renal retention of PAMAM dendrimers report the localization of these polymers in the lysosomes of proximal tubule cells [33]. This uptake is only possible upon filtration of the dendrimers, providing access to reabsorption into the proximal tubules. The biodistribution of acetylated PAMAM G5.0 has been reported and the construct has shown negligible kidney accumulation [34]. Acetylation may increase the hydrodynamic size of the PAMAM beyond the glomerular filtration cutoff (> 5.0 nm) thereby denying access to proximal tubule cells for uptake.

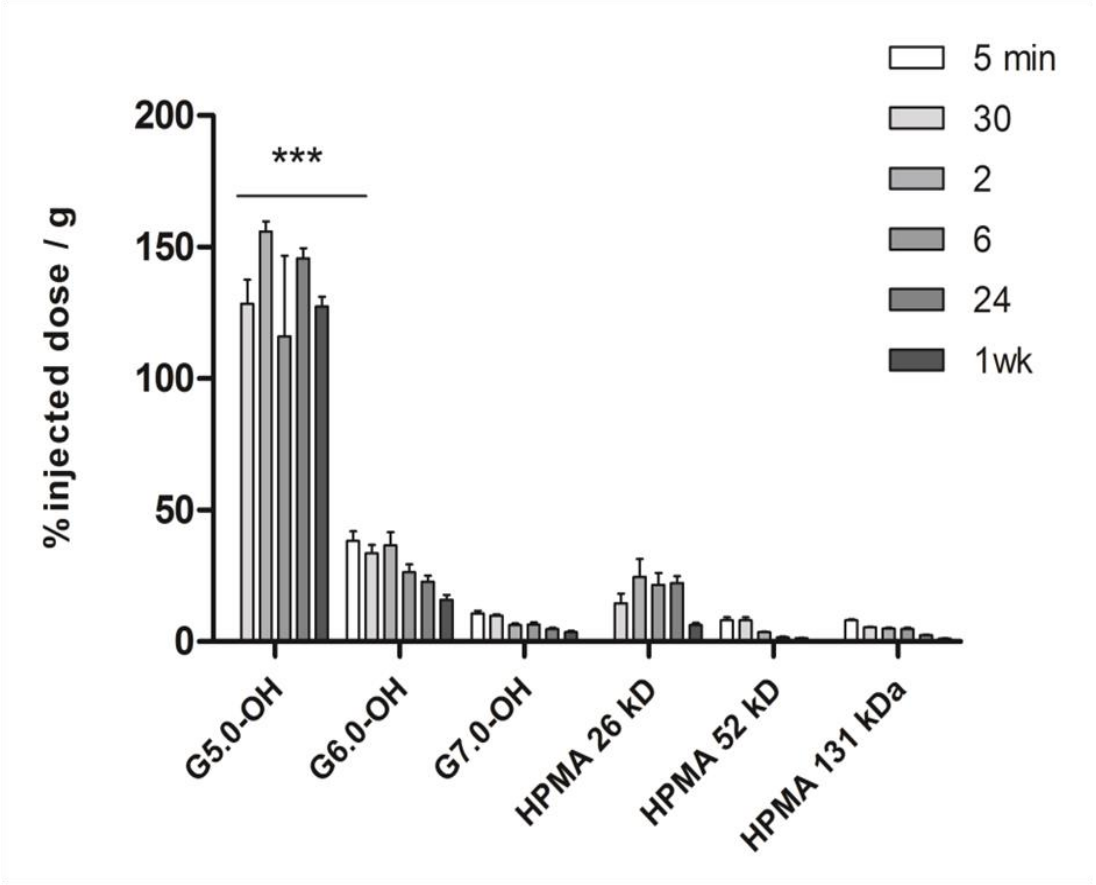

Figure 3-11. Percentage of injected dose / g of kidney tissue for PAMAM dendrimers and HPMA copolymers. Values are Mean +/- SEM; n=5; except n=4 for 5 minute HPMA copolymer (52 kDa), 2 hour HPMA copolymer (26 kDa) and G5.0-OH, 6 hour HPMA copolymer (131 kDa); 6 hour and 24 hour G7.0-OH and n=3 for 1 week HPMA copolymer (52 kDa), 5 minute, 30 minute, 2 hour HPMA copolymer (131 kDa). *** indicates a statistically significant difference as per ANOVA and Bonferroni's multiple comparison test comparing G5.0-OH with all other treatment groups, $p < 0.001$. Kidney exposure calculated by area under the curve using trapezoidal rule was statistically significantly different ($p<0.001$) for G5.0-OH compared with other treatment groups as per ANOVA and Bonferonni's multiple comparison test.

PAMAM G6.0-OH (R_h = 3.0 nm, Table 3-2) and G7.0-OH (R_h = 4.0 nm, Table 3-2) studied here are not readily filtered due to their hydrodynamic sizes being above the filtration threshold cutoff and hence do not show prolonged renal retention comparable to G5.0-OH (Figure 3-11). However, the renal accumulation of G6.0-OH was greater than HPMA copolymer of 52 kDa suggesting that polymer architecture affected renal retention (Figure 3-11). The renal uptake for PAMAM G7.0-OH is comparable to that of pegylated G4.0-NH_2 dendrimers reported in the literature [32]. This indicates that it is possible to reduce non-specific kidney uptake by increasing dendrimer generation to a hydrodynamic size beyond kidney filtration pore size cut-off. The smaller generation G5.0-OH that is observed to accumulate in the kidney may be used for kidney imaging to detect renal tubular damage [35, 33]. The constructs suggested for this application have been dendrimer-based-magnetic resonance imaging (MRI) contrast agents that are amine terminated [35, 33]. A hydroxyl-terminated dendrimer such as PAMAM G5.0-OH shows the same or higher extent of kidney accumulation and is likely to be less toxic *in vivo* than the amine terminated dendrimer of same generation [13]. Inspite of persistent kidney accumulation, PAMAM G5.0-OH did not show elevated kidney toxicity markers at 1 week (refer to Appendix A). An elevated white blood cell count was observed (refer to Appendix A). It has been observed that physicochemically modified HPMA copolymers accumulate in the kidney to a higher extent than their non-modified counterparts [8]. The introduction of peptide moieties was found to increase kidney accumulation and a direct correlation was observed between the amount of carboxyl and hydrazide groups on the HPMA copolymer and the extent of kidney localization [36]. HPMA copolymer of 26 kDa, under study, had a slightly negative zeta potential indicative of the presence of

carboxyl groups which could potentially explain its renal accumulation. HPMA copolymers functionalized with the targeting peptide RGDfK and DTPA (1,2-diamine-N,N-N′,N′,N″,N″-pentaacetic acid) chelating moiety in the side chains showed persistent kidney accumulation that correlated with the amount of peptide loading [29]. It would be interesting to study the effect of surface modification of PAMAM dendrimers with peptides on kidney accumulation and establish a systematic correlation of the same in non-linear, hyperbranched polymers.

PAMAM dendrimers (G5.0-OH and G6.0-OH) accumulated to a larger extent in the liver than HPMA copolymers of similar molecular weight (26 kDa and 52 kDa) (Figure 3-12). PAMAM G6.0-OH, with a hydrodynamic radius of 3.0 nm (Table 3-1) is on the threshold of kidney filtration size cutoff. It showed a high extent of accumulation observed in the liver (Figure 3-12). PAMAM G7.0-OH with its rigid sphere-like globular structure and a hydrodynamic radius of 4.0 nm circulates longer in the plasma than PAMAM G6.0-OH (Figure 3-12). Its liver accumulation is less than G6.0-OH at the time points under study. However, there is a possibility of an increase in RES organ uptake when the polymer may be eliminated from the tumor (beyond the range of the time points under study). It has been shown that amine terminated PAMAM Generation 4.0 and 5.0 interact with plasma proteins such as human serum albumin, bovine serum albumin and enzymes such as human erythrocyte acetyl cholinesterase and alter the protein conformation and enzyme activity [37-40]. It has also been shown that in the case of other nanoparticulate constructs, smaller particles with higher surface curvature had a better retention of the native protein structure and function than larger nanoparticles [41]. There is, therefore, a possibility that PAMAM G6.0-OH with a smaller hydrodynamic

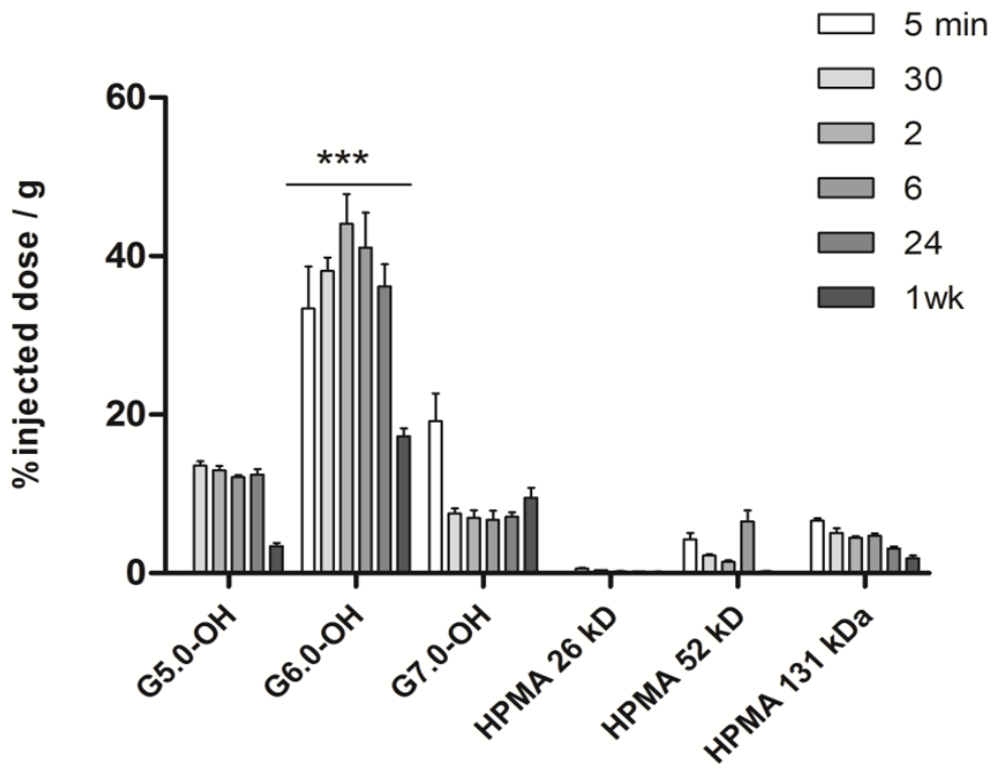

Figure 3-12. Percentage of injected dose / g of liver tissue for PAMAM dendrimers and HPMA copolymers. Values are Mean +/- SEM; n=5; except n=4 for 5 minute HPMA copolymer (52 kDa), 2 hour HPMA copolymer (26 kDa) and G5.0-OH, 6 hour HPMA copolymer (131 kDa); 6 hour and 24 hour G7.0-OH and n=3 for 1 week HPMA copolymer (52 kDa), 5 minute, 30 minute, 2 hour HPMA copolymer (131 kDa). *** indicates a statistically significant difference as per ANOVA and Bonferroni's multiple comparison test comparing G6.0-OH with all other treatment groups, $p < 0.001$. Liver exposure calculated by area under the curve using trapezoidal rule was statistically significantly different ($p<0.001$) for G6.0-OH compared with other treatment groups as per ANOVA and Bonferonni's multiple comparison test. Using the same statistical tests, liver exposure was different for PAMAM dendrimers compared to HPMA copolymers of comparable MW.

radius than G7.0-OH and a less dense surface exterior may interact differently with opsonizing proteins, causing it to be taken up by the liver. It would be necessary to investigate how the interaction of the PAMAM dendrimer with opsonizing proteins affects macrophage uptake and consequently *in vivo* fate. Accumulation of PAMAM G6.0-OH up to 40% dose/gram of liver tissue did not affect liver function as indicative of plasma levels of alanine aminotransferase and aspartate aminotransferase (data not shown). The liver accumulation of the higher molecular weight polymers of varying architecture- HPMA copolymer (131 kDa) and G7.0-OH was not different, suggesting that in this molecular weight range, polymer architecture did not affect liver uptake.

Within a given polymer series, tumor accumulation was correlated to hydrodynamic sizes as measured by dynamic light scattering. The largest dendrimer under study PAMAM G7.0-OH (R_h = 4.0 nm) showed the highest and most persistent tumor accumulation of about 4-6 percent injected dose/gram of tumor tissue up to a week (Figure 3-13). As is characteristic of the EPR effect, PAMAM G7.0-OH showed time-dependent accumulation in the tumor that peaked at 6 hours and persisted for up to 1 week with a tumor to blood ratio (T/B ratio) of about 12.75 [35, 42]. Inspite of the R_h of HPMA 131 kDa being twice that of G7.0-OH of comparable MW, the extent of tumor accumulation of HPMA copolymer of 131 kDa was less than that of G7.0-OH ($p < 0.001$). Additional studies are needed to understand the effect of the linear and hyperbranched polymer architecture on rates and extent of microvascular extravasation to explain this difference in accumulation. The extent of tumor accumulation of HPMA 52 kDa was less than the HPMA homopolymer of comparable MW reported in the literature [8]. This can be attributed to intramolecular interactions amongst tyrosine-containing side

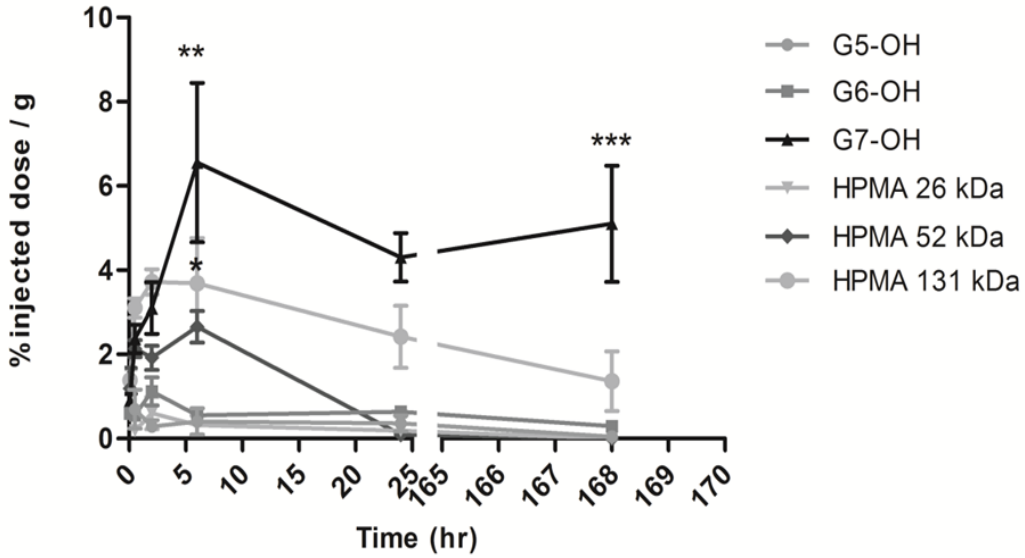

Figure 3-13. Percentage of injected dose / g of tumor tissue for PAMAM dendrimers and HPMA copolymers; Values are Mean +/- SEM; n=5; except n=4 for 5 minute HPMA copolymer (52 kDa), 2 hour HPMA copolymer (26 kDa) and G5.0-OH, 6 hour HPMA copolymer (131 kDa); 6 hour and 24 hour G7.0-OH and n=3 for 1 week HPMA copolymer (52 kDa), 5 minute, 30 minute, 2 hour HPMA copolymer (131 kDa).*/**/*** indicates a statistically significant difference with $p<0.05$, $p<0.01$ and $p < 0.001$, respectively, as per ANOVA and Bonferroni's multiple comparison test comparing G7.0-OH and HPMA 131 kDa with smaller MW polymers.

chains (0.22 mmol/g of polymer) on the HPMA copolymer leading to a decrease in hydrodynamic radius (3.3 nm, Table 3-2) as compared to 4.2 nm for the HPMA homopolymer standards, emphasizing the importance of nanoscale size variations in deciding *in vivo* fate. PAMAM G5.0-OH and HPMA copolymer of 26 kDa were cleared from circulation by kidney filtration and hence did not show tumor accumulation. The tumor accumulation data indicated a hydrodynamic radius cutoff of about 4.0 nm, below which prolonged tumor retention was not observed for the orthotopic ovarian carcinoma tumors under study. The HPMA copolymer of 52 kDa with a radius of 3.3 nm showed enhanced tumor accumulation up to 2 % injected dose/gram of tumor. However, unlike the HPMA copolymer of 131 kDa, it did not show enhanced retention. PAMAM G6.0-OH with a hydrodynamic radius of 3.0 nm did not passively target the tumor (Figure 3-13).

The plasma exposure of the polymers is consistent with the hydrodynamic sizes of the macromolecules under study (Figure 3-14). The largest carriers in each of the polymer series HPMA copolymer (131 kDa, Rh = 8.1 nm) and G7.0-OH (R_h = 4.0 nm) showed the highest plasma exposures. The extended circulation times of these polymers allowed enhanced tumor accumulation. Comparing the linear and branched polymers of similar MW, percentage of injected dose / g of plasma tissue was statistically significantly different between HPMA copolymer (131 kDa) and G7.0-OH (117 kDa) of comparable molecular weights with the HPMA showing longer plasma circulation than PAMAM. This can be attributed to the hydrodynamic size of the HPMA copolymer being twice that of PAMAM. HPMA copolymer of 52 kDa circulated in the plasma for a slightly longer duration than PAMAM G6.0-OH of comparable MW. This can be

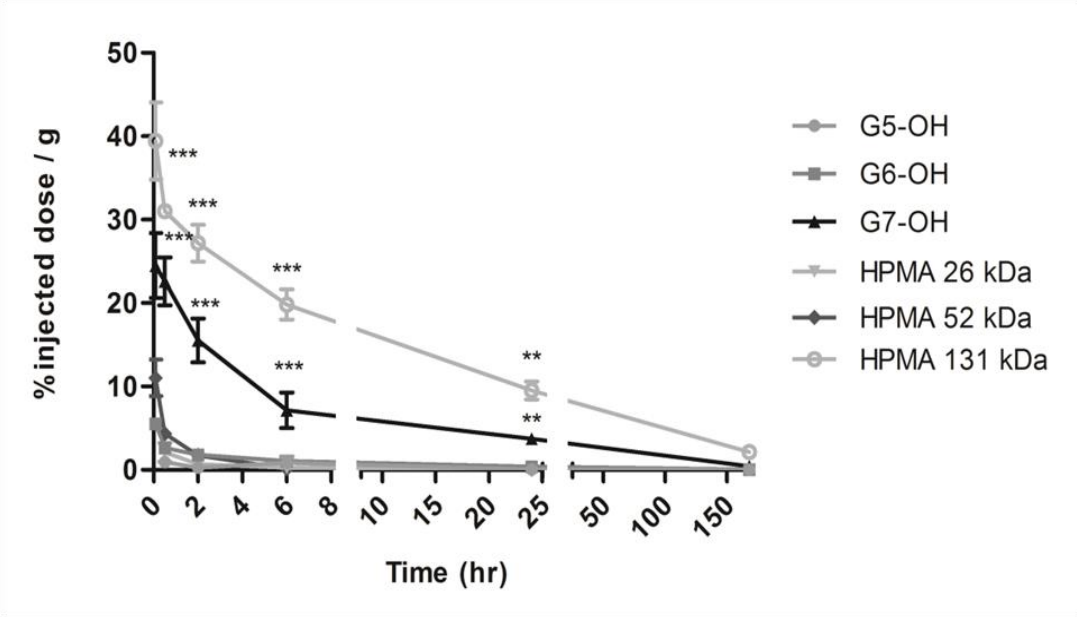

Figure 3-14. Percentage of injected dose / g of plasma tissue for PAMAM dendrimers and HPMA copolymers. Values are Mean +/- SEM; n=5; except n=4 for 5 minute HPMA copolymer (52 kDa), 2 hour HPMA copolymer (26 kDa) and G5.0-OH, 6 hour HPMA copolymer (131 kDa); 6 hour and 24 hour G7.0-OH and n=3 for 1 week HPMA copolymer (52 kDa), 5 minute, 30 minute, 2 hour HPMA copolymer (131 kDa).**/*** indicates a statistically significant difference, $p < 0.01$ and $p < 0.001$, respectively, as per ANOVA and Bonferroni's multiple comparison test comparing G7.0-OH and HPMA 131 kDa with smaller MW polymers.

attributed to a slightly higher hydrodynamic radius of the HPMA copolymer (R_h = 3.3 nm) as compared to the compact dendrimer (R_h = 3.0 nm) that reduces kidney filtration. PAMAM G6.0-OH was also extensively taken up by the liver, thus reducing its plasma circulation time.

The biodistribution results of the polymeric constructs under study have implications in the choice of carriers for drug delivery and imaging. Due to its selective and persistent kidney accumulation, PAMAM G5.0-OH should be used with caution to deliver drugs such as cisplatinum, methotrexate, stroptozotocin and mitomycin that cause kidney toxicity, but these polymers may be effectively used for kidney imaging to detect renal tubular damage and assess kidney function [33, 43]. This polymer also has the potential to treat kidney diseases due to preferential renal targeting, which is an area of growing interest. Although G5.0-OH did not show signs of acute renal toxicity over the period of the study (Appendix A), its prolonged retention could lead to chronic renal toxicity. PAMAM dendrimers accumulated in the liver to a higher extent than the HPMA copolymers under study and hence should be used with caution to deliver drugs like adriamycin, methotrexate, 6-mercaptopurine, carboplatin, L-asparaginase and pentostatin that can cause liver damage. High generation PAMAM G7.0-OH showed reduced non-specific uptake in the liver and kidney comparable to that of PEGylated dendrimers [32].

The effect of polymer architecture on drug loading, drug release, cellular delivery and pharmacological activity have been evaluated *in vitro* [20, 44]. In this study, we have evaluated the influence of polymer architecture on *in vivo* fate utilizing orthotopic A2780 ovarian tumor-bearing nude mouse models. Polymer architecture affected renal and hepatic uptake of the constructs under study. The branched PAMAM dendrimers

accumulated to a larger extent in the liver than the linear HPMA copolymers. For polymers that could be easily filtered through the kidney, PAMAM dendrimers persisted for a longer period of time in the kidney tissue as compared to HPMA copolymers. This is indicative of a difference in the extravasation of polymers of varying architecture through fenestrations of healthy tissue [45]. Inspite of a greater hydrodynamic size and longer plasma circulation, the HPMA copolymer (131 kDa) accumulated in the tumor to a lesser extent than G7.0-OH of comparable MW. More work is needed to understand the effect of linear and hyperbranched polymer architecture on rates and extent of microvascular extravasation.

3.5. Conclusion

Macromolecular architecture affected the increment in hydrodynamic radius of the polymer with increase in molecular weight**.** Along with molecular weight, polymer architecture and hydrodynamic volume were critical to the *in vivo* fate of the macromolecules. Specifically, polymer architecture affected renal and hepatic uptake of the constructs under study, with the hyperbranched PAMAM dendrimers showing more persistent accumulation than their linear HPMA copolymer counterparts. The difference in hepatic and renal accumulation between PAMAM dendrimers and HPMA copolymers is indicative of a difference in the extravasation of polymers of varying architecture through fenestrations of healthy tissue. The tumor accumulation data indicated a hydrodynamic radius cutoff of about 4.0 nm, below which prolonged tumor retention was not observed for orthotopic ovarian carcinoma tumors under study. However, the hyperbranched PAMAM G7.0-OH (117 kDa) showed a higher tumor uptake than the

linear HPMA copolymer (131 kDa) of comparable molecular weight suggesting that polymer architecture affected tumor uptake. Additional studies are needed to understand the effect of the linear and hyperbranched polymer architecture on rates and extent of microvascular extravasation. A pharmacokinetic analysis of the data can give insight into the same (discussed in Chapter 4). The biodistribution result of the polymeric constructs guides the choice of a carrier of certain architecture and hydrodynamic size for preferential organ accumulation, which can be exploited for drug delivery and imaging applications.

3.6. References

1. Duncan R. The dawning era of polymer therapeutics. Nat Rev Drug Discovery. 2003;2(5):347-60.

2. Fang J, Nakamura H, Maeda H. The EPR effect: unique features of tumor blood vessels for drug delivery, factors involved, and limitations and augmentation of the effect. Adv Drug Deliv Rev. 2011;63(3):130-51.

3. Kopeček J, Kopečková P. HPMA copolymers: origins, early developments, present, and future. Adv Drug Deliv Rev. 2010;62(2):122-49.

4. Pike DB, Ghandehari H. HPMA copolymer-cyclic RGD conjugates for tumor targeting. Adv Drug Deliv Rev. 2010;62(2):167-83.

5. Ulbrich K, Subr V. Structural and chemical aspects of HPMA copolymers as drug carriers. Adv Drug Deliv Rev. 2010;62(2):150-66.

6. Duncan R. Polymer conjugates as anticancer nanomedicines. Nat Rev Cancer. 2006;6(9):688-701.

7. Konak C, Rathi RC, Kopečková P, Kopeček J. Effect of side-chains on solution properties of N-(2-hydroxypropyl) methacrylamide copolymers in aqueous solvents. Polymer. 1993;34(22):4767-73.

8. Lammers T, Kühnlein R, Kissel M, Subr V, Etrych T, Pola R et al. Effect of physicochemical modification on the biodistribution and tumor accumulation of HPMA copolymers. J Control Release. 2005;110(1):103-18.

9. Svenson S, Tomalia DA. Dendrimers in biomedical applications--reflections on the field. Adv Drug Deliv Rev. 2005;57(15):2106-29.

10. Tomalia D, Reyna L, Svenson S. Dendrimers as multi-purpose nanodevices for oncology drug delivery and diagnostic imaging. Biochem Soc Trans. 2007;35:61-7.

11. Tomalia DA, Baker H, Dewald J, Hall M, Kallos G, Martin S et al. A new class of polymers: starburst-dendritic macromolecules. Polym J. 1985;17(1):117-32.

12. Tomalia DA, Fréchet JMJ. Discovery of dendrimers and dendritic polymers: a brief historical perspective. J Polym Sci, Part A: Polym Chem. 2002;40(16):2719-28.

13. Duncan R, Izzo L. Dendrimer biocompatibility and toxicity. Adv Drug Deliv Rev. 2005;57(15):2215-37.

14. Kitchens KM, El-Sayed MEH, Ghandehari H. Transepithelial and endothelial transport of poly (amidoamine) dendrimers. Adv Drug Deliv Rev. 2005;57(15):2163-76.

15. Malik N, Wiwattanapatapee R, Klopsch R, Lorenz K, Frey H, Weener JW et al. Dendrimers: relationship between structure and biocompatibility *in vitro*, and preliminary studies on the biodistribution of 125I-labelled polyamidoamine dendrimers *in vivo*. J Control Release. 2000;65(1-2):133-48.

16. Jevprasesphant R, Penny J, Jalal R, Attwood D, McKeown NB, D'Emanuele A. The influence of surface modification on the cytotoxicity of PAMAM dendrimers. Int J Pharm. 2003;252(1-2):263-6.

17. Roberts JC, Bhalgat MK, Zera RT. Preliminary biological evaluation of polyamidoamine (PAMAM) starburst^{TM} dendrimers. J Biomed Mater Res A. 1996; 30(1):53-65.

18. Vicent MJ, Duncan R. Polymer conjugates: nanosized medicines for treating cancer. Trends Biotechnol. 2006;24(1):39-47.

19. Fox ME, Szoka FC, Frechet JMJ. Soluble polymer carriers for the treatment of cancer: the importance of molecular architecture. Acc Chem Res. 2009;42(8):1141-51.

20. Khandare J, Jayant S, Singh A, Chandna P, Wang Y, Vorsa N et al. Dendrimer versus linear conjugate: influence of polymeric architecture on the delivery and anticancer effect of paclitaxel. Bioconjug Chem. 2006;17(6):1464-72.

21. Kopeček J, Kopečková P, Minko T, Lu ZR. HPMA copolymer–anticancer drug conjugates: design, activity, and mechanism of action. Eur J Pharm Biopharm. 2000;50(1):61-81.

22. Strohalm J, Kopecek J. Poly N-(2-hydroxypropyl) methacrylamide. 4. Heterogeneous polymerization. Angew Makromol Chem. 1978;70:109-18.

23. Greenaway J, Moorehead R, Shaw P, Petrik J. Epithelial-stromal interaction increases cell proliferation, survival and tumorigenicity in a mouse model of human epithelial ovarian cancer. Gynecol Oncol. 2008;108(2):385-94.

24. Fritzinger B, Scheler U. Scaling behaviour of PAMAM dendrimers determined by diffusion NMR. Macromol Chem Phys. 2005;206(13):1288-91.

25. Tande B, Wagner N, Mackay M, Hawker C, Jeong M. Viscosimetric, hydrodynamic, and conformational properties of dendrimers and dendrons. Macromolecules. 2001;34(24):8580-5.

26. Uppuluri S, Keinath S, Tomalia D, Dvornic P. Rheology of dendrimers. I. Newtonian flow behavior of medium and highly concentrated solutions of polyamidoamine (PAMAM) dendrimers in ethylenediamine (EDA) solvent. Macromolecules. 1998;31(14):4498-510.

27. Kobayashi H, Brechbiel M. Nano-sized MRI contrast agents with dendrimer cores. Adv Drug Deliv Rev. 2005;57(15):2271-86.

28. Venditto V, Regino C, Brechbiel M. PAMAM dendrimer based macromolecules as improved contrast agents. Mol Pharm. 2005;2(4):302-11.

29. Borgman M, Coleman T, Kolhatkar R, Geyser-Stoops S, Line B, Ghandehari H. Tumor-targeted HPMA copolymer-(RGDfK)-(CHX-A"-DTPA) conjugates show increased kidney accumulation. J Control Release. 2008;132(3):193-9.

30. Kodaira H, Tsutsumi Y, Yoshioka Y, Kamada H, Kaneda Y, Yamamoto Y et al. The targeting of anionized polyvinylpyrrolidone to the renal system. Biomaterials. 2004;25(18):4309-15.

31. Rippe C, Asgeirsson D, Venturoli D, Rippe A, Rippe B. Effects of glomerular filtration rate on Ficoll sieving coefficients (theta) in rats. Kidney Int. 2006;69(8):1326-32.

32. Kojima C, Regino C, Umeda Y, Kobayashi H, Kono K. Influence of dendrimer generation and polyethylene glycol length on the biodistribution of PEGylated dendrimers. Int J Pharm. 2010;383(1-2):293-6.

33. Kobayashi H, Kawamoto S, Jo SK, Sato N, Saga T, Hiraga A et al. Renal tubular damage detected by dynamic micro-MRI with a dendrimer-based magnetic resonance contrast agent. Kidney Int. 2002;61(6):1980-5.

34. Kukowska-Latallo J, Candido K, Cao Z, Nigavekar S, Majoros I, Thomas T et al. Nanoparticle targeting of anticancer drug improves therapeutic response in animal model of human epithelial cancer. Cancer Res. 2005;65(12):5317.

35. Jun YJ, Kim JI, Jun MJ, Sohn YS. Selective tumor targeting by enhanced permeability and retention effect. Synthesis and antitumor activity of polyphosphazene-platinum (II) conjugates. J Inorg Biochem. 2005;99(8):1593-601.

36. Lammers T, Subr V, Ulbrich K, Hennink W, Storm G, Kiessling F. Polymeric nanomedicines for image-guided drug delivery and tumor-targeted combination therapy. Nano Today. 2010;5(3):197-212.

37. Gabellieri E, Strambini GB, Shcharbin D, Klajnert B, Bryszewska M. Dendrimer-protein interactions studied by tryptophan room temperature phosphorescence. BBA-Proteins Proteom. 2006;1764(11):1750-6.

38. Klajnert B, Bryszewska M. Fluorescence studies on PAMAM dendrimers interactions with bovine serum albumin. Bioelectrochemistry. 2002;55(1-2):33-5.

39. Klajnert B, Sadowska M, Bryszewska M. The effect of polyamidoamine dendrimers on human erythrocyte membrane acetylcholinesterase activity. Bioelectrochemistry. 2004;65(1):23-6.

40. Klajnert B, Stanisawska L, Bryszewska M, Paecz B. Interactions between PAMAM dendrimers and bovine serum albumin. BBA-Proteins Proteom. 2003;1648(1-2):115-26.

41. Lundqvist M, Sethson I, Jonsson BH. Protein adsorption onto silica nanoparticles: conformational changes depend on the particles' curvature and the protein stability. Langmuir. 2004;20(24):10639-47.

42. Maeda H, Fang J, Inutsuka T, Kitamoto Y. Vascular permeability enhancement in solid tumor: various factors, mechanisms involved and its implications. Int Immunopharmacol. 2003;3(3):319-28.

43. Dear JW, Kobayashi H, Brechbiel MW, Star RA. Imaging acute renal failure with polyamine dendrimer-based MRI contrast agents. Nephron Clinical Practice. 2006;103(2):c45-9.

44. Perumal O, Khandare J, Kolhe P, Kannan S, Lieh-Lai M, Kannan R. Effects of branching architecture and linker on the activity of hyperbranched polymer- drug conjugates. Bioconjug Chem. 2009;20(5):842-6.

45. El-Sayed M, Kiani MF, Naimark MD, Hikal AH, Ghandehari H. Extravasation of poly (amidoamine)(PAMAM) dendrimers across microvascular network endothelium. Pharm Res. 2001;18(1):23-8.

CHAPTER 4[1]

COMPARATIVE PHARMACOKINETICS OF PAMAM–OH DENDRIMERS AND HPMA COPOLYMERS

4.1. Introduction

The pharmacokinetics of hyperbranched PAMAM dendrimers has been correlated to its physicochemical properties-generation or molecular weight, chemical composition of core and nature of surface groups as well as type of surface modification [1-3]. The linear HPMA copolymers have also been well characterized for the influence of co-monomer structure, composition and charge on solution properties, molecular conformation as well as *in vivo* biodistribution and pharmacokinetics [4-6].

Along with the molecular weight, polymer architecture and hydrodynamic size are also known to affect the biodistribution and consequently the pharmacokinetics of the polymeric carriers [7-10]. The shape and ability of macromolecules to deform have been

---

[1]Note- Reprinted with permission from S. Sadekar, O. Linares, GJ. Noh , D. Hubbard, A. Ray, M. Janát-Amsbury, C. M. Peterson, J. Facelli, H. Ghandehari, Comparative Pharmacokinetics of PAMAM-OH Dendrimers and HPMA Copolymers in Ovarian-Tumor-Bearing Mice, *Drug Delivery and Translational Research, In press, DOI 10.1007/s13346-012-0119-6.*

reported to influence their glomerular filtration and consequently elimination clearance and blood exposure [8]. In Chapter 3, a head to head comparison of the *in vivo* fate of hyper-branched hydroxyl-terminated poly(amido amine) or PAMAM-OH dendrimers with linear HPMA copolymers of comparable molecular weights in tumor-bearing mice was described. It was observed that along with molecular weight, hydrodynamic size and polymer architecture were critical in affecting the accumulation of these polymers in the tumor and elimination organs such as kidney and liver [10]. The purpose of this study was to model the previously obtained experimental data on the biodistribution of HPMA copolymers and PAMAM-OH dendrimers by compartmental pharmacokinetic analysis. By modeling the biodistribution data, the pharmacokinetic parameters of these polymeric carriers of varying hydrodynamic sizes and architecture were quantified in order to understand their effect on *in vivo* kinetics.

4.2. Pharmacokinetic analysis

The radioactive readings obtained in counts per minute from blood, tumor, liver, kidney, urine and feces were expressed as milligram of dose (weight of polymer) using the correlation of administered dose in mg/kg of mouse and total counts per minute of radioactivity measured for each dose. The blood weights of each mouse were expressed in milliliters (volume of blood) assuming the density of mouse blood to be 1.05 g/mL. Consequently, the plasma concentration of polymers (C_p) was expressed as the weight of PAMAM-OH dendrimer / HPMA copolymer per unit volume of blood (mg/ml). The organ accumulations for tumor, liver and kidney were expressed in milligram of polymer per gram of organ weight (mg/g). The biodistribution data was modeled using a naïve

pooled data approach. Blood concentration data was fitted to one and two-compartmental models with single bolus input using WinNonlin® 2.1 (Pharsight, a Certara Company, St. Louis, Missouri). The Akaike Information Criterion (AIC) values obtained from each of the model fits indicated that the two-compartment model fit the blood concentration time profile better than the one-compartment model (Appendix A). The blood data was therefore modeled by two-compartment analysis using Winnonlin® 2.1 to obtain elimination clearance (E.CL) and blood exposure (AUC_{blood}). Renal clearance (CL_R) was calculated from urine data collected over 1 week (Equations (1) and (2), Section A.8., Appendix A). A compartmental model was set up in order to link the blood and the tumor compartments (Figure 4-1, 4-2). The model allowed a two-compartmental distribution for the blood between the central blood (C_p) and the peripheral fast distribution compartment (C_f) (as determined from fitting blood data alone). For the lower molecular weight polymers that did not show tumor retention, the tumor compartment (C_t) allowed elimination of the polymers back into the blood via the rate constant K_5 (model 1, Figure 4-1). For the higher molecular weight polymers that showed prolonged retention in the tumor, the tumor compartment was subdivided into two compartments, linked serially to the blood (model 2, Figure 4-2). The first compartment (C_{t1}) allowed elimination of the polymers back into the blood. For model 2, the second tumor compartment (C_{t2}) did not allow elimination in order to account for the tumor retention of the higher MW polymers observed in the study and in accordance with the EPR effect. An alternate model (model 3) was also attempted where elimination was allowed from the second tumor compartment (C_{t2}) into the first tumor compartment (C_{t1}) via a first order elimination rate

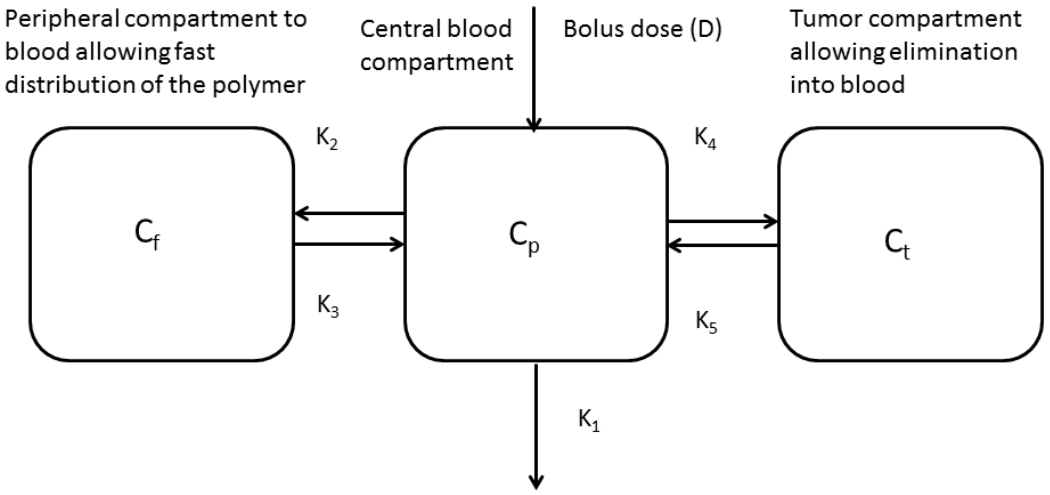

Figure 4-1. Compartmental model linking the blood and the tumor compartment. Model 1- For lower MW polymers that did not show prolonged retention in the tumor. Model allows elimination from a single tumor compartment (t) back into the plasma compartment.

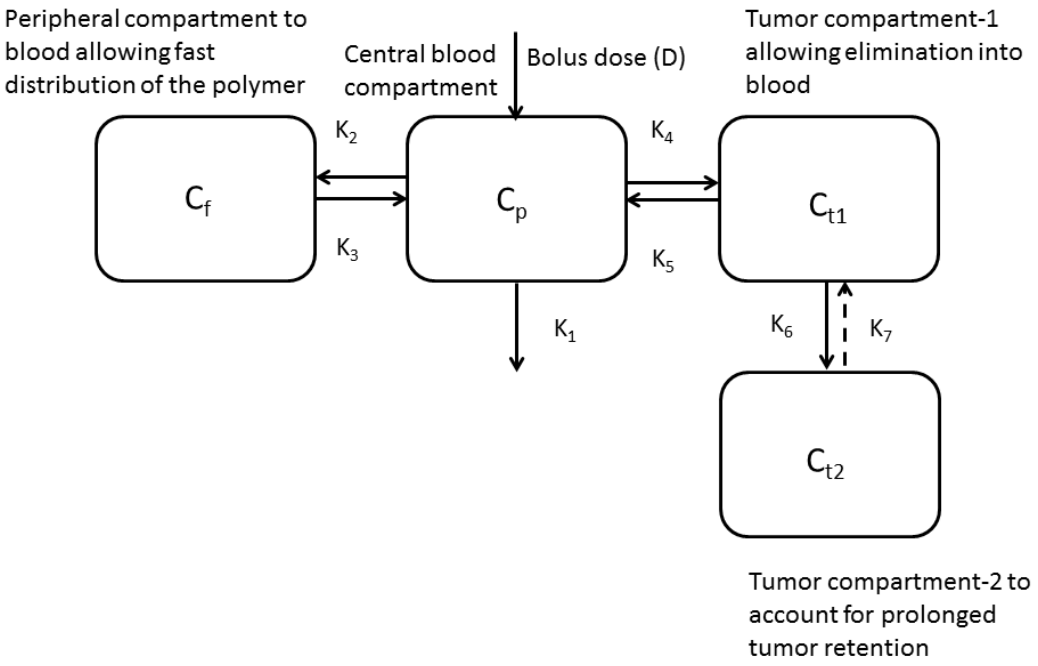

Figure 4-2. Compartmental model linking the blood and the tumor compartment. Model 2- for higher MW polymers with prolonged retention in the tumor. Model allows elimination from the first tumor compartment (t1) via rate constant K_5 back into the plasma compartment but does not allow elimination from the second tumor compartment (t2). Model 3- Extension of model 2 where elimination is allowed from the second tumor compartment (t2) to the first tumor compartment (t1) by a first order rate constant K_7 (indicated by dotted line).

constant K_7. The blood elimination (K_1) and distribution (K_2, K_3) rate constants were initially fixed as per the two-compartmental distribution of the blood data. The model was fitted to experimental blood and tumor data by varying the tumor extravasation (K_4, K_6) and elimination (K_5, K_7) rate constants using multivariable constrained optimization solver in Matlab® to obtain initial estimates of the tumor rate constants. Using initial estimates of the tumor rate constants as well as blood elimination and distribution rate constants, the model was refitted to experimental blood and tumor data by varying all of the rate constants by the multivariable constrained optimization solver in Matlab®. The AIC of model 3 for all the high MW polymers except G7.0-OH was slightly higher than the AIC of model 2 (that did not allow elimination from the second tumor compartment) (Appendix A). Hence, for high MW polymers showing prolonged retention, model 2 was chosen to fit blood and tumor data of higher MW polymers G6.0-OH and HPMA 131 kDa while model 3 was chosen to fit data of G7.0-OH (compartmental model equations, optimization code, AIC and χ^2 values given in Section A.11., Appendix A).

Tumor exposures (AUC_{tumor}) were computed from area under the tumor concentration time profile curve by the linear trapezoidal method. Blood and tumor exposures were dose normalized assuming linear pharmacokinetics over the dose ranges studied for the polymers (20-50 mg/Kg).

4.3. Results

4.3.1. Blood exposure

The polymers showed a biphasic exponential blood circulation with an apparent fast distribution component and a much slower elimination component (Figure 4-3).

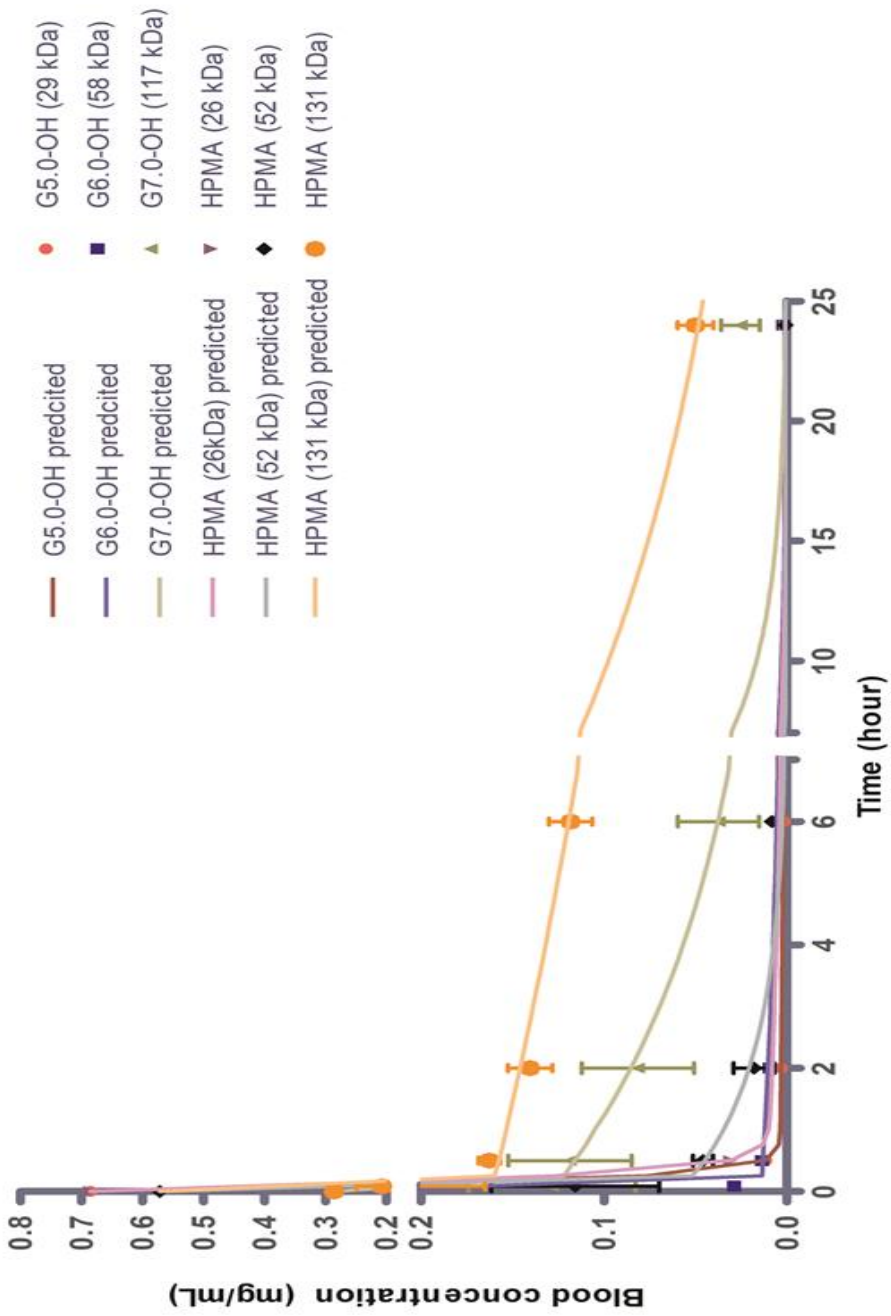

Figure 4-3. Blood concentration-time profile of PAMAM-OH dendrimers and HPMA copolymers. Experimental data are represented in symbols-mean ± SEM. Model predicted best fit values are represented as a line.

The two-compartmental pharmacokinetic parameter estimates showed a significant difference across molecular weights for each of the polymer series-PAMAM-OH dendrimers and HPMA copolymers (Table 4-1). The dose normalized blood exposure (AUC_{blood}/dose) increased with increase in molecular weight or hydrodynamic size for the PAMAM-OH dendrimers (Table 4-1, Figure 4-4). The HPMA copolymers had similar blood exposures for the 26 and 52 kDa copolymers, while the blood exposure increased drastically for the HPMA copolymer (131 kDa) (Table 4-1, Figure 4-4). Consistent with the trend for elimination clearance (Section 4.3.2), HPMA copolymer (26 kDa) (R_h = 1.4 nm) had a higher blood exposure in spite of being smaller in hydrodynamic size than G5.0-OH (R_h = 2.3 nm) of comparable MW. The opposite was seen for HPMA copolymer (52 kDa) (R_h = 3.3 nm) and G6.0-OH (R_h = 3.0 nm) of comparable MW with the hyperbranched dendrimer showing higher blood exposure than HPMA copolymer of comparable MW even though the dendrimer was slightly smaller than the HPMA copolymer. This observation can also be attributed to the trend in elimination clearance where the linear HPMA copolymer on the threshold of kidney filtration eliminated faster than the branched dendrimer (elaborated in Section 4.3.2). Owing to its hydrodynamic size being twice that of G7.0-OH (R_h = 4.0 nm), HPMA copolymer (131 kDa) (R_h = 8.2 nm) had a much higher blood exposure than G7.0-OH of comparable MW.

Table 4-1. Blood compartmental pharmacokinetic parameter estimates for PAMAM-OH dendrimers and HPMA copolymers.*

Parameter	G5.0-OH (29 kDa)	G6.0-OH (58 kDa)	G7.0-OH (117 kDa)	HPMA copolymer (26 kDa)	HPMA copolymer (52 kDa)	HPMA copolymer (131 kDa)
Clearance (mL/h)						
Elimination Clearance (E.CL)	10.50 ± 1.30	5.00 ± 1.00	0.79 ± 0.21	7.24 ± 0.58	6.02 ± 0.82	0.17 ± 0.03
Renal Clearance (CL_R)	0.266	0.087	0.007	1.179	0.807	0.041
Dose normalized Exposure						
$AUC_{plasma(0-24h)}$ (mg.h/mg.mL)	0.1 ± 0.01	0.2 ± 0.04	1.27 ± 0.34	0.14 ± 0.01	0.13 ± 0.02	5.88 ± 0.97
$AUC_{tumor(0-168h)}$ (mg.h/mg.g)	0.48	0.82	7.99	0.21	0.23	3.48
AUC_{tumor}/ AUC_{plasma}	5.06	4.12	6.31	1.52	1.70	0.59
Correlation Coefficient	0.9785	1	0.9954	0.9765	0.9999	0.9967

*Elimination clearance and plasma exposure were computed by two-compartmental analysis with bolus input. Renal clearances were computed from urine data and were pooled for all animals in a treatment group. Tumor AUCs were computed from area under the tumor concentration profile curve. Data are presented as mean ± standard error.

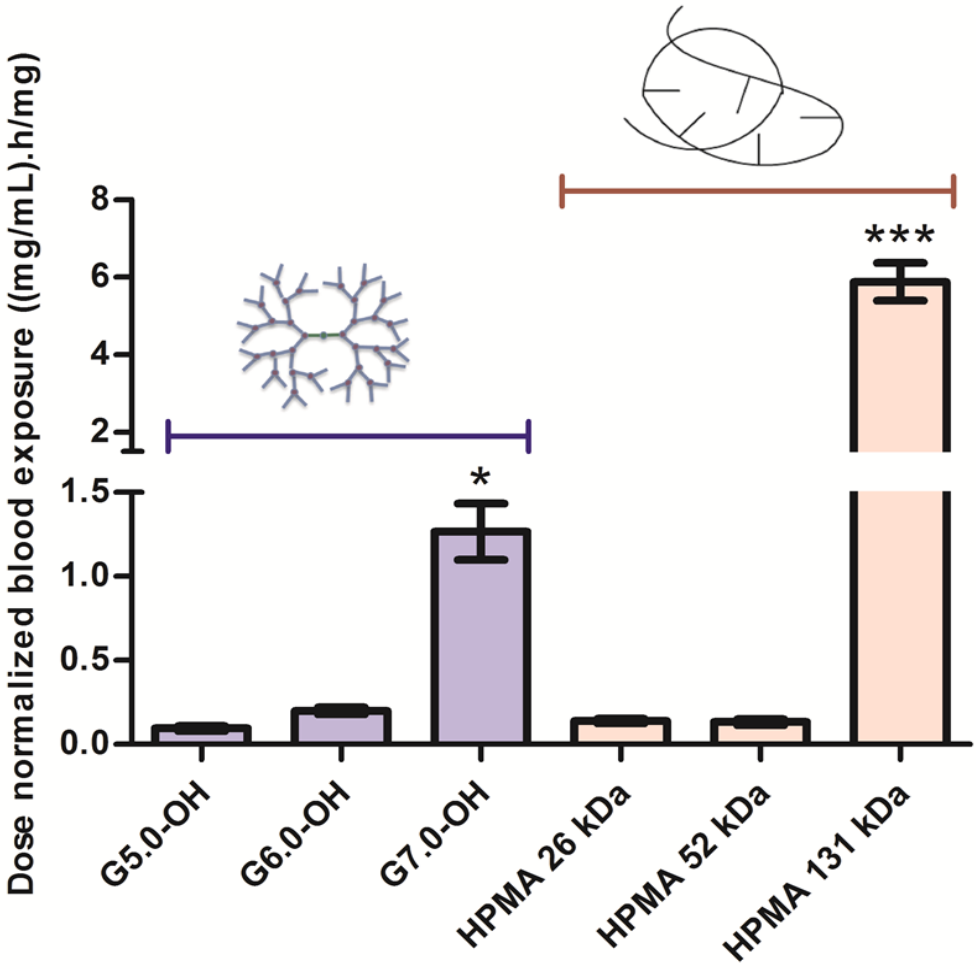

Figure 4-4. Dose normalized blood exposure (0-24 h) of PAMAM-OH dendrimers and HPMA copolymers computed from model fit. Data are represented as mean estimate ± standard error of fit. Dose normalized blood exposure of G7.0-OH and HPMA 131 kDa is statistically significantly different from lower MW polymers with $p<0.5$ and $p<0.001$, respectively, as per ANOVA and Bonferroni's multiple comparison tests comparing G7.0-OH and HPMA 131 kDa with all other treatment groups.

4.3.2. Elimination clearance-correlation with hydrodynamic size

Elimination clearance decreased with increase in MW within each of the polymer series (Table 4-1). The hydrodynamic diameter of G5.0-OH (29 kDa) and HPMA (26 kDa) were below the threshold diameter for kidney filtration (~ 6.0 nm) [11]. In spite of being greater in hydrodynamic size, the blood elimination clearance of G5.0-OH (R_h = 2.3 nm) was significantly higher than that of HPMA (26 kDa) (R_h = 1.4 nm) of comparable MW. In this size range, the highly compact structure of the PAMAM dendrimer may facilitate extravasation faster than the linear HPMA copolymer, explaining its faster rate of disappearance from the blood compartment. These observations demonstrate that polymer architecture affected elimination clearance below kidney filtration threshold. G6.0-OH (58 kDa) and HPMA copolymer (52 kDa) were on the threshold of kidney filtration cutoff diameter (6.0 nm). Their elimination clearances were comparable with the HPMA (R_h = 3.3 nm) being eliminated from the blood slightly faster than the G6.0-OH (R_h = 3.0 nm). This difference was not statistically significant. However this observation suggests that at the kidney filtration threshold size, the linear copolymer was eliminated faster than the hyperbranched dendrimer, even though it was slightly greater in hydrodynamic size. G7.0-OH was almost half the hydrodynamic size of HPMA (131 kDa) and had a faster clearance than the HPMA copolymer (131 kDa) of comparable MW. Over the MW range studied, elimination clearance decreased log linearly with increase in hydrodynamic size within each of the polymer series (Figure 4-3). However, elimination clearance decreased more rapidly for PAMAM-OH dendrimers with increase in hydrodynamic volume as compared to HPMA copolymers indicated by slopes (Figure 4-5). This can be attributed to the effect of architecture on the change in

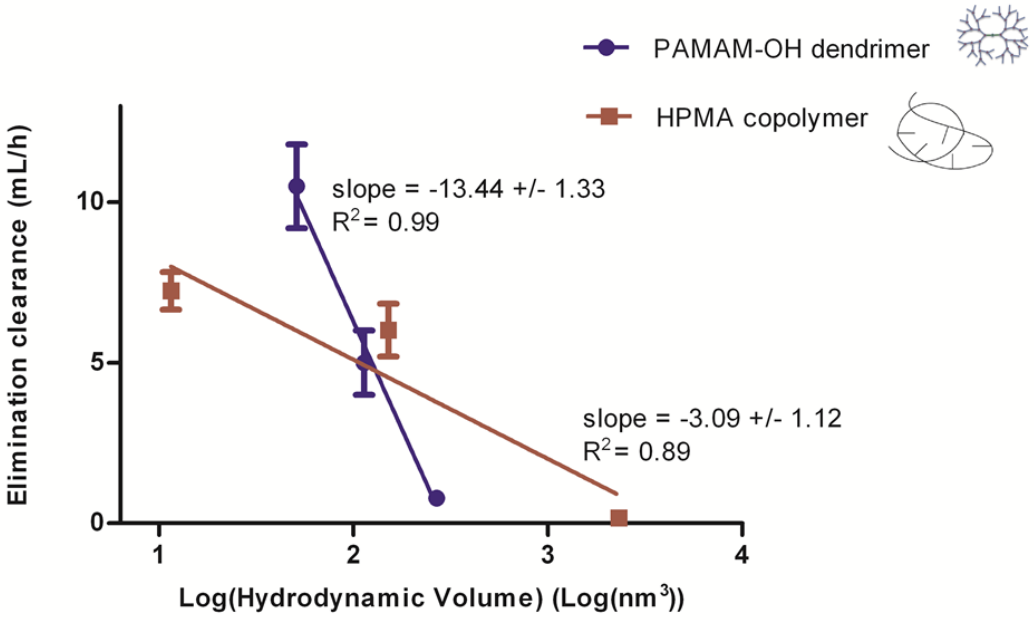

Figure 4-5. Correlation of elimination clearance of PAMAM-OH dendrimers and HPMA copolymers to hydrodynamic size. Data are represented as mean estimate ± standard error of fit.

molecular conformation of polymers with increase in MW (elaborated in detail in Section 4.4) [12, 13]. The observed trend of decrease in elimination clearance is only expected to hold over this range of molecular weights since the polymers transition from being small enough to be readily filtered through the kidney: G5.0-OH and HPMA copolymer 26 kDato being on the threshold of kidney filtration (G6.0-OH, HPMA copolymer (52 kDa)), and further to being long circulating in the blood (G7.0-OH, HPMA copolymer (131 kDa)) with a minimal renal clearance. This trend is not expected to hold outside of this molecular weight or size range, where the elimination clearance is likely to be independent of hydrodynamic size, although such studies warrant further investigation [14].

4.3.3. Renal clearance

Renal clearance decreased with increase in hydrodynamic size for each of the polymer series (Table 4-1, Figure 4-6). However, at comparable molecular weights, linear HPMA copolymers were eliminated renally to a higher extent (by an order of magnitude) than hyperbranched PAMAM-OH dendrimers (Table 4-1, Figure 4-6). In spite of the hydrodynamic size of HPMA copolymer (131 kDa) (R_h = 8.2 nm) being double that of G7.0-OH (R_h = 4.0 nm), HPMA copolymer (131 kDa) was eliminated renally to a greater extent than G7.0-OH. This can potentially be attributed to the unique ability of a linear polymer to reptate through a renal filtration pore while the branched polymer has to deform in order to pass through [8, 15]. Renal clearance was significantly less than the total elimination clearance for all of the polymers under study. This is

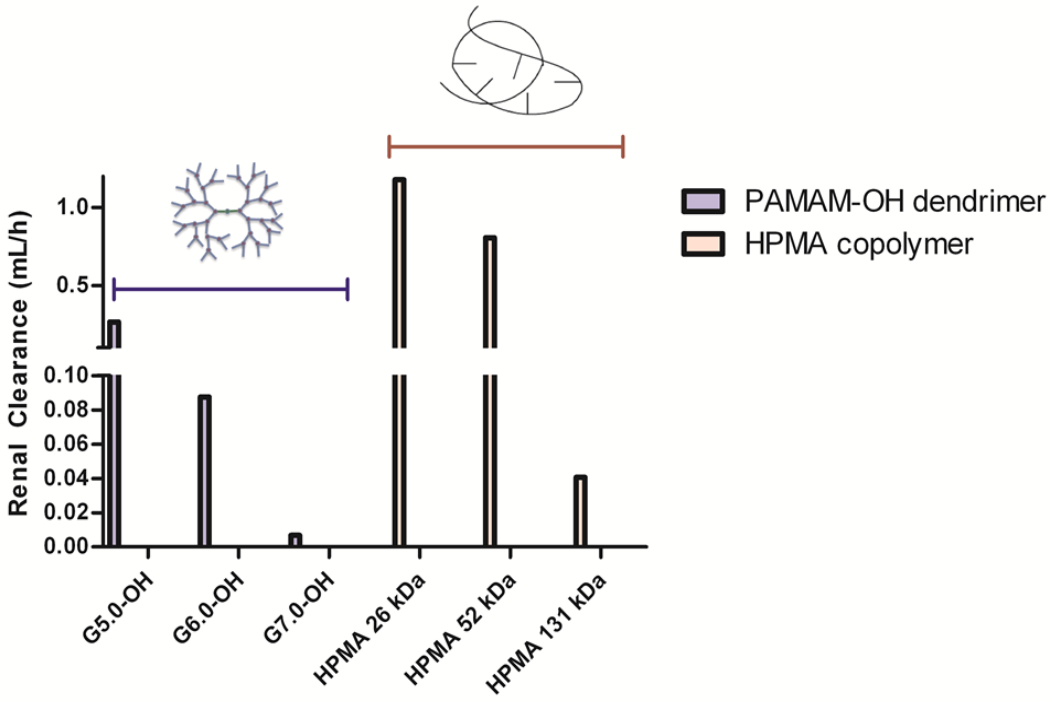

Figure 4-6. Renal clearances of PAMAM-OH dendrimers and HPMA copolymers. Data are represented as mean clearance calculated from data pooled for all animals in each treatment group.

indicative of the presence of other clearance mechanisms, potentially through the liver and the spleen.

4.3.4. Tumor exposure

Tumor concentration peaked at about 0.5-6 hours for the polymers under study with the larger molecular weight polymers showing a greater T_{max} than the lower molecular weight polymers (Figure 4-7) indicating a longer diffusion time for the larger polymers into the tumor. The dose normalized tumor exposure (AUC_{tumor}/dose) increased with increase in molecular weight or hydrodynamic size within a given polymer series (Table 4-1, Figure 4-8). However, the tumor exposure of the PAMAM-OH dendrimers was greater than that of HPMA copolymers of comparable molecular weights. In spite of a smaller hydrodynamic radius, faster elimination and lesser blood exposure, G7.0-OH (Rh = 4.0 nm) accumulated in the tumor twice as much as HPMA copolymer (131 kDa) (Rh = 8.2 nm) of comparable MW. The tumor to blood exposure ratios indicate that the polymers in circulation passively accumulated in the tumor and this accumulation was greater for the PAMAM dendrimers than the HPMA copolymers under study. The tumor to blood exposure ratios suggest that when in circulation, PAMAM-OH dendrimers have a higher affinity to accumulate in the tumor than the HPMA copolymers (Figure 4-9).

4.3.5. Blood and tumor extravasation and elimination rate constants

In accordance with the trend in elimination clearance, discussed in detail in Section 4.3.2, blood elimination rate constant (K_1) decreased with an increase in MW / R_h

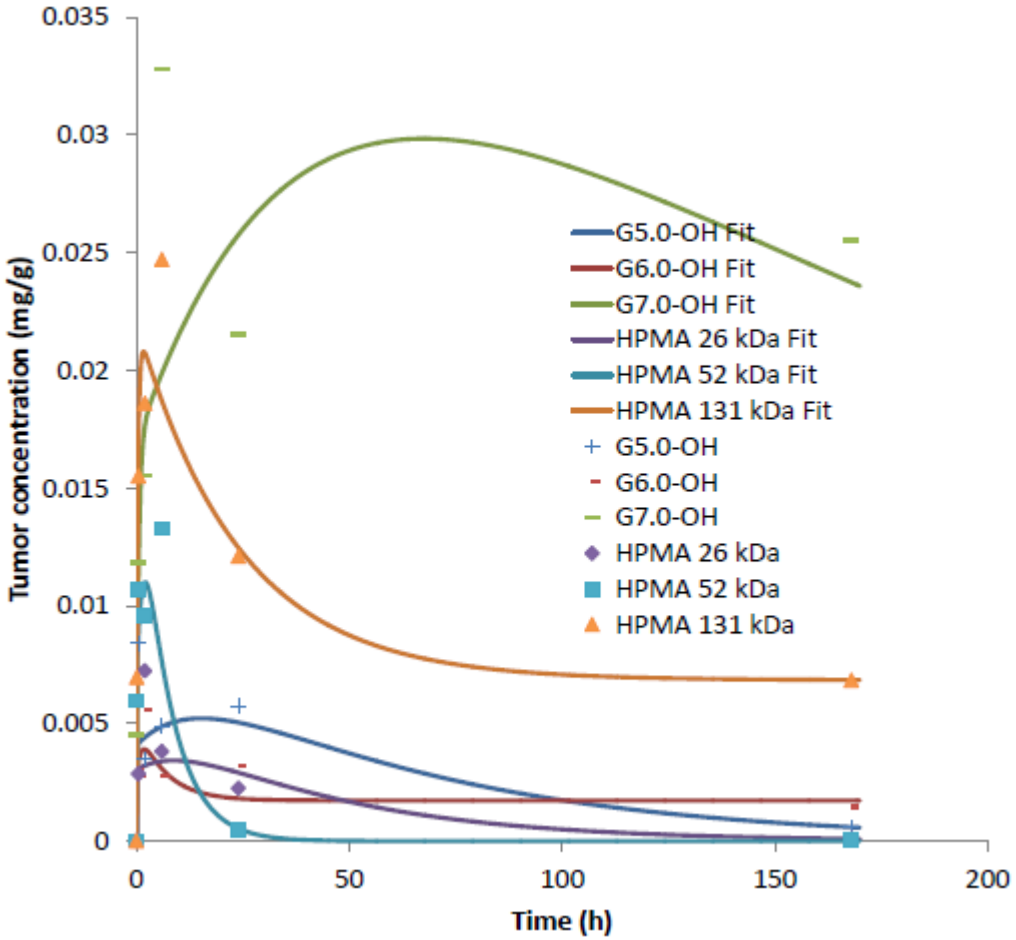

Figure 4-7. Tumor concentration-time profile of PAMAM-OH dendrimers and HPMA copolymers. Experimental data are represented in symbols-mean ± SEM. Model predicted best fit values are represented as a line. Tumor accumulation of G7.0-OH is statistically significantly higher than HPMA 131 kDa at 6 hours and 24 hours with a $p<0.01$ and $p<0.001$, respectively. Tumor accumulation of HPMA 131 KDa is higher than accumulation of lower MW polymers (except G7.0-OH) at 6 hours, $p<0.5$.

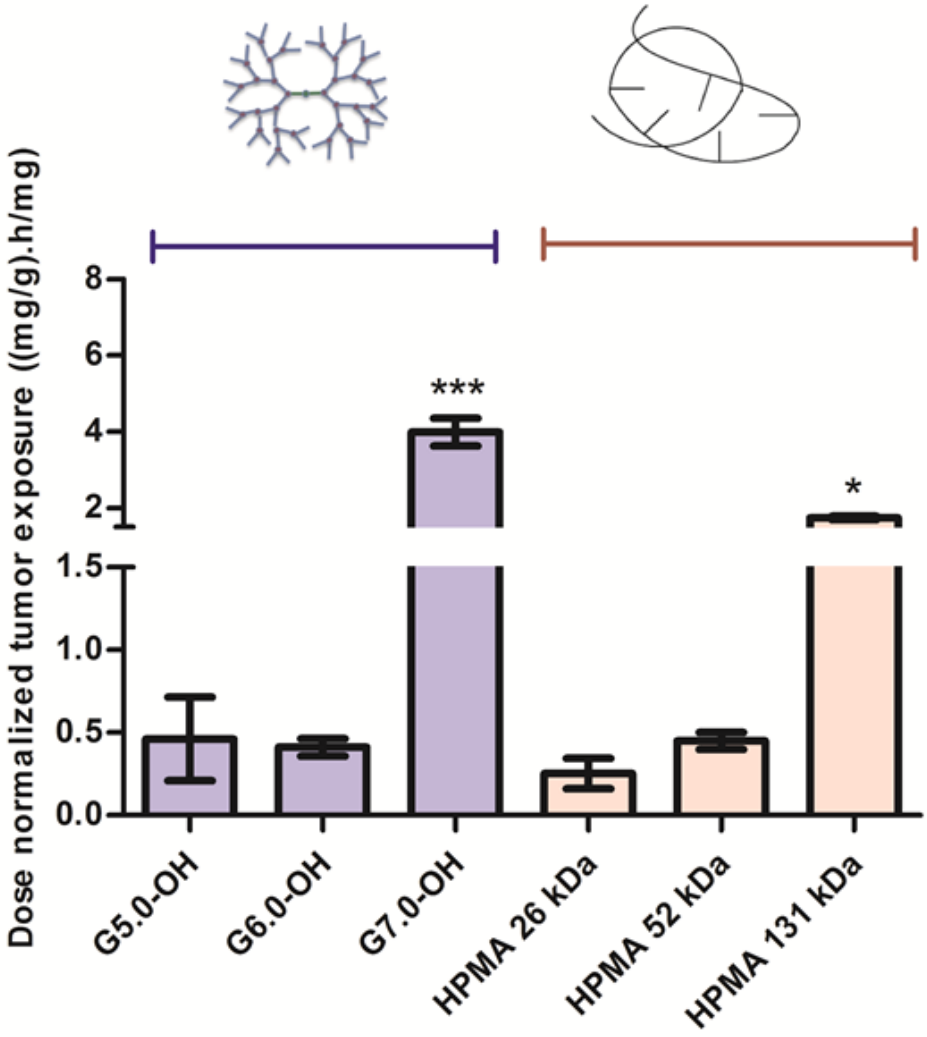

Figure 4-8. Dose normalized tumor exposure (0-168 h) of PAMAM-OH dendrimers and HPMA copolymers. Tumor exposure calculated by area under the curve using the trapezoidal rule was statistically significantly different for G7.0-OH ($p<0.001$) compared with other treatment groups as per ANOVA and Bonferonni's multiple comparison test. Using the same statistical tests, tumor exposure was different for HPMA 131 kDa compared to smaller MW polymers ($p<0.05$) and G7.0-OH ($p<0.001$) under study.

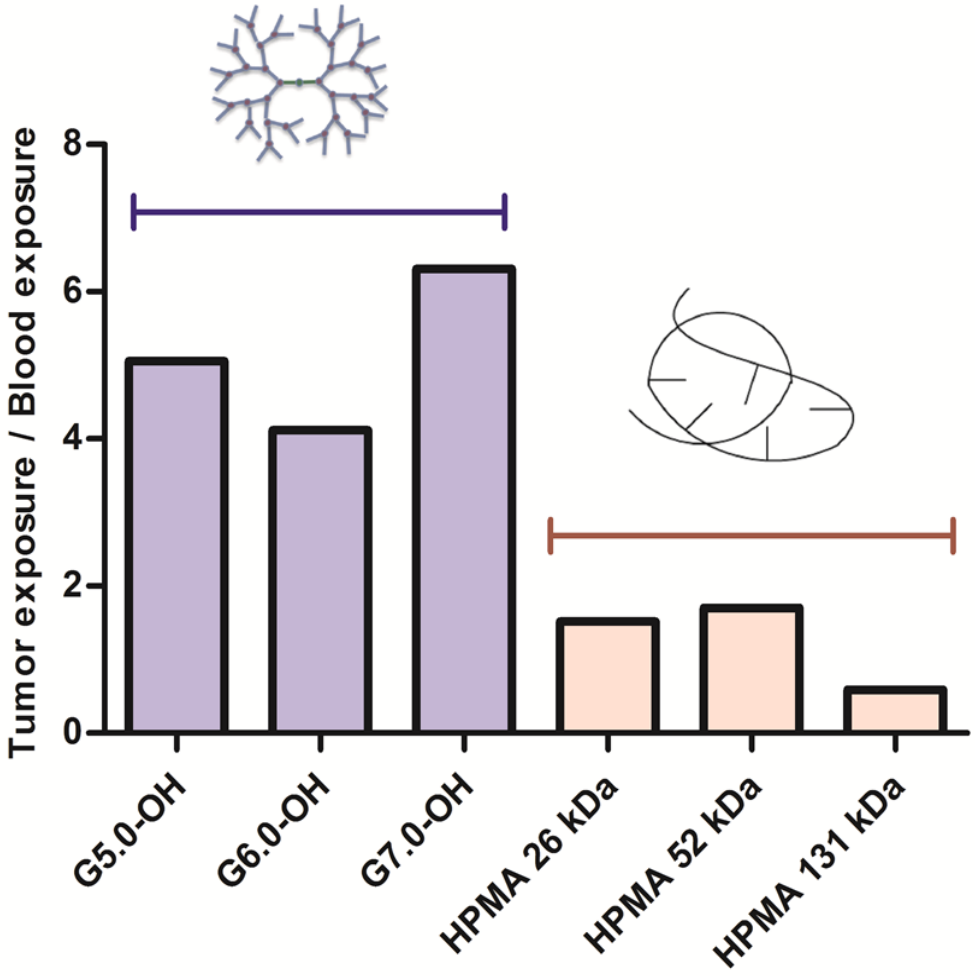

Figure 4-9. Ratio of tumor/blood exposure of PAMAM-OH dendrimers and HPMA copolymers.

of polymers within a given series (Table 4-2). As a consequence of increased blood circulation, tumor extravasation rate constant (K_2) increased with increase in molecular weight/hydrodynamic size within a polymer series (Table 4-2). It was also observed that PAMAM dendrimers extravasated into the tumor slightly faster than their equivalent molecular weight counterparts in the HPMA polymer series. It should be noted that all the rate constants computed by the global curve fitting method had significant error associated to them. In most cases, error was greater than 100%. Some of the χ^2 values (Appendix A) were high for the curve fits of all models. This suggests either inadequate estimation of standard deviation (obtained from experimental data limited in sample size) or inadequate choice and assumptions in model.

Blood and tumor data from smaller MW polymers G5.0-OH and HPMA 26 kDa as well as HPMA 52 kDa was fitted to model 1 without the second tumor compartment. These polymers showed diffusion in and out of tumor but did not show prolonged tumor retention over 1 week. Hence model 1 was used to globally curve fit blood and tumor data (Figure 4-1). For the higher MW polymers-G7.0-OH and HPMA 131 kDa as well as G6.0-OH, rate constant K_6 facilitated extravasation into the second tumor compartment and prolonged tumor retention over the time period of study which is in agreement with the EPR effect. Blood and tumor accumulation data of PAMAM G6.0-OH fit model 2 while that of HPMA 52 kDa, comparable in MW to G6.0-OH, fit model 1 indicating that the G6.0-OH showed a more prolonged tumor retention than HPMA copolymer of comparable MW (χ^2 values in Appendix A). G7.0-OH also had a higher extravasation rate constant into the second tumor compartment (K_6) than HPMA 131 kDa of comparable MW (Table 4-2). This suggests that PAMAM dendrimers had higher

Table 4-2. Extravasation and elimination rate constants of the blood-tumor link model.

Parameter (h^{-1})	**G5.0-OH (29 kDa) (Model 1)**	**G6.0-OH (58 kDa) (Model 2)**	**G7.0-OH (117 kDa) (Model 3)**	**HPMA copolymer (26 kDa) (Model 1)**	**HPMA copolymer (52 kDa) (Model 1)**	**HPMA copolymer (131 kDa) (Model 2)**
K_1	4.97 ± 5.16	2.86 ± 0.61	0.10 ± 0.24	4.17 ± 2.44	2.46 ± 1.84	0.08 ± 0.01
K_2	4.15 ± 4.78	30.17 ± 1.32	39.79 ±146.61	2.71 ± 2.31	21.79 ± 2.71	4.98 ± 1.28
K_3	0.13 ± 0.27	1.88 ± 0.27	10.88 ± 43.48	0.15 ± 0.21	1.62 ± 0.76	6.21 ± 1.88
K_4	0.06 ± 0.03	0.33 ± 0.14	0.53 ± 3.08	0.03 ± 0.02	0.31 ± 0.36	0.36 ± 0.39
K_5	0.02 ± 0.04	0.96 ± 0.65	1.71 ± 12.86	0.02 ± 0.07	0.66 ± 1.17	2.40 ± 3.00
K_6	-	0.05 ± 0.04	0.05 ± 0.36	-	-	0.01 ± 0.02
K_7	-	-	0.01 ± 0.04	-	-	-

PAMAM G5.0-OH, HPMA 26 and 52 kDa were modeled as per model 1, Figure 4-1A.
PAMAM G6.0-OH, HPMA 131 kDa were modeled as per model 2, Figure 4-1B.
PAMAM G7.0-OH was modeled as per model 3, Figure4-1B.
Choice of models was based on AIC and reduced χ^2 values of fits, see Appendix A.

tumor retention than HPMA copolymers in the orthotopic xenograft ovarian tumors under study. This propensity of the PAMAM dendrimers to passively target the tumor was also reflected in tumor to blood exposure ratios of the polymer discussed in Section 4.3.4 (Figure 4-9). Both models 2 and 3 facilitated prolonged tumor retention with the second tumor compartment (Figure 4-2). However, model 3 allowed elimination from the second tumor compartment (via rate constant K_7) while model 2 did not. Amongst the higher MW polymers showing prolonged tumor retention, data from G6.0-OH and HPMA 131 kDa showed a better fit for model 2 while that from G7.0-OH showed a better fit for model 3 (χ^2 values in Appendix A). For all of these polymers, the presence of the elimination rate constant from second tumor compartment (K_7) marginally decreased fit error (χ^2 values in Appendix A). However, this decreased error came at the cost of increased model parameterization. The Akaike Information Criterion (AIC), which is a balance of both fit error as well as degrees of freedom was lower for model 2 in the case of G6.0-OH and HPMA 131 kDa (AIC values in Appemdix A). In case of G7.0-OH, AIC was lower for model 3. Within the scope of the given experimental dataset (12 experimental data points), the models that were set up are tending to be over-parameterized (6 parameters for model 2 and 7 for model 3). Hence, choice of model, based on a lower value of AIC, is limited by degrees of freedom. If these experiments are designed to include more time points, it is likely that model 3 would fit all of the higher MW polymers better than model 2.

4.4. Discussion

Polymeric carriers used in drug delivery have a favorable pharmacokinetic profile over small molecular weight drugs owing to their reduced renal clearance and resulting long circulation half-life in the blood [16]. Unlike small molecular weight drugs which are known to have instantaneous distribution into blood-perfused organs, macromolecular distribution to both target organs such as tumor, and clearance organs such as kidney and liver is limited by their size [16]. Target organs like the tumor are known to have increased uptake and retention of macromolecules due to the enhanced permeability and retention effect [17]. The extent of accumulation of macromolecules in these organs and their blood pharmacokinetics depend on their physicochemical attributes such as chemical composition, molecular weight, hydrodynamic size, charge, extent of blood protein binding and molecular architecture [18]. Architecture of a polymeric carrier is determined by its molecular conformation, chain flexibility, deforming capability and extent of branching [8]. The polymeric carriers that were evaluated had distinct architectures: PAMAM-OH dendrimers are hyperbranched polymers with a globular shape while the HPMA copolymers are linear with side chains, known to assume a random coil conformation in solution [12, 13]. PAMAM dendrimers become more rigid at higher generations [19, 12]. With every increase in generation, extent of branching increases and so does surface congestion. This affects the molecular conformation and deforming capability of the dendrimer. The smaller generation PAMAMs (G0.0-3.0) are flexible, floppy and disc-like. Generations 4.0 through 6.0 have a hollow core and permeable outer shells that render them as nano-containers. Generations 7.0 onwards, the dendrimers start to possess a very rigid surface scaffolding with a globular shape [19].

The PAMAM-OH dendrimers under study, i.e., G5.0 through G7.0 lie in a range where they transition from a more flexible conformation for G5.0-OH to a more rigid, globular shape for G7.0-OH. The HPMA copolymers on the other hand are not known to undergo a significant conformational change for the range of molecular weights that were studied (26-131 kDa). This trend in molecular conformational change of polymers of different architecture affected their pharmacokinetics. The polymers under study interacted minimally with blood proteins due to their neutral charge (Section A.9., Appendix A). Hence, blood protein binding is not expected to influence observed trends in biodistribution and pharmacokinetics.

Elimination clearance decreased more rapidly for PAMAM dendrimers with increase in molecular weight or hydrodynamic size than for HPMA copolymers for the same increase in molecular weight (Figure 4-5). These results are in agreement with other studies which show that the shape and ability of the polymer to deform play important roles in the glomerular filtration rate and hence elimination clearance [8, 9, 20, 21]. Previous reports suggest that increased hydrodynamic size, decreased flexibility and increased extent of branching of polymer chains limits passage of a polymer through a pore of comparable size and reduces elimination through the kidneys [8]. *In vitro* diffusion studies of polymers through porous structures have shown that transport of linear polymers in tissue containing complex extracellular matrix is different from that of branched polymers [15, 22-25]. The exponent for power law stating the molecular weight dependence on diffusion coefficient through a membrane with defined pore sizes is different for a linear (exponent = -1 to -2.5) versus branched (exponent = -0.33) polymer. These observations are explained by de Gennes's polymer reptation theory where a linear

polymer can move through a network of fibrous obstacles presented by the extracellular matrix while the branched polymer cannot [26]. The branched polymer has to deform in order to diffuse through. *In vivo*, the glomerular basement membrane, which is a complex fibrous network is known to be the primary barrier to filtration of neutral macromolecules [27]. Hence, it has been considered fairly realistic to apply the theory of molecular sieving in polymeric gels to the glomerular filtration of macromolecules [27]. For the lower molecular weight polymers, in spite of a higher hydrodynamic radius, G5.0-OH (R_h = 2.3 nm) eliminated faster than HPMA copolymer (26 kDa) (R_h = 1.4 nm), possibly due to a compact and flexible structure that allowed faster extravasation. The conformational change of PAMAM dendrimers with increase in hydrodynamic size can affect their deforming capability and drastically reduce transport through the capillary endothelium of clearance organs thereby reducing their clearance. G6.0-OH (R_h = 3.0 nm) eliminated slower than HPMA copolymer (52 kDa) (R_h = 3.3 nm) of comparable MW, possibly due to increased rigidity and consequently slower extravasation. HPMA copolymers, owing to a linear architecture can potentially reptate through pores of capillary endothelium, even if their effective hydrodynamic radii are greater than pore size of fenestration. Hence, even though the elimination clearance for G7.0-OH (R_h = 4.0 nm) was greater than HPMA copolymer (131 kDa) (R_h = 8.2 nm) of comparable MW, the rate at which the elimination clearance changed over a fixed MW range was different for the two polymers of varying architecture. The elimination clearance changed less rapidly with increase in molecular weight and hydrodynamic size of HPMA copolymers as compared to PAMAM dendrimers. In addition to differences in interstitial transport rates of PAMAM-OH dendrimers and HPMA copolymers, their intrinsic differences in

physicochemical properties could potentially alter their rate and extent of endocytosis and transcytosis through cells, directly affecting their blood clearances. Extensive kidney accmumlation of G5.0-OH and liver accumulation of G6.0-OH also suggests differences in cellular uptake of these polymers based on accumulation size and architecture [10].

Renal clearance showed a trend similar to the elimination clearance where along with hydrodynamic size, the polymer architecture affected this parameter (Figure 4-5). The effective pore size for glomerular filtration through the kidney is 3.7-6.0 nm in hydrodynamic diameter [11]. PAMAM G5.0-OH and HPMA copolymer (26 kDa) fall below the size cutoff of glomerular filtration and should readily eliminate through the kidneys. However, renal clearance of G5.0-OH was less than HPMA copolymers of comparable molecular weight since G5.0-OH showed persistent accumulation in the kidney (up to 80% injected dose) (Chapter 3) [10]. Limited mechanistic studies for renal retention of PAMAM dendrimers report the localization of these polymers in the lysosomes of proximal tubule cells upon glomerular filtration [28]. G6.0-OH (R_h = 3.0 nm) and HPMA copolymer (52 kDa) (R_h = 3.3 nm) are comparable in hydrodynamic size and fall on the threshold of the size cutoff range for kidney filtration. HPMA copolymer (52kDa) was renally cleared to a higher extent than G6.0-OH. HPMA copolymer (131 kDa) (R_h = 8.2 nm) is twice the hydrodynamic size of G7.0-OH (R_h = 4.0 nm), and yet was renally cleared to a greater extent than its PAMAM counterpart of comparable MW. This can be explained by the architectural difference in the two constructs. The primary impediment to renal clearance of these polymers is likely to be the tortuous path through the fibrous mesh of the glomerular basement membrane [27]. While the linear HPMA copolymers can potentially reptate through a pore smaller in size than their hydrodynamic

radii in a random coil conformation, PAMAM dendrimers have to deform in order to permeate across the pores (Figure 4-10). With increase in molecular weight or generation, the deforming capacity of PAMAM-OH dendrimers is known to decrease, making it harder for higher generation PAMAM-OH dendrimers to sieve through the glomerulus as compared to HPMA copolymers of comparable molecular weights.

Renal clearance was however significantly less than the total elimination clearance suggesting clearance through the liver and spleen. It could also suggest distribution of the polymers into other compartments outside the central compartment (blood). Specifically renal clearance was significantly less for PAMAM dendrimers than HPMA copolymers. PAMAM-OH dendrimers showed high liver accumulation (15-50% injected dose/g of liver tissue), which could potentially be indicative of biliary clearance [10].

Polymer concentration in a given tumor type is a function of blood clearance rate and vascular exposure along with kinetics of transendothelial transport within the tumor or effective interstitial diffusion coefficient [29, 18]. These factors are governed by a number of physicochemical characteristics of the polymer including size, surface characteristics, shape, and rigidity [18]. Of these properties affecting interstitial tumor transport, the molecular conformation or polymer architecture has been the least studied. In general, polymers with a flexible conformation have demonstrated more ideal tumor transport properties leading to higher tumor accumulation [30-32]. Findings reported in this analysis, however are contradicting this literature-reported trend with the globular, rigid PAMAM dendrimers showing higher tumor to blood exposure ratio and extravsation rate constants (K_2, K_6) than the random coil, flexible HPMA copolymers of

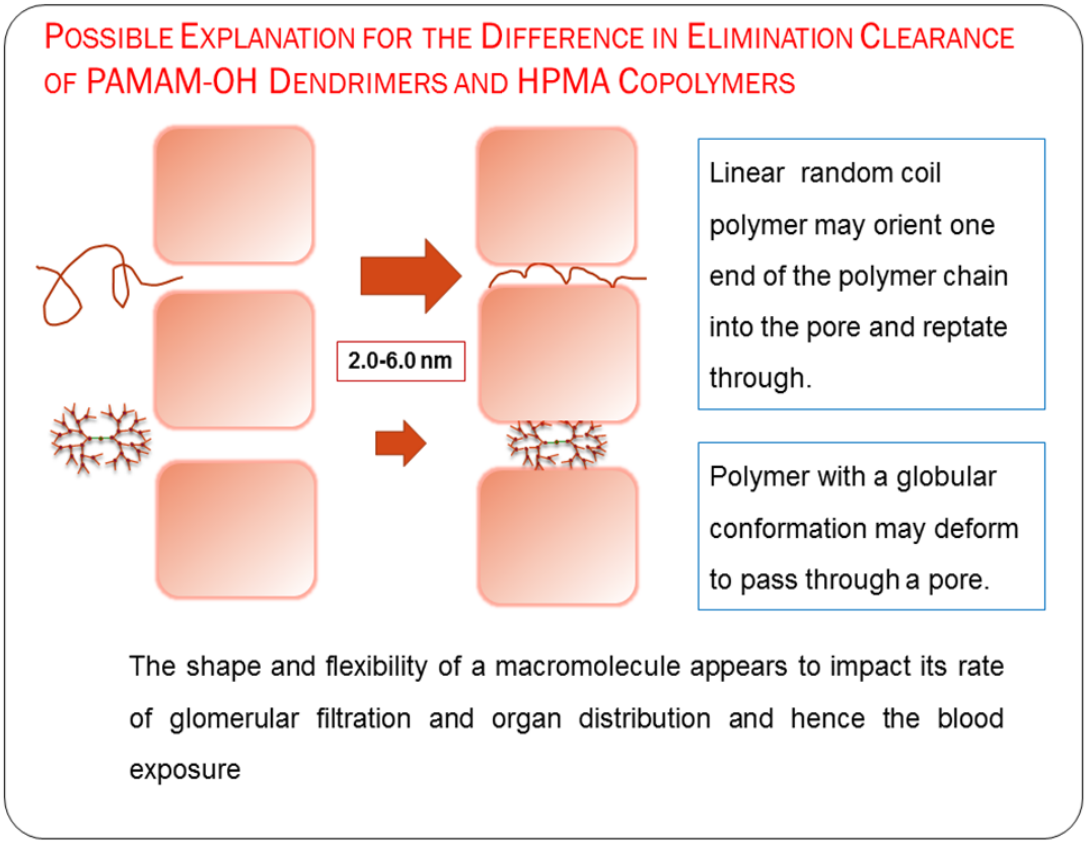

Figure 4-10. Proposed explanation for the difference in elimination clearance of PAMAM-OH dendrimers and HPMA copolymers. Adapted from Ref [8].

comparable MW (Figure 4-9). This could be indicative of a phenomenon in the complex fibrous extracellular matrix of angiogenic neovasculature where rigid nanoscale constructs may show higher permeability than coiled polymers that can entangle in the matrix. Besides the conformation, the difference in hydrodynamic size of polymers of varying architecture and comparable molecular weights could also contribute to differences in tumor extravsation rate constant (K_6) and total exposure (AUC_{tumor}/dose). For instance, HPMA copolymer (131 kDa) (R_h = 8.2 nm) is twice the hydrodynamic size of G7.0-OH (R_h = 4.0 nm) of comparable molecular weight. It is known that the primary impediment for the transvascular extravasation of particles across the blood-tumor-barrier is at the level of the glycocalyx that coats the surface of pores formed in the trans-endothelial cell fenestrations and inter-endothelial cell gaps [18, 22]. The luminal glycocalyx layer acts as a nanofilter for transvascular flow creating an effective physiological upper limit of pore size for the blood-tumor-barrier [18, 22]. This pore size cutoff can vary for different tumor types and is not precisely known for the orthotopic xenograft A2780 ovarian carcinoma tumors under study. However, based on the pore size range for other tumor types, it could range between the hydrodynamic sizes of HPMA copolymer (131 kDa) and G7.0-OH [33]. This could potentially explain the difference in tumor accumulation of these higher molecular weight polymers. These findings suggest that further investigation and optimization of polymer size and conformation is necessary for optimal tumor transport and accumulation.

4.5. Conclusion

Along with MW and hydrodynamic size, polymer architecture was critical in affecting the blood pharmacokinetics of the PAMAM-OH dendrimers and HPMA copolymers. Over the MW range studied, elimination clearance decreased more rapidly with increase in R_h for PAMAM-OH dendrimers as compared to HPMA copolymers. Linear HPMA copolymers were eliminated renally to a higher extent than hyperbranched PAMAM-OH dendrimers. These results were indicative of a difference in extravasation of polymers of varying architecture through fenestrations of the kidney tissue. In addition, PAMAM-OH dendrimers had a higher tumor to blood exposure ratio than HPMA copolymers indicating that when in circulation, PAMAM-OH were taken up in the tumor to a greater extent than HPMA copolymers.

4.6. References

1. Duncan R, Izzo L. Dendrimer biocompatibility and toxicity. Adv Drug Deliv Rev. 2005;57(15):2215-37.

2. Malik N, Wiwattanapatapee R, Klopsch R, Lorenz K, Frey H, Weener JW et al. Dendrimers: relationship between structure and biocompatibility *in vitro*, and preliminary studies on the biodistribution of 125I-labelled polyamidoamine dendrimers *in vivo*. J Control Release. 2000;65(1-2):133-48.

3. Wijagkanalan W, Kawakami S, Hashida M. Designing dendrimers for drug delivery and imaging: pharmacokinetic considerations. Pharm Res. 2011;28(7):1500-19.

4. Borgman M, Coleman T, Kolhatkar R, Geyser-Stoops S, Line B, Ghandehari H. Tumor-targeted HPMA copolymer-(RGDfK)-(CHX-A"-DTPA) conjugates show increased kidney accumulation. J Control Release. 2008;132(3):193-9.

5. Konak C, Rathi RC, Kopečková P, Kopeček J. Effect of side-chains on solution properties of N-(2-hydroxypropyl) methacrylamide copolymers in aqueous solvents. Polymer. 1993;34(22):4767-73.

6. Lammers T, Kuhnlein R, Kissel M, Subr V, Etrych T, Pola R et al. Effect of physicochemical modification on the biodistribution and tumor accumulation of HPMA copolymers. J Control Release. 2005;110(1):103-18.

7. Chen B, Jerger K, Fréchet JMJ, Szoka Jr FC. The influence of polymer topology on pharmacokinetics: differences between cyclic and linear PEGylated poly (acrylic acid) comb polymers. J Control Release. 2009;140(3):203-9.

8. Fox ME, Szoka FC, Fre chet JMJ. Soluble polymer carriers for the treatment of cancer: the importance of molecular architecture. Acc Chem Res. 2009;42(8):1141-51.

9. Nasongkla N, Chen B, Macaraeg N, Fox ME, Fre chet JMJ, Szoka FC. Dependence of pharmacokinetics and biodistribution on polymer architecture: effect of cyclic versus linear polymers. J Am Chem Soc. 2009;131(11):3842-3.

10. Sadekar S, Ray A, Jana t-Amsbury M, Peterson C, Ghandehari H. Comparative biodistribution of PAMAM dendrimers and HPMA copolymers in ovarian-tumor-bearing mice. Biomacromolecules. 2011;12(1):88-96.

11. Rippe C, Asgeirsson D, Venturoli D, Rippe A, Rippe B. Effects of glomerular filtration rate on Ficoll sieving coefficients (theta) in rats. Kidney Int. 2006;69(8):1326-32.

12. Tande B, Wagner N, Mackay M, Hawker C, Jeong M. Viscosimetric, hydrodynamic, and conformational properties of dendrimers and dendrons. Macromolecules. 2001;34(24):8580-5.

13. Ulbrich K, Subr V. Structural and chemical aspects of HPMA copolymers as drug carriers. Adv Drug Deliv Rev. 2010;62(2):150-66.

14. Schmidt MM, Wittrup KD. A modeling analysis of the effects of molecular size and binding affinity on tumor targeting. Mol Cancer Ther. 2009;8(10):2861-71.

15. Deen W, Bohrer M, Epstein N. Effects of molecular size and configuration on diffusion in microporous membranes. AlChE J. 1981;27(6):952-9.

16. Nishikawa M, Takakura Y, Hashida M. Pharmacokinetic evaluation of polymeric carriers. Adv Drug Deliv Rev. 1996;21(2):135-55.

17. Maeda H, Wu J, Sawa T, Matsumura Y, Hori K. Tumor vascular permeability and the EPR effect in macromolecular therapeutics: a review. J Control Release. 2000;65(1-2):271-84.

18. Chauhan VP, Stylianopoulos T, Boucher Y, Jain RK. Delivery of molecular and nanoscale medicine to tumors: transport barriers and strategies. Annu Rev Chem Biomol. 2011;2:281-98.

19. Tomalia D, Reyna L, Svenson S. Dendrimers as multi-purpose nanodevices for oncology drug delivery and diagnostic imaging. Biochem Soc Trans. 2007;35:61-7.

20. Gillies ER, Dy E, Fréchet JMJ, Szoka FC. Biological evaluation of polyester dendrimer: poly (ethylene oxide)"bow-tie" hybrids with tunable molecular weight and architecture. Mol Pharm. 2005;2(2):129-38.

21. Lim J, Guo Y, Rostollan CL, Stanfield J, Hsieh JT, Sun X et al. The role of the size and number of polyethylene glycol chains in the biodistribution and tumor localization of triazine dendrimers. Mol Pharm. 2008;5(4):540-7.

22. Jain RK. Transport of molecules in the tumor interstitium: a review. Cancer Res. 1987;47(12):3039.

23. Ohlson M, Sörensson J, Lindström K, Blom AM, Fries E, Haraldsson B. Effects of filtration rate on the glomerular barrier and clearance of four differently shaped molecules. Am J Physiol-Renal. 2001;281(1):F103-13.

24. Venturoli D, Rippe B. Ficoll and dextran vs. globular proteins as probes for testing glomerular permselectivity: effects of molecular size, shape, charge, and deformability. Am J Physiol-Renal. 2005;288(4):F605-13.

25. Pluen A, Netti PA, Jain RK, Berk DA. Diffusion of macromolecules in agarose gels: comparison of linear and globular configurations. Biophys J. 1999;77(1):542-52.

26. Gennes PGd. Reptation of a polymer chain in the presence of fixed obstracles. J Chem Phys. 1971;55(2):572-9.

27. Deen WM, Bohrer MP, Brenner BM. Macromolecule transport across glomerular capillaries: application of pore theory. Kidney Int. 1979;16(3):353-65.

28. Kobayashi H, Kawamoto S, Jo SK, Sato N, Saga T, Hiraga A et al. Renal tubular damage detected by dynamic micro-MRI with a dendrimer-based magnetic resonance contrast agent. Kidney Int. 2002;61(6):1980-5.

29. Dreher MR, Liu W, Michelich CR, Dewhirst MW, Yuan F, Chilkoti A. Tumor vascular permeability, accumulation, and penetration of macromolecular drug carriers. J Natl Cancer Inst. 2006;98(5):335-44.

30. Uzgiris E. The role of molecular conformation on tumor uptake of polymeric contrast agents. Invest Radiol. 2004;39(3):131-7.

31. Uzgiris E, Cline H, Moasser B, Grimmond B, Amaratunga M, Smith JF et al. Conformation and structure of polymeric contrast agents for medical imaging. Biomacromolecules. 2004;5(1):54-61.

32. Uzgiris EE. A cell-surface polymer reptation mechanism for tumor transendothelial transport of macromolecules. Technol Cancer Res T. 2008;7(3):257-68.

33. Sarin H, Kanevsky AS, Wu H, Sousa AA, Wilson CM, Aronova MA et al. Physiologic upper limit of pore size in the blood-tumor barrier of malignant solid tumors. J Transl Med. 2009;7(1):51.

CHAPTER 5

PAMAM DENDRIMERS AS ORAL ABSORPTION ENHANCERS FOR ORAL DELIVERY OF CAMPTOTHECIN

5.1. Introduction

5.1.1. Oral delivery of camptothecin

Oral administration of chemotherapeutics has treatment advantages of patient preference, convenience of administration, cost-effectiveness and improving quality of life in palliative care [1, 2]. In terms of treatment outcomes, oral chemotherapeutics are advantageous for protracted dosage regimens as is the case for schedule-dependent cytotoxic drugs [1, 3]. Camptothecin and its derivatives are potent topoisomerase-I inhibitors that show a schedule-dependent activity which means that they are more efficacious with low and frequent oral dosage regimens [4]. However, the oral delivery of camptothecins is limited by poor and variable bioavailability attributed to low solubility, low permeability and P-gp efflux of the drug [5].

Camptothecin and its derivatives have been solubilized in various micellar, liposomal, microsphere, microemulsion and cyclodextrin-based formulations [6-10]. A

number of water-soluble analogues and prodrugs have also been synthesized [6, 11-18]. However, the majority of these formulations have not been evaluated for oral delivery.

5.1.2. Poly(amido amine) or PAMAM dendrimers as oral drug carriers

Poly(amido amine) (PAMAM) dendrimers are a class of hyperbranched polymers [19]. They are synthesized with alternating repeating units of ethylene diamine and methyl acrylate and can be terminated to have primary amines, carboxylic acids or hydroxyl-terminated groups [20, 19]. As a result of the repeated branching, PAMAM dendrimers have a dense surface exterior and a relatively hollow interior, where they are known to solubilize hydrophobic moieties by encapsulation or surface interactions [21-32].

PAMAM dendrimers have also been extensively evaluated *in vitro* for potential oral drug delivery applications as intestinal penetration enhancers as well as carriers for transepithelial transport of small molecules [33]. Both cationic, amine-terminated as well as anionic, carboxylic acid-terminated PAMAM dendrimers are known to modulate tight junctions and increase paracellular transport of small molecules [34-36]. They are also known to be translocated across the intestinal epithelial barrier by endocytic mechanisms [37-40]. Additionally, cationic PAMAM dendrimers are known to interact with lipid bilayers on cell membranes increasing their cellular uptake [41]. Their solubilizing potential combined with their transepithelial transport make PAMAM dendrimers attractive for oral delivery of biopharmaceutics classification system (BCS) class IV drugs such as camptothecin [15-17]. There have been very limited studies *in vivo* to evaluate PAMAM dendrimers for oral drug delivery [42, 43]. In this study, camptothecin

was formulated and co-delivered with cationic, amine-terminated PAMAM dendrimer generation 4 (G4.0) and anionic, carboxylate-terminated generation 3.5 (G3.5) in CD-1 mice.

5.2. Materials and methods

5.2.1. Materials

Poly(amido amine) dendrimers generation 4 (G4.0-NH_2) and generation 3.5 (G3.5-COONa) were purchased from Dendritech (Midland, MI). Camptothecin was procured from A.K.Scientific (Union City, CA). Tritium (^3H)-labeled camptothecin and ^{14}C-labeled Mannitol were purchased from American Radiolabeled Chemicals (St. Louis, MO). Reagents for beta detection were purchased from Perkin Elmer (Waltham, MA).

5.2.2. Methods

5.2.2.1. Physicochemical characterization of PAMAM dendrimers

The chromatographic elution profiles of the PAMAM dendrimers under study, G4.0-NH_2 and G3.5-COONa, were obtained using a Fast Protein Liquid Chromatography (FPLC) system with an analytical Superose 6^{TM} 10/300 GL column (GE Healthcare) and an ultraviolet detector (GE Healthcare) in order to evaluate relative elution volumes and to check for the absence of small molecular weight impurities (Appendix B). The mobile phase for elution was 20% (v/v) acetonitrile and 80% (v/v) phosphate buffer saline (137 mM NaCl, 2.7 mM KCl, 10 mM Na_2HPO_4, 1.76 mM KH_2PO_4, pH 7.4) at a flow rate of 1.0 mL/minute. Eluted peaks were detected at a wavelength of 280 nm. PAMAM dendrimers were further characterized for hydrodynamic radius (R_h) using a Dynamic

Light Scattering (DLS) detector (Helleos II) attached to the FPLC system and analyzed using Astra^{TM} 5.3.4.13 software (Wyatt Technologies Corp).

5.2.2.2. Camptothecin formulations with poly(amido amine) dendrimers

The camptothecin alone (0.5 mg/mL, 14.4 x 10^{-4} M) was formulated in a solution of DMSO: 0.05M borate buffer-pH 8.5: poly(ethylene glycol) 400 in the ratio 1:9.5:9.5. For the formulations of camptothecin co-delivered with PAMAM, a dispersion of camptothecin (0.5mg/mL, 14.4 x 10^{-4} M) was prepared using the solvent system DMSO: deionized water: poly(ethylene glycol) 400 in the ratio 1:9.5:9.5. Methanolic solutions of PAMAM dendrimers were evaporated up to the constant weight. The drug dispersion was stirred with PAMAM dendrimers at room temperature for 12 hours by mixing with varying concentrations and generations of PAMAM dendrimers (Table 5-1)

The pH of all the formulations including the camptothecin was adjusted to be between 8.5-9.0, to facilitate head to head comparison of the oral absorption of camptothecin across different treatment groups. The ratios of drug to dendrimer were chosen based on maximum tolerated oral doses of the two as well as the reported solubilization potential of PAMAM dendrimers specifically for camptothecin [44, 30]. In order to ascertain the solubility of the formulations, they were filtered through a 100 kDa centrifugal membrane filter (Nanosep 100K Omega, Pall Corporation, Ann Arbor, MI) that was pretreated with 5 weight % solution of Triton-X to minimize adsorption to the membrane. The filtrate obtained after spinning the centrifuge tubes at 14,000g for 20 minutes was spectrophotometrically analyzed for camptothecin content at an absorbance maximum of 370 nm (Spectramax M2, Molecular Devices, LLC., Sunnyvale, CA).

Table 5-1. Formulation ratios of PAMAM to camptothecin

PAMAM concentration (mg/kg)	**PAMAM concentration (M)**	**PAMAM/camptothecin Molar ratio**
CPT + G4.0-NH_2 (100 mg/kg)	7.1×10^{-4}	0.49
CPT + G4.0-NH_2 (300 mg/kg)	21.1×10^{-4}	1.47
CPT + G3.5-COONa (300 mg/kg)	23.2×10^{-4}	1.61
CPT + G3.5-COONa (1000 mg/kg)	77.4×10^{-4}	5.38

5.2.2.3. Mannitol oral absorption

Mannitol alone (0.5 mg/mL) was dissolved in a solution of DI water. Methanolic solutions of PAMAM dendrimers were evaporated up to the constant weight. For the mixtures of mannitol co-delivered with PAMAM, the mannitol solution was mixed with the highest doses of PAMAMs of various generations under study as follows:

1. G4.0-NH_2 (30 mg/mL or 21.1 x 10^{-4} M)-300 mg/kg

2. G3.5-COONa (100 mg/mL or 77.4 x 10^{-4} M)-1000 mg/kg

The pH values of all the solutions were adjusted to be between 8.5-9.0, to facilitate head-to-head comparison of the paracellular transport of mannitol across different treatment groups.

5.2.2.4. Characterization of camptothecin – PAMAM formulations

To evaluate the percentage of camptothecin associated with the PAMAM dendrimers in the formulations, they were diluted 5x with DI water and filtered through a 3.5 kDa centrifugal membrane (Amicon® Ultra 0.5 mL, EMD Millipore, Billerica, MA) that was pretreated with 5 weight % solution of Triton-X to minimize adsorption to the membrane. The filtrate obtained after spinning the tubes at 14,000g for 20 minutes was spectrophotometrically analyzed for camptothecin content at an absorbance maximum of 370 nm (Spectramax M2, Molecular Devices, LLC.) (U.V absorbance standard curve in Appendix B).

In order to assess the percentage of camptothecin in the lactone and carboxylate forms, camptothecin alone and PAMAM camptothecin formulations were eluted on a reverse phase C18 (5 µm, 250 mm x 5 mm) high performance liquid chromatography

column (XTerra, Waters®; Agilent HPLC system). The mobile phase used was acetonitrile: aqueous triethylamine acetate buffer (prepared using 0.1% v/v triethylamine, adjusted with glacial acetic acid to pH 5.5), in the ratio of 27:73 delivered at a flow rate of 1.0 ml/min with an injection volume of 20 µl (method adapted from [30]). Camptothecin in the lactone form was detected at an absorbance wavelength of 370 nm and a retention time of 11.47 ± 0.12 minute. Camptothecin in the carboxylate sodium salt form was detected at an absorbance wavelength of 370 nm and a retention time of 4.16 ± 0.03 min. The camptothecin calibration curve for the lactone form was y =75.19x-5.50 (r^2 = 0.99), when the peak area was plotted vs concentration of camptothecin in µg/mL (Appendix B). The camptothecin calibration curve for the carboxylate sodium salt form was y =58237x+100.88 (r^2 = 0.99) when the peak area was plotted vs concentration of camptothecin in mg/mL (Appendix B). The solution for the camptothecin lactone form standard curve was prepared in DMSO acidified with 0.1N HCl while the solution for the camptothecin carboxylate sodium salt form standard curve was prepared in 0.1N NaOH. The solvent system of the HPLC run (pH 5.5) did not cause inter-conversion of the lactone and carboxylate forms during the duration of the run.

In order to check the precipitation kinetics of the drug when formulated with PAMAM, camptothecin alone and PAMAM-camptothecin formulations were incubated with simulated gastric (0.2% w/v NaCl, 0.7% w/v HCl) and intestinal (6.8% w/v KH_2PO_4, 0.9% w/v NaOH) fluids at 37^0C. 500 µL of solutions were sampled at the end of 2 hours for simulated gastric fluid (SGF), and 3 hours for simulated intestinal fluid (SIF), and filtered through a 100 kDa centrifugal membrane filter (Nanosep 100K Omega, Pall Corporation, Ann Arbor, MI) that was pretreated with 5 weight % solution

of Triton-X to minimize adsorption to the membrane. The filtrate obtained after spinning the centrifugal tubes at 14,000g for 20 minutes was buffered back by incubation with 1:1 0.1N HCl at 37^0C for 2 hours. The filtrate was spectrophotometrically analyzed for camptothecin content at an absorbance maximum of 370 nm (Spectramax M2, Molecular Devices, LLC., Sunnyvale, CA). Formulations were evaluated in the simulated instestinal fluid for only 3 hours because the absorption enhancement action of PAMAM dendrimers is known to be in the upper gastrointestinal tract [42, 43].

5.2.2.5. *In vivo* oral absorption

Six-to eight-week female CD-1 mice were dosed by oral gavage with 0.2 mL of camptothecin alone (5 mg/kg) and camptothecin (5 mg/kg) mixed with PAMAM G4.0-NH_2 (100 and 300 mg/kg) and G3.5-COONa (300 and 1000 mg/kg) (Dose preparation detailed in Section 5.2.2.2). *In vivo* dose selection of PAMAM dendrimers was based on maximum tolerated oral doses evaluated previously [44]. In addition, 6-to 8-week female CD-1 mice were dosed by oral gavage with 0.2 mL of mannitol alone (5 mg/kg) and mannitol (5 mg/kg) mixed with the highest doses of PAMAMs under study- G4.0-NH_2 (300 mg/kg) and G3.5-COONa (1000 mg/kg). (Dose preparation detailed in Section 5.2.2.3). Camptothecin and mannitol were tritium and ^{14}C-labeled respectively to facilitate detection. For the camptothecin formulations, animals were sacrificed at 0.5, 1, 2, 4 and 8 hours. Blood and liver samples were analyzed by ^{3}H-Camptothecin beta detection (procedure detailed below). For the mannitol solutions, animals were sacrificed at 2 hours, the T_{max} of mannitol absorption and blood samples were analyzed by ^{14}C-mannitol beta detection.

For tissue digestion, blood (50 µL) and liver (50 mg) samples were digested using 0.5 mL of Solvable™ (PerkinElmer, Inc.) and Soluene™-350 (PerkinElmer, Inc.) respectively with incubation and shaking at 60^0C for 1 hour.

For tissue bleaching, 50 µL of 0.1M EDTA solution was added to the digested samples to minimize foaming during the bleaching process. 150 µL of a 30% solution of hydrogen peroxide was added to the digested tissue samples in 3 aliquots of 50 µL each, over 30 minutes, with intermittent shaking. Samples were allowed a reaction time of 30 minutes at room temperature and subsequently incubated at 60^0C for 30 minutes. This facilitated the quenching of excess free radicals generated during the bleaching process.

For beta detection, the bleached blood and liver samples were mixed with 4.5 mL of liquid scintillation cocktails-Ultima Gold™ and Hionic Fluor™ (PerkinElmer, Inc.), respectively. The samples were light and temperature adapted for 24 hours and counted using a liquid scintillation system (Beckman LS 6000IC, Beckman Coulter, Inc.).

Beta detection of tissue samples is sensitive to the ratio of digestion, bleaching and detection agents. This ratio was optimized to obtain the lowest luminescence interference and the most optimal processing parameters and efficiencies (Table 5-2).

5.2.2.6. Histologic assessment of small intestinal segments

Six- to eight-week female CD-1 mice were dosed by oral gavage with 0.2 mL of saline, G4.0-NH_2 (100 and 300 mg/kg) and G3.5-COONa (300 and 1000 mg/kg) to evaluate changes in intestinal histology by dendrimers. In addition, 6- to 8-week female CD-1 mice were dosed by oral gavage with 0.2 mL of CPT alone (5 mg/kg) and CPT (5 mg/kg) mixed with PAMAM G4.0-NH_2 (100 and 300 mg/kg) and G3.5-

Table 5-2. Processing parameters of Tritium and ^{14}Carbon counting from blood and liver

	^{3}H	**^{14}C**
Blood		
Lumex (%)	4.19 ± 3.19	0.17 ± 0.02
Extraction Efficiency (%)	75.48 ± 6.09	88.26 ± 0.01
Blank Blood	46.28 ± 11.35	37.17 ± 0.76
Liver		
Lumex (%)	1.14 ± 0.63	-
Extraction Efficiency (%)	77.39 ± 4.81	-
Blank Blood	41.23 ± 9.82	-

COONa (300 and 1000 mg/kg) (Dose preparation detailed in section 5.2.2.2). *In vivo* dose selection of PAMAM dendrimers was based on maximum tolerated oral doses evaluated previously [44]. Animals were sacrificed at 4 hours. Tissue samples were taken from different sections of the small intestine and stained by H and E staining to evaluate morphological changes in the small intestinal segments using a dark-field microscope (Olympus® BH-2, Olympus Corp., Center Valley, PA) and a digital camera for imaging (DXM1200C, Nikon Instruments Inc., Melville, NY). Small intestinal segments were also evaluated by Transmission Electron Microscopy (Hitachi I-7100 operated at 75 kV using a Leica EMUC6 ultramicrotome, South San Francisco, CA) to assess microvilli integrity.

5.3. Results and discussion

5.3.1. Characteristics of the formulation of PAMAM dendrimers with camptothecin

With increase in PAMAM generation or extent of branching, these dendrimers are known to undergo a conformational change [20, 45]. Owing to a high functional group density on the surface, PAMAM generations 3.5 and 4.0 are known to have a relatively hollow interior and a dense exterior possessing nano-container-like properties by which they efficiently encapsulate and complex small hydrophobic molecules [46]. PAMAM generations 3.5-COONa and 4.0-NH_2 are reported to have a molecular weight of 12,927.69 and 14,214.17 kDa respectively, assuming perfect dendrimer synthesis [19]. The hydrodynamic radius range of G3.5 was 1.3 ± 0.1 nm and that of G4.0 was 1.7 ± 0.1 nm as measured by dynamic light scattering. The surface functionality of PAMAM G4.0

is a primary amine group (n= 64) with a reported pKa of 8-9 while that of PAMAM G3.5 is a carboxylic acid group (n=64) with a pKa of 3-4 [20]. The interior of the PAMAM G4.0 and G3.5 has 62 tertiary nitrogen atoms (pKa of 3-6) [20]. These functional groups on the surface and the interior of the PAMAM dendrimers are known to interact with guest molecules via electrostatic interactions, hydrogen bonding and hydrophobic interactions [22, 21]. This interaction depends on a number of factors, some of which are PAMAM generation and core, ratio of dendrimer to drug, physicochemical properties of drugs and pH [22, 21]. Camptothecin formulated with PAMAM G4.0 showed up to 80% association with the dendrimer (Table 5-3). The concentration of G4.0 did not influence this association. On the other hand, camptothecin formulated with PAMAM G3.5 showed only a 20-30% association with the dendrimer (Table 5-3). In case of G4.0, at a 100 mg/kg dose, there was one molecule of PAMAM for every two molecules of camptothecin while at 300 mg/kg, there were two molecules of PAMAM for every molecule of camptothecin (Table 5-1). Every molecule of PAMAM also has 64 primary amine surface functionalities, 62 internal tertiary nitrogens and other internal hydrogen bonding sites contributed by the amide bonds. Camptothecin has a lactone E-ring that hydrolyzes around pH 7.0 to yield the carboxylate form of the drug [47]. When camptothecin was solubilized with PAMAM G4.0 at pH 8-9, the primary amine group (protonated about 50%) hydrolyzed the lactone of the camptothecin to yield the carboxylate form (as observed by HPLC, Figure 5-1). The carboxylate group of camptothecin potentially formed an ionic bond with the protonated primary amine groups on the PAMAM surface.

Table 5-3. Association of camptothecin with PAMAM dendrimers

Formulation	Percentage associated with PAMAM
CPT + G4.0-NH_2 (100 mg/kg)	80.27 ± 0.66
CPT + G4.0-NH_2 (300 mg/kg)	81.80 ± 0.24
CPT + G3.5-COONa (300 mg/kg)	29.57 ± 3.31
CPT + G3.5-COONa (1000 mg/kg)	23.23 ± 0.46

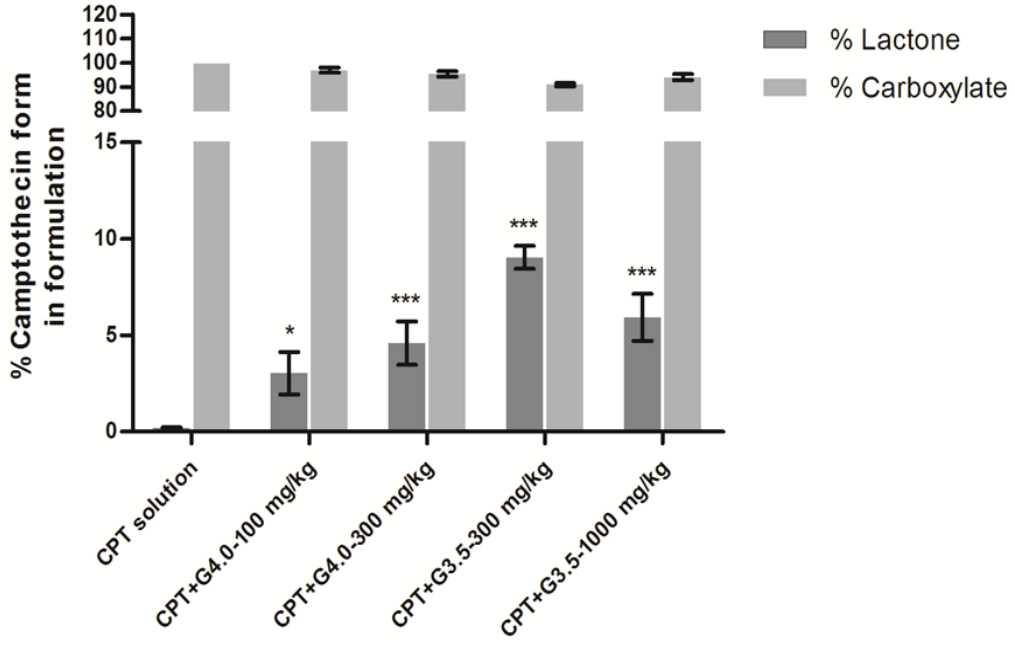

Figure 5-1. Percentage of camptothecin in the lactone form in its formulation alone and with PAMAM G4.0 (100 and 300 mg/kg), and G3.5(300 and 1000 mg/kg). Statistically significant difference between camptothecin alone and camptothecin formulation with G4.0, G3.5, * $p<0.05$, ***$p<0.001$ by one-way ANOVA and Bonferroni's multiple comparison tests comparing PAMAM-CPT formulations with CPT alone. Camptothecin formulated with PAMAM to form a soluble formulation had a higher % of drug in the lactone (unionized form) compared to camptothecin solution alone suggesting potential encapsulation of camptothecin within the interior cavities of both cationic G4.0 and anionic G3.5.

In addition to surface electrostatic interaction, camptothecin could also have been partially encapsulated into the dendrimer interior. The association of camptothecin to the interior of PAMAM G4.0 can be attributed to hydrophobic interactions between the drug and the relatively hydrophobic interior of the dendrimer (tertiary nitrogens will not be protonated at pH 8-9) compared to the external aqueous environment. It could also be due to hydrogen bonding between the drug and the dendrimer interior. The dense dendrimer interior could result in local pH environments to facilitate hydrogen bonding that stabilizes the lactone form of the drug, accounting for the small percentage of camptothecin in the lactone form when formulated with the PAMAM dendrimers (Figure 5-1). Detailed 2D-NOESY NMR spectroscopy studies on the interaction of cationic PAMAM dendrimers and anionic guest molecules have demonstrated that there exists an inclusion complex of the anionic hydrophobic drug with the cationic PAMAM dendrimer in addition to the surface electrostatic interactions [28, 48, 49]. Camptothecin formulated with PAMAM G3.5 showed significantly less association with the dendrimer (Table 5-3). This can be attributed to electrostatic repulsion between the negatively-charged PAMAM surface and the carboxylate group on the drug. Unlike PAMAM G4.0, there was no potential for surface interaction with PAMAM G3.5. The partial association observed can be attributed to encapsulation of the drug in the PAMAM interior (similar for both PAMAM G4.0 and G3.5). Concentration of the dendrimer influenced this association. A smaller ratio of G3.5 to camptothecin (1.61) showed a slightly higher drug association (29.57 ± 3.31) than a larger ratio (5.38) which showed a drug association of 23.23 ± 0.46 (Tables 5-1 and 5-3). This can be attributed to a higher extent of electrostatic repulsion in the formulation with a higher dose of G3.5 that potentially reduced encapsulation. As a

consequence of lesser encapsulation, the percentage of lactone form of camptothecin in the higher dose of G3.5 (1000 mg/kg) was also slightly less than the percentage of lactone in the formulation with a smaller dose of G3.5 (300 mg/kg) (Figure 5-1). Such a difference in the association of drug to the cationic and anionic dendrimers has been reported for the solubilization of the hydrophobic drug sylibin (containing ionizable phenol groups) and indomethacin (containing carboxylic acid groups) [43, 50]. Both these drugs associated to a higher extent to the cationic dendrimers due to a surface electrostatic interaction that was not likely in case of the anionic dendrimer. This trend was not observed for nifedipine which does not have an ionizable group that can electrostatically interact with cationic surfaces [27]. Camptothecin delivered alone precipitated in the gastric fluid at 2 hours to a higher extent than when co-delivered with PAMAM suggesting that both cationic and anionic PAMAM dendrimers controlled release and precipitation kinetics of camptothecin at pH 1.2 (Figure 5-2). It is known that the solubilization potential of cationic dendrimers for anionic molecules decreases with decrease in pH due to elimination of electrostatic interaction. [25, 43, 48, 51]. At pH 1.2, the tertiary nitrogen atoms in the interior of the PAMAM dendrimers G4.0 and G3.5 and the primary nitrogen atoms on the surface of G4.0 will be completely protonated but the carboxylate group will be unionized, thus not available for ionic interaction. However, there is a possibility of intermolecular hydrogen bonding between: 1) the hydrogen atom of the carboxylic acid of camptothecin and the carbonyl group from the amide bond of the PAMAM, and 2) the hydrogen atom of the secondary nitrogen from the amide bond and the oxygen atom from the carbonyl group of camptothecin. This stabilizes the drug as a carboxylic acid and also partially solubilizes it. This has been postulated for other

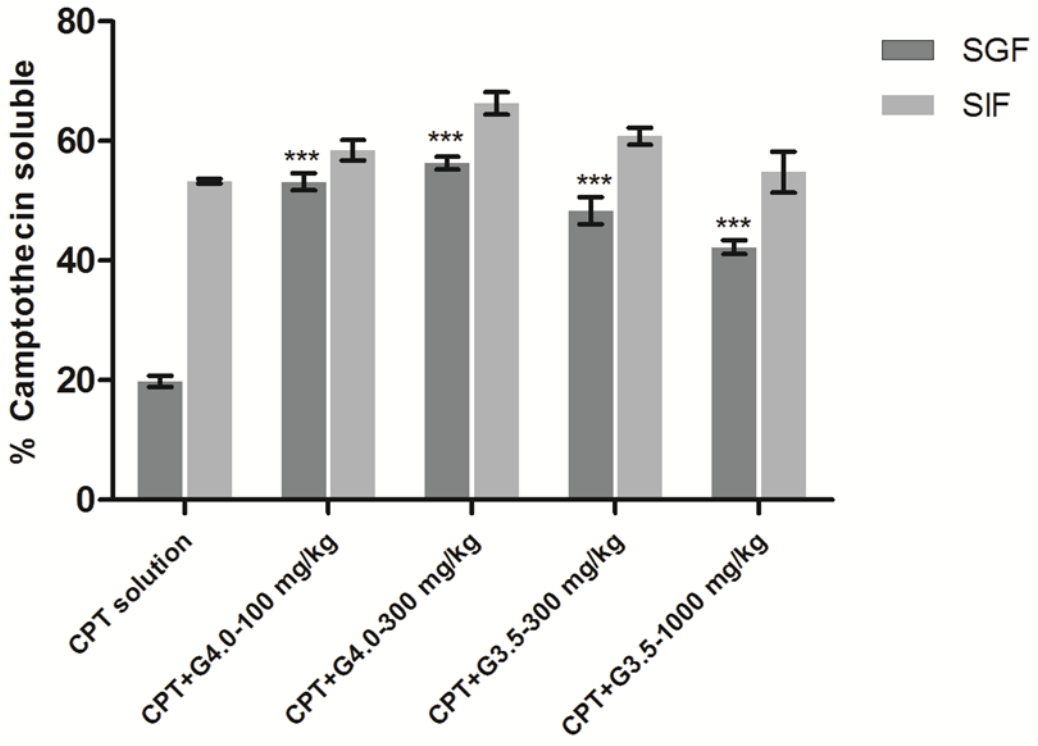

Figure 5-2. Percentage of total camptothecin solubilized in simulated gastric and intestinal fluids at 2 and 3 hours, respectively. n=3. Statistically significant difference between camptothecin alone and camptothecin formulation with G4.0, G3.5, *** $p<0.001$ by one-way ANOVA and Bonferroni's multiple comparison tests comparing PAMAM-CPT formulations with CPT alone.

carboxylic acid-containing hydrophobes like benzoic acid [32]. Inclusion complexes of drug with PAMAM dendrimer can also potentially control release of the drug thus altering precipitation kinetics over 2 hours [51, 43]. In case of the camptothecin solution alone, majority of the drug (80%) precipitated out of solution. However, only 40 % of the drug precipitated out of solution over 2 hours when camptothecin was formulated with PAMAM G4.0 and G3.5.

In the simulated intestinal fluid, there was no difference in the precipitation of the drug when formulated with the PAMAM, with about 40% of the drug precipitating out of solution in 3 hours. At pH 6.8, the carboxylic acid group of the drug is ionized thus preventing intermolecular hydrogen bonding in the dendrimer interior. The primary amine groups of the cationic dendrimer will also not be protonated eliminating surface electrostatic interactions. However, the tertiary nitrogens (pKa 3-6) could be partially protonated, facilitating electrostatic interaction between the ionized drug and the dendrimer interior. This internal association (similar for both cationic and anionic dendrimers) was not reflected in the precipitation kinetics in the SIF due to the water-solubility of the drug in the ionized form at pH 6.8. Inclusion complexes of the dendrimer-drug can, however, control drug release and improve oral bioavailability as seen for oral absorption studies with cationic PAMAM solubilized drugs sylibin and doxorubicin [42, 43].

5.3.2. *In vivo* oral absorption of camptothecin co-delivered with PAMAM dendrimers

Both cationic, amine-terminated PAMAM G4.0-NH_2 and anionic, carboxylic-acid terminated PAMAM G3.5-COONa dendrimers caused an approximate 2- to 3-fold oral absorption enhancement of camptothecin *in vivo* at 2 hours (T_{max} of camptothecin oral absorption). For both G4.0-NH_2 (100-300 mg/kg) and G3.5-COOH (300-1000 mg/kg), there was no statistically significant dose-dependence on absorption enhancement at 2 hours in the dosing range studied (Figure 5-3). Camptothecin levels in the blood when delivered alone or with G4.0 (300 mg/kg) and G3.5 (1000 mg/kg) increased in the first 2 hours and plateaued up to 8 hours (Figure 5-4). The drug exposure of camptothecin (AUC = 3.9 ± 0.1 μg-h/mL) increased 2.2 and 2.5–fold respectively when codelivered with PAMAM G4.0 (AUC = 8.6 ± 0.6 μg-h/mL) and G3.5 (AUC = 9.4 ± 0.8 μg-h/mL). The camptothecin lactone E-ring is known to hydrolyze to the carboxylate form in the plasma and bind to human serum albumin, thus prolonging its circulation half-life to 36 hours [52].

All of the formulations tested had the same drug content but varied in the surface charge and concentration of PAMAM dendrimer and hence in the extent of drug association. The increase in absorption of camptothecin was similar for the cationic (80% camptothecin associated with PAMAM) and anionic dendrimer (20-30% camptothecin associated with PAMAM). Total amount of bioavailable drug in this formulation would be a result of multiple factors. These are drug association to PAMAM, drug solubilization in the simulated gastric and intestinal environments by PAMAM, fraction of drug retained in the unionized form by PAMAM, drug release rate from PAMAM, species

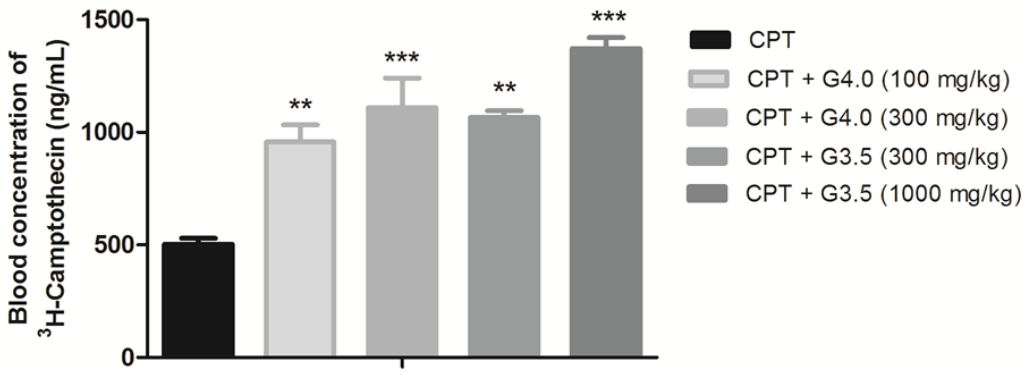

Figure 5-3. Blood concentration of orally administered ^{3}H-Camptothecin at 2 hours alone and co-delivered with PAMAM G4.0 at 100 mg/kg, 300 mg/kg and G3.5 at 300 mg/kg and 1000 mg/kg, n= 3 animals per time point, PAMAM dendrimers G4.0 and G3.5 statistically significantly increased the blood concentration of ^{3}H-Camptothecin, **$p<0.01$, ***$p<0.001$ by one-way ANOVA and Bonferroni's multiple comparison tests comparing PAMAM-CPT formulations with CPT alone.

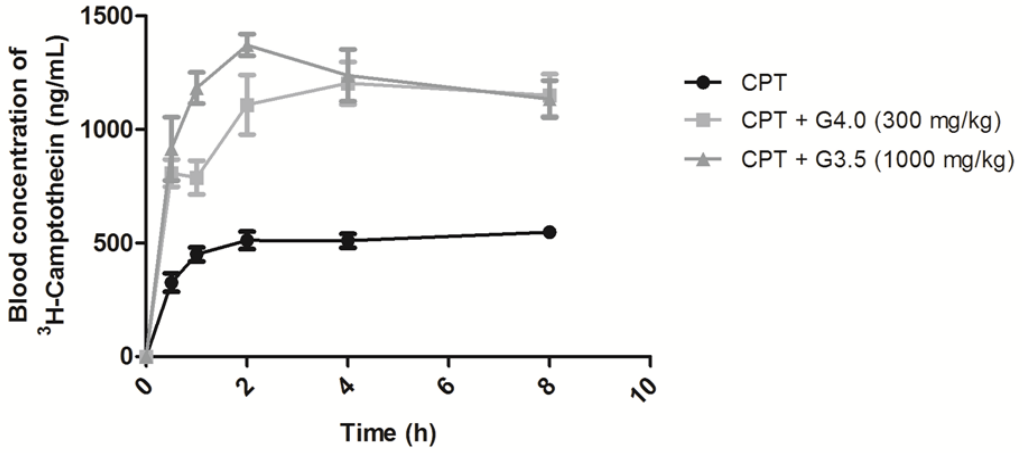

Figure 5-4. Blood concentration-time profile of orally administered ^{3}H-Camptothecin alone and co-delivered with PAMAM G4.0 (300 mg/kg) and G3.5 (1000 mg/kg), n= 3 animals per time point, PAMAM dendrimers statistically significantly increased the blood exposure (AUC computed by the trapezoidal rule) of ^{3}H-Camptothecin, $p<0.001$ by one-way ANOVA and Bonferroni's multiple comparison tests comparing PAMAM-CPT formulations with CPT alone.

being absorbed (free drug or drug associated dendrimer) and tight junction modulation by the polymer. Drug solubilization in SGF and SIF as well as fraction of drug retained in unionized lactone form by PAMAM was similar for both cationic and anionic PAMAM dendrimers at varying concentrations tested (Figure 5-1, 5-2). Limited reports have shown that association of drugs with PAMAM dendrimers controls drug solubilization and release, thereby increasing the oral bioavailability [42, 43]. It is expected therefore that the higher the extent of association, the higher would be the bioavailability of the drug. However, the surface electrostatic interaction between cationic PAMAM and carboxylate group of drug was diminished at lower pH (below pKa of terminal primary amine groups of G4.0), thus suggesting that drug inclusion in PAMAM interior controlled solubilization in SGF, SIF and oral bioavailability. It was also observed that the cationic PAMAM dendrimers bind to mucous layer restricting their interaction with the epithelial barrier *in vivo*. Anionic PAMAM dendrimers did not show this phenomenon. This difference in mucosal interaction and access to epithelial barrier can affect drug release and absorption *in vivo*. Tight junction modulation, which is a factor that affects drug absorption was not seen for either the cationic or the anionic PAMAM dendrimers at doses tested (discussed in Section 5.3.3).

Along with enhancement in blood levels, both cationic, amine-terminated PAMAM G4.0-NH_2 (300 mg/kg) and anionic, carboxylic-acid terminated PAMAM G3.5-COOH (1000 mg/kg) caused an approximate 2-fold increase in liver accumulation of camptothecin *in vivo* at 2 hours (Figure 5-5). Campthtecin derivative (Irinotecan) is approved for hepatic metastasis of colorectal cancer [53]. Oral delivery of camptothecin offers a route through the hepatic portal vein to access the liver directly reducing drug

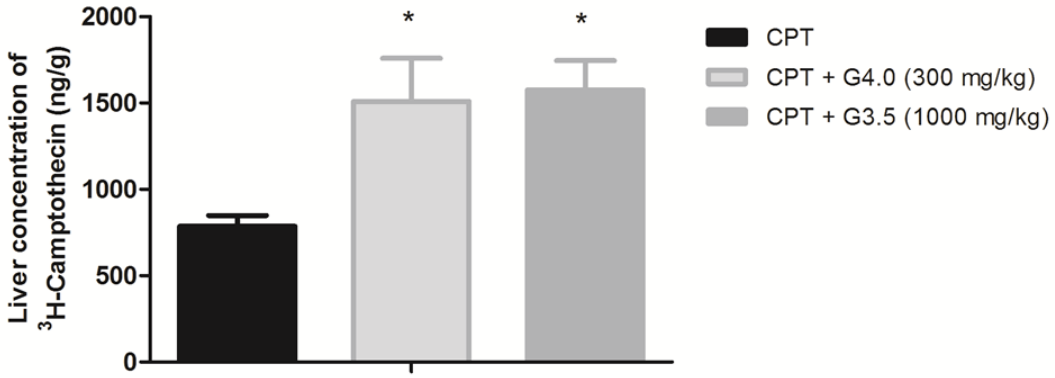

Figure 5-5. Liver concentration of orally administered ^{3}H-Camptothecin at 2 hours alone and co-delivered with PAMAM G4.0 (300 mg/kg) and G3.5 (1000 mg/kg), n= 3 animals per time point, PAMAM dendrimers statistically significantly increased the liver concentration of ^{3}H-Camptothecin, *$p<0.05$ by one-way ANOVA and Bonferroni's multiple comparison tests comparing PAMAM-CPT formulations with CPT alone.

exposure to plasma and consequently reducing non-specific systemic toxicities. It has been reported that liver/blood exposure of camptothecin is higher when camptothecin is delivered orally [54]. However, the oral delivery of camptothecin is limited by variable and low absorption [54]. An increase in oral absorption of camptothecin will allow a therapeutic dose to reach the liver, while decreasing blood exposure of the drug as compared to a similar dose given intravenously.

5.3.3. *In vivo* oral absorption of paracellular marker-mannitol

PAMAM dendrimers did not cause an increase in blood levels of the paracellular marker ^{14}C-mannitol at 2 hours. (T_{max} of Mannitol) (Figure 5-6). This observation suggests that at doses of 300mg/kg for amine-terminated PAMAM G4.0-NH2 and 1000 mg/kg for carboxylic acid-terminated PAMAM G3.5-COONa, tight junction modulation was not observed and that the increase in absorption of camptothecin was not due to opening of tight junctions.

Previous *in vitro* transepithelial transport studies of PAMAM dendrimers across Caco-2 monolayers have reported tight junction modulation by amine and carboxylic acid-terminated PAMAM dendrimers as investigated by TEER (transepithelial electrical resistance) measurements and the permeability of ^{14}C-mannitol [39, 35, 34]. Tight junction modulation was observed to be a function of PAMAM surface chemistry, concentration and incubation time [35]. Both PAMAM G4.0-NH_2 (partially surface modified by FITC) and G3.5-COOH were shown to cause a sharp decline in TEER and a 5- to 10-fold increase in mannitol flux at concentrations of 1.0 mM, when incubated for 2 hours with Caco-2 cell monolayers [34, 35]. The highest doses of the PAMAM

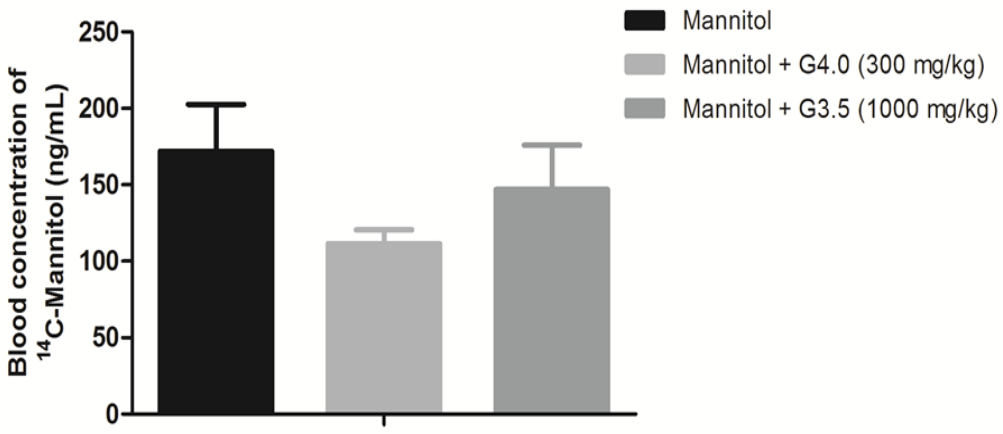

Figure 5-6. Blood concentration of orally administered ^{14}C-Mannitol at 2 hours alone and co-delivered with PAMAM G4.0 (300 mg/kg), G3.5 (1000 mg/kg), n= 5 animals per time point, No statistical significance as per ANOVA.

formulations tested in the current *in vivo* study were 2.1 mM for G4.0-NH_2 (corresponding to 300 mg/kg in animals) and 7.7 mM (corresponding to 1000 mg/kg in animals) for G3.5-COOH. These doses are slightly higher than the doses tested *in vitro* across Caco-2 However, the PAMAM dendrimers dosed in this study were subjected to variables in the *in vivo* GIT system like dilution in the gastric and intestinal fluid, gastrointestinal transit and mucosal barrier. This potentially reduced the effective concentration and incubation time of PAMAM dendrimers at the intestinal surface at which tight junction modulation was not achieved.

5.3.4. Histologic assessment of small intestinal segments

At the PAMAM G4.0-NH_2 and G3.5-COOH doses tested, no clinically significant histologic changes were observed. No morphological changes were noted at the villi (Figure 5-7 and Appendix B) or the microvilli levels (Figure 5-8 and Appendix B). Slight irregularities of microfilaments were observed for the group treated with saline (Figure 5-8 and Appendix B). Previous studies *in vitro* have shown that anionic PAMAM G3.5 (1.0 mM) did not affect microvilli structure in Caco-2 cell monolayers over a 2 hour incubation period while at the same concentration, cationic PAMAM G4.0 showed disruption and loss of microvilli [38]. The influence of surface groups on histologic morphology was not observed in this study. PAMAM G4.0 doses at concentrations of 0.7 mM (100 mg/kg) and 2.1 mM (300 mg/kg) and PAMAM G3.5 doses at 2.3 mM (300 mg/kg) and 7.7 mM (1000 mg/kg) were subjected to gastrointestinal transit time and dilution variables which reduced their effective concentration at the epithelial layer *in vivo* as compared to that on Caco-2 cell monolayers *in vitro*. The camptothecin dosed

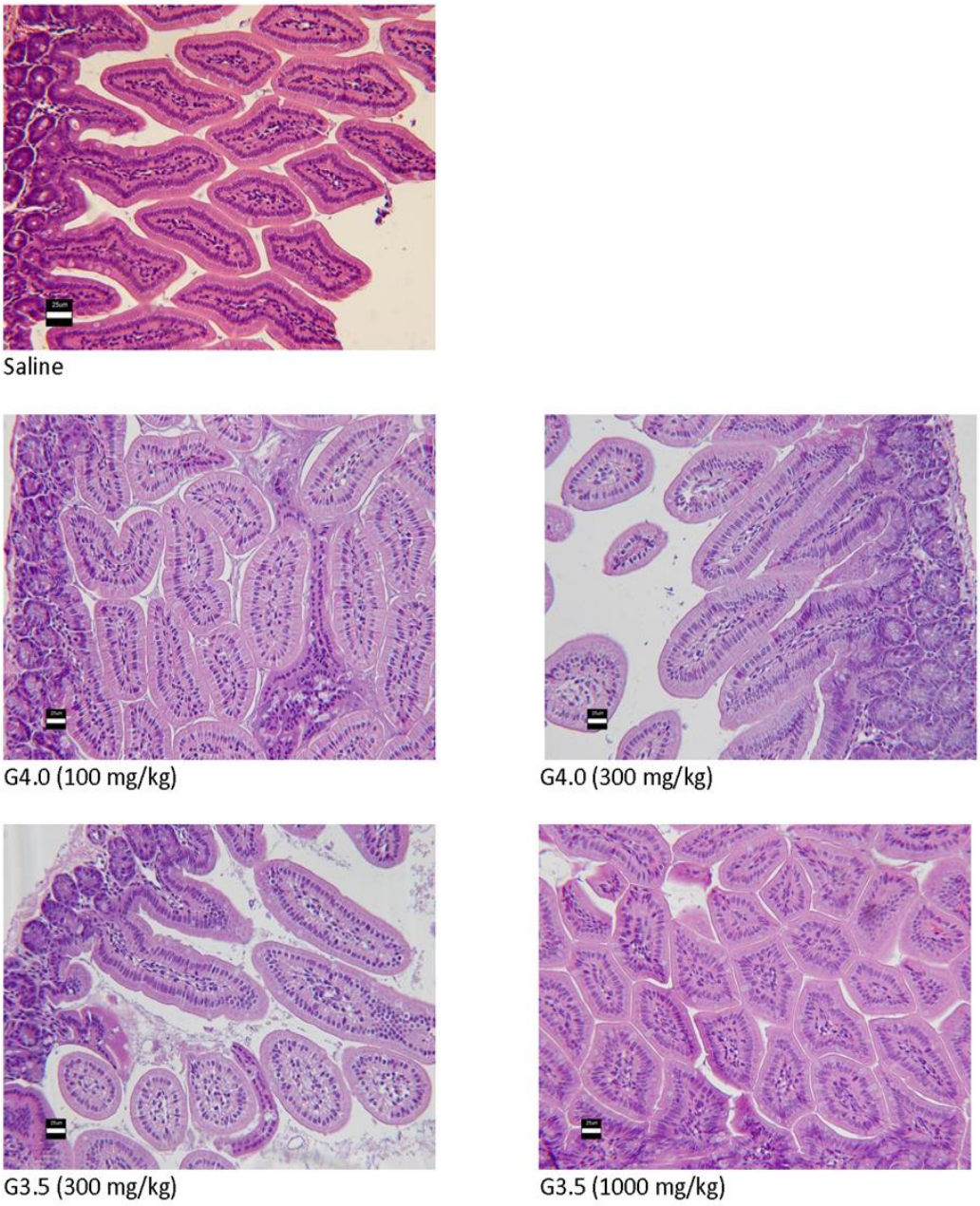

Figure 5-7. H and E staining of the small intestinal segments of CD-1 mice orally administered with saline, G4.0 (100 mg/kg), G4.0 (300 mg/kg), G3.5 (300 mg/kg), G3.5 (1000 mg/kg). Scale Bar = 25 μm.

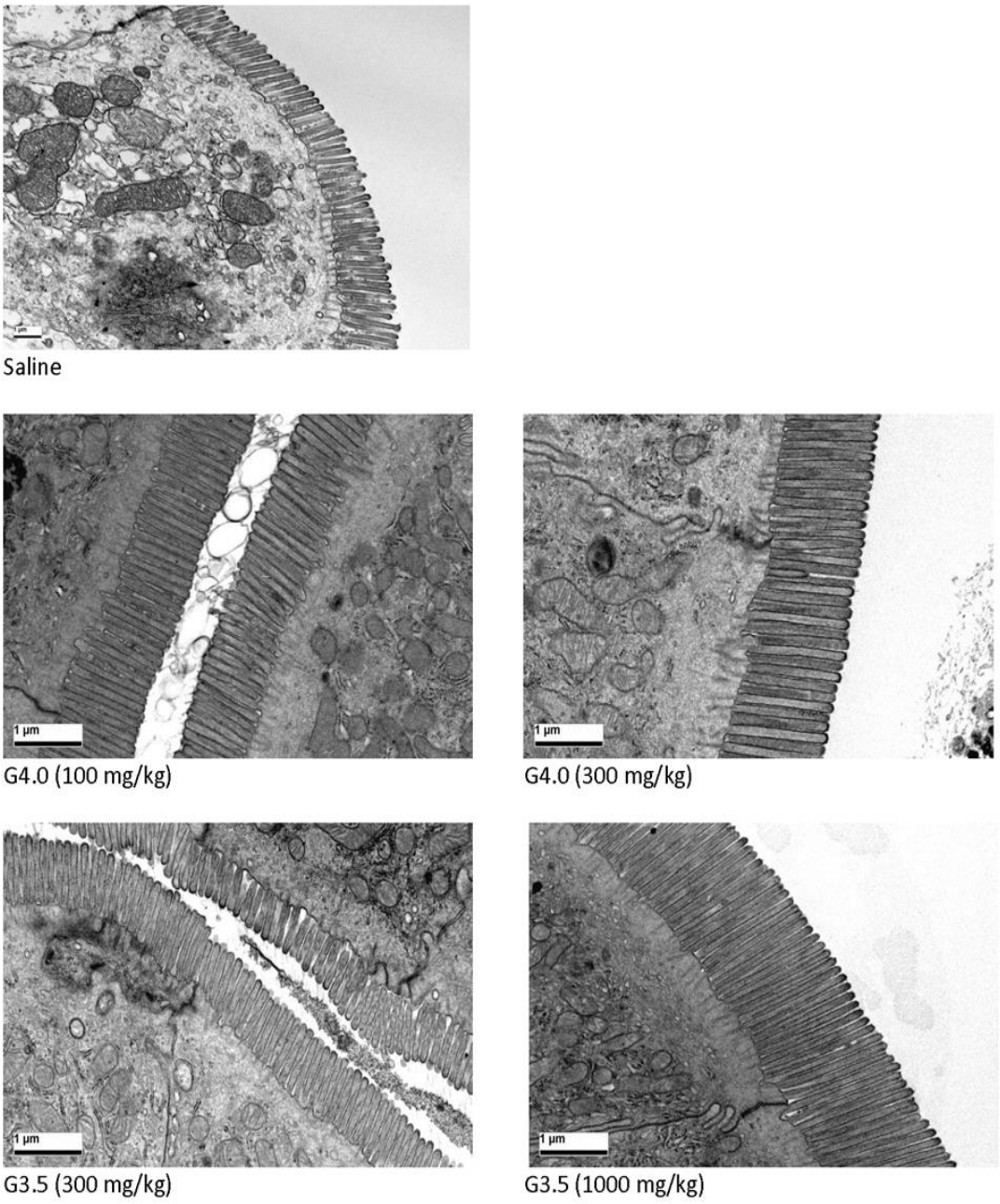

Figure 5-8. TEM images of the small intestinal segments of CD-1 mice orally administered with saline, G4.0 (100 mg/kg), G4.0 (300 mg/kg), G3.5 (300 mg/kg), G3.5 (1000 mg/kg). Scale Bar = 1 µm.

alone or with the PAMAM dendrimers under study also did not cause any apparent morphological changes to the villi of the small intestinal segments being evalulated (Figure 5-9 and Appendix B). However, slight irregularities in the plasma membranes and microfilaments of microvilli were observed for the camptothecin dosed alone (Figure 5-10 and Appendix B). Disruption of microvilli has been previously noted in cells treated with camptothecin [55, 56]. When the camptothecin was dosed with the PAMAM dendrimers-G4.0 and G3.5, the microvilli did not show swelling and the microfilaments inside the microvilli were well organized (Figure 5-10 and Appendix B). This suggests a protective effect of the PAMAM dendrimers to the potential histologic changes caused by camptothecin, probably due to encapsulation of the drug within the interior cavities of the dendrimers. H and E staining of small intestinal segments in animals dosed with camptothecin + G4.0 or G3.5 as well as saline showed dilated lymphatics indicative of an absorptive process (Figure 5-7, Figure 5-9 and Appendix B).

5.4. Conclusion

When formulated with cationic, amine-terminated PAMAM generation 4.0 and anionic, carboxylate-terminated G3.5, camptothecin associated to a higher extent with G4.0 than G3.5 due to an electrostatic interaction on the surface of G4.0. Inspite of a difference in drug association, both G4.0 and G3.5 caused a 2- to 3-fold increase in oral absorption of camptothecin when co-delivered with the drug at 2 hours (the T_{max} of camptothecin absorption). This was attributed to better solubilization of the drug in simulated gastric fluid which can affect drug association with PAMAM, precipitation kinetics and release in the simulated intestinal fluid that in turn affects oral

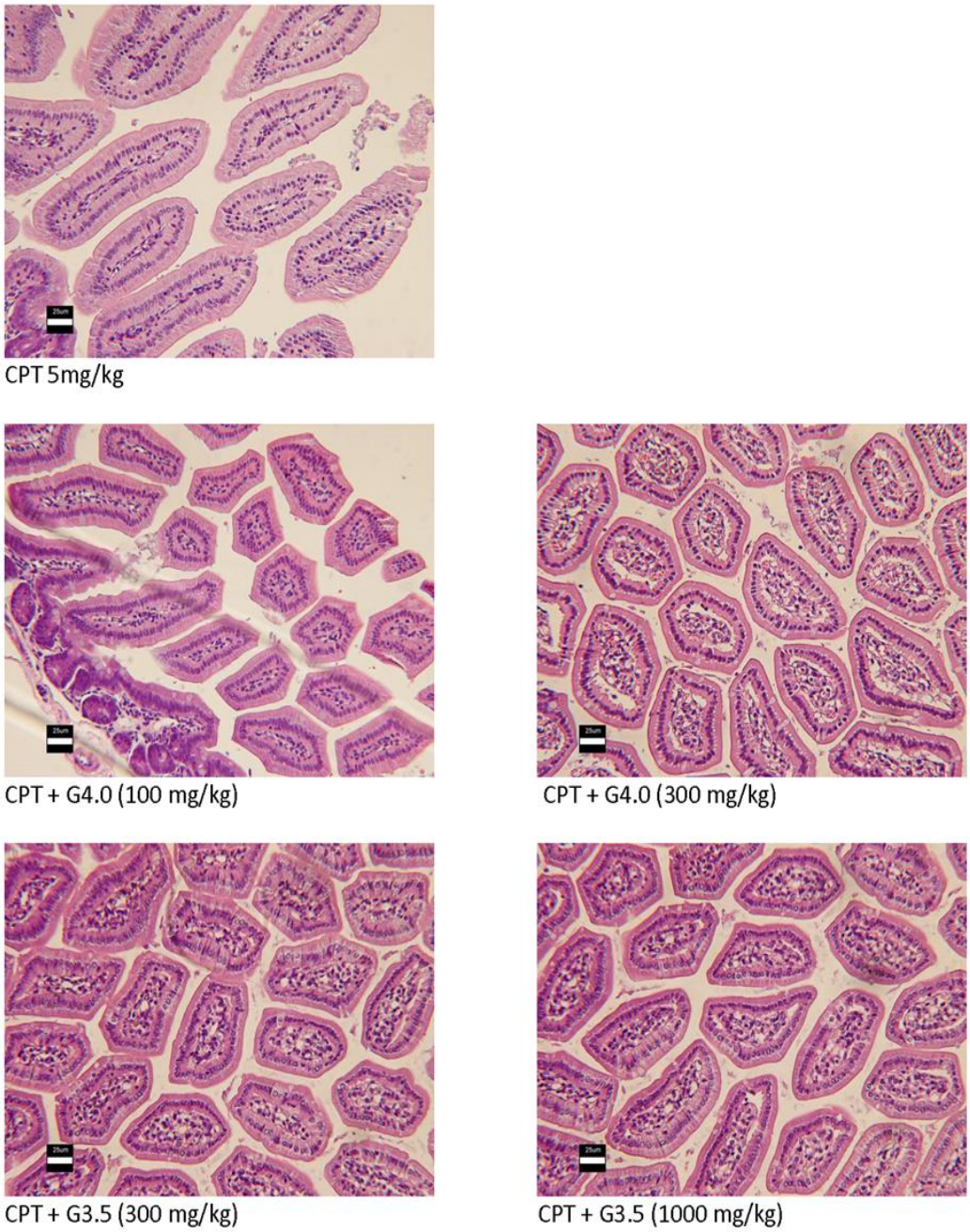

Figure 5-9. H and E staining of the small intestinal segments of CD-1 mice orally administered with CPT (5 mg/kg), CPT + G4.0 (100 mg/kg), CPT + G4.0 (300 mg/kg), CPT + G3.5 (300 mg/kg), CPT + G3.5 (1000 mg/kg). Scale Bar = 25 μm.

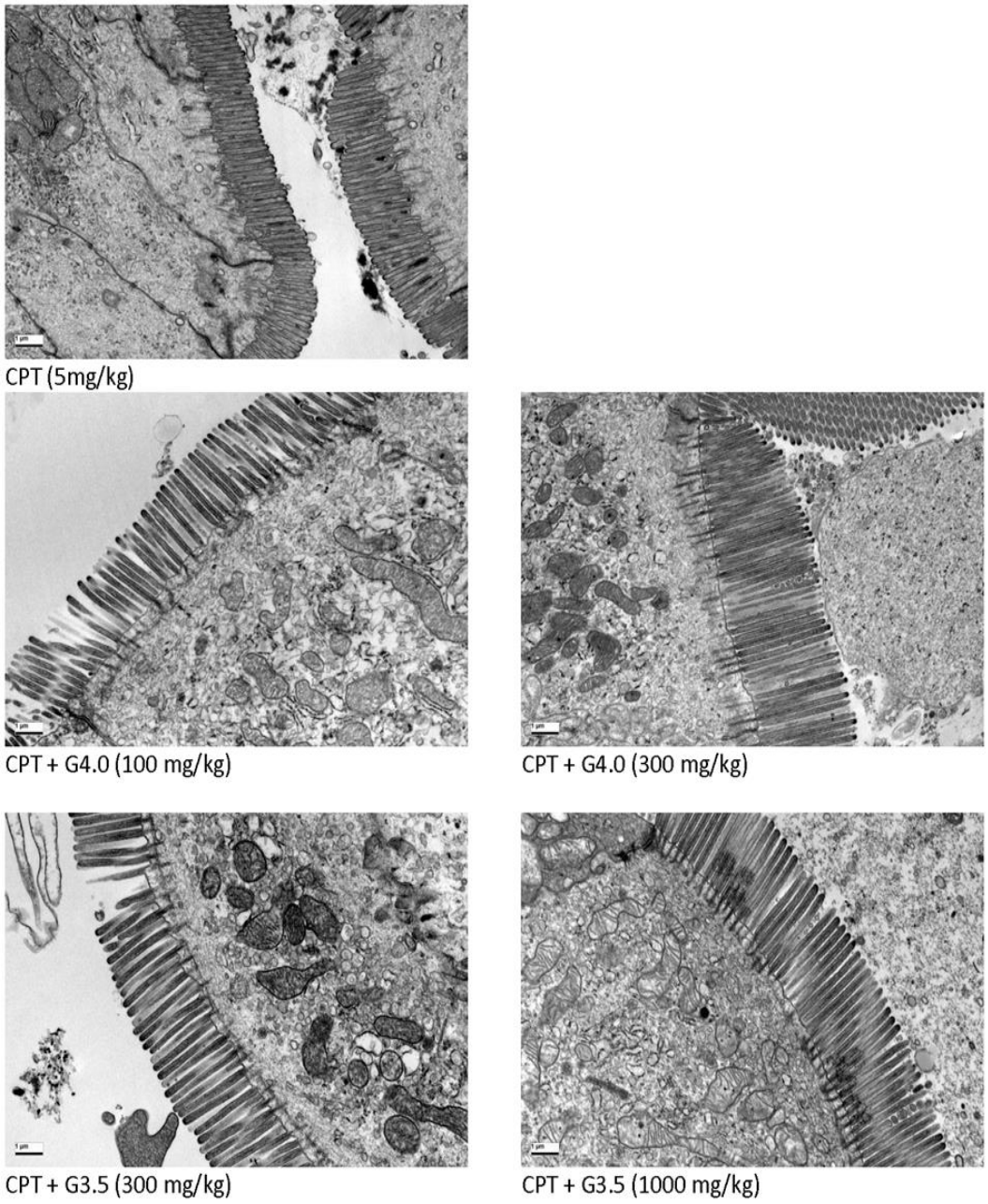

Figure 5-10. TEM images of the small intestinal segments of CD-1 mice orally administered with CPT (5 mg/kg), CPT + G4.0 (100 mg/kg), CPT + G4.0 (300 mg/kg), CPT + G3.5 (300 mg/kg), CPT + G3.5 (1000 mg/kg). Scale Bar = 1 μm.

bioavailability. Increased oral absorption of camptothecin was also attributed to a higher fraction of the drug in the unionized form (lactone) when formulated with PAMAM dendrimers. There was no significant difference in drug solubilization in SGF and SIF by either cationic or anionic PAMAM dendrimers. This was attributed to the absence of surface electrostatic interaction with G4.0 at lower pH. PAMAM G4.0 and G3.5 did not cause tight junction modulation at the doses tested suggesting that increase in oral absorption of camptothecin was not due to tight junction modulation. At doses tested, PAMAM dendrimers did not cause any histologic changes to the epithelial layer of the gastrointestinal tract at 4 hours post dosing. This study demonstrates that both cationic and anionic PAMAM dendrimers were equally effective in enhancing the oral absorption of camptothecin. Results suggest that drug inclusion in PAMAM interior controlled drug solubilization in SGF and SIF, and increased oral bioavailability.

5.5. References

1. DeMario MD, Ratain MJ. Oral chemotherapy: rationale and future directions. J Clin Oncol. 1998;16(7):2557-67.

2. Aisner J. Overview of the changing paradigm in cancer treatment: oral chemotherapy. Am J Health Syst Pharm. 2007;64(9 Supplement 5):S4-7.

3. Terwogt JMM, Schellens JHM, Huinink WW, Beijnen JH. Clinical pharmacology of anticancer agents in relation to formulations and administration routes. Cancer Treat Rev. 1999;25(2):83-101.

4. O'Leary J, Muggia F. Camptothecins: a review of their development and schedules of administration. Eur J Cancer. 1998;34(10):1500-8.

5. Stehlin JS, Natelson EA, Hinz HR, Giovanella BC, Ipolyi P, Fehin K et al. In: Potmesil M, Pinedo H, editors. Camptothecins: new anticancer agents. Florida: CRC Press, Inc.; 1995. p. 59-65.

6. Hatefi A, Amsden B. Camptothecin delivery methods. Pharm Res. 2002;19(10):1389-99.

7. Sugarman SM, Zou YY, Wasan K, Poirot K, Kumi R, Reddy S et al. Lipid-complexed camptothecin: formulation and initial biodistribution and antitumor activity studies. Cancer Chemother Pharmacol. 1996;37(6):531-8.

8. Lundberg B. Biologically active camptothecin derivatives for incorporation into liposome bilayers and lipid emulsions. Anticancer Drug Des. 1998;13(5):453-61.

9. Emerson DL. Liposomal delivery of camptothecins. Pharm Sci Technol To. 2000;3(6):205-9.

10. Cortesi R, Esposito E, Maietti A, Menegatti E, Nastruzzi C. Formulation study for the antitumor drug camptothecin: liposomes, micellar solutions and a microemulsion. Int J Pharm. 1997;159(1):95-103.

11. Singer JW, Vries P, Bhatt R, Tulinsky J, Klein P, Li C et al. Conjugation of camptothecins to poly(l-glutamic acid). Ann N Y Acad Sci. 2000;922(1):136-50.

12. Sakuma S, Lu ZR, Kopečková P, Kopeček J. Biorecognizable HPMA copolymer–drug conjugates for colon-specific delivery of 9-aminocamptothecin. J Control Release. 2001;75(3):365-79.

13. Kingsbury WD, Boehm JC, Jakas DR, Holden KG, Hecht SM, Gallagher G et al. Synthesis of water-soluble (aminoalkyl) camptothecin analogs: inhibition of topoisomerase I and antitumor activity. J Med Chem. 1991;34(1):98-107.

14. Harada M, Sakakibara H, Yano T, Suzuki T, Okuno S. Determinants for the drug release from T-0128, camptothecin analogue-carboxymethyl dextran conjugate. J Control Release. 2000;69(3):399-412.

15. Vijayalakshmi N, Ray A, Malugin A, Ghandehari H. Carboxyl-terminated PAMAM-SN38 conjugates: synthesis, characterization, and *in vitro* evaluation. Bioconjug Chem. 2010;21:1804-10.

16. Thiagarajan G, Ray A, Malugin A, Ghandehari H. PAMAM-camptothecin conjugate inhibits proliferation and induces nuclear fragmentation in colorectal carcinoma cells. Pharm Res. 2010;27:2307-16.

17. Goldberg D, Vijayalakshmi N, Swaan P, Ghandehari H. G3.5 PAMAM dendrimers enhance transepithelial transport of SN38 while minimizing gastrointestinal toxicity. J Control Release. 2011;150:318-25.

18. Conover CD, Greenwald RB, Pendri A, Gilbert CW, Shum KL. Camptothecin delivery systems: enhanced efficacy and tumor accumulation of camptothecin following its conjugation to polyethylene glycol via a glycine linker. Cancer Chemother Pharmacol. 1998;42(5):407-14.

19. Tomalia DA, Baker H, Dewald J, Hall M, Kallos G, Martin S et al. A new class of polymers: starburst-dendritic macromolecules. Polym J. 1985;17(1):117-32.

20. Tomalia DA, Naylor AM, Goddard WA. Starburst dendrimers: molecular-level control of size, shape, surface chemistry, topology, and flexibility from atoms to macroscopic matter. Angewandte Chemie International Edition in English. 1990;29(2):138-75.

21. D'Emanuele A, Attwood D. Dendrimer–drug interactions. Adv Drug Del Rev. 2005;57(15):2147-62.

22. Gupta U, Agashe HB, Asthana A, Jain N. Dendrimers: novel polymeric nanoarchitectures for solubility enhancement. Biomacromolecules. 2006;7(3):649-58.

23. Yiyun C, Tongwen X. Dendrimers as potential drug carriers. Part I. Solubilization of non-steroidal anti-inflammatory drugs in the presence of polyamidoamine dendrimers. Eur J Med Chem. 2005;40(11):1188-92.

24. Pistolis G, Malliaris A, Paleos C, Tsiourvas D. Study of poly (amidoamine) starburst dendrimers by fluorescence probing. Langmuir. 1997;13(22):5870-5.

25. Pistolis G, Malliaris A. Study of poly (propylene imine) dendrimers in water, by exciplex formation. Langmuir. 2002;18(1):246-51.

26. Ooya T, Lee J, Park K. Hydrotropic dendrimers of generations 4 and 5: synthesis, characterization, and hydrotropic solubilization of paclitaxel. Bioconjug Chem. 2004;15(6):1221-9.

27. Devarakonda B, Hill RA, de Villiers MM. The effect of PAMAM dendrimer generation size and surface functional group on the aqueous solubility of nifedipine. Int J Pharm. 2004;284(1):133-40.

28. Cheng Y, Wu Q, Li Y, Xu T. External electrostatic interaction versus internal encapsulation between cationic dendrimers and negatively charged drugs: which contributes more to solubility enhancement of the drugs? J Phys Chem B. 2008;112(30):8884-90.

29. Cheng Y, Qu H, Ma M, Xu Z, Xu P, Fang Y et al. Polyamidoamine (PAMAM) dendrimers as biocompatible carriers of quinolone antimicrobials: an *in vitro* study. Eur J Med Chem. 2007;42(7):1032-8.

30. Cheng Y, Li M, Xu T. Potential of poly (amidoamine) dendrimers as drug carriers of camptothecin based on encapsulation studies. Eur J Med Chem. 2008;43(8):1791-5.

31. Chauhan AS, Jain NK, Diwan PV, Khopade AJ. Solubility enhancement of indomethacin with poly (amidoamine) dendrimers and targeting to inflammatory regions of arthritic rats. J Drug Target. 2004;12(9-10):575-83.

32. Beezer A, King A, Martin I, Mitchel J, Twyman L, Wain C. Dendrimers as potential drug carriers; encapsulation of acidic hydrophobes within water soluble PAMAM derivatives. Tetrahedron. 2003;59(22):3873-80.

33. Sadekar S, Ghandehari H. Transepithelial transport and toxicity of PAMAM dendrimers: implications for oral drug delivery. Adv Drug Del Rev. 2012;64(6):571-88.

34. Kitchens KM, Kolhatkar RB, Swaan PW, Eddington ND, Ghandehari H. Transport of poly (amidoamine) dendrimers across Caco-2 cell monolayers: influence of size, charge and fluorescent labeling. Pharm Res. 2006;23(12):2818-26.

35. El-Sayed M, Ginski M, Rhodes CA, Ghandehari H. Influence of surface chemistry of poly (amidoamine) dendrimers on Caco-2 cell monolayers. J Bioact Compatible Polym. 2003;18(1):7-22.

36. El-Sayed M, Ginski M, Rhodes C, Ghandehari H. Transepithelial transport of poly (amidoamine) dendrimers across Caco-2 cell monolayers. J Control Release. 2002;81(3):355-65.

37. Kitchens KM, Kolhatkar RB, Swaan PW, Ghandehari H. Endocytosis inhibitors prevent poly (amidoamine) dendrimer internalization and permeability across Caco-2 cells. Mol Pharm. 2008;5(2):364-9.

38. Kitchens KM, Foraker AB, Kolhatkar RB, Swaan PW, Ghandehari H. Endocytosis and interaction of poly (amidoamine) dendrimers with Caco-2 cells. Pharm Res. 2007;24(11):2138-45.

39. El-Sayed M, Rhodes CA, Ginski M, Ghandehari H. Transport mechanism (s) of poly (amidoamine) dendrimers across Caco-2 cell monolayers. Int J Pharm. 2003;265(1-2):151-7.

40. Goldberg D, Ghandehari H, Swaan P. Cellular entry of G3.5 poly (amido amine) dendrimers by clathrin-and dynamin-dependent endocytosis promotes tight junctional opening in intestinal epithelia. Pharm Res. 2010;27:1547-57.

41. Lin Y, Khanafer K, El-Sayed MEH. Quantitative evaluation of the effect of poly (amidoamine) dendrimers on the porosity of epithelial monolayers. Nanoscale. 2010;2(5):755-62.

42. Ke W, Zhao Y, Huang R, Jiang C, Pei Y. Enhanced oral bioavailability of doxorubicin in a dendrimer drug delivery system. J Pharm Sci. 2008;97(6):2208-16.

43. Huang X, Wu Z, Gao W, Chen Q, Yu B. Polyamidoamine dendrimers as potential drug carriers for enhanced aqueous solubility and oral bioavailability of silybin. Drug Dev Ind Pharm. 2011;37(00):419-27.

44. Thiagarajan G, Khaled G, Ghandehari H. Charge affects the oral toxicity of poly(amido amine) dendrimers. *Submitted* 2012.

45. Maiti PK, Cagin T, Wang G, Goddard III WA. Structure of PAMAM dendrimers: generations 1 through 11. Macromolecules. 2004;37(16):6236-54.

46. Svenson S, Tomalia DA. Dendrimers in biomedical applications—reflections on the field. Adv Drug Del Rev. 2005;57(15):2106-29.

47. Fassberg J, Stella VJ. A kinetic and mechanistic study of the hydrolysis of camptothecin and some analogues. J Pharm Sci. 1992;81(7):676-84.

48. Hu J, Cheng Y, Wu Q, Zhao L, Xu T. Host−guest chemistry of dendrimer-drug complexes. 2. Effects of molecular properties of guests and surface functionalities of dendrimers. J Phys Chem B. 2009;113(31):10650-9.

49. Markowicz M, Szymański P, Ciszewski M, Kłys A, Mikiciuk-Olasik E. Evaluation of poly (amidoamine) dendrimers as potential carriers of iminodiacetic derivatives using solubility studies and 2D-NOESY NMR spectroscopy. J Biol Phys. 2012:1-20.

50. Chauhan AS, Sridevi S, Chalasani KB, Jain AK, Jain SK, Jain N et al. Dendrimer-mediated transdermal delivery: enhanced bioavailability of indomethacin. J Control Release. 2003;90(3):335-43.

51. Hu J, Cheng Y, Ma Y, Wu Q, Xu T. Host−guest chemistry and physicochemical properties of the dendrimer− mycophenolic acid complex. J Phys Chem B. 2008;113(1):64-74.

52. Scott DO, Bindra DS, Stella VJ. Plasma pharmacokinetics of the lactone and carboxylate forms of 20 (S)-camptothecin in anesthetized rats. Pharm Res. 1993;10(10):1451-7.

53. Rothenberg ML. Irinotecan (CPT-11): recent developments and future directions-colorectal cancer and beyond. Oncologist. 2001;6(1):66.

54. Gupta E, Vyas V, Ahmed F, Sinko P, Cook T, Rubin E. Pharmacokinetics of orally administered camptothecins. Ann N Y Acad Sci. 2000;922(1):195-204.

55. Lin J, Liu X, Bao Y, Hou S, An L, Lin X. Effects of isocamptothecin, a novel camptothecin analogue, on proliferation, apoptosis and telomerase activity in HaCaT cells. Exp Dermatol. 2008;17(6):530-6.

56. Bredholt T, Dimba EAO, Hagland HR, Wergeland L, Skavland J, Fossan KO et al. Camptothecin and khat (Catha edulis Forsk.) induced distinct cell death phenotypes involving modulation of c-FLIP. Mol Cancer. 2009;8:101.

CHAPTER 6

CONCLUSIONS AND FUTURE DRIECTIONS

6.1. Conclusions

In this dissertation, PAMAM dendrimers were evaluated as polymeric carriers for delivery of anticancer agents. The hypothesis in the first part of the dissertation was that the difference in polymer architecture and molecular conformation of PAMAM dendrimers from traditionally used linear polymers can influence its hydrodynamic size and deforming capacity, which in turn influences biodistribution and pharmacokinetics of these polymers (Chapters 3 and 4). Polymer architecture affected the increase of hydrodynamic size with molecular weight [1]. PAMAM dendrimers are generally known to be more globular and compact structures than linear polymers that assume a random coil or an extended conformation in solution [2-5]. An interesting observation in the size characterization of these polymers was that there was a MW cutoff (40 kDa) below which the HPMA copolymers was smaller than the PAMAM dendrimer of comparable MW [1, 6]. With increase in MW, the size of PAMAM dendrimers grew at a much slower rate than HPMA copolymers by virtue of the compact nature of their divergent growth from the core [1, 6].

The biodistribution study showed that along with MW, hydrodynamic size and polymer architecture influenced blood circulation, nonspecific uptake in the kidney and liver as well as site-specific uptake in the tumor [1]. In general, the PAMAM dendrimers had a higher tumor to blood ratio. This suggests that given the same opportunity to be taken up into the tumor when circulating in the blood, hyperbranched PAMAM dendrimers had a higher affinity to the tumor tissue than HPMA copolymers [6]. PAMAM dendrimers, therefore, had better passive targeting potential than HPMA copolymers in the orthotopic ovarian carcinoma tumors under study. However, PAMAM dendrimers also had a higher and more persistent accumulation in the liver and kidney tissue than HPMA copolymers. This could potentially cause long-term, non-specific toxicities in these elimination organs affecting primary physiological functions, although we did not observe any acute toxicity at doses tested. The pharmacokinetic analysis of blood data revealed that the clearance decreased more drastically for PAMAM dendrimers over the molecular weight range studied as compared to HPMA copolymers over the same molecular weight range [6]. It should be noted that although the MW of the polymers being studied was comparable, the hydrodynamic size range was not. The largest HPMA copolymer (131 kDa) was twice the size of the largest PAMAM dendrimer (G7.0-OH). Clearance is known to decrease exponentially with hydrodynamic size for polymers over a range of MWs or hydrodynamic size, where they can be partially filtered through the kidney. However, below or above this range, the clearance is likely to be independent of molecular weight, in which case the glomerulus is not a rate-limiting barrier for the smaller polymers and other mechanisms of elimination such as the RES uptake or biliary excretion kick in for the larger polymers. This study only included a

range of sizes where clearance was seen to be a function of MW. In this size range, the linear polymers were excreted renally to a greater extent than the PAMAM dendrimers. The renal and elimination clearance trends suggested that the deforming capacity of PAMAM dendrimers decreases more drastically with increase in generation, size or MW than that of HPMA copolymers, affecting their extravasation rates across glomerular basement membrane. Head-to-head comparative study of HPMA copolymers and PAMAM dendrimers can guide the rational design and development of carriers based on these systems for delivery of bioactive and imaging agents.

In Chapter 5, PAMAM dendrimers were evaluated for oral delivery of camptothecin, a schedule-dependent chemotherapeutic. The drug was co-delivered with different ratios of cationic, amine-terminated PAMAM G4.0-NH_2 and anionic, carboxylic acid-terminated PAMAM G3.5-COOH. The drug associated to a greater extent to the PAMAM G4.0-NH_2 than PAMAM G3.5-COOH due to the potential for surface electrostatic interaction between the carboxylate group on drug and the amine group on G4.0 (unstable under gastric conditions) [7]. Inspite of this difference in association, both G4.0 and G3.5 increased oral absorption of camptothecin to the same extent (2-fold at 2 hours post dosing) [7]. This was attributed to partial encapsulation of the drug in the PAMAM interior via hydrogen bonding or hydrophobic interactions, solubilizing it under gastric conditions [7]. It was also attributed to a small percentage of drug in the unionized form when encapsulated in the PAMAM, which is a more favorable form for absorption [7]. Mannitol absorption remained unchanged at 2 hours after dosing and no histological toxicity was observed at 4 hours after dosing in presence of both cationic and anionic PAMAM dendrimers, indicating that they did not modulate tight junctions and were

biocompatible *in vivo* at these doses [7]. This was contradictory to previously observed results *in vitro* at comparable doses [8-10]. These findings suggest that *in vivo* variables such as presence of the mucous layer, and gastrointestinal transit time diluted the effective concentration of the dendrimer at the epithelial layer. This study demonstrates the potential of PAMAM G4.0 and G3.5 to enhance the oral absorption of camptothecin, possibly by altering precipitation kinetics of the encapsulated drug in the GI.

6.2. Future directions

In Chapters 3 and 4, two polymer series, PAMAM dendrimers and HPMA copolymers over a certain size range, were evaluated and shown that clearance decreased exponentially with hydrodynamic size. However, this trend is not expected to hold for polymers with hydrodynamic sizes outside of this range, where clearance is likely to be independent of MW or size of polymers. A systematic evaluation of each of the polymer series across a broader range of MWs or hydrodynamic sizes is likely to result in a sigmoidal curve when clearance is plotted as a function of hydrodynamic size [11]. Different sigmoidal curves can be generated for polymers of varying architecture which can help simulate elimination clearance of a polymer with known molecular weight and conformation in solution.

Molecular conformation of a polymer is known to depend on the physicochemical properties and extent of cargo loaded on the polymer [12]. A slight increase in tyrosine loading caused the hydrodynamic size of HPMA copolymer to decrease as compared to that of HPMA homopolymer of comparable MW (Chapter 3). It is expected that the hydrodynamic size, molecular conformation and consequently the *in vivo* fate of the

PAMAM dendrimers and HPMA copolymers will change with loading of drugs and targeting moieties. The architecture of the polymeric carrier is likely to influence this change as well. The presentation of the targeting moiety and the resulting active targeting potential of a polymer can be affected by polymer architecture. A systematic study evaluating the effect of drug loading and targeting moieties on hydrodynamic size, molecular conformation, biodistribution and pharmacokinetics of polymers of varying architecture will aid in the rational choice of a polymeric carrier.

Polymer architecture was also seen to influence tumor uptake in the biodistribution studies (Chapter 4). This can be attributed to: 1) differences in the extravasation of the polymer in the tumor interstitium, and 2) difference in cellular uptake of polymers of varying architecture. The extravasation rates of polymers of varying architecture in the tumor can be studied by intravital microscopy. Such study can give insight into the influence of polymer architecture on depth of polymer penetration in the tumor, which is known to be one of the limitations in tumor-targeted delivery.

It should be noted that the conclusions drawn from Chapters 3 and 4 were based on an orthotopic xenograft ovarian carcinoma tumor model. The type of tumor model is known to influence EPR due to differences in interstitial pressure as well as vascularization [13, 14]. A comparison of polymers of varying architecture in different tumor models would help understand the influence of tumor interstitial, cellular and angiogenic environment on polymer uptake.

Camptothecin or its derivatives have been conjugated to PAMAM G4.0 and G3.5 via a glycine spacer [15, 16]. It is critical to achieve linker stability sufficient to prevent gastrointestinal toxicity and a release rate efficient and specific enough for effective

therapy. Identifying site-specific elevated enzymes and designing linkers to be specifically cleaved by them is necessary to overcome this problem. These constructs have shown promise *in vitro* as oral delivery constructs by demonstrating a good balance of stability in the GIT, site-specific release in presence of liver carboxylesterases and enhanced transepithelial transport compared to drug alone [15, 16]. There has been no *in vivo* demonstration of the absorption of an intact dendrimer-drug conjugate. It would be beneficial to compare camptothecin exposure *in vivo* to GIT, blood and liver (site-specific organ of interest) when complexed and conjugated with PAMAM dendrimers. Such a study will provide insight into the advantages of either complexation or conjugation to improving the oral delivery of camptothecin. It is possible that a combination of solubilization, penetration enhancement and transepithelial translocation will be beneficial for oral drug delivery using PAMAM dendrimers.

Several surface modifications for PAMAMs such as acetyl groups, fatty acids and amino acids have shown increased permeability across Caco-2 cell monolayers or isolated intestinal tissue [17, 18]. Studying the effect of these surface modifications on the drug encapsulating potential and absorption enhancing effect of PAMAM on hydrophobic and hydrophilic drugs *in vivo* could lead to the establishment of a structure-activity relationship between surface modification and absorption-enhancement effect.

In vitro models employed to assess transepithelial transport have been useful to rank the translocation of PAMAM dendrimers of different generations and surface functionalities. However, they lack the variables of mucous membrane barrier, gastrointestinal transit time and/or enzymatic milieu pertinent to the gastrointestinal tract

[19]. Systematic modeling and correlation of *in vitro* transport to *in vivo* absorption can facilitate high throughput screening of PAMAM-based conjugates and complexes.

6.3. References

1. Sadekar S, Ray A, Jana t-Amsbury M, Peterson C, Ghandehari H. Comparative biodistribution of PAMAM dendrimers and HPMA copolymers in ovarian-tumor-bearing mice. Biomacromolecules. 2011;12:88-96.

2. Ulbrich K, Subr V. Structural and chemical aspects of HPMA copolymers as drug carriers. Adv Drug Deliv Rev. 2010;62(2):150-66.

3. Maiti PK, Cagin T, Wang G, Goddard III WA. Structure of PAMAM dendrimers: generations 1 through 11. Macromolecules. 2004;37(16):6236-54.

4. Mansfield ML, Klushin L. Intrinsic viscosity of model starburst dendrimers. J Phys Chem. 1992;96(10):3994-8.

5. Tomalia DA, Naylor AM, Goddard III WA. Starburst dendrimers: molecular-level control of size, shape, surface chemistry, topology, and flexibility from atoms to macroscopic matter. Angew Chem Int Ed. 1990;29(2):138-75.

6. Sadekar S, Linares O, Noh GJ, Hubbard D, Ray A, Janát-Amsbury M et al. Comparative pharmacokinetics of PAMAM-OH dendrimers and HPMA copolymers in ovarian tumor-bearing mice. Drug Deliv Transl Res. 2012. doi:10.1007/s13346-012-0119-6.

7. Sadekar S, Thiagarajan G, Bartlett K, Hubbard D, Ray A, L.D.McGill et al. Poly(amido amine) dendrimers as absorption enhancers for oral delivery of camptothecin. Int J Pharm. *Submitted*.

8. El-Sayed M, Ginski M, Rhodes C, Ghandehari H. Transepithelial transport of poly (amidoamine) dendrimers across Caco-2 cell monolayers. J Control Release. 2002;81(3):355-65.

9. El-Sayed M, Ginski M, Rhodes CA, Ghandehari H. Influence of surface chemistry of poly (amidoamine) dendrimers on Caco-2 cell monolayers. J Bioact Compatible Polym. 2003;18(1):7-22.

10. Kitchens KM, Kolhatkar RB, Swaan PW, Eddington ND, Ghandehari H. Transport of poly (amidoamine) dendrimers across Caco-2 cell monolayers: influence of size, charge and fluorescent labeling. Pharm Res. 2006;23(12):2818-26.

11. Deen WM, Bohrer MP, Brenner BM. Macromolecule transport across glomerular capillaries: application of pore theory. Kidney Int. 1979;16(3):353-65.

12. Konak C, Rathi RC, Kopečková P, Kopeček J. Effect of side-chains on solution properties of N-(2-hydroxypropyl) methacrylamide copolymers in aqueous solvents. Polymer. 1993;34(22):4767-73.

13. Ho KS, Poon PC, Owen SC, Shoichet MS. Blood vessel hyperpermeability and pathophysiology in human tumour xenograft models of breast cancer: a comparison of ectopic and orthotopic tumours. BMC Cancer. 2012;12(1):579.

14. Xiao K, Luo J, Li Y, Xiao W, Lee JS, Gonik AM et al. The passive targeting of polymeric micelles in various types and sizes of tumor models. Nanoscience and Nanotechnology Letters. 2010;2(2):79-85.

15. Thiagarajan G, Ray A, Malugin A, Ghandehari H. PAMAM-camptothecin conjugate inhibits proliferation and induces nuclear fragmentation in colorectal carcinoma cells. Pharm Res. 2010;27:2307-16.

16. Vijayalakshmi N, Ray A, Malugin A, Ghandehari H. Carboxyl-terminated PAMAM-SN38 conjugates: synthesis, characterization, and *in vitro* evaluation. Bioconjug Chem. 2010;21:1804-10.

17. Kolhatkar RB, Kitchens KM, Swaan PW, Ghandehari H. Surface acetylation of polyamidoamine (PAMAM) dendrimers decreases cytotoxicity while maintaining membrane permeability. Bioconjug Chem. 2007;18(6):2054-60.

18. Jevprasesphant R, Penny J, Jalal R, Attwood D, McKeown NB, D'Emanuele A. The influence of surface modification on the cytotoxicity of PAMAM dendrimers. Int J Pharm. 2003;252(1-2):263-6.

19. Borchardt R SP, Wilson G, editor. Models for assessing drug absopriton and metabolism: Pharmaceutical biotechnology volume 8, New York, N.Y., Plenum Press, A division of Plenum Publishing Corporation; 1996.

APPENDIX A

BIODISTRIBUTION AND PHARMACOKINETIC MODELING PARAMETERS OF PAMAM-OH DENDRIMERS AND HPMA COPOLYMERS

A.1. Dose recoveries of PAMAM-OH dendrimers and HPMA copolymers in the biodistribution study

Table A-1. Percentage of recovered doses of PAMAM dendrimers and HPMA copolymers

Polymer	**Percentage recovered dose**
G5.0-OH (29 kDa)*	71.58 +/- 17.04
G6.0-OH (58 kDa)	97.22 +/- 12.99
G7.0-OH (117 kDa)	85.99 +/- 12.83
HPMA copolymer (26 kDa)*	20.38 +/- 7.28
HPMA copolymer (52 kDa)	70.44 +/- 32.82
HPMA copolymer (131 kDa)	57.65 +/- 9.73

*Carcass unaccounted; lower dose recovery of HPMA copolymer (26 kDa) may be attributed to losses in urinary excretion.

A.2. Dose recovery of PAMAM dendrimers and HPMA copolymers in urine and stool in the biodistribution study

Table A-2. Percentage of administered dose in urine and stool per animal for PAMAM dendrimers and HPMA copolymers.

Time points (hour)	**Polymers**	**G5.0-OH**	**G6.0-OH**	**G7.0-OH**	**HPMA copolymer (26 kDa)**	**HPMA copolymer (52 kDa)**	**HPMA copolymer (131 kDa)**
0.5	Urine	0.888	-	-	6.246	-	-
	Stool	-	-	0.008	0.016	-	-
2	Urine	1.69	-	0.862	11.916	-	12.34
	Stool	0.648	0.112	0.138	0.832	0.338	0.14
6	Urine	2.764	1.47	0.978	9.298	3.664	12.81
	Stool	2.052	0.09	0.302	-	1.32	0.41
24	Urine	2.312	1.198	1.332	13.288	16.292	23.62
	Stool	1.444	0.352	2.99	1.952	1.774	1.76

Values are pooled for each group, n=5, except n=4 for 2 hour HPMA copolymer (26 kDa) and G5.0-OH; 6 hour and 24 hour G7.0-OH; n=3 for 5 minute, 30 minute, 2 hour; n=4 for 6 hour for HPMA 131 kDa.

A.3. Size exclusion chromatographs of ^{125}Iodine-labeled PAMAM-OH dendrimers and HPMA copolymers

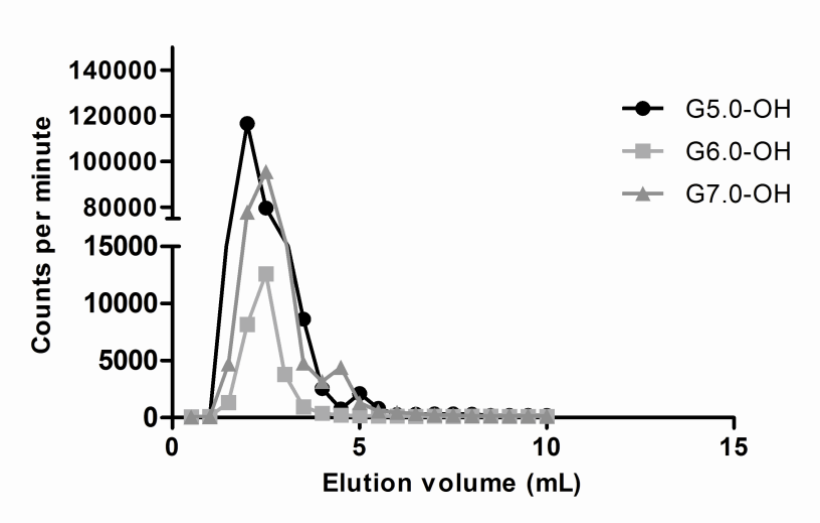

Figure A-1. Size exclusion chromatograms of ^{125}Iodine-labeled PAMAM dendrimers (PD-10, GE Healthcare). Absence of radioactivity between 6.0 to 8.0 mL indicates that there is no free ^{125}Iodine in the radiolabeled polymer samples.

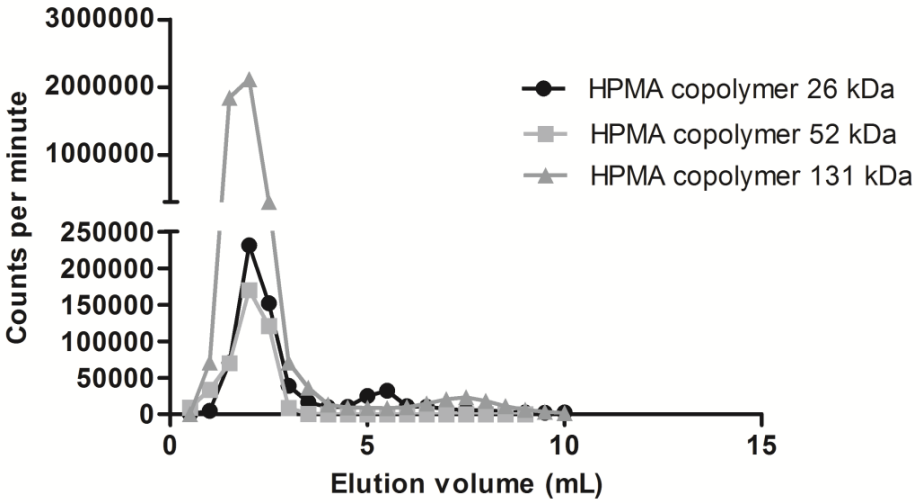

Figure A-2. Size exclusion chromatograms of ^{125}Iodine-labeled HPMA copolymers (PD-10, GE Healthcare). Absence of radioactivity between 6.0 to 8.0 mL indicates that there is no free ^{125}Iodine in the radiolabeled polymer samples.

A.4. *In vivo* toxicity of PAMAM-OH dendrimers and HPMA copolymers

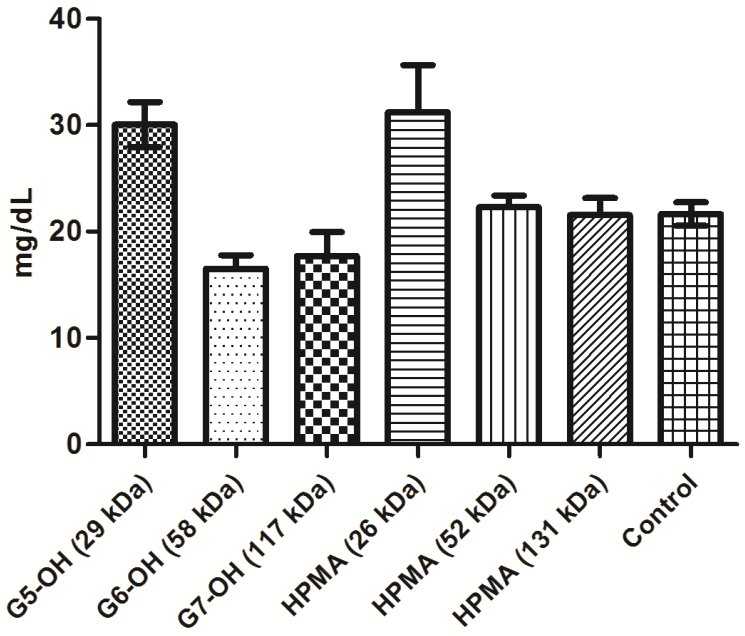

Figure A-3. Blood urea nitrogen levels in plasma of A2780 orthotopic ovarian tumor bearing mice at 1 week. Values are mean +/- SEM, n=5.

Note- The PAMAM dendrimers and HPMA copolymers were assessed for *in vivo* toxicity at doses corresponding to those used for the *in vivo* biodistribution study. The doses were prepared in 0.2 mL sterile saline. Five A2780 orthotopic ovarian tumor bearing nude mice were used per study group along with a control group (administered with saline) for the experiment. Acute toxicity was evaluated over 1 week by monitoring whole blood counts and organ function. Organ function was assessed by measuring enzyme levels for liver and kidney function monitored using a HESKA Blood analysis instrument (HESKA, Loveland, Colorado) with Fuji Dri-Chem slides (Fujifilm Global, Tokyo, Japan) for the toxicity marker enzymes.

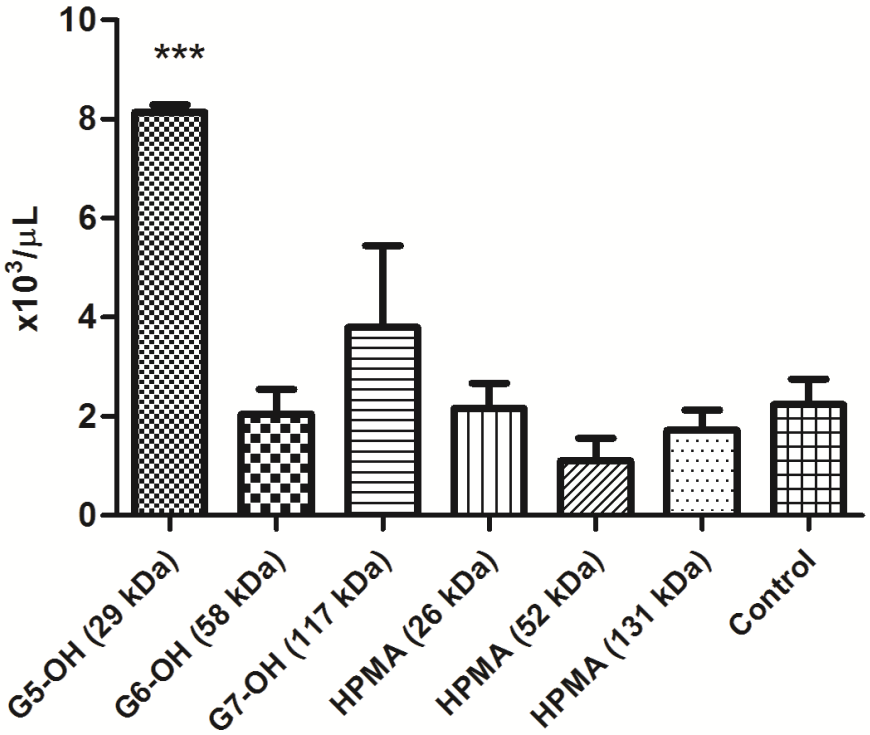

Figure A-4. White blood cell count in plasma of A2780 orthotopic ovarian tumor bearing mice at 1 week. Values are mean +/- SEM, n=5; *** indicates a statistically significant difference from control $p<0.001$.

Note-The differential blood count (RBC, WBC, Platelets) and haemoglobin levels were monitored using a HESKA CBC Diff (HESKA, Loveland, Colorado).

A.5. Size exclusion chromatograms of PAMAM-OH dendrimers and HPMA copolymers

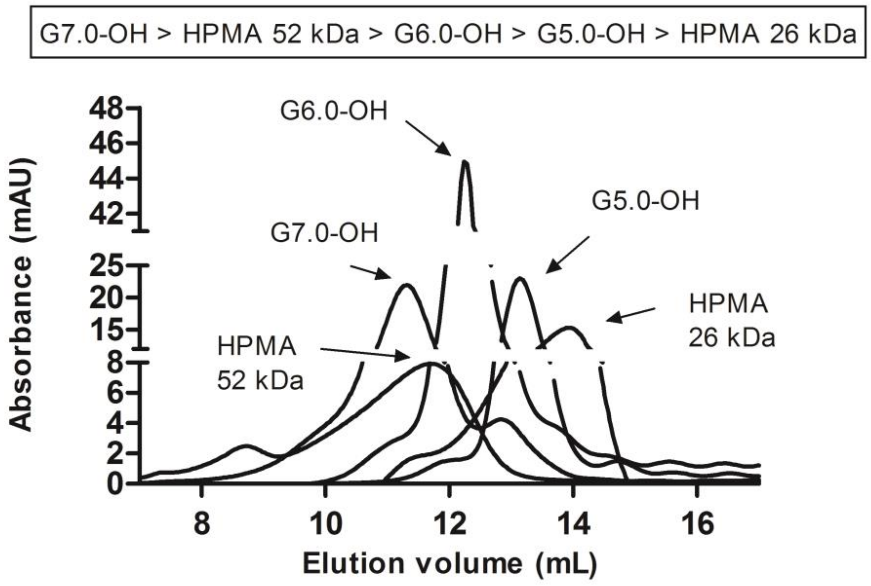

Figure A-5. Size exclusion chromatograms of PAMAM G5.0-OH, G6.0-OH, G7.0-OH and HPMA copolymers 26 and 52 kDa (Superose 6^{TM}, GE Healthcare). Reprinted with permission from S. Sadekar, A. Ray, M. Janàt-Amsbury, C. M. Peterson, H. Ghandehari, Comparative Biodistribution of PAMAM Dendrimers and HPMA Copolymers in Ovarian-Tumor-Bearing Mice, *Biomacromolecules,* 2011, *12,* 88–96. Copyright 2011 American Chemical Society.

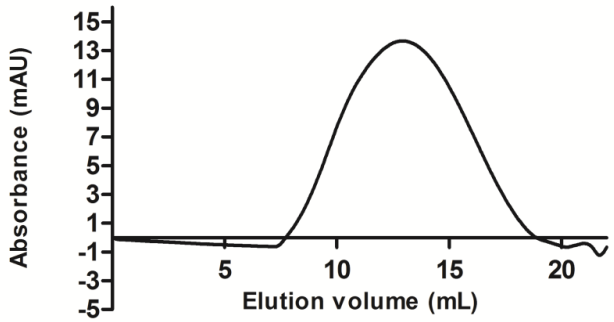

Figure A-6. Size exclusion chromatogram of HPMA copolymer (131 kDa) (Superose 6^{TM}, GE Healthcare).

A.6. Kidney accumulation of PAMAM G5.0-OH

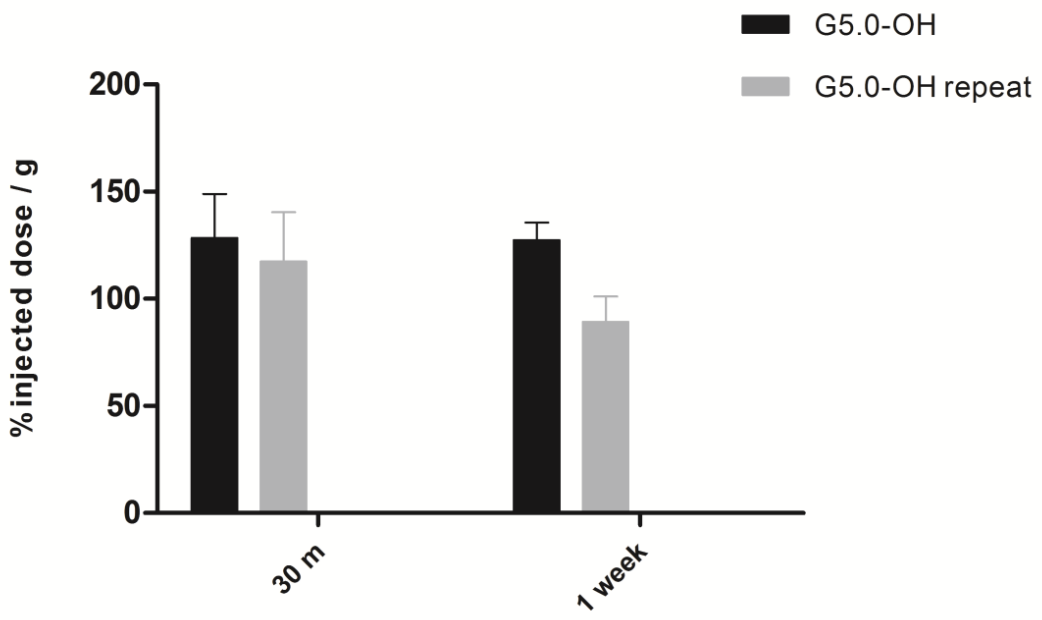

Figure A-7. Percentage of injected dose/g of kidney tissue. Black bars represent the biodistribution of PAMAM G5.0-OH from the experiment reported in Chapter 3. Grey bars represent the biodistribution of PAMAM G5.0-OH from a repeat biodistribution experiment of the dendrimer at 30 m and 1 week. In both experiments, PAMAM G5.0-OH showed a high and extended kidney accumulation of 90-130 % injected dose/g confirming the tendancy of this polymer to be uptaken and retained over one week in the kidney tissue.

A.7. Blood compartmental modeling

Table A-3. Akaike Information Criterion (AIC) for blood compartmental model analysis of PAMAM-OH dendrimers and HPMA copolymers.

Polymer	**AIC** One- compartment model	**AIC** Two-compartment model
G5.0-OH	-4.16	-78.41
G6.0-OH	-17.42	-77.87
G7.0-OH	-24.63	-43.61
HPMA copolymer (26 kDa)	-5.23	-74.08
HPMA copolymer (52 kDa)	-8.42	-62.57
HPMA copolymer (131 kDa)	-29.06	-47.66

AIC was computed using Winnonlin® Version 2.1 for compartmental analysis

Note-The AIC values (Table A-3) indicated that a two-compartmental model with bolus input was a better fit for the polymer biodistribution data as compared to a one compartmental model with bolus input.

A.8. Renal clearance

Renal clearance was calculated from urine data collected over time using the following equations:

$$Cl\,R = \frac{U,ti}{AUC\ blood,0-ti} \quad (1)$$

$$U,ti = \int_0^{ti}\left(\frac{dU}{dt}\right)dt \quad (2)$$

Cl_R: Renal clearance

AUC blood, 0-ti: Area under the blood concentration-time curve of the polymer

U, ti: Extent of accumulation of polymer in urine at time ti

A.9. Polymer interaction with bovine serum albumin

Stock solutions of BSA (10 μmol/L) and polymers (160 μmol/L) were prepared in phosphate buffer saline (PBS: 150 mmol/l NaCl, 1.9 mmol/l NaH_2PO_4, 8.1 mmol/l Na_2HPO_4, pH 7.4). Polymers were serially diluted to study the interaction of PAMAM-OH dendrimers and HPMA copolymers with BSA at a concentration range of 2.5-80 μmol/L for the polymers and 5μmol/L for BSA [4-6]. After a 30-minute incubation at room temperature, sample solutions were measured for fluorescence quenching in a 96 well black polymer BTM P-D-L plate (Nalge Nunc International, Rochester, NY) with opaque walls for wells. The spectrofluorometer used was SpectraMax® M2 (Molecular Devices Corporation, Sunnyvale, CA). The excitation wavelength employed was 280 nm and the emission spectra were recorded from 300 to 500 nm. Quenching data was collected for BSA and polymers alone and for BSA upon addition of each polymer at varying concentrations. The fluorescence intensity at the absorption maximum (λ_{max} =

380 nm) was noted in presence and absence of quenching agent (BSA) and plotted as per the Stern-Volmer equation:

$$\frac{Fo}{F} = 1 + Ksv\,[Q]$$

F_0 = Fluorescence intensity of BSA in absence of quencher (polymer)

F = Fluorescence intensity of BSA in presence of quencher (polymer)

Ksv = Quenching coefficient

[Q] = Concentration of quencher (polymer)

Serum albumin is a major component of the soluble proteins present in plasma [7]. Bovine serum albumin has two tryptophan residues (Trp-134 and Trp-212) that possess intrinsic fluorescence. This fluorescence is sensitive to the presence of a quenching agent in the vicinity of the BSA molecule. The extent of fluorescence quenching is known to be indicative of the binding affinity of the quenching agent to BSA. Therefore, the quenching coefficient (Ksv) is indicative of the interaction of the polymer with bovine serum albumin (BSA) [8]. The higher the Ksv value, the greater is the interaction of the polymer with BSA. All of the polymers had very low Ksv values close to zero, suggesting that these polymers interacted minimally with bovine serum albumin (Table A-4).

Table A-4. Quenching coefficients (Ksv) for the interaction of PAMAM-OH dendrimers and HPMA copolymers with bovine serum albumin.

Polymer	**Ksv**
G5.0-OH (29 kDa)	-0.0001 +/- 0.0005
G6.0-OH (58 kDa)	0.0042
G7.0-OH (117 kDa)	0.0107
HPMA copolymer(26 kDa)	-0.0016 +/- 0.0019
HPMA copolymer (52 kDa)	0.0059
HPMA copolymer (131 kDa)	0.0064

Note: The quenching of BSA fluorescence observed is static or ground state quenching. Such quenching is better analyzed using a binding isotherm. The graph of F_0/F was linear as a function of quencher concentration for all the polymers under study, suggesting that the BSA was not saturated with the quencher or polymer over the concentration range studied. Bound and unbound fractions of polymer with BSA were also not measured in the experiment. Hence, it was not possible to analyze the data using binding isotherms. Alternatively, the Stern-Volmer method, originally derived for dynamic or excited state quenching was used. Also, note that quenching coefficient values cannot be negative. Negative values of Ksv for polymers G5.0-OH and HPMA 26 kDa have a standard deviation with a higher limit in the positive range. The Ksv values of these polymers are likely to fall within the higher range of error where they will be positive numbers.

A.10. Blood concentration time profile and terminal blood half-life

Table A-5. Blood concentration-time profile and terminal blood half-life

Polymer	**Equation governing blood concentration-time profile**	**Terminal half-life (h)**
G5.0-OH (29 kDa)	$C_p = 0.682\ e^{-8.86}t + 0.004\ e^{-0.12}t$	6.36
G6.0-OH (52 kDa)	$C_p = 0.271\ e^{-34.75}t + 0.014\ e^{-0.15}t$	4.49
G7.0-OH (117 kDa)	$C_p = 0.158\ e^{-50.53}t + 0.128\ e^{-0.2}t$	3.4
HPMA copolymer (26 kDa)	$C_p = 0.674\ e^{-6.95}t + 0.011\ e^{-0.16}t$	4.23
HPMA copolymer (52 kDa)	$C_p = 0.513\ e^{-25.75}t + 0.058\ e^{-0.52}t$	1.34
HPMA copolymer (131 kDa)	$C_p = 0.127\ e^{-11.3}t + 0.159\ e^{-0.05}t$	12.78

Note: Terminal half-life is a function of both blood clearance and peripheral distribution. Hence a long terminal blood half-life can be attributed to larger volume of distribution or smaller blood clearance or both. Therefore, terminal half-life is not the most robust parameter to assess the ability of the body to eliminate the polymer. On the other hand, blood clearance expresses the ability of the body to eliminate the polymer. Hence, blood clearance has been used to correlate the blood pharmacokinetics to MW/R_h of polymers.

A.11. Blood-tumor link model

Equations describing the Blood-Tumor Link model (Figure 4-1):

Concentration profile of the central blood compartment (C_p) was modeled using the following equation:

$$\frac{dCp(t)}{dt} = \text{-K1*Cp(t)-K2*Cp(t)-K4*Cp(t)} + \text{K3*Cf(t)} + \text{K5*Ct1(t)}$$

Concentration profile of tumor compartment-1 (C_{t1}) was modeled using the following equation:

$$\frac{dCt1(t)}{dt} = \text{K4} * \text{Cp(t)} - \text{K5} * \text{Ct1(t)} - \text{K6} * \text{Ct1(t)}$$

Concentration profile of tumor compartment-2 (C_{t1}) was modeled using the following equation:

$$\frac{dCt2(t)}{dt} = \text{K6} * \text{Ct1(t)}$$

Concentration profile of peripheral fast distribution compartment (C_f) was modeled using the following equation:

$$\frac{dCf(t)}{dt} = \text{K2} * \text{Cp(t)} - \text{K3} * \text{Cf(t)}$$

Initial conditions: $C_f(0) = C_{t1}(0) = C_{t2}(0) = 0$; Cp(0) = Dose of polymer / Blood volume

Assumptions:

1. It was assumed that the distribution of polymer in each of the compartments was instantaneous and homogenous.
2. The intercompartmental rate constants were assumed to be first order.

Optimization code for Global curve fitting of experimental blood and tumor

The generalized methodology of solving a set of simultaneous first order linear differential equations with unknown coefficients involves utilizing linear optimization techniques in finding the least square fit to the observed experimental data. Initially, K_1, K_2 and K_3 were fixed while optimizing K_4, K_5 and K_6 to obtain the desired best fit. The obtained values of K_4, K_5 and K_6 were then used as initial estimates and both blood and tumor data were refitted by varying all rate constants. Due to the complexity of the problem, an unconstrained search for global minimum is often challenging and time intensive. Therefore, to circumvent this issue, we have used the Optimization toolbox in Matlab® software that offers routines for searching constrained minimum values of multivariable scalar functions with intelligible initial estimates. The algorithm starts with a user supplied initial guess on rate constants and solves the set of differential equations with known initial conditions (namely, blood and tumor compartment 1 and 2 concentrations at time t=0). It then determines the absolute squared error normalized to the experimental value for each data point in every concentration set (C_p, C_{t1} and C_{t2}).

$$\sum_{k=1}^{n}\left(\frac{C_p(t_k)-Y_p(t_k)}{C_p(t_k)}\right)^2+\sum_{i=1}^{n}\left(\frac{C_{t1}(t_k)+C_{t2}(t_k)-Y_{t1}(t_k)-Y_{t2}(t_k)}{C_{t1}(t_k)+C_{t2}(t_k)}\right)^2$$

where Y_p, Y_{t1} and Y_{t2} are the blood and tumor compartment 1 and 2 concentrations at each time points t_k, calculated by solving the set of differential equations based on present values of rate constants and eventually summed over all measured time points. This error is minimized using a constrained linear optimization tool in Matlab® that iterates through all possible combinations of rate constants under pre-specified lower and upper bounds on the same to determine the best fit (Error values in Table A-6.).

Table A-6. Akaike Information Criteria (AIC) and Reduced Chi square (χ^2) values of blood-tumor link model (1, 2 and 3) (Chapter 4)

	G5.0-OH (29 kDa)	**G6.0-OH (58 kDa)**	**G7.0-OH (117 kDa)**	**HPMA copolymer (26 kDa)**	**HPMA copolymer (52 kDa)**	**HPMA copolymer (131 kDa)**
AIC (Model 1)	145.16	40.15	-	17.07	23.64	-
Reduced χ^2 (Model 1)	41.60	5.02	-	1.77	2.27	-
AIC (Model 2)	-	29.64	27.40	-	-	28.36
Reduced χ^2 (Model 2)	-	2.94	2.57	-	-	2.73
AIC (Model 3)	-	30.13	22.03	-	-	29.25
Reduced χ^2 (Model 3)	-	2.69	1.39	-	-	2.54

Model 1- Schematic represented in Figure 4-1A, Chapter 4. Elimination from a single tumor compartment into blood via K_5 for lower MW polymers not showing prolonged tumor retention.

Model 2- Schematic represented in Figure 4-1B, Chapter 4. Model allows elimination from the first tumor compartment (t1) via rate constant K_5 back into the plasma compartment but does not allow elimination from the second tumor compartment (t2) to account for the prolonged retention seen in tumors over the time period of the experiment.

Model 3: Elimination is allowed from the second tumor compartment (t2) to the first tumor compartment (t1) by a first order rate constant K_7

A.12. References

1. Strohalm J, Kopecek J. Poly N-(2-hydroxypropyl) methacrylamide. 4. Heterogeneous polymerization. Angew Makromol Chem. 1978;70:109-18.

2. Šubr V, Ulbrich K. Synthesis and properties of new *N*-(*2*-hydroxypropyl) methacrylamide copolymers containing thiazolidine-2-thione reactive groups. React Funct Polym. 2006;66(12):1525-38.

3. Sadekar S, Ray A, Janat-Amsbury M, Peterson C, Ghandehari H. Comparative biodistribution of PAMAM dendrimers and HPMA copolymers in ovarian-tumor-bearing mice. Biomacromolecules. 2011;12(1):88-96.

4. Klajnert B, Bryszewska M. Fluorescence studies on PAMAM dendrimers interactions with bovine serum albumin. Bioelectrochemistry. 2002;55(1-2):33-5.

5. Klajnert B, Stanisawska L, Bryszewska M, Paecz B. Interactions between PAMAM dendrimers and bovine serum albumin. BBA-Proteins Proteom. 2003;1648(1-2):115-26.

6. Mandeville J, Tajmir-Riahi H. Complexes of dendrimers with bovine serum albumin. Biomacromolecules. 2010;11(2):465-72.

7. Owens III DE, Peppas NA. Opsonization, biodistribution, and pharmacokinetics of polymeric nanoparticles. Int J Pharm. 2006;307(1):93-102.

8. Lakowicz JR, Masters BR. Principles of fluorescence spectroscopy. J Biomed Opt. 2008;13:029901.

APPENDIX B

PHYSOCOCHEMICAL CHARACTERISTICS AND HISTOLOGICAL ASSESSMENT OF SMALL INTESTINAL TOXICITY OF PAMAM CPT FORMULATIONS

B.1. Size exclusion chromatogram of elution profiles of PAMAM G4.0-NH2 and G3.5-COOH

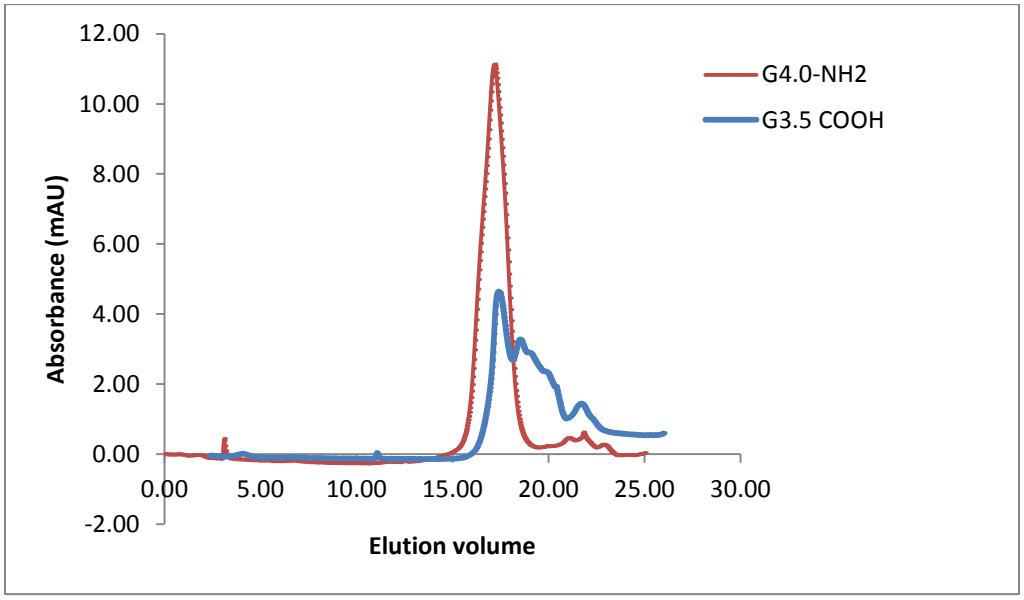

Figure B-1. Size exclusion chromatograms of PAMAM G4.0-NH_2 and G3.5-COOH (Superose 6^{TM} 10/300 GL column (GE Healthcare).

B.2. Spectroscopic detection of camptothecin-lactone form

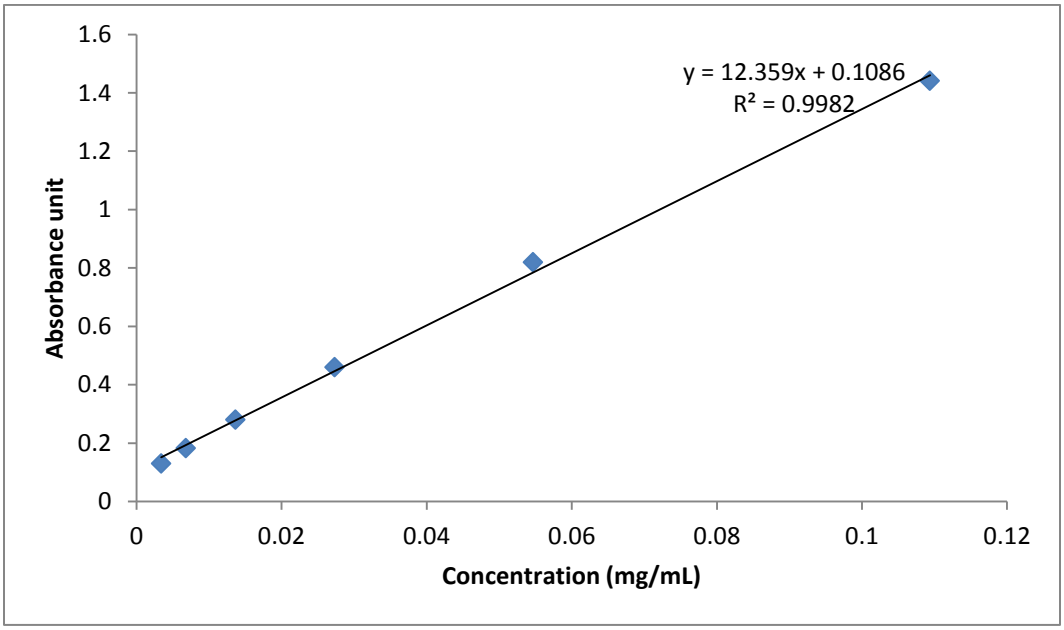

Figure B-2. Absorbance of camptothecin-lactone form over a range of concentrations at λ=370 nm.

B.3. High performance liquid chromatography detection of camptothecin-lactone form

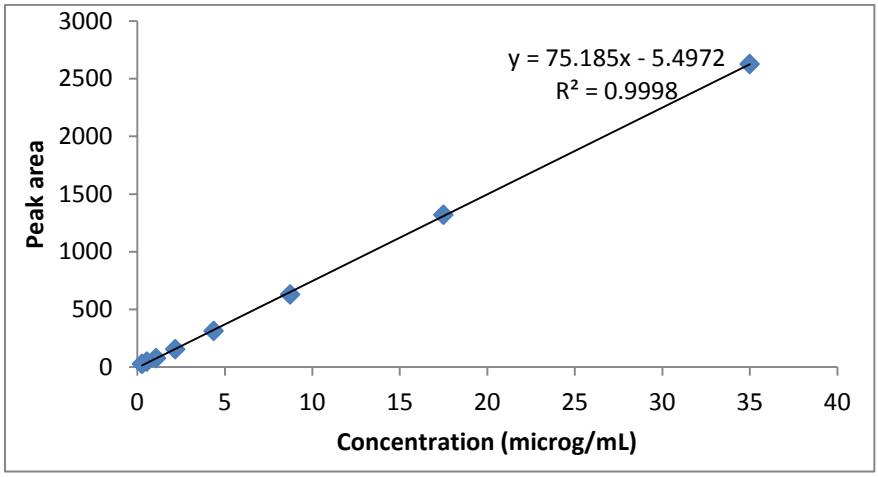

Figure B-3. Peak area of camptothecin-lactone form eluted on a C18 reverse phase HPLC column (XTerra, Waters®; Agilent HPLC system) over a range of concentrations at λ=370 nm.

B.4. High performance liquid chromatography detection of camptothecin-carboxylate form

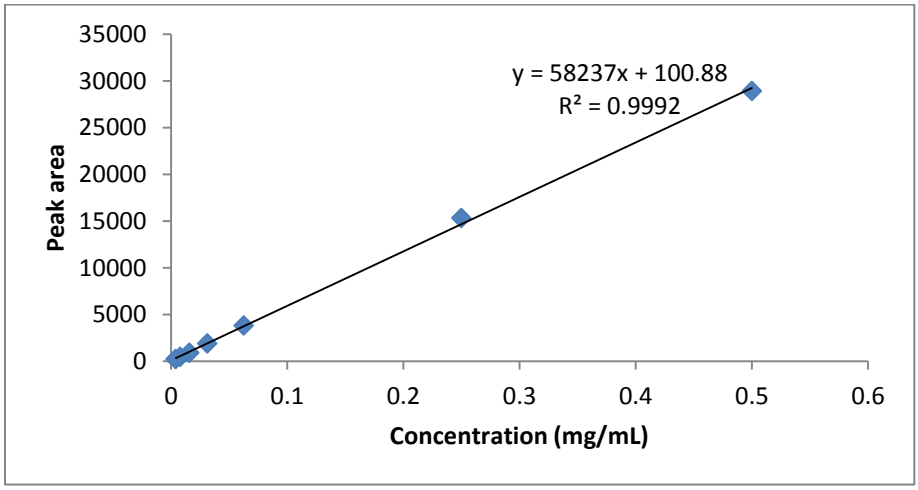

Figure B-4. Peak area of camptothecin-carboxylate form eluted on a C18 reverse phase HPLC column (XTerra, Waters®; Agilent HPLC system) over a range of concentrations at λ=370 nm.

B.5. Histologic assessment of small intestinal segments of animals dosed with PAMAM dendrimer

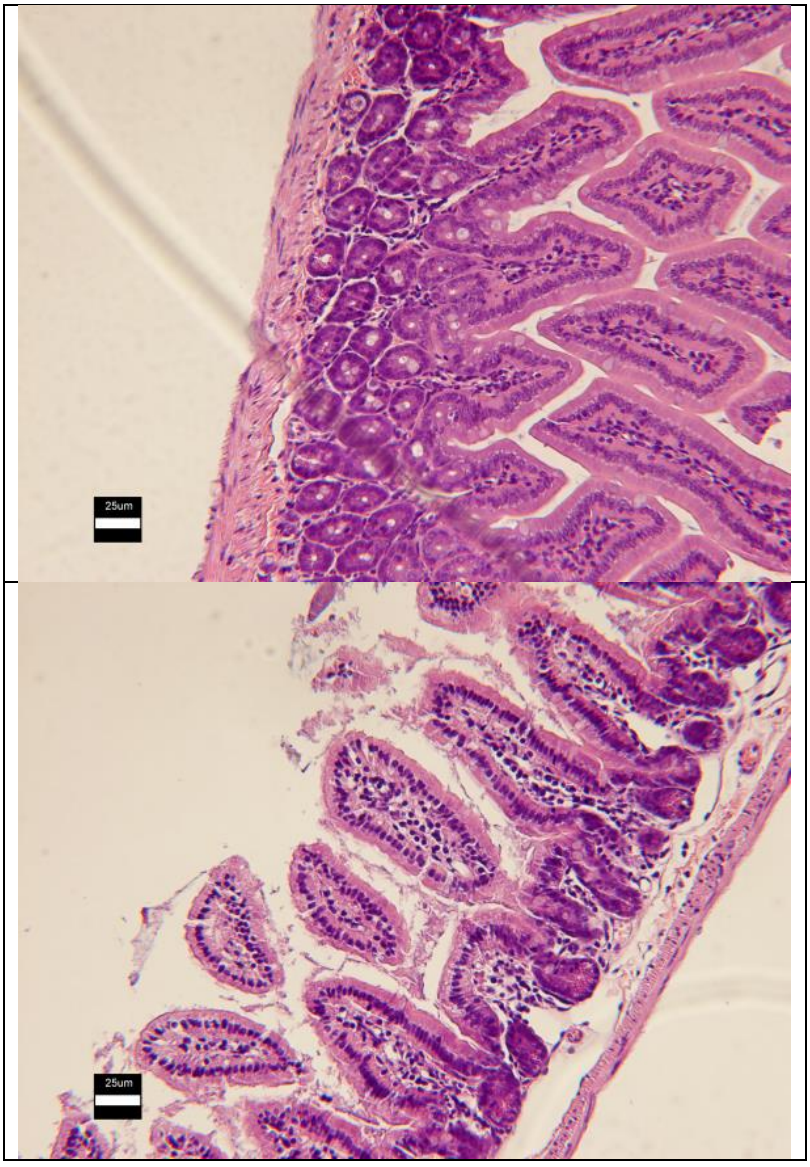

Figure B-5. H and E staining of the small intestinal segments of CD-1 mice orally administered with saline. Scale Bar = 25 μm.

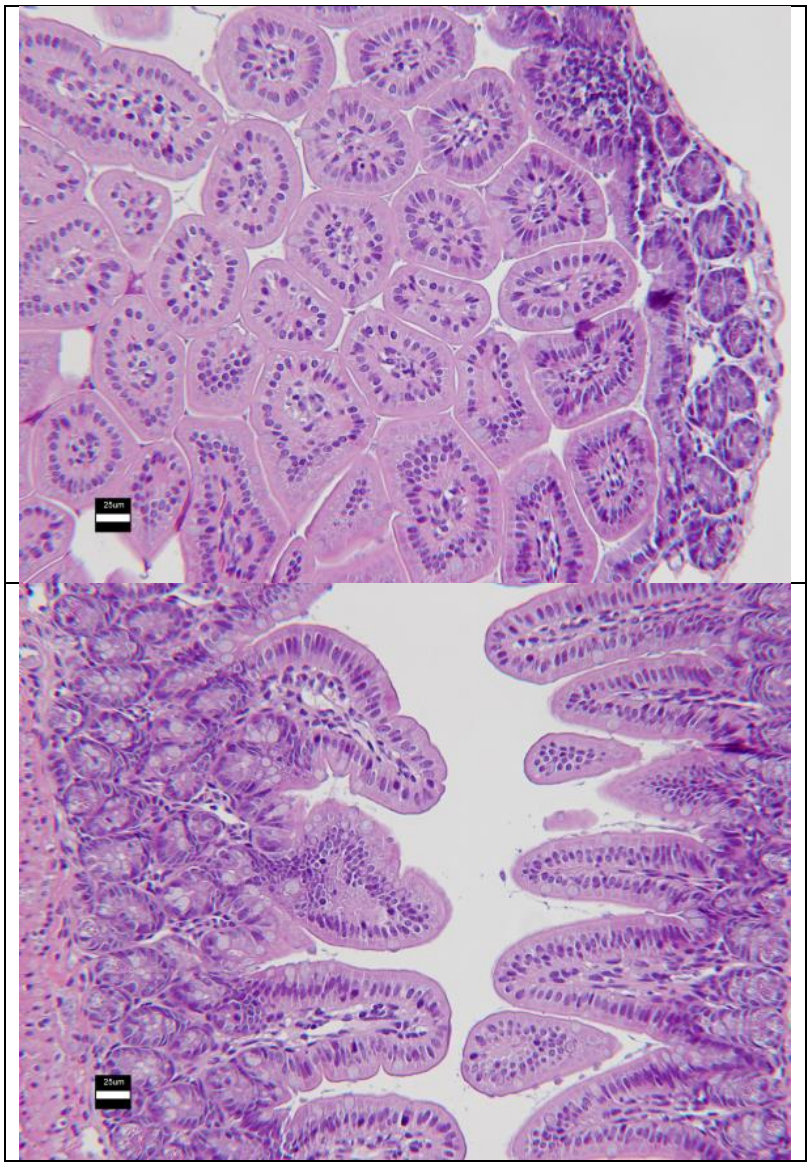

Figure B-6. H and E staining of the small intestinal segments of CD-1 mice orally administered with G4.0 (100 mg/Kg). Scale Bar = 25 µm.

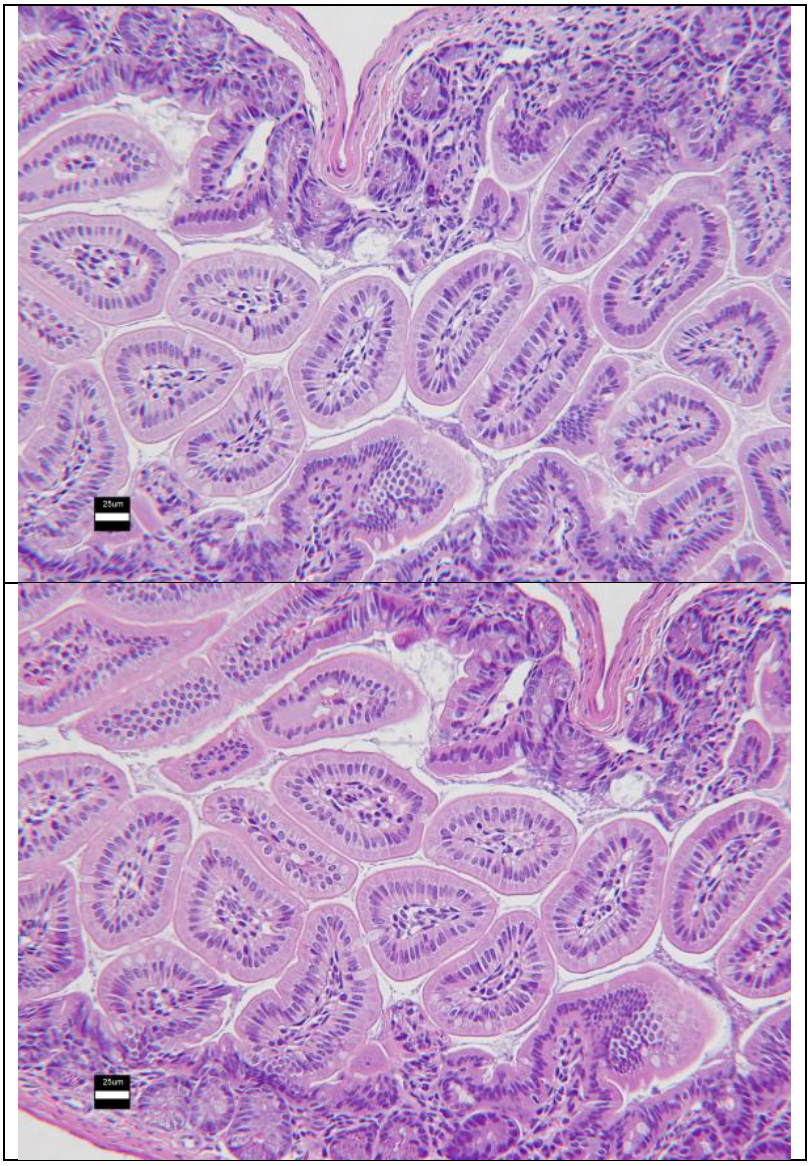

Figure B-7. H and E staining of the small intestinal segments of CD-1 mice orally administered with G4.0 (300 mg/Kg). Scale Bar = 25 µm.

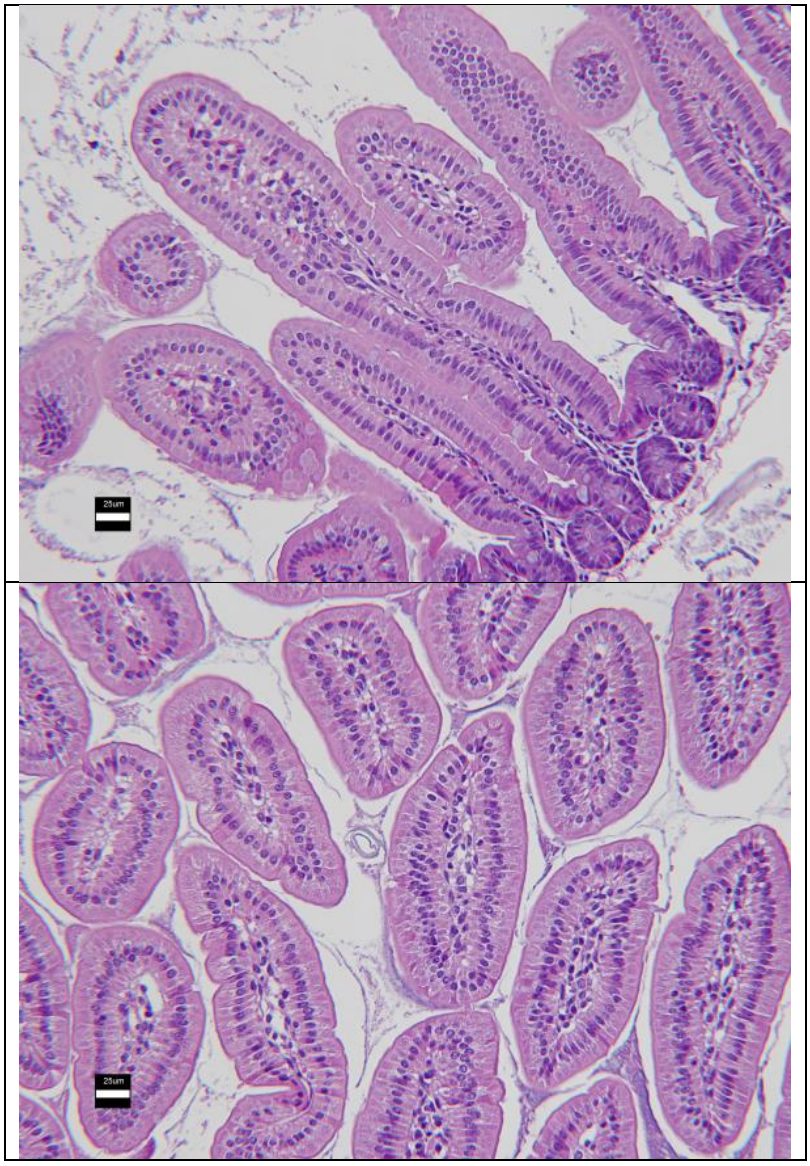

Figure B-8. H and E staining of the small intestinal segments of CD-1 mice orally administered with G3.5 (300 mg/Kg). Scale Bar = 25 µm.

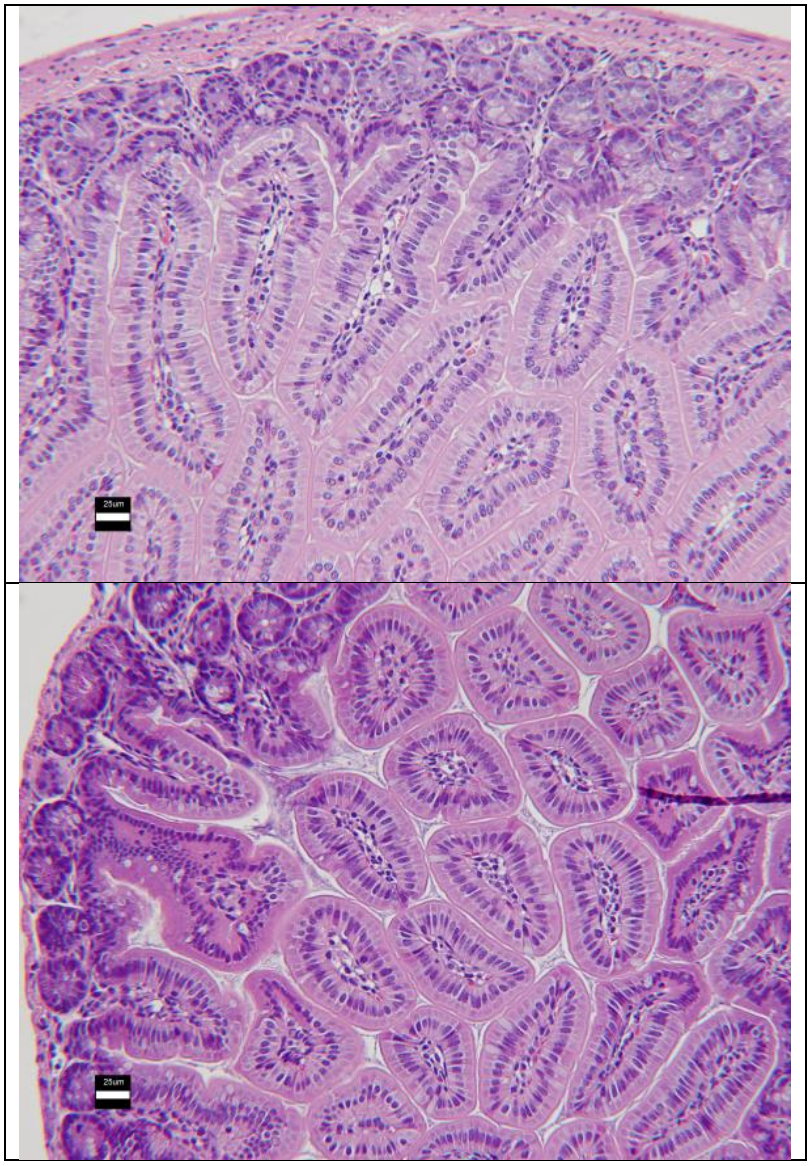

Figure B-9. H and E staining of the small intestinal segments of CD-1 mice orally administered with G3.5 (1000 mg/Kg). Scale Bar = 25 µm.

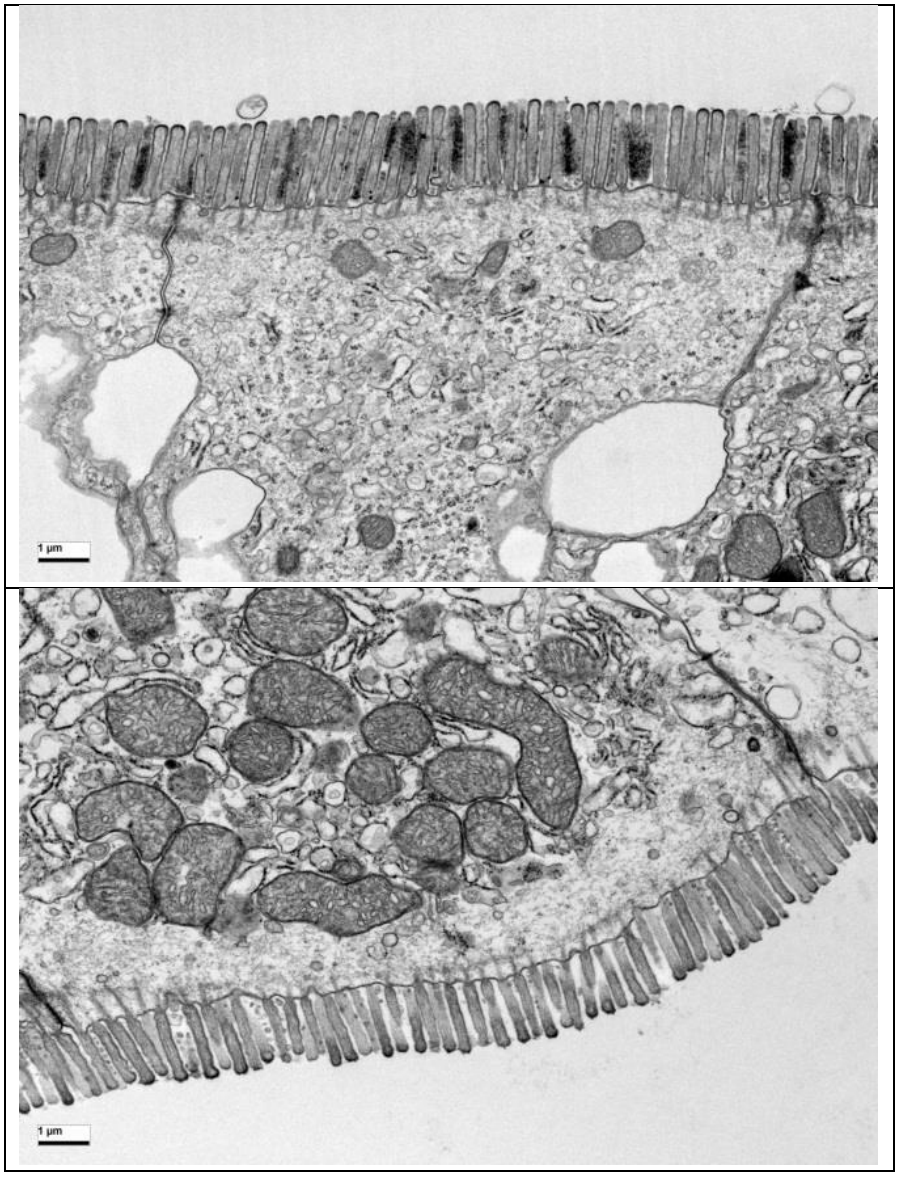

Figure B-10. TEM images of the small intestinal segments of CD-1 mice orally administered with saline. Scale Bar = 1 µm.

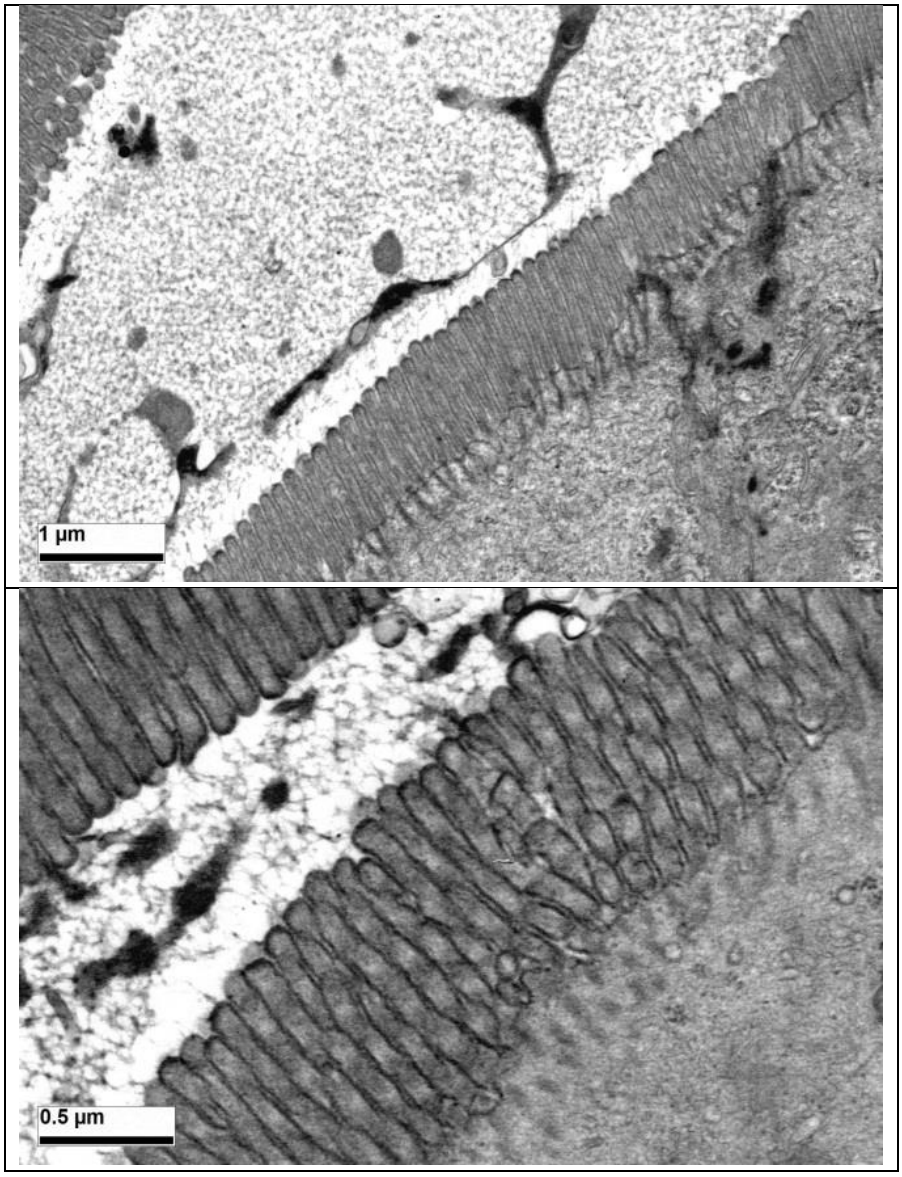

Figure B-11. TEM images of the small intestinal segments of CD-1 mice orally administered with G4.0 (100 mg/Kg). Scale Bar = 1 µm (left); 0.5 µm (right).

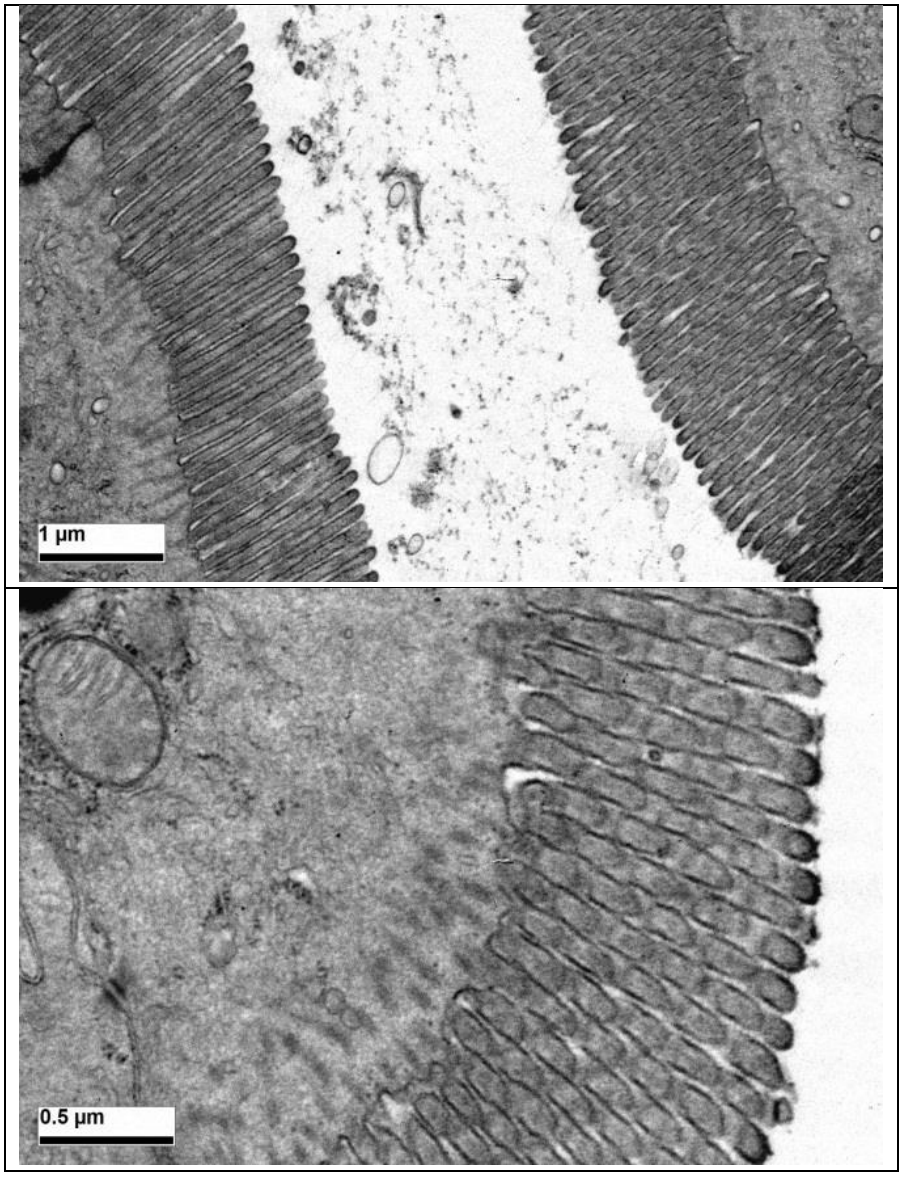

Figure B-12. TEM images of the small intestinal segments of CD-1 mice orally administered with G4.0 (300 mg/Kg). Scale Bar = 1 µm (left); 0.5 µm (right).

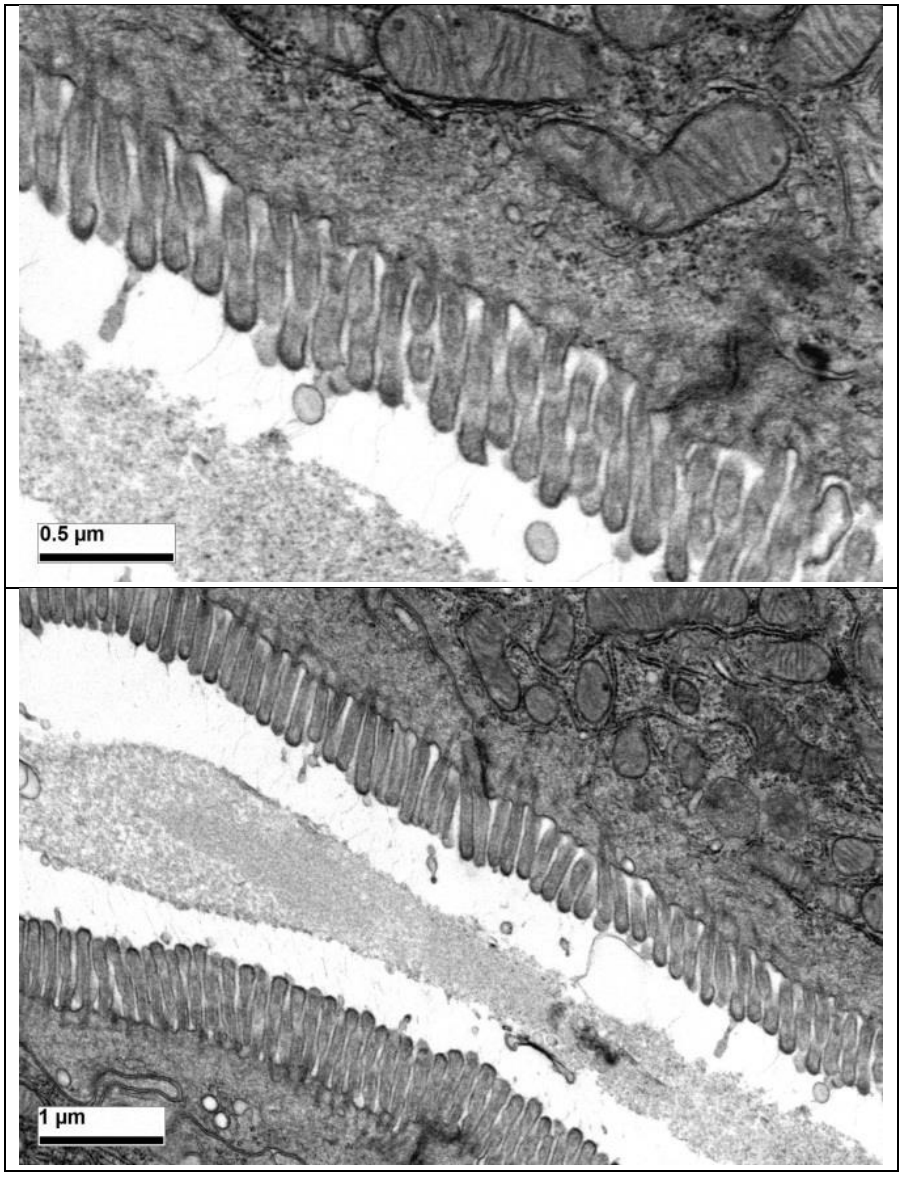

Figure B-13. TEM images of the small intestinal segments of CD-1 mice orally administered with G3.5 (300 mg/Kg). Scale Bar = 0.5 µm (left); 1 µm (right).

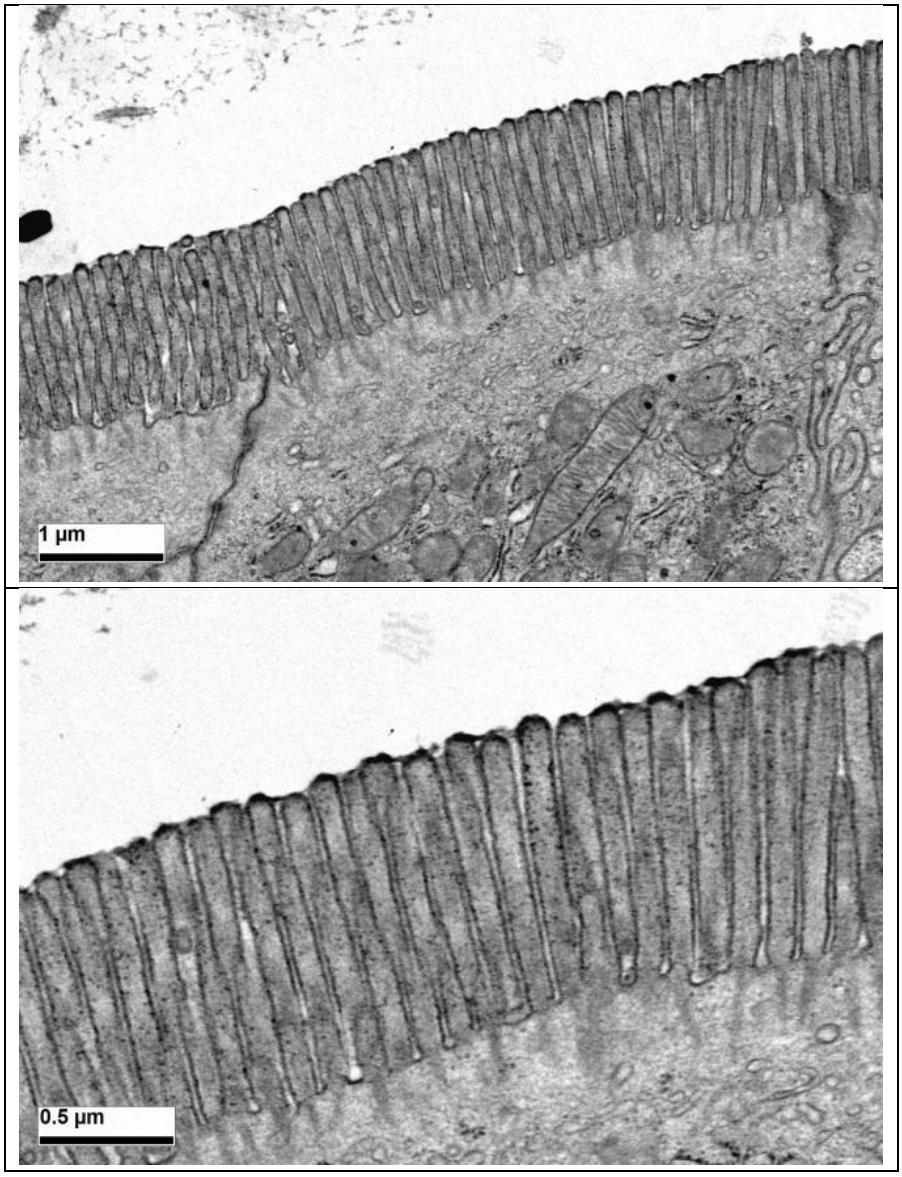

Figure B-14. TEM images of the small intestinal segments of CD-1 mice orally administered with G3.5 (1000 mg/Kg). Scale Bar = 1 µm(left); 0.5 µm(right).

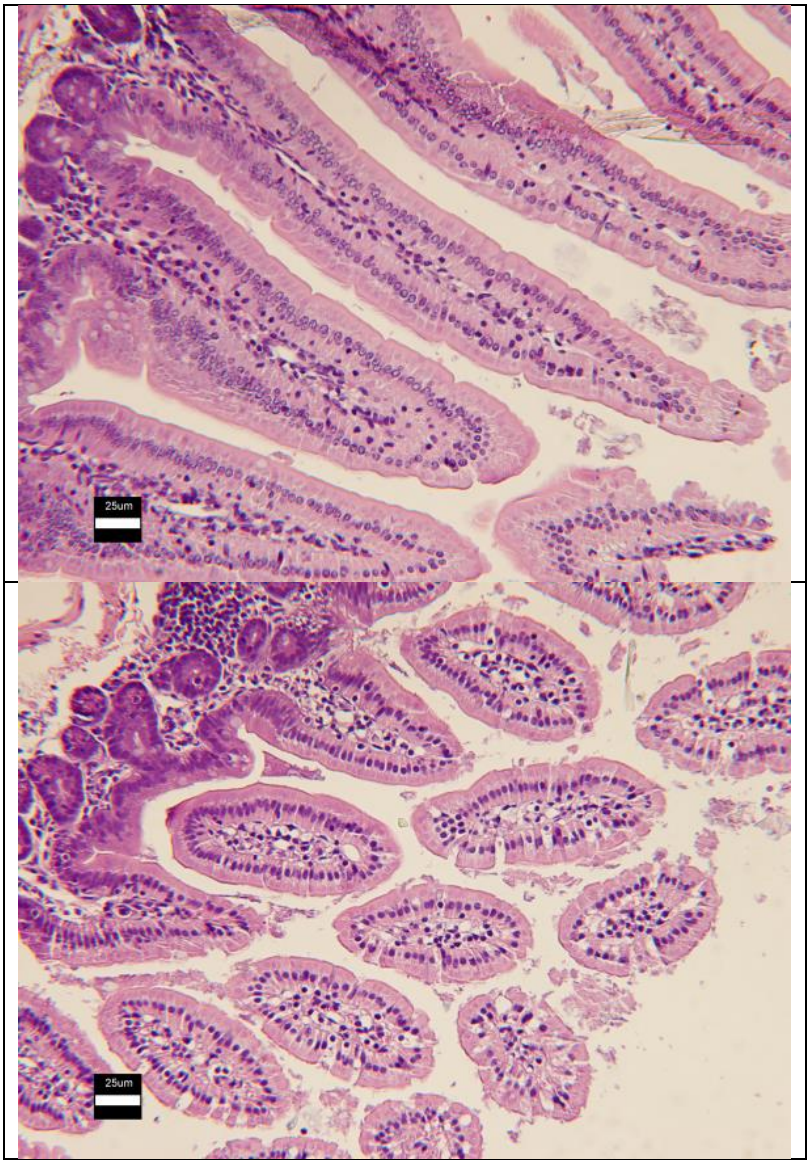

Figure B-15. H and E staining of the small intestinal segments of CD-1 mice orally administered with CPT (5 mg/Kg). Scale Bar = 25 µm.

Figure B-16. H and E staining of the small intestinal segments of CD-1 mice orally administered with CPT + G4.0 (100 mg/Kg). Scale Bar = 25 µm.

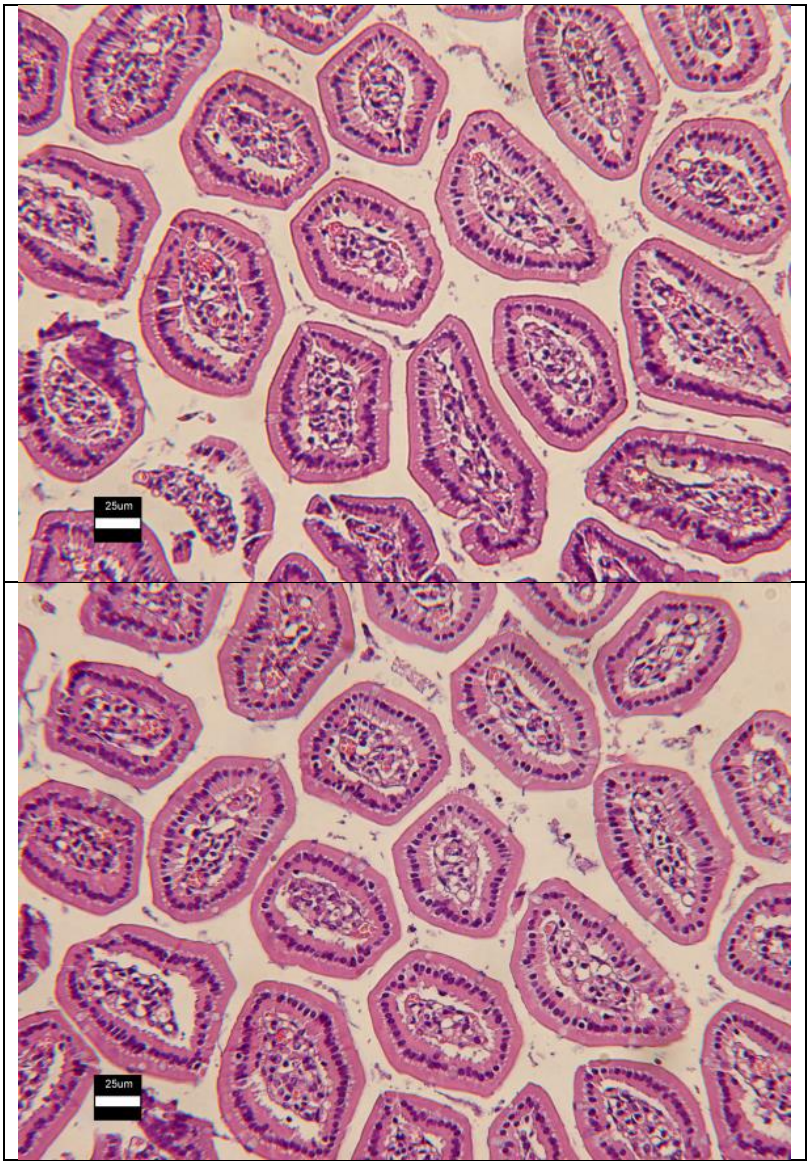

Figure B-17. H and E staining of the small intestinal segments of CD-1 mice orally administered CPT + G4.0 (300 mg/Kg). Scale Bar = 25 µm.

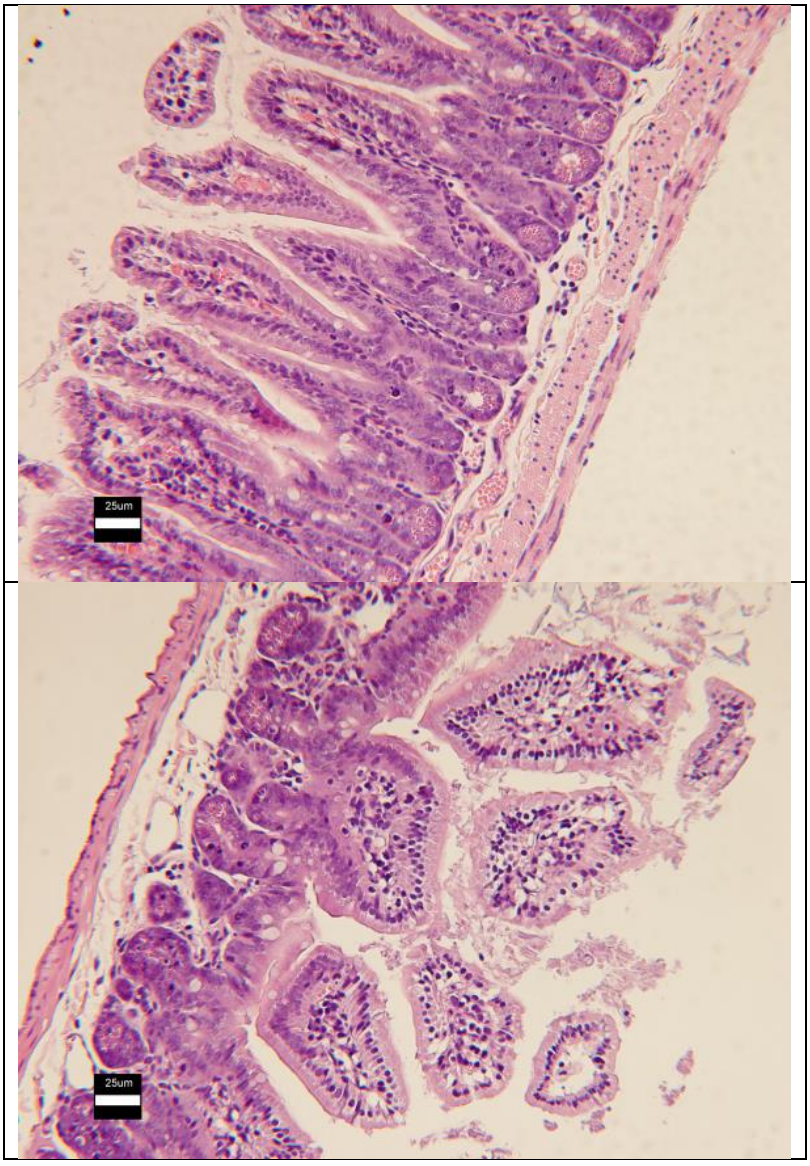

Figure B-18. H and E staining of the small intestinal segments of CD-1 mice orally administered with CPT + G3.5 (300 mg/Kg). Scale Bar = 25 μm.

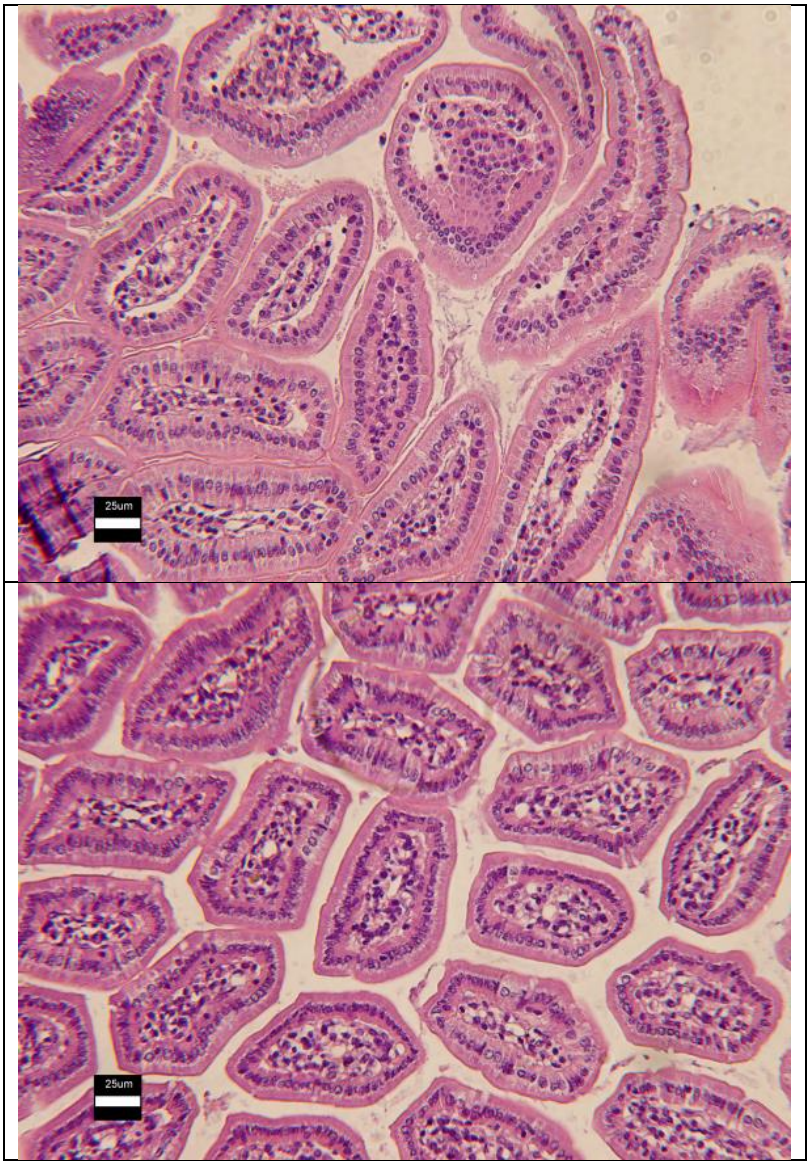

Figure B-19. H and E staining of the small intestinal segments of CD-1 mice orally administered with CPT + G3.5 (1000 mg/Kg). Scale Bar = 25 µm.

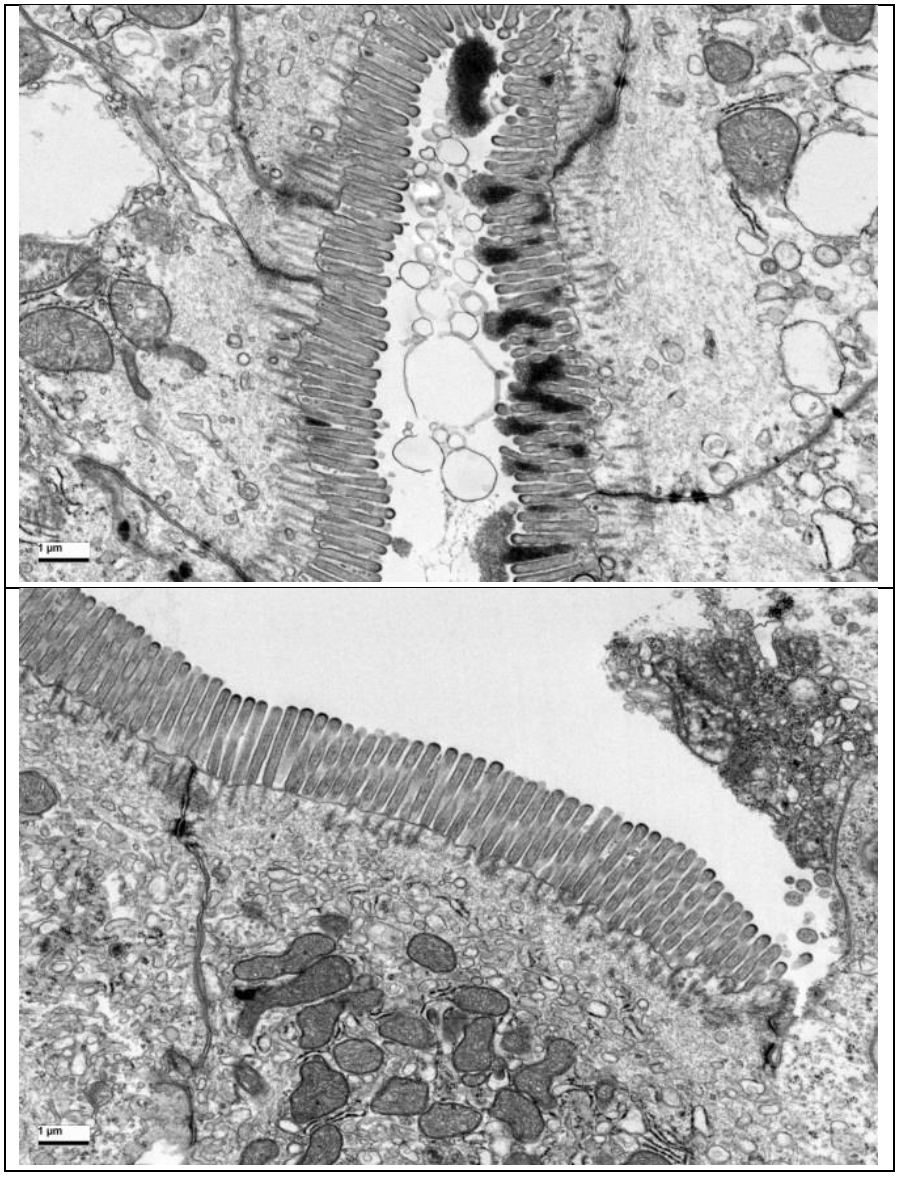

Figure B-20. TEM images of the small intestinal segments of CD-1 mice orally administered with CPT (5 mg/Kg). Scale Bar = 1 µm.

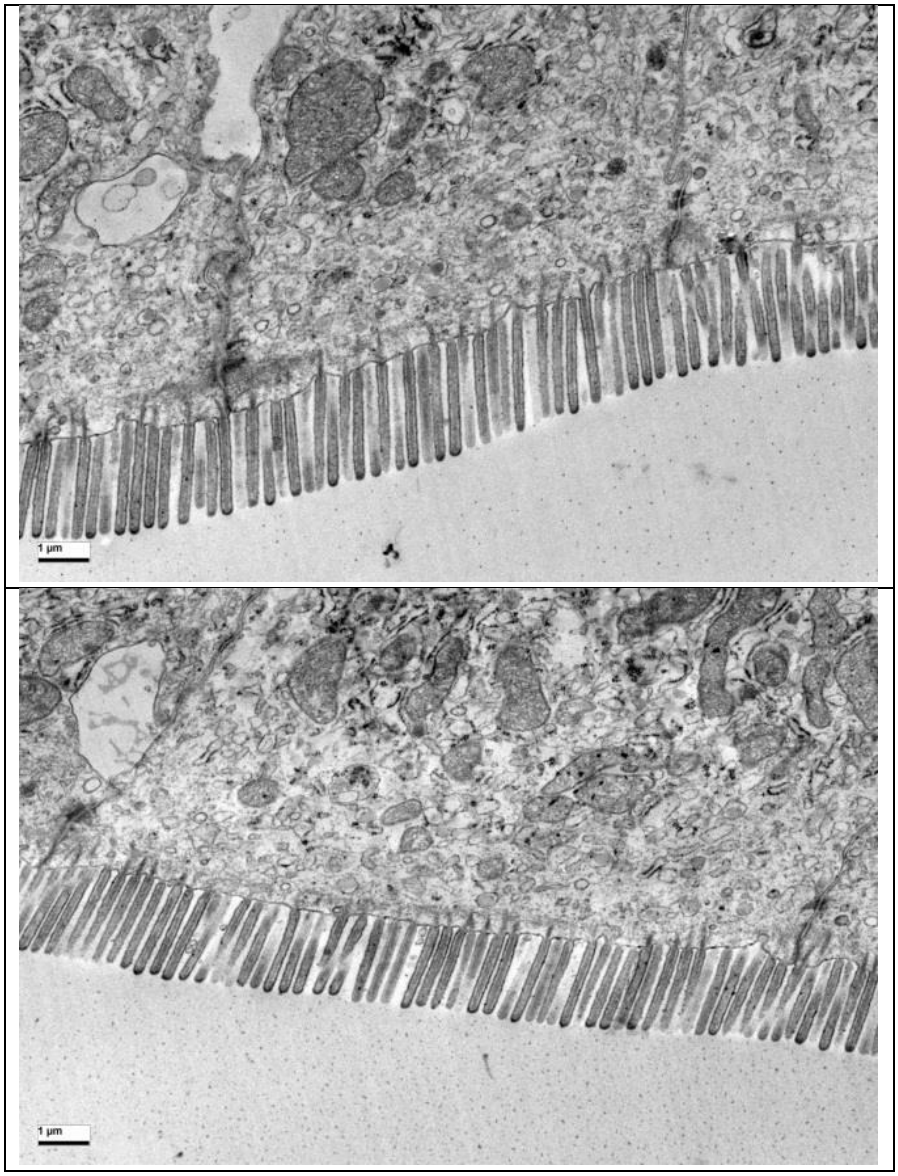

Figure B-21. TEM images of the small intestinal segments of CD-1 mice orally administered with CPT + G4.0 (100 mg/Kg). Scale Bar = 1 µm.

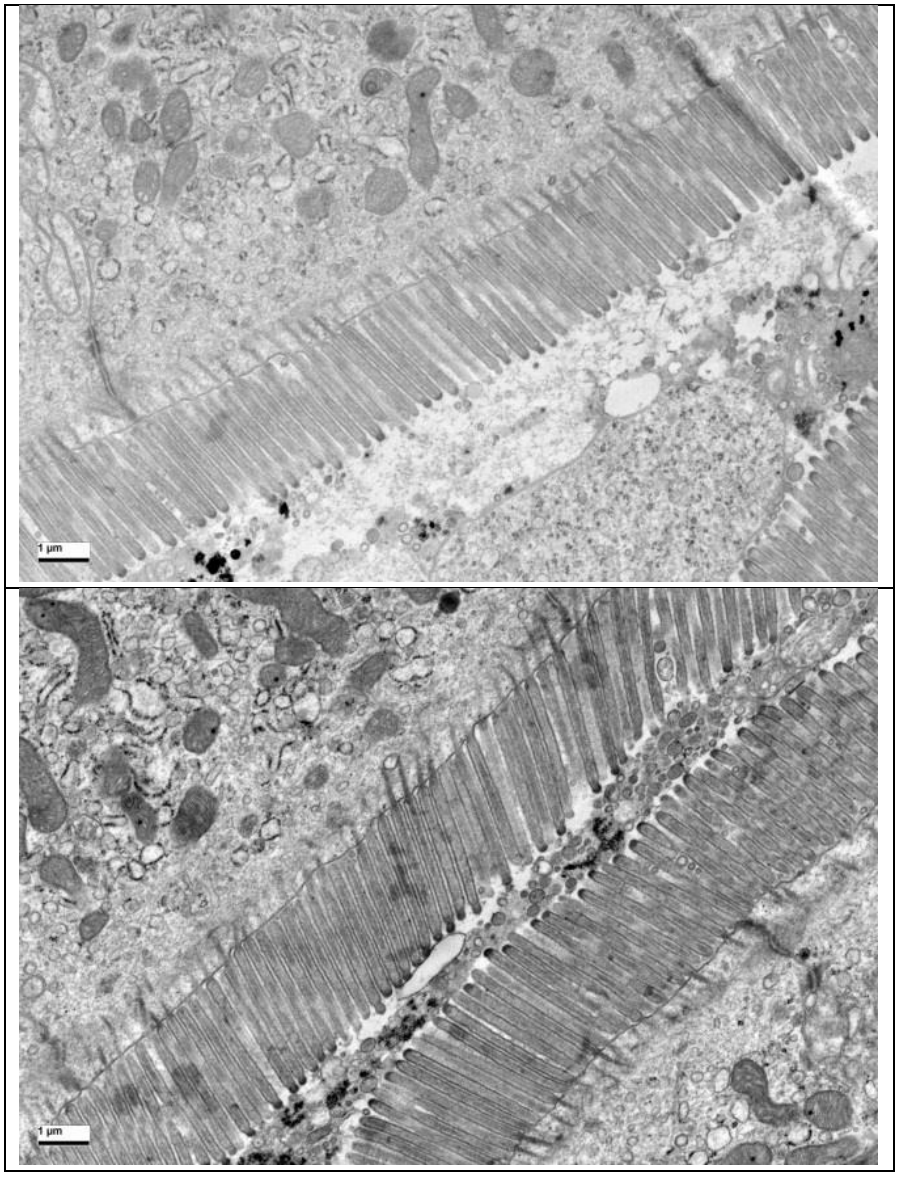

Figure B-22. TEM images of the small intestinal segments of CD-1 mice orally administered with CPT + G4.0 (300 mg/Kg). Scale Bar = 1 µm.

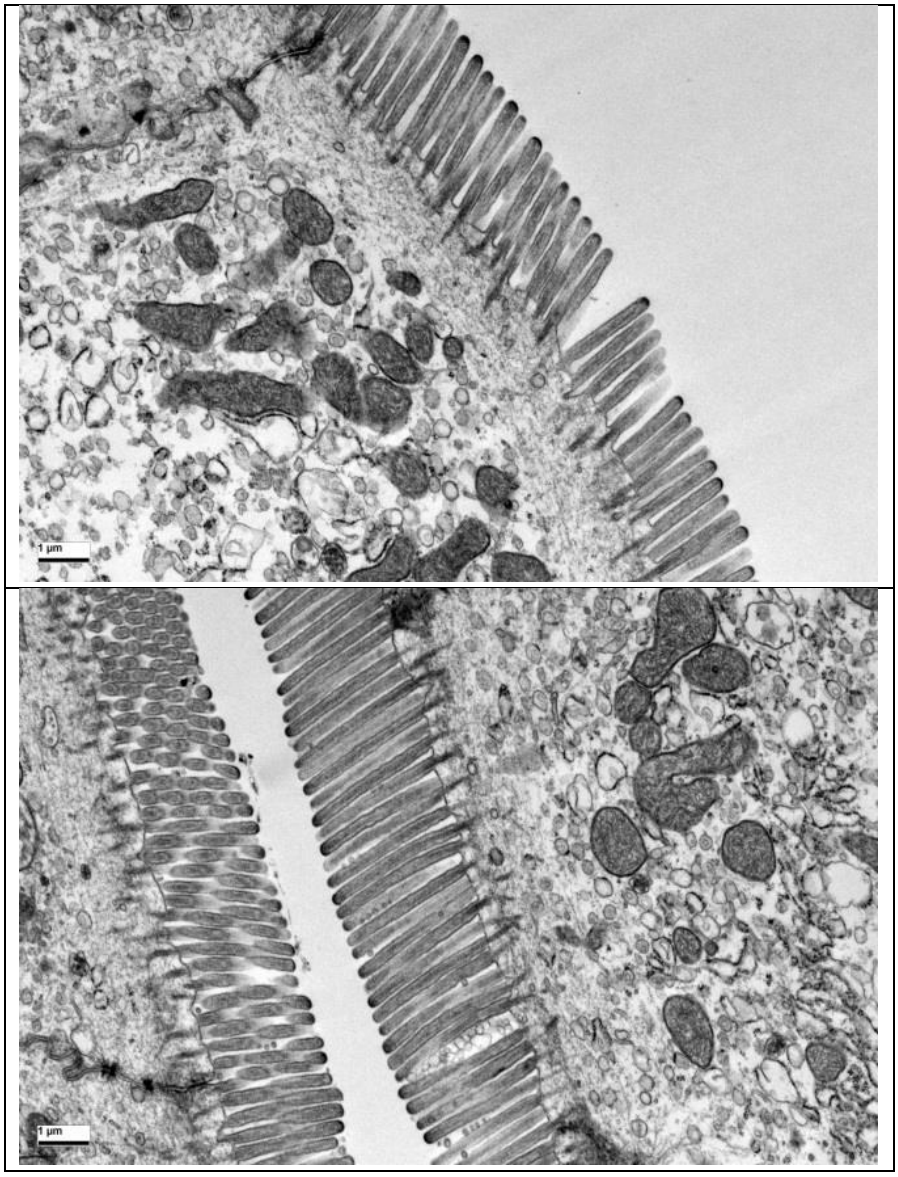

Figure B-23. TEM images of the small intestinal segments of CD-1 mice orally administered with CPT + G3.5 (300 mg/Kg). Scale Bar = 1 µm.

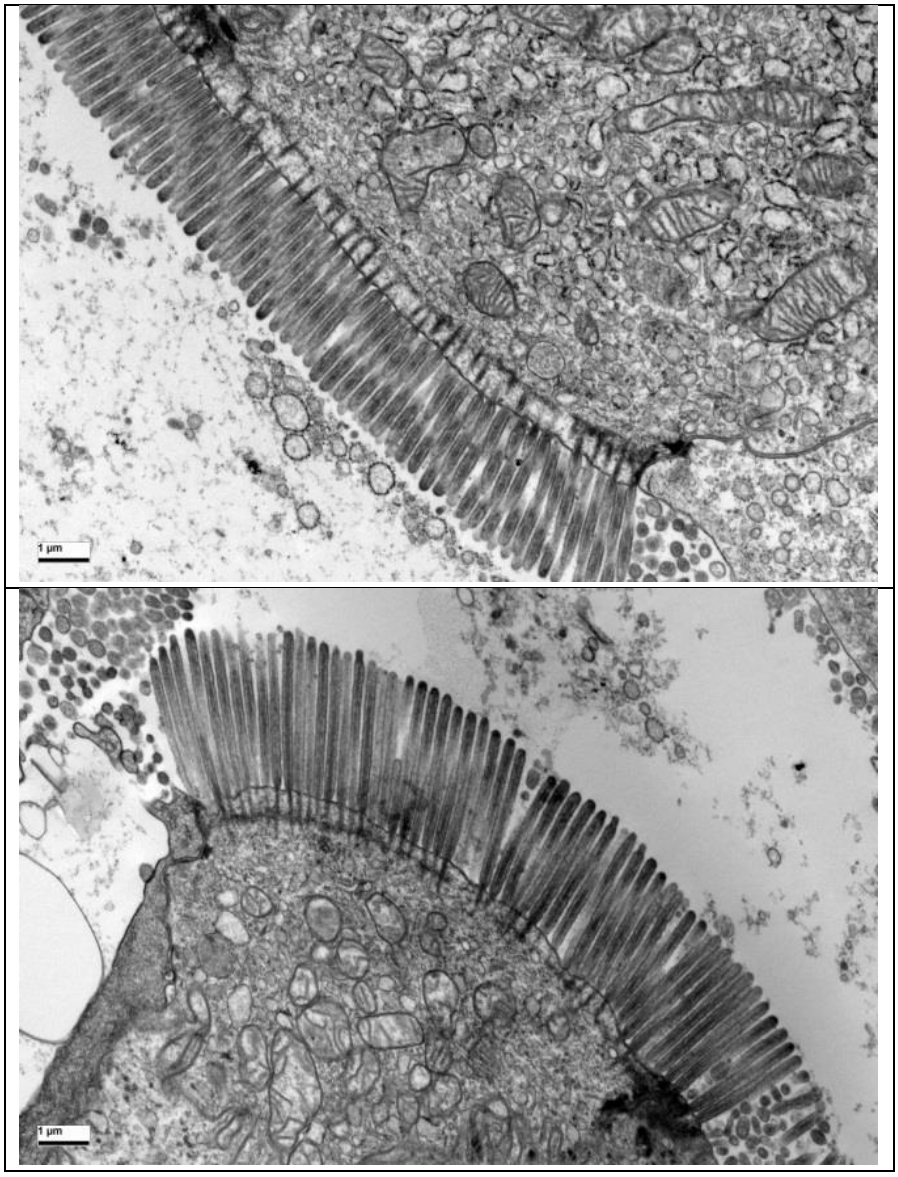

Figure B-24. TEM images of the small intestinal segments of CD-1 mice orally administered with CPT + G3.5 (1000 mg/Kg). Scale Bar = 1 µm.